UNIVERSITÀ DEGLI STUDI DI PAVIA

DOTTORATO IN SCIENZE CHIMICHE E FARMACEUTICHE

XXIX CICLO

Coordinatore: Chiar.mo Prof. Mauro Freccero

Identification of molecules targeting the PKC/ELAV/mRNA cascade as innovative pharmacological tools

Tutore

Chiar.ma Dr.ssa Daniela Rossi

Tesi di Dottorato di

Rita Nasti

a.a. 2015- 2016

Foreword

Recent evidence in literature has shown that dysregulation of the Protein Kinase C (PKC)/Embrionic Lethal Abnormal Vision (ELAV) proteins pathway have led to a significant alteration in gene codifying expression of proteins (i.e TNFa, GAP-43, VEGF) primarily involved in various pathologies such as cancer, inflammation and neurodegeneration., Based on this evidence my PhD has mainly focused on the discovery of new molecules capable of modulating the PKC/ELAVs/mRNA cascade, targeting either PKC or ELAV proteins. In addition, my research also focused on the chiral resolution of racemic compounds of pharmaceutical interest (i.e butyro lactones and A_3 adenosine receptor antagonist) *via* enantioselective chromatography combined with the assignment of the absolute configuration of the pure enantiomers by means of chiroptical spectroscopic techniques [i.e including Vibrational Circular Dichroism(VCD), Electronical Circular Dichroism (ECD), Optical Rotatory Dispersion (ODR)] combined with Density Functional Theory (DFT) calculations.

My research shows a high degree of interdisciplinarity and requires the full integration of complementary activities. For these reasons, my research has been carried out in collaboration with national and international research groups who have all the competences required to successfully fulfil the aims of the project. Two research networks in particular, working on the identification of PKC ligands and the discovery of ELAV targeting compounds, have been successfully collaborating on the project, as summarized in Figure A.

As regards the configurational study of enantiopure compounds, activity has been performed in close collaboration with Prof. Abbate's research group which shares the competences in the field of chiroptical spectroscopy, and Prof. Potenza's research group, which supports the configurational assignment by NMR spectroscopy.
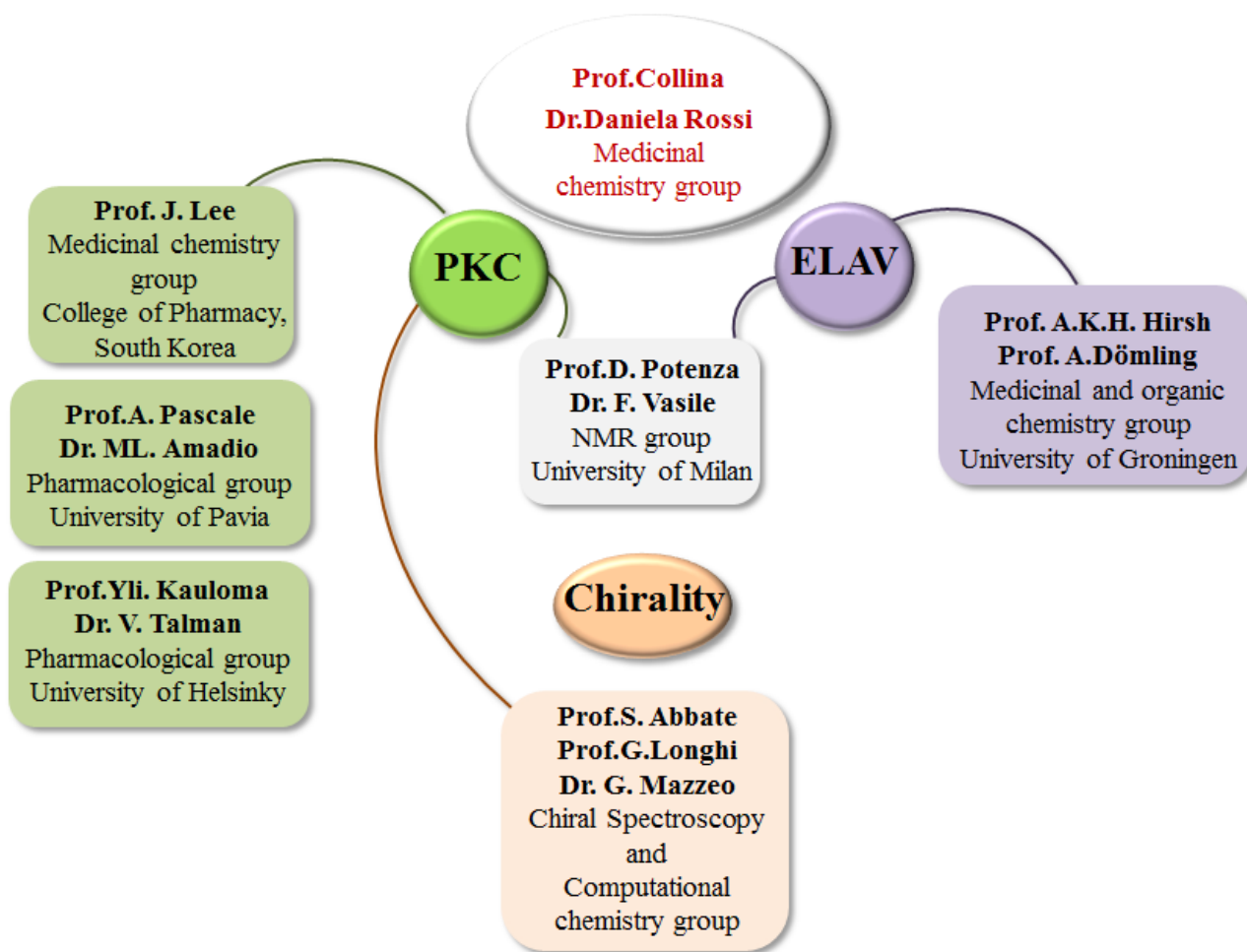
Figure A: research networks

Table of contests

Chapter I

1. Introduction

Protein kinase C (PKC) is a super-family of ten serine/threonine kinases discovered in 1977 by professor Yasutomi Nishizuka.[1] This family is one of the most important regulators of cellular functions due to its ability to phosphorylate a large number of substrates after it has been activated by second messengers Calcium (Ca^{2+}) and Diacyl glycerol (DAG). In mammals the PKC family is classified in conventional (cPKCs: α, ßI, ßII and γ), novel (nPKCs: δ, ε, η and θ) and atypical (aPKCs: ζ, ι and λ) subfamilies based on both isoform structure and sensitivity to the activators (Figure 1) The cPKCs in particular are activated by both Ca^{2+} and DAG, nPKCs which are insensitive to Ca^{2+}, while aPKCs are not regulated by either activator.

From a structural standpoint, PKCs are generally characterized by a primary amino acid sequence composed of a single polypeptide chain which includes conserved domains (named C1–C4) linked by a hinge region (Figure 1). The N-terminal regulatory region hosts C1 and C2 domains that control the kinase activity of the enzyme as well as its subcellular localization. The C1 domain presents the binding motif for the endogenous activator DAG as well as for the exogenous activators, such as phorbol esters (Figure 1). Going into structural detail, this regulatory domain is divided into two portions each containing 30 amino acids classified as C1a and C1b domains. The first one binds the activator DAG while the second sub-domain has an affinity for phorbol esters and structurally related molecules.

The C2 domain coordinates binding to anionic phospholipids on the cell membrane and, in the case of cPKCs, includes the binding site for Ca^{2+} [2-4]. In the nPKC, this domain is called C2-like domain due to the lack of conserved aspartate residues necessary for Ca^{2+} binding, which are capable of binding phospholipids.[5,6] The C3 and C4 domains are localized in the C-terminal kinase region of the enzyme and are designated to bind ATP and the substrate, respectively. Moreover, PKCs present a pseudo-substrate sequence (PS) empowered to maintain the protein in inactive conformation and to prevent false activation.
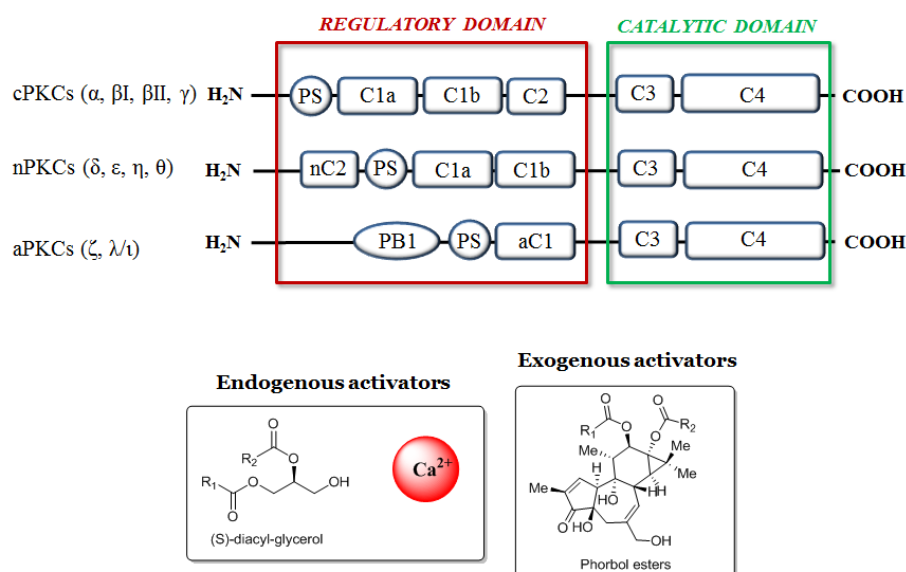
Figure 1. Schematic structures of PKC isoforms and their activators

Over the past 30 years the physiological activities of the PKC sub-families have been thoroughly studied and described and their role in various cellular functions, such as cell migration, proliferation, differentiation, apoptosis and cellular metabolism have been proved. Although the PKC isoforms have a high degree of homology (75-80%), they are capable of modulating a specific cellular function by acting on definite proteic substrate.[7]

1.1 PKCs and diseases

On the basis of the above considerations, it is easy to understand that alteration of PKCs functions are involved in different pathological conditions. In particular, dysregulations of many PKC isoforms have been documented in human cancer, suggesting that these family members may function as oncogenes or tumor suppressors. Numerous studies in particular have shown an overexpression of PKCα and PKCß in breast, liver, kidney and prostate cancer, while aPKCs seem to be expressed in malignant lung carcinoma. [8-12]

Furthermore, the involvement of PKCs in the aethiology of neurodegenerative diseases have been largely documented .[13, 14] In brief, in physiological conditions PKCα and ε enhance the α-secretasi activity leading to a decrease in the production of amyloid precursor protein (APP). Moreover, PKCα is involved in synaptic remodeling through the phosphorilation of neuronal Embrionic Lethal Abnormal Vision protein (n-ELAVs). The activation of n-ELAV led to an improvement in the expression of GAP-43, a protein designed to improve signal transduction. The activity of these PKC isoforms is switched off in pathological conditions, especially in Alzheimer's disease (AD), causing an alteration of the pathway described above.

In addition, the involvement of PKC in diabetes has been proved. Going into more detail, iper-activation of PKCß is tightly linked to the uncontrolled phosphorylation of the ubiquitous ELAV (ELAVL1 or HuR), leading to an over-expression of the *Vascular Endothelian Growth Factor* (VEGF) protein which is primarly implicated in diabetic retinopathy. [15]

1.2 PKC's modulators

1.2.1 Catalytic domain's ligands

In the past few years, the high therapeutic value of PKC modulators have been widely demonstrated. Research in this field has been firstly addressed to develop ligands able to interact with the catalytic domain of PKCs. The ATP binding inhibitors are the most well known and explored PKC modulators acting *via* a competitive inhibition mechanism. Several classes of compound have been identified, including: mimicks of the ATP moiety, natural ligands and their synthetic derivatives, and lastly bisubstrate analogs.

Concerning the first compound class, a sequence of a miniumum 5 aminoacids and a maximum of 20 were synthetized as mimicks of the ATP binding site. The second class of inhibitors is represented by both natural and synthetic molecules. Among natural componds, Staurosporine (Figure 3) was isolated in 1977 from *Streptomyces staurosporeus*.[16] and represents the precursor of several classes of synthetic derivatives which maintain the indolocarbazoles scaffold.[17] Some of these, such as Enzasturin and Lestaurtinib (Figure 3) for example, are undergoing clinical trials as chemotherapeutic agents and their selectivity of action is strictly related to substitution on the rings. [18-22]

The third class of inhibitors is represented by the bisubstrate analog inhibitors, that were designed with the basic idea to mimic the phosphate donor (ATP) and the acceptor components (Ser-, Thr-, or Tyr-containing peptides) maintaining a specific distance between these two components. Sulfonamides, sulfonylbenzoyl, carboxylic acid, dipeptidyl and N-acylated peptide, phosphodiester derivatives are representative examples of this class of inhibitors (Figure 3). [23-27]

Recently, a new class of diaminopyrimide was discovered by High Throughput screening (HTS) as selective ligands for ATP moiety of PKCθ, showing an affinity that ranged from low nanomolar to high micromolar.(Figure 3)[28]

Although the high potency showed by the PKC ligands targeted the catalytic domain, they cannot be considered selective enough for a specific kinase class. Indeed, it has to be noted that that the ATP-site is highly conserved among 500 kinases expressed by the human genome, therefore the design of specific and selective ligands for this target definitely represents a challenge.
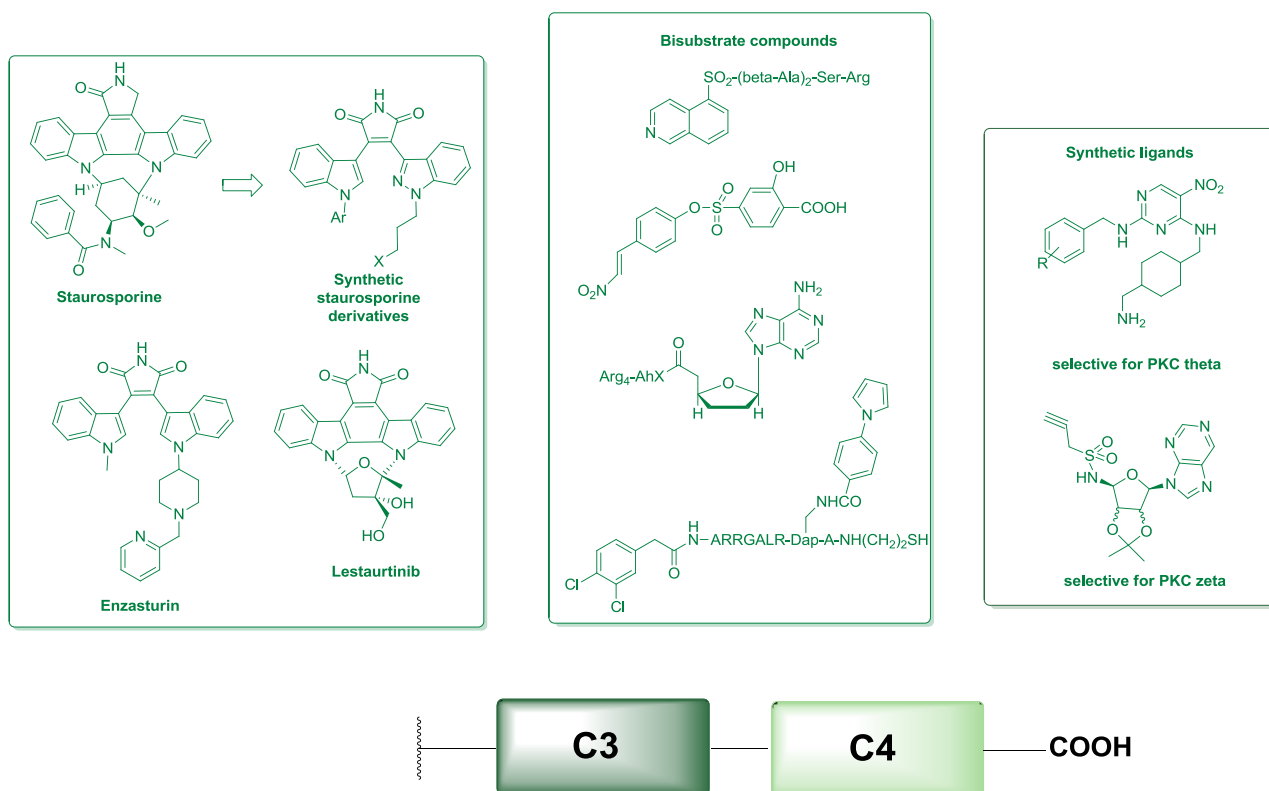
Figure 3: examples of PKC ligands targeting the catalytic domain

1.2.2 Regulatory domain's ligands

The C1 domain of PKC represents an intriguing pharmacological target for developing new PKC activators, which may be useful in the treatment of various diseases including AD. The most well known PKC activators targeting the C1 domain are Phorbol and Bryostatin-1, both of natural origin (Figure 4). Phorbol is considered the exogenous ligand of regulatory domain par excellence. It was discovered in 1934 and its derivative phorbol-12-myristate-13-acetate (PMA, Figure 4), is widely used in biochemical assay. Bryostatin-1 is a macrolide lactone isolated in 1967 from a *Bugula neritina.*[29] Several Bryostatin-1 synthetic analogs targeting the regulatory domain of PKCs have been prepared and characterized (Figure 4). It is interesting that they seem to specifically target novel PKC isoforms. [30, 31]
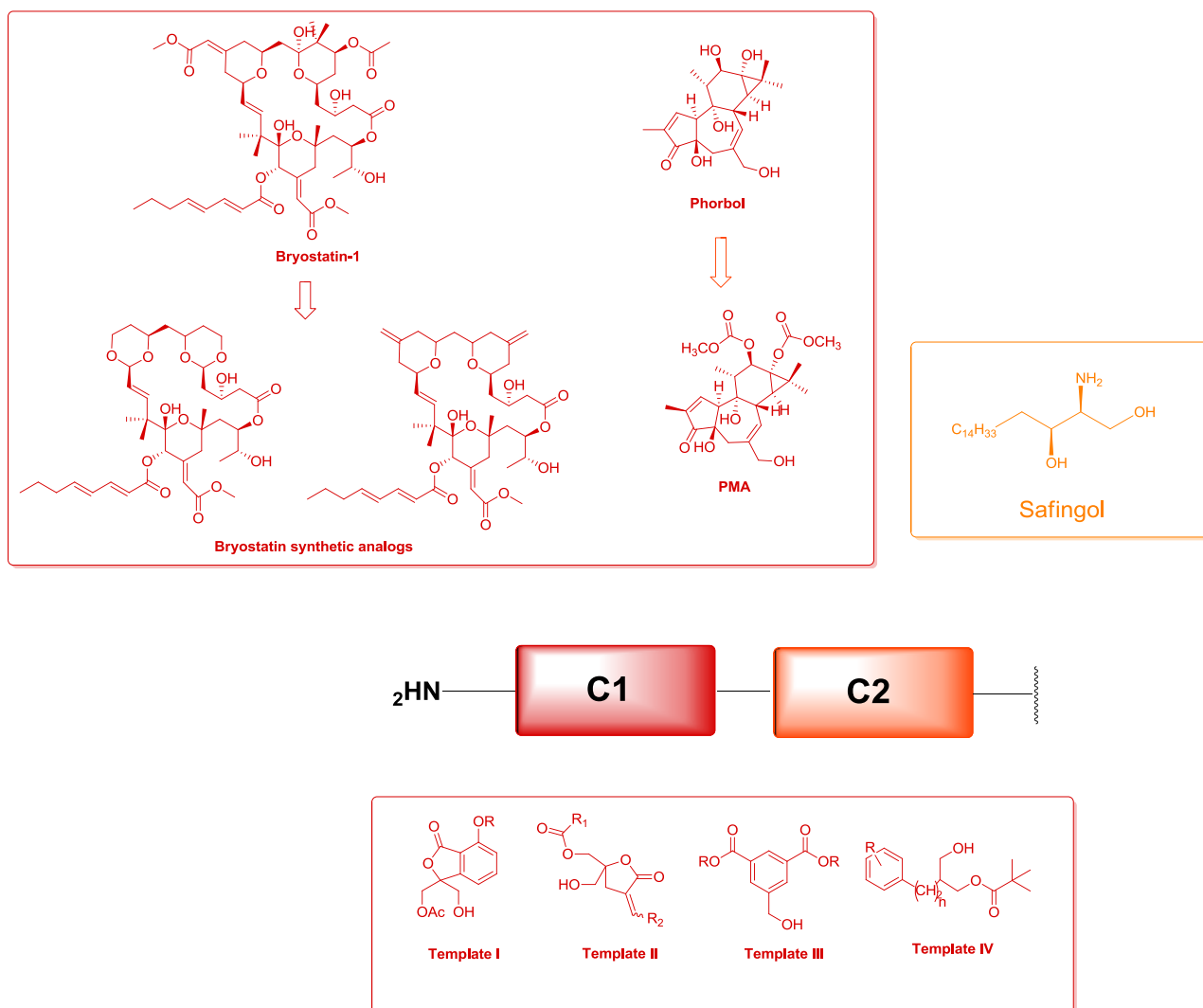
Figure 4. examples of ligands target regulatory domain and of template of the most promising PKC ligands targeting the C1-domain

It is worth noting that the crystal structure of C1b domain of the PKC delta co-crystallized with phorbol-13-*O*-acetate was solved 1995 (PDB code: 1PTR), thus providing insights into the structural features directly involved in ligand-target interaction. Going into detail, five H-bonds between the ligand and Gly 253, Thr 242 and Leu 251 were highlighted as important for the interaction. (Figure 6) [32]

Since 1995 research into the field of C1 domain-targeting ligands has increased significantly. In particular, numerous synthetic C1-targeting compounds belonging to various templates (Templates I-IV, Figure 4). were designed and prepared, and their affinity for PKC isoforms were evaluated and proposed.[33-37]

Going into detail, monocyclic Templates I and II [33-35] were designed with the aim of reducing the part of the entropic penalty associated with the binding of the flexible glycerol backbone of

DAG, displaying affinity in the submicromolar range. Indeed, the rigid analogs of the DAG matched well with two/three points of the pharmacophore model of phorbol ester including $C_3=O$, C_9-OH and C_{20}-OH of the phorbol ester. As an alternative approach, new compounds were designed based on both the dialkyl 5-(hydroxymethyl)isophthalate template III,[36] and the 2-phenyl- and 2-benzyl-3-hydroxypropyl pivalate template IV.[37]
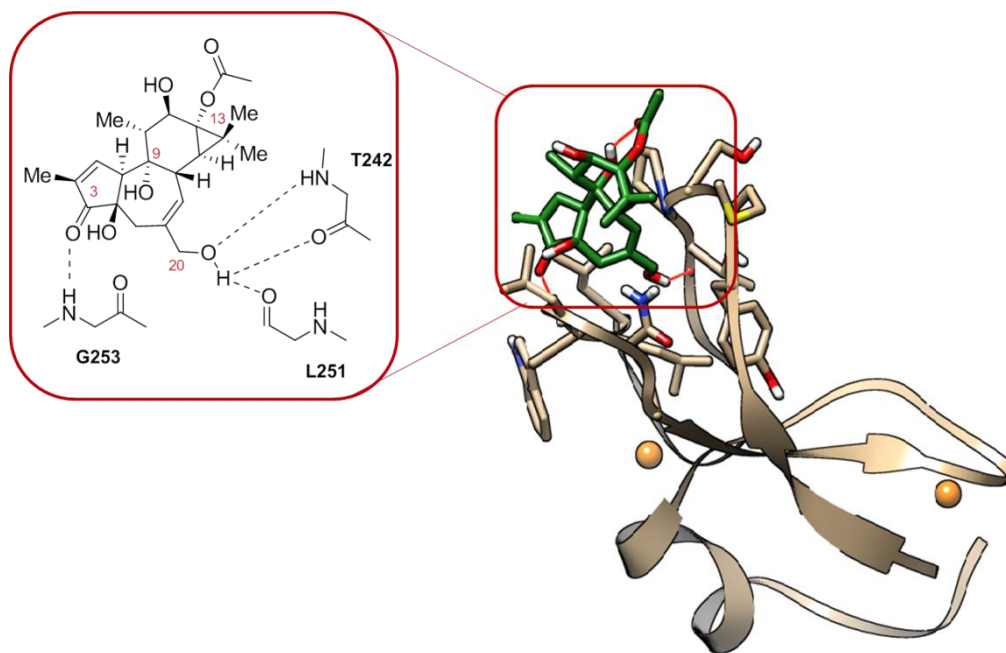
Figure 6. C1 domain of PKCδ complexed with phorbol ester (PDB code: 1PTR). Color code: protein (shown as a cartoon): light gray; Aminoacids; C: light gray, N: blue, O: red, S: yellow. Phorbol ester (shown as stick): C, green; O, red; zinc: orange. Hydrogen bonds below 3.5 Å shown as red lines.

With regards to C2 domain-targeting compounds, the L-threo-dihydrosphingosine is noteworthy (known as Safingol, Figure 4). This is the first PKC inhibitor to enter clinical trials as a chemotherapeutic agent. It is interesting that it seems to act especially on PKCδ, ε and ßI.[38]

2. Design and synthesis of new PKC's ligands

Among the compounds belonging to template IV, compound **1** (Figure 7), emerged as the most promising C1-targeting- PKC ligand, showing high affinity for PKC alpha (0.7 uM). As reported in our *paper 1* [D. Rossi, Med.Chem.Com., 2016], the research in my PhD was firstly aimed at understanding which structural modifications of reference compound **1** were allowed to preserve or increase the affinity for the C1-domain of PKCs. For this purpose, we designed a small library of thirteen new compounds characterized by structural variability at aromatic and carboxylic moieties, as summarized in Figure 7. The study was conducted in synergic collaboration with the groups of

Professor Lee at College University of South Korea, Professor Gustav Boije Af Gennas and Professor Jari Yli Kauhaluoma at the University of Helsinki.
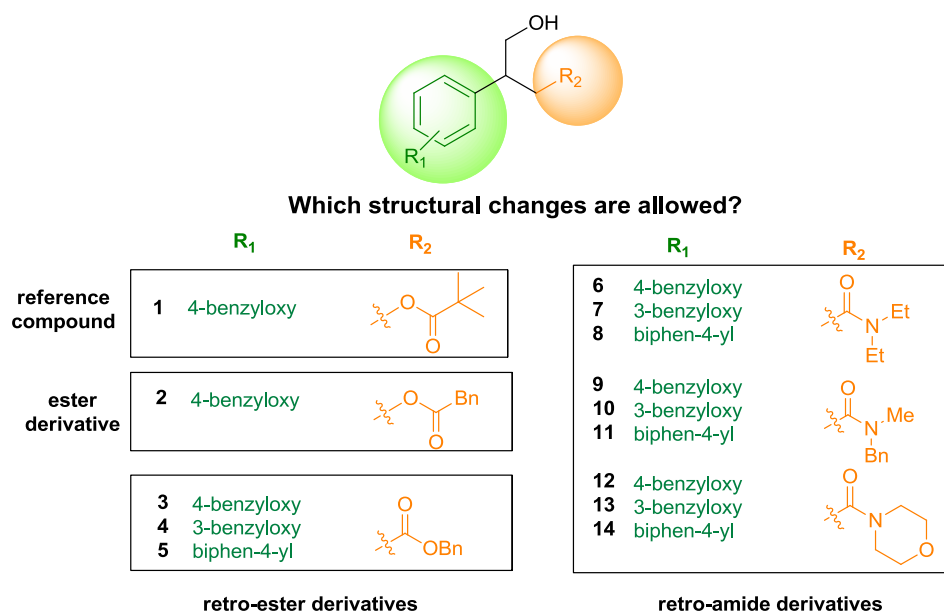
Figure 7. structure of compound **1–14**

The work flow can be summarized as follows: i) docking experiments to investigate if compounds **2–14** would bind to the binding groove of the C1 domain of PKC, ii) synthesis of designed compounds, iii) biological assay. Additionally, given the presence of a chiral centre in the structure of our PKC ligands, and considering that the enantiomers of a biologically active compound may show different interactions to the target protein and, more generally, different behavior in the biological environment, we also investigated the role of chirality in the ligand-target interaction by preparing and testing the pure enantiomers of the most promising compounds.

Concerning docking experiments, results clearly showed that all designed compounds can be considered able to interact with the target and thus are suitable for the study. In Figure 8, a snapshot of compounds (*S*)-**2** and (*S*)-**3** docked docked to the C1b domain of PKCδ is reported as an example.
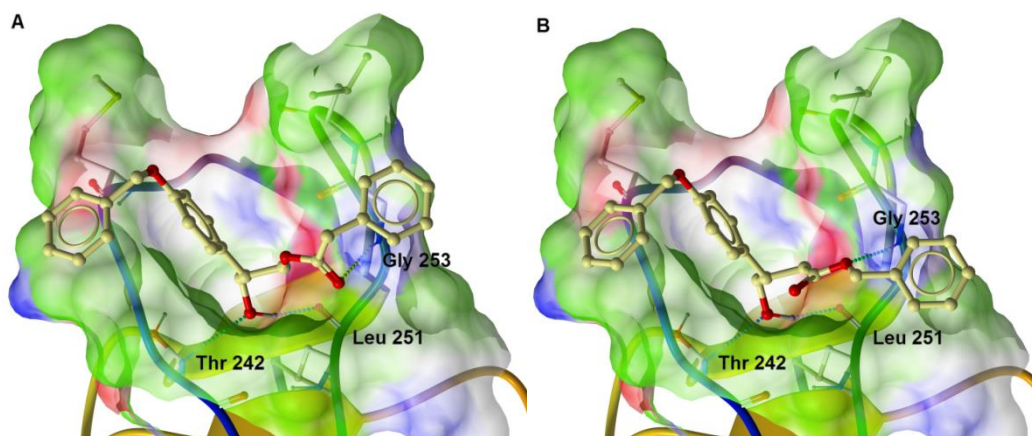
Figure 8 (**A**) Compound (*S*)-**2** and (**B**) (*S*)-**3** docked to the C1b domain of PKC δ (PDB ID: 1PTR).20 Hydrogen bonds are represented as green spheres and the surface of the binding pocket of the protein is colored as following: hydrogen bond acceptor area (red), hydrogen bond donor area (blue) and hydrophobic area (green). The figure was created using ICM-Browser (version 3.7-2a,Molsoft L.L.C.).

The synthesis of designed compounds was then accomplished according to the procedure reported in Schemes 1 and 2. Compounds **1** and **2** were prepared in accordance with the synthetic pathway developed by Professor J. Lee's research group, with the appropriate modifications. (scheme 1).

Scheme 1. Synthesis of **1** and **2**. Reagents and conditions: (a) LiAlH$_4$, diethyl ether, 0 °C, then reflux, 30 min; (b) SOCl$_2$, DCM, 0 °C, 1 h; (c) NaCN, DMF, 100 °C, 2 h; (d) 30% NaOH (aq), reflux, overnight; (e) H$_2$SO$_4$, MeOH, reflux, 2 h; (f) NaH, 1,4-dioxane, 0 °C, then rt, 30 min; g) (MeO)$_2$CO, 1,4-dioxane, 0 °C then reflux, 2 d; (h) LiAlH$_4$, THF, 0 °C, then rt, 2 h; (i) (Me$_3$)$_3$CCOCl, pyridine, DCM, 0 °C, then rt, 2 h; (l) PhCH$_2$COCl, pyridine, DCM, 0 °C, then rt, 2 h.

As regards compounds **3-14,** a retro-synthetic analysis was initially accomplished, suggesting the synthetic pathway summarized in scheme 2. In brief, the key step for the synthesis of compounds **3-14** was the preparation of 3-unsaturated γ-butyrolactones **28-30** (Scheme 2), that was easily achieved through a two-step reaction sequence. Firstly the Heck reaction, performed according to our previously optimized phosphine-free protocol, gave the α,β-unsaturated esters **25-27** as mixtures of (*E,Z*)-isomers. Subsequently, crude **25-27** underwent allylic oxidation with selenium dioxide and *tert*-butyl hydroperoxide without further purification, providing the desired oxidation products **28-30**. γ-Butyrolactones **28-30** were then subjected to microwave-assisted catalytic hydrogenation under phase transfer conditions, yielding intermediates **31-33**. It has to be noted that catalytic hydrogenation of **28** and **29** resulted in the simultaneous reduction of the double bond and the cleavage of benzyloxy group, thus providing compounds **31** and **32**, respectively. These, in turn, were fully *O*-benzylated, to yield the desired γ-butyrolactones **34** and **35**. The γ-butiro lactones **31-34-35** were finally converted into the retro-esters **3-5** and the retro-amides **6-14**, applying a tandem hydrolysis-esterification process and an aminolysis reaction, respectively. The aminolysis reation was performed according to the protocol developed by Lesimple, applying the appropriate

modifications. In order to speed up the synthetic procedure, we decided to take advantage of microwave irradiation instead of using conventional heating thus obtaining the desired products in a very short reaction time (40 minutes vs 6 hours).

Scheme 2. Synthesis of compound **3-14**. Reagents and conditions: (a) TBAC, AcONa, Pd(OAc)$_2$, DMF, reflux, overnight; (b) SeO$_2$, tBuOOH, DCE, reflux, overnight; (c) HCOONH$_4$, 10% Pd/C, MW conditions: 100 °C, 100 W, 180 s; (d) Cs$_2$CO$_3$, benzyl bromide, MeCN, MW conditions: 100 °C, 60 W, 40 min; (e) 10% NaOH (aq), MeOH, reflux, 3 h, then K$_2$CO$_3$, benzyl bromide, H$_2$O/DMF (1:10), rt, overnight; (f) 10% NaOH (aq), MeOH, reflux, 3 h, then AlCl$_3$, amine, DCE, MW conditions: 100 °C, 60 W, 25 min.

The affinity of compounds **1-14** was then tested on both C1 domain of PKCα and δ through binding assays at concentrations ranging from 1-100 uM. The percentages of residual [^{3}H]PDBu binding after exposure to **1-14** at 100 μM concentration are presented in Table 1. As regards affinity to PKCα, the new compound **2** displaced [^{3}H]PDBu in a concentration-dependent manner with an IC$_{50}$ value of 73.9 μM, showing a binding profile very similar to that of reference compound **1** (IC$_{50}$ = 37.5 μM). The retro-ester derivatives **3-5** also exhibited clear concentration-dependent binding to the C1 domain of PKCα although they were less potent than compounds **1** and **2** in displacing [^{3}H]PDBu. No significant displacement of [^{3}H]PDBu was observed for the retro-amides **6-14**; not even at the highest concentration tested (100 μM). With regards to affinity to PKCδ, the results were consistent with those obtained from the PKCα binding assays: compounds **1** and **2** exhibited the highest affinity (IC$_{50}$ values of 33.2 μM and 39.9 μM, respectively;), while compounds **3-5** displaced [^{3}H]PDBu from PKCδ in a concentration-dependent manner, but with lower potency.

Cmpd	Residual [³H]PDBu binding to PKCα (% of control)	Residual [³H]PDBu binding to PKCδ (% of control)
1	41.6±2.7 (4)	29.3±2.1 (4)
2	51.3±5.8 (4)	34.8±2.2 (4)
3	73.9±8.0 (2)	61.6±0.4 (2)
4	67.4±2.1 (2)	52.5±1.3 (2)
5	64.4±11.5 (2)	56.7±3.5 (2)
6	100.5±12.2 (2)	*n.d.*
7	90.0±11.6 (2)	*n.d.*
8	84.4±4.9 (3)	n.d.
9	80.6±10.3 (3)	n.d.
10	72.4±10.7 (3)	*n.d.*
11	76.1±7.7 (3)	*n.d.*
12	106.7±7.8 (3)	*n.d.*
13	99.7±0.9 (2)	*n.d.*
14	86.6±11.9 (3)	*n.d.*

Table 1: [a]The binding affinities were studied as described in the Electronic supplementary information of the attached paper and are expressed as mean ± SEM of residual [3H]PDBu binding (% of control) with 100 μ M ligand concentration. The number of independent experiments is presented in brackets for each value. *n.d.*, not determined.

In the light of these experimental data, **2** emerged as the most interesting compound together with reference ligand **1** and thus **1** and **2** were selected to be investigated further. With the purpose of studying the role of the chirality in the interaction with the target, enantiomers of **1** and **2** were prepared and their biological activity evaluated. Based on our experience in the chiral chromatography field, the resolution of **1** and **2** was carried out by semi-preparative High Pressure Liquid Chromatography (HPLC) using chiral stationary phase (CSPs). In order to identify the optimal experimental conditions for the enantioresolution of **1** and **2**, a standard screening protocol was applied to both Chiralcel OJ-H (0.46 cm diameter × 15 cm length, 5 μm) and Chiralpak IC (0.46 cm diameter × 25 cm length, 5 μm columns). For both compounds the best enantioresolution were achieved on Chiralpak IC eluting with with *n*-hexane/2-propanol (90/10, v/v), at a flow rate of 1 mL min-1[*t*r1 19.9 min, *t*r2 22.5 min, α 1.16 and *R*s 2.00 for **1**, Figure 9A; *t*r1 36.7 min, *t*r2 47.1 min, α 1.31 and *R*s 4.16 for **2,** Figure 9B]. These experimental conditions were scaled-up to a semi-preparative scale (Table 2). yielding the corresponding isomers of **1** and **2** in amount and optical

purity suitable for biological investigations, as proved by the analytical control of the collected fractions. In brief, 48 mg of **1** was processed in 24 cycles accordingly, yielding 20.0 mg of the first eluted enantiomer **1A** (*e.e* 99.9%, α_{405}^{20}= +37.7, *c* 0.6 in methanol) and 19.3 mg of the second eluted enantiomer **1B** (*e.e* 99.9%, α_{405}^{20}= -37.2, *c* 0.6 in methanol), together with 7.5 mg of an intermediate fraction as a mixture of the two enantiomers. As regards **2**, 30 mg of racemate was processed in 5 cycles, providing 14.2 mg of the first eluted enantiomer **2A** (*e.e* 99.9%, α_{405}^{20}= +37.5, *c* 0.4 in methanol) and 13.1 mg of the second eluted enantiomer **2B** (*e.e* 99.9%, α_{405}^{20}= -37.4, *c* 0.4 in methanol), together with 1.1 mg of intermediate fraction.
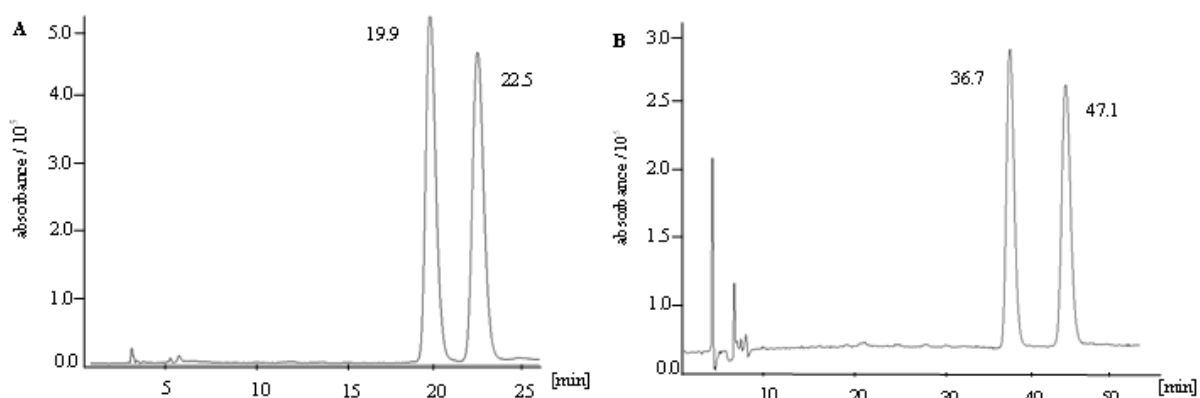

Figure 9. Analytical separation of (**A**) compound **1** (detection at 274 nm) and (**B**) compound **2** (detection at 254 nm) on Chiralpak IC column (0.46 cm diameter × 25 cm length, 5 μm), mobile phase: *n*-hex/ 2-propanol (90/10, v/v), flow rate: 1 mL min^{-1}.

Cmpd	*n*-hexane/2-propanol	Flow rate [mL min^{-1}]	t_{r1} [min]	t_{r2} [min]	Inj.vol [mL]	Conc. [mg mL^{-1}]	λ [nm]
1	90/10	3	29.5	33.5	0.2	10	274
2	90/10	2	48.1	63.5	1	6	254

Table 2 Semi-preparative resolution of 1 and 2 on Chiralpak IC column (10 mm diameter × 250 mm length, 5 μm), eluting with *n*-hexane/2-propanol (90/10, v/v).

The ability of enantiomers of **1** and **2** to displace [³H]PDBu from the C1 domain of PKC was finally evaluated according to the procedure described above. Results showed that, for both compounds **1** and **2**, the *dextro* (**1A** and **2A)** and the *levo* (**1B** and **2B**) isomers possess almost the same binding profile as the corresponding racemates (displacement at 100 μ M equal to: 34.6% for **1A**, 36.3% for **1B**, 27.3% for **2A** and 26.3% for **2B**), thus suggesting that chirality does not seem to play a significant role in the ligand-target interaction.

In conclusion, the results obtained in our study clearly pointed out that:

- the presence of the ester function is essential for the ligand-target interaction.

- in order to preserve the C1 domain affinity only a few structural modifications at the ester group are allowed. Indeed, only the normal ester derivative **2** showed affinity for the C1 domain of PKC comparable to that of reference compound **1**, while the retro-ester derivatives **3-5** bound to the target more loosely, thus suggesting that the medicinal chemistry impact of modifying the normal ester functional group is very high, regardless of the aromatic moiety of the molecules.

- as regards the role of chirality in the ligand-target interaction, we showed that the C1 domain of PKC does not seem to exhibit enantio preference for the pure stereoisomers of compounds **1** and **2**.

All in all, our observations provide further insights into the ligand-target interactions of the PKC C1 domain and represent a step-forward for the future development of more specific and effective PKC ligands. In particular, the most interesting feature of the results presented herein appears to be the observation that, at least for ligands belonging to the template IV series, only few structural modifications are tolerated by the C1 domain of PKC.

3. Configurational study of 1 and 2 isomers

As a part of the research in the PKC field, my PhD also focused on the assignment of the absolute configuration of the enantiomers of **1** and **2** which were previously isolated. For this purpose, several methods were experimented, including chiroptical spectroscopies techniques and NMR spectroscopy (manuscript in preparation). A detailed discussion of the methods used is reported in the following paragraphs.

3.1 Configurational study by Chiroptical spectroscopies

In the last decade, innovation in spectroscopy has permitted the association of various techniques to Density Functional Theory (DFT) calculations in order to easily establish the absolute configuration of organic molecules with a high degree of success. Initially, a full set of chiral spectroscopies such as Vibrational Circular Dichroism (VCD), Electronic Circular Dichroism (EDC) and Optical Rotatory Dispersion (ORD) were experimented together with computational prediction by DFT calculations. This work was performed in tight collaboration with Prof. Sergio Abbate, Prof. Giovanna Longhi and Dr. Giuseppe Mazzeo at the University of Brescia. They made available the instrumentation and more importantly, they supported the study significantly by sharing their knowledge of both the fields of spectroscopic and computational chemistry.

VCD is the extension of electronic CD within infrared and near-infrared regions of the spectrum

where vibrational transitions occur in the ground neutral electronic state of the molecule. More specifically, VCD spectra are obtained by vibrational difference spectra compared to left and right circularly polarized radiation. The principal area of application of VCD is structure elucidation of biologically significant molecules including peptides, proteins, nucleic acids, carbohydrates, natural products and molecules of pharmaceutical interest.[39]

The assignment of the absolute configuration by means of chiroptical spectroscopies and their computational prediction was obtained by comparing the calculated and experimental VCD, ECD and ORD spectra. This approach requires the initial conformational search for all possible conformers of compounds studied at the Molecular Mechanics level. All the conformers found within 10 kcal/mol in energy compared to the most stable one, are fully optimized at DFT level. Only the optimized conformers which differ from the most stable ones within 2 kcal/mol in relative free energy are taken into account for calculation properties. Chiroptical properties are then calculated for each conformer found and the total property is given as the weighted average over the Boltzmann populations.[40]

It is very clear why it is important to obtain accurate calculated geometries and energies in order to achieve a correct simulation. Furthermore, one more problem in applying this approach could arise from flexible systems which have a large number of conformations even with opposite chiroptical property values. In this case, an inaccurate prediction of conformer distribution, geometries or energies could lead to the incorrect assignment of absolute configuration.

In brief, the first [(+)-1A and (+)-2A] and the second [(-)-1B and (-)-2B] eluted enantiomers of both **1** and **2** were investigated by IR and VCD first, then by UV and ECD. The results are summarized in Figure 10. The enantiomers of both **1** and **2** showed a good response in fingerprint region of IR which did not find a correspondence in VCD spectra. The weakness of the signals did not allow us to fully appreciate the inversion of the signals corresponding to two enantiomers of **1** and **2**. Similarly, the molecules seem to have a good UV profile showing two important bands at 190 and 230 nm. but the response to ECD was only moderate (Figure 10). However, the ECD spectra of the two pairs of enantiomers are good mirror images of each other (Figure 10) although the intensity of the signals are weak. Overall, given the absence of significant signals especially in the VCD spectra, the theoretical calculation of the spectra was not possible. These negative outcomes could be due to the high flexibility of the molecules, as clearly showed by the conformational analysis (at MM level) which evidenced the presence of more than 200 conformers for the compounds studied.
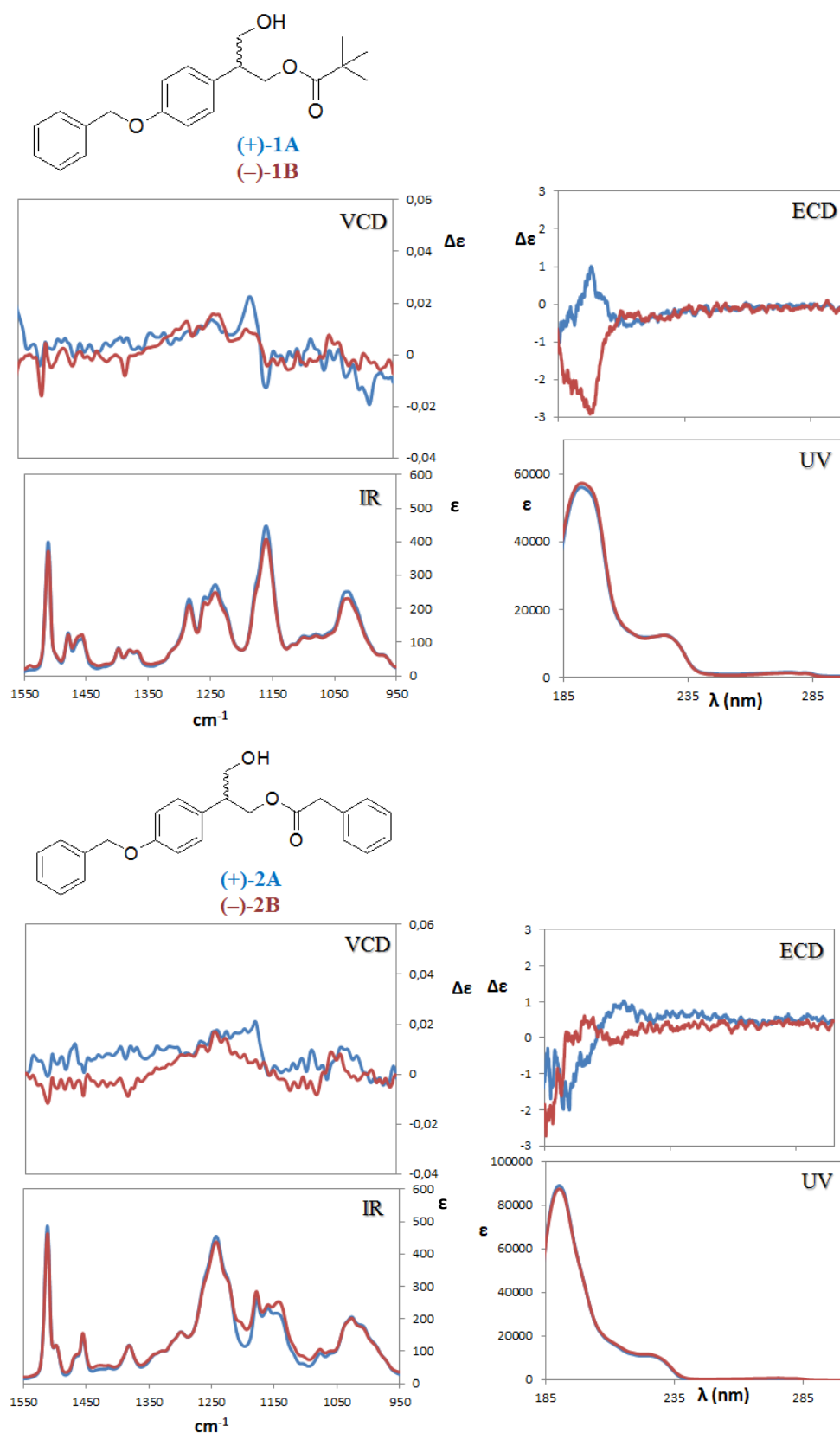
Figure 10. Superimposed VCD spectra, in the fingerprint region (first column), ECD spectra (second column) of molecules **1** (first row) and **2** (second row). Color-coded: blue, first eluted enantiomer (+)-1A and (+)-2A; red, second eluted (-)-1B and (-)-2B.

As previously discussed, the high conformational freedom of enantiomers **1** and **2** seems to be the reason why the spectroscopic techniques experimented did not succeed in the configurational study.

14

Accordingly, we decided to convert racemic **1** and **2** into the corresponding derivatives **36** and **37** (Scheme 4), which lack the O-benzyl group and thus possess lower conformational freedom compared to parent compounds **1** and **2**. A conformational analysis of **36** and **37** was first accomplished, highlighting a significant decrease in the number of conformers compared to the parent compounds. Indeed approximately 60 conformers were estimated within a range of 10 Kcal/mol for **36** and **37**, while more than 200 conformers were observed for **1** and **2**, as stated above when the same cut-off was applied. Encouraged by these theoretical data, the cleaving of benzylic group of **1** and **2** was then accomplished by MW- assisted hydrogenation under transfer phase conditions, as reported in Scheme 4. Briefly the reaction was conducted in presence of Pd/C 10% as catalyst and ammonium formiate as hydrogen source.
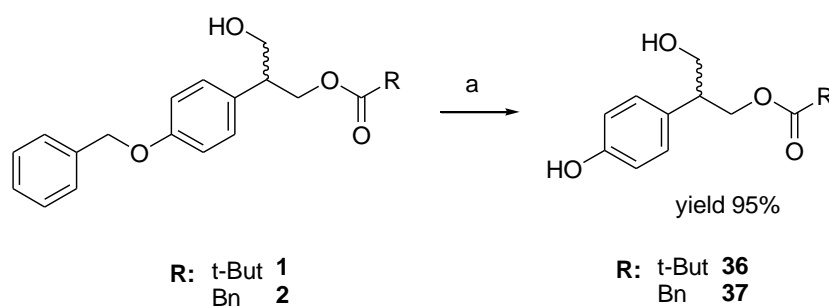
Scheme 4. Reagents and condition a: Pd/C 10%, ammonium formiate, MW 140°C, 20 min

The resolution of racemic**36** and **37** was finally achieved by chiral chromatography in (semi)-preparative scale. In order to identify the best experimental conditions for scale-up a standard screening protocol was applied to Chiralpak AD-H column (0.45 x 15 cm, 5 uM) eluting with different mobile phases, including alcohols methanol, ethanol and iso-propanol (MeOH, EtOH and IPA) either as pure solvents or in mixtures as well as mixtures of *n*-hexane (*n*-Hex)and alcohols as polar modifiers. Results of the screening protocol are reported in Table 3, expressed in terms of retention factor (k_A or k_B), separation factor (α), and resolution factor (R_S). As shown in Table 3, no resolution for **36** and **37** was observed following elution with pure alcohols. On the contrary, good enantioseparation was achieved for both compounds eluting with mixtures of alkane and polar modifier. More specifically, the best results in terms of enantioresolution were obtained eluting with *n*-Hex/EtOH (95/5, v/v) for **36** (α= 1.25, Rs= 4.25) and with *n*-Hex/IPA (95/5, v/v) for **37** (α= 1.17, Rs= 2.29), but analysis was quite time-consuming (*tr1*= 33.37 min, *tr2*= 41.43 min for **36**; *tr1*= 83.14 min, *tr2*= 96.85 min for **37**) and thus not suitable for (semi)preparative purposes. . Interestingly, , a significant decrease in the retention times without significant modifications to the enantiorelution was observed for both compounds by increasing the percentage of the polar modifier in the mobile phase compositions from 5 to 10%,(*tr1*= 10.16 min, *tr2*= 12.07 min, α= 1.24,

Rs= 3.25 for **36** eluting with *n*-Hes/EtOH 90/10, v/v; *tr1*= 17.44 min, *tr2*= 19.72 min, α= 1.15, *Rs*= 1.69 for **37** eluting with *n*-Hes/IPA 90/10, v/v, Figure 11). Considering that the shortest retention times possible is an important pre-requisite for the economic and productive (semi)-preparative enantiomeric separation, these experimental conditions were selected for the next (semi)-preparative scale-up.

	Chiralpak AD-H							
Eluent [a]	**36**				**37**			
	k_A	k_B	α	Rs	k_A	k_B	α	Rs
A	0.84		n.a	n.a	0.95		n.a	n.a
B	0.83		n.a	n.a	0.16		n.a	n.a
C [b]	1.04		n.a	n.a	4.6		n.a	n.a
D	0.92		n.a	n.a	n.t			
E	4.2	4.4	n.a	n.a	**8.08**	**9.27**	**1.15**	**1.7**
F	n.t				42.07	49.18	1.17	2.3
G	16.63	20.88	1.25	4.27	n.t			
H	**3.86**	**4.77**	**1.24**	**3.25**	9.61		n.a	n.a
I	n.t				2.35		n.a	n.a

Table 3: screening conditions

[a] Mobile phases: A: MeOH (100, v/v); B: EtOH (100, v/v); C: IPA (100, v/v); D: *n*-Hes/IPA (80/20, v/v); E: *n*-Hes/IPA (90/10, v/v); F *n*-Hes/IPA (95/5, v/v); G: *n*-Hes/EtOH (95/5, v/v); H: *n*-Hes/EtOH (90/10, v/v) ; I: *n*-Hes/EtOH (80/20, v/v);

[b] flow rate: 0.5 mL/min
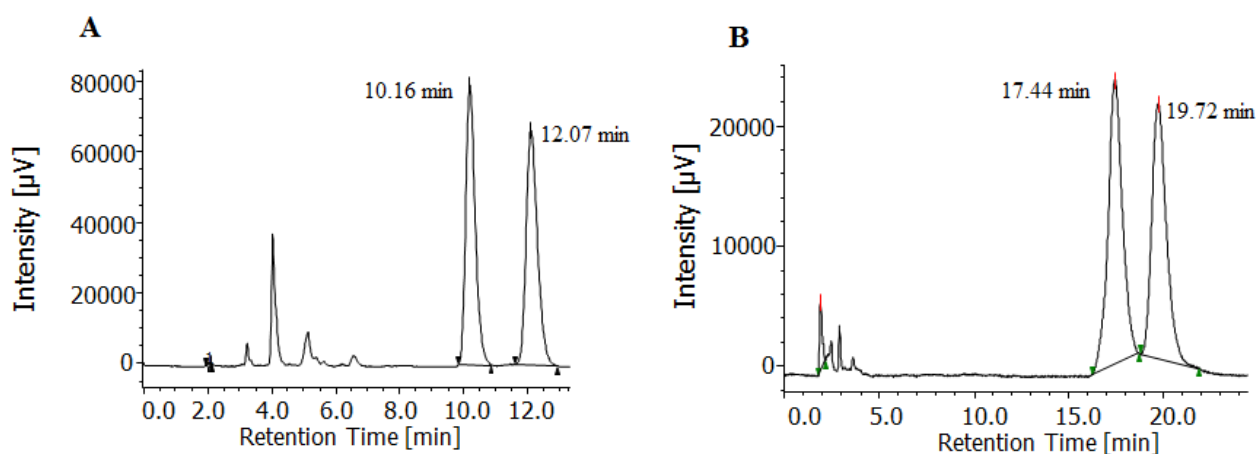
n.t: not tested; n.a: not applicable

Figure 11: Analytical separation on Chiralpack AD-H (150 mm x 4.6 mm, 5 μm) of (**A**) compound **36,** mobile phase: *n*-Hex/EtOH 90/10 (v/v) and (**B**) compound **37** mobile phase: *n*-Hex/ IPA 90/10 (v/v); flow rate: 1 mL min^{-1}, injection volume 10 μL, detection at 254 nm.

The separation of **36** and **37**-enantiomers in (semi)preparative scale was then achieved using a RegisPack column (250 mm × 10 mm, 5 μm) according to the conditions reported in Table 4, providing the desired enantiomers in terms of amount and optical purity suitable for the configurational study.

In brief, 12 mg of **36** were processed in 3 cycles, yielding 5.4 mg of the first eluted enantiomer **36A** (*e.e* 95%) and 5.6 mg of the second eluted enantiomer **36B** (*e.e* 90%). With regard to **37,** 11 mg were processed in 2 cycles, giving 5.1 mg of the first eluted enantiomer **37A** (*e.e* 99.9%) and 4.9 mg of the second eluted enantiomer, **37B** (*e.e* 99.9%)

Cmpd	Mobile phase	Flow rate [mL min^{-1}]	t_{r1} [min]	t_{r2} [min]	Inj.vol [mL]	Conc. [mg mL^{-1}]	λ [nm]
36	*n*-Hex/EtOH (90/10, v/v)	4	15.6	18.5	1	4	254
37	*n*-Hex/2-propanol (90/10, v/v)	4	38.1	42.8	1	5.5	254

Table 4 Semi-preparative resolution of **36** and **37** on RegisPack column (10 mm diameter × 250 mm length, 5 μm)

At this point, we attempted to measure the VCD-IR spectra of enantiomers **36** and **37** in CDCl$_3$. As shown in Figure 12, non significant variations were observed in measured VCD spectra compared to those of **1** and **2**. The experimental ECD spectra of both enantiomers **36** and **37** were still specular and weak. These results suggested that the chiroptical spectroscopies employed were not sensitive to the flexibility of benzylic moiety but they would probably be much more sensitive to the conformational freedom of the alkylic chain of the molecules.
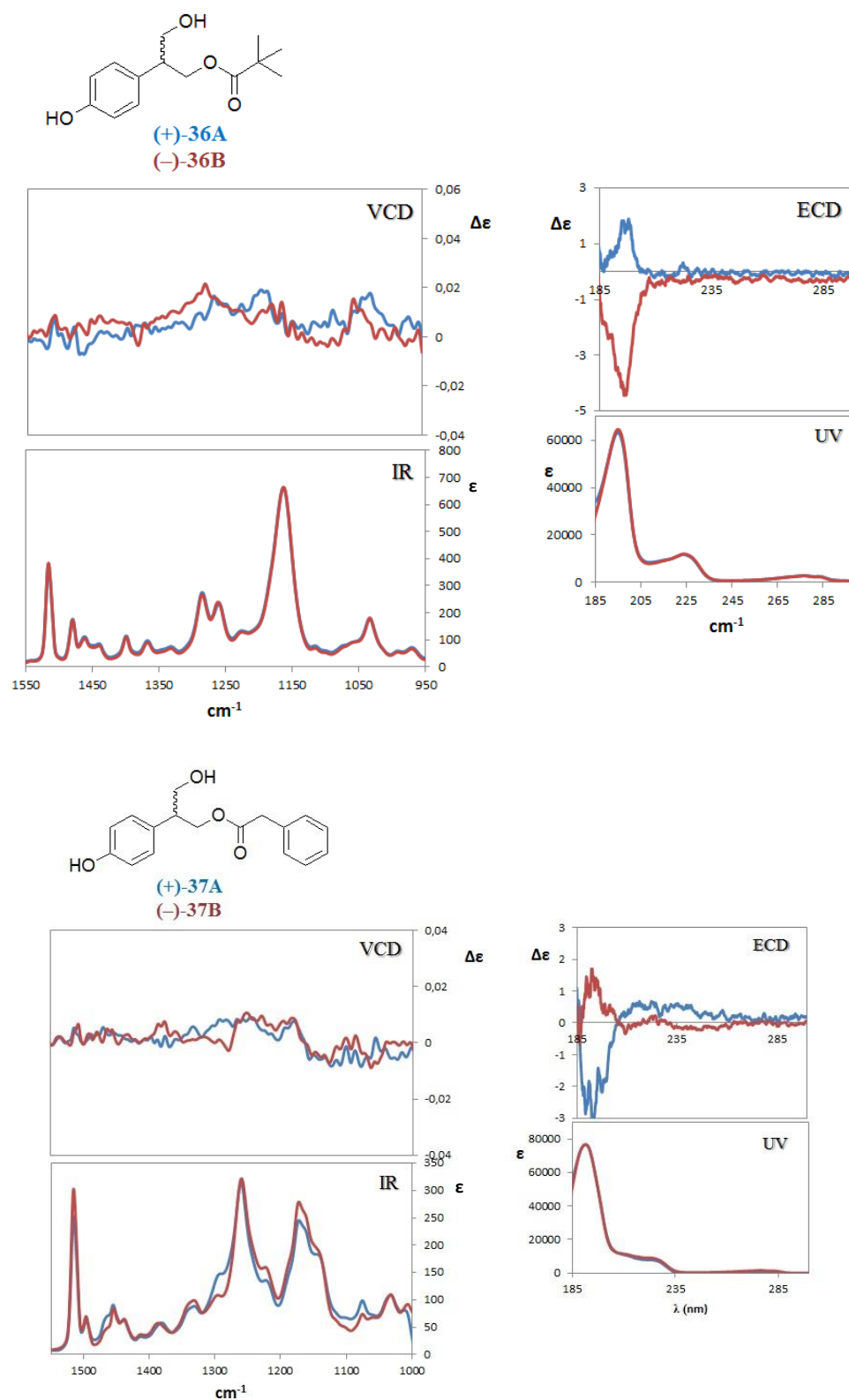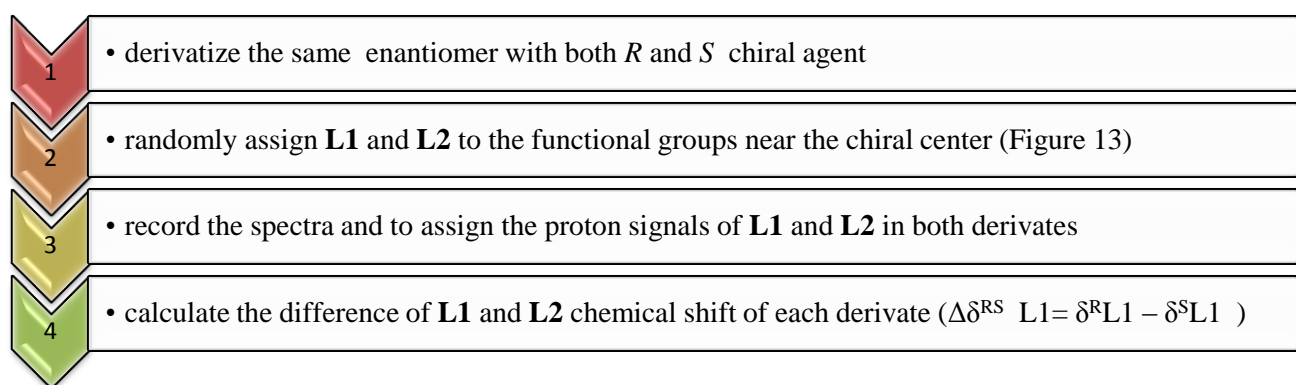
Figure 12. Superimposed VCD spectra, in the fingerprint region (first column), ECD spectra (second column) of molecules **36** (first row) and **37** (second row). Color-coded: blue, first eluted enantiomer (+)-36A and (+)-37A; red, second eluted (-)-36B and (-)-37B.

3.2 Configurational study by NMR

The determination of the absolute configuration of organic compounds by NMR constitutes an area of research of increasing interest due to the general availability of the instruments, the small amount of sample needed, and the simplicity of the method.[43]

The presence of primary alcohol in ß-position at chiral center in **1** and **2** made the molecules suitable candidates for being derivatised with a chiral agent. The double derivatisation of enantiomer with both *S* and *R* chiral agents is strongly recommended for improving the confidence level of assignment. The methodology has been widely described and summarised in Scheme 5:

1	• derivatize the same enantiomer with both *R* and *S* chiral agent
2	• randomly assign **L1** and **L2** to the functional groups near the chiral center (Figure 13)
3	• record the spectra and to assign the proton signals of **L1** and **L2** in both derivates
4	• calculate the difference of **L1** and **L2** chemical shift of each derivate ($\Delta\delta^{RS}$ L1= δ^{R}L1 – δ^{S}L1)

Scheme5: workflow
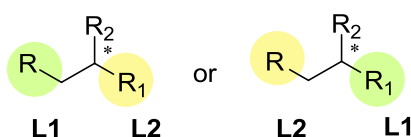
Figure 13

The approach for the assignment of the absolute configuration of primary alcohols is based on the use of 9-anthrylmethoxyacetic acid (9-AMA) (Figure 14), since it possesses two very important characteristics: (a) a higher conformational preference (the syn-periplanar form, sp), than other AMAA reagents (Figure 3), and (b) the anthryl ring in the main conformer (sp) is particularly well-oriented in terms of projecting its strong aromatic magnetic cone on substituent near the chiral center.[44]

Figure 14. most known AMAA chiral agent

However, the commercially available reagents Methoxy-phenylacetic acid (MPA) and Methoxy-α-trifluoromethyl-α-phenylacetic acid (MPTA) are currently widely used for determination of absolute stereochemistry. MTPA is one of the most popular chirality recognition reagents,[45] probably because the quaternary character of its chiral center suppresses the risk of racemization [46] and because it allows stereochemistry to be studied by ^{19}F NMR as well as ^{1}H NMR spectroscopy.[47]
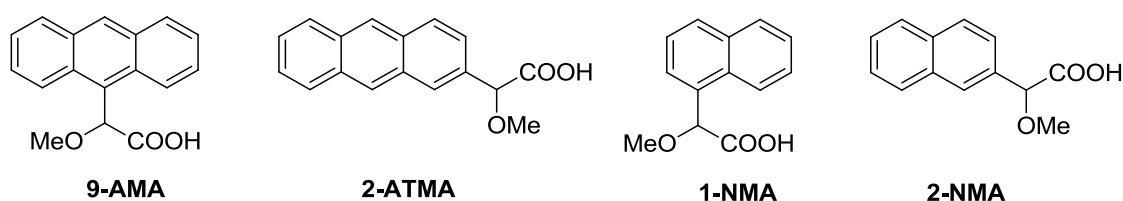
In 1973 and for the first time, Mosher used ^{19}F NMR to detect the chemical shifts of the CF_3 groups for the assignment of the absolute configuration of a series of secondary alcohols and amines. In later studies, he used by ^{1}H and ^{13}C NMR to study the chemical shifts of the protons and C atoms of the chiral alcohol under examination.[48] The absolute configuration of the substrates was deduced by interpreting the signs of $\Delta\delta^{RS}$ values using an empirical model where the spatial position of **L1** and **L2** was in correlation with the anisotropic effect of phenyl group MTPA(Figure 15).
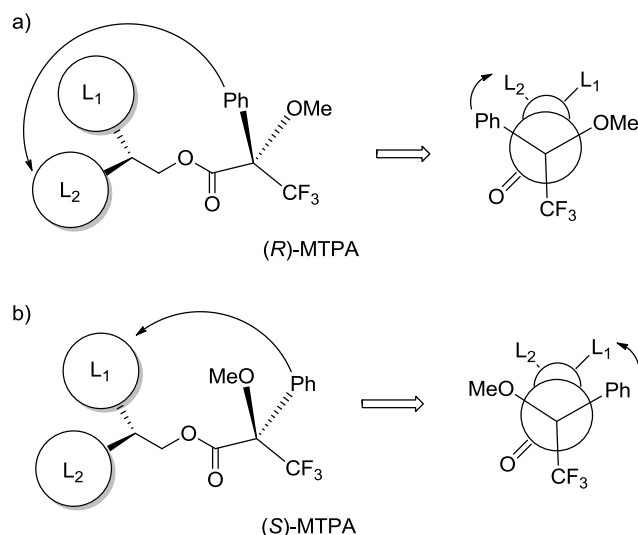
Figure 15. Models proposed by Mosher (a, b) for the assignment of configuration by ^{1}H NMR

On the basis of various experimental data, Mosher assumed empirically that the most representative conformation of diasteromeric esters of MTPA was that in which the carbonyl group and CF_3 group were situated in the same plane. This assumption was confirmed by X-ray studies conducted on the (*R*)-MTPA esters of secondary alcohols in particular the 4-trans-tert-butylcyclohexano and 1-(*R*)-hydroxy-2-(*R*)-bromo- 1,2,3,4-tetrahydronaphthalene.[48-49]

Successively, Riguera affirmed that the empirical model described by Mosher was not representative of the real position of the MTPA phenyl group. Indeed, computational studies indicated that the conformational composition of MTPA was complex, showing three preferred rotamers at low-energy: one *ap* form and two *sp* forms.(Figure 16) Each conformer of the MPTA ester contributes different shielding/dishielding effects resulting in low $\Delta\delta^{RS}$ values.[50]

a)

b)

Figure 16. Low-energy conformations of *(R)*-MTPA (a) and *(S)*-MTPA (b)

To predict the absolute configuration, a reliable model can be drawn on the basis of the experimental values ($\Delta\delta^{RS}$).[51] The idealized conformation depicted in Figure 17. Due to the diamagnetic effect of the benzene ring of the chiral agent, the $H_{A,B,C(n)}$ NMR signals of the (*R*) - MTPA ester should appear upfield compared to those of the (*S*)-MTPA ester. The reverse should hold true for $H_{,X,Y,\,(n)}$. (Figure 17a)

Therefore, when $\Delta\delta = \delta^R - \delta^S$, protons on the left side of the MTPA plane (Figure 17b) have negative values ($\Delta\delta < 0$) the protons on the right side of the plane have positive values ($\Delta\delta > 0$).

a)

b)

Figure 17. model for ACA

So far, not many examples have been reported in the literature regarding the derivatization of primary alcohol with Mosher's reagent. This approach could be difficult as it may be limited by two factors: i) the distance between groups L1/L2 of the substrate and the aryl ring of the auxiliary reagent is greater than that in secondary alcohols, because the asymmetric center is at the ß position,

and ii) The presence of an extra C-C bond between the chiral center and the auxiliary reagent reduces the conformational preference by increasing rotational freedom.

Taking these observations into consideration, the configurational study of **1** and **2** was dealt with MTPA as a chiral auxiliary with the additional purpose of investigating the effect of this chiral agent on ß-primary alcohol.

For these aims, we arbitrarily selected the second eluted enantiomer of both **1** and **2,** labelling **L1** to aromatic moiety and **L2** to carboxylic moiety. A small amount of the enantiomer was derivatised in parallel with the acyl chloride of (*R*) and (*S*)- MPTA.[48] The reaction was conducted in DCM using 4-dimethylaminopyridine (DMAP) supported on resin as catalyst in order to simplify the work-up procedure.(Scheme 6)
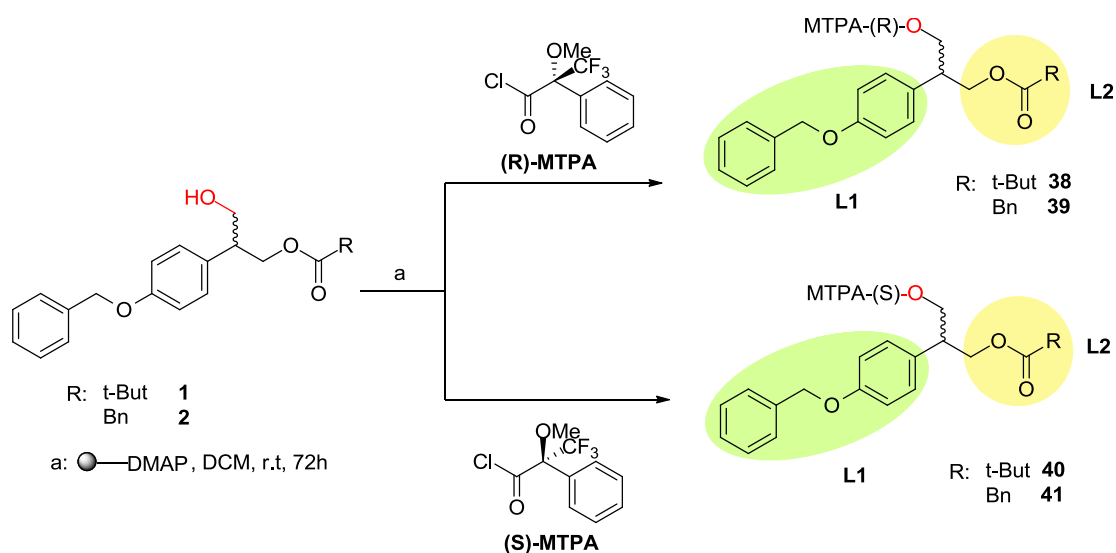
Scheme 6: work scheme

The ^{1}H-NMR spectrum of each diasteromeric ester was then recorded in chloroform deuterated and the $\Delta\delta^{RS}$ **L$_1$** and **L$_2$** were calculated. Moreover, the disappearance of the signal at ppm corresponding to the diasterotopic protons close the primary alcohol and the appearance of new signals at lower fields is confirmation of the resulting esterification reaction. Predictably, the difference in terms of the chemical shift of **L1** and **L2** between **38-40** and **39-41** are small but significant. The shifts are appreciable especially in the aromatic field (L1). The signals of aromatic protons close to the chiral center of **38** shifted to high field [δ (ppm): 7.03-7.01; 6.82-6.80] compared to the signals of **40** that shifted to a slightly lower field [δ (ppm): 7.04-7.02; 6.83-6.81], with a calculated $\Delta\,\delta^{RS}$ **L$_1$** equal to -0.01. (Figure 18) As regards the *R* and *S* MTPA derivatives of **2,** a similar trend is shown: the signals of aromatic protons in immediate proximity to the chiral center of **39** [δ (ppm): 6.92-6.91; 6.77-6.76] shifted to a slightly lower field respect compared to the

signal of **41**[δ (ppm): 6.93-6.92; 6.79-6.77] with a calculated $\Delta\ \delta^{RS}$ **L₁** equal to -0.01ppm.(Figure 18). Additionally, the signals of the proton linked to the carbon of benzylic groups (-OC*H₂*Ar) of **38** and **39** [δ (ppm): 4.97] moved to higher field than **40** and **41** [δ (ppm): 4.98], with a $\Delta\ \delta^{RS}$ **L₁** equal to -0.01 ppm. (Figure 18)
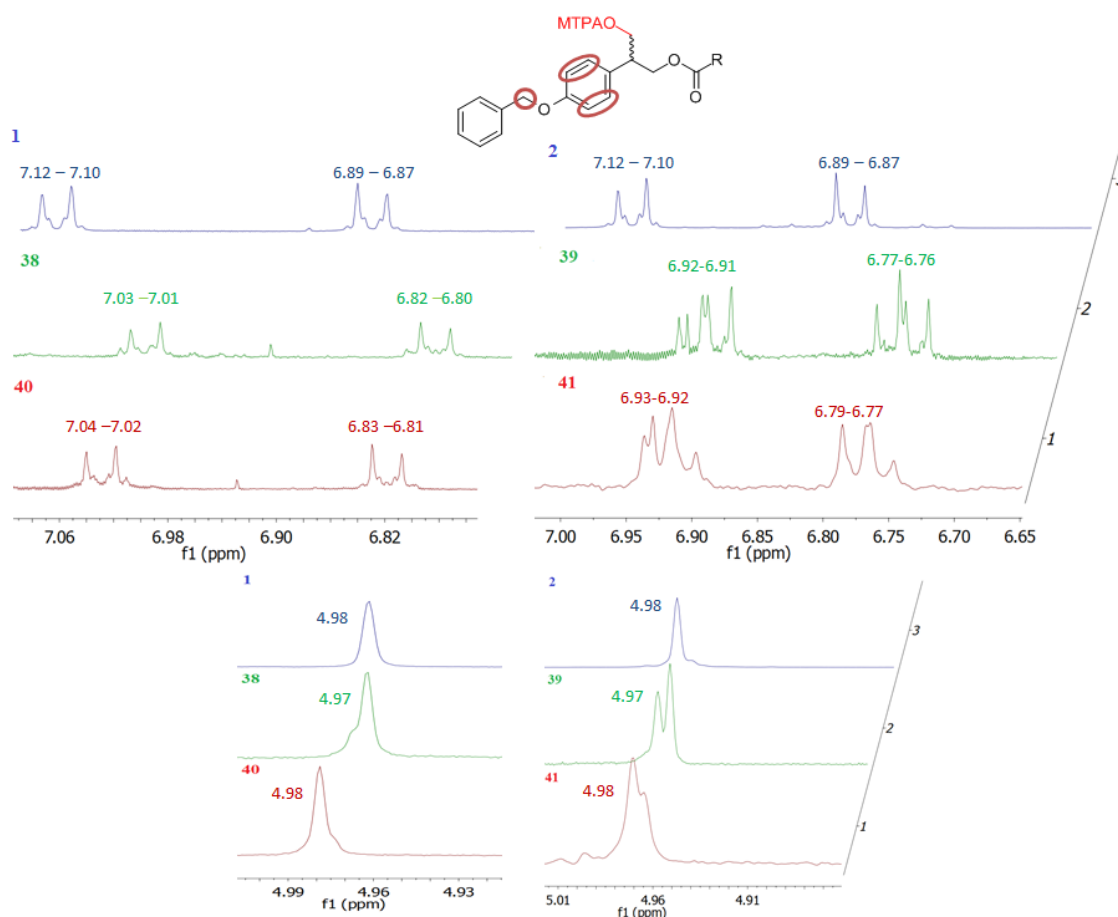

Figure 18. Partial ¹H NMR spectra of **L1** moiety of diastereomeric esters of **1** and **2** in CDCl3 at 400 MHz

Regardless of the moiety of **L2**, the shifting signals of the carboxylic chain protons (**L2**) are visually appreciable in both diasteromeric esters **1** and **2**, although the calculation of their difference in terms of chemical shift were difficult to detect as the variations were too small.

The difference was only detectable as regards the diasterotopic protons of the carbon close to the chiral center. The signals of **38** slightly shifted to a lower field [δ (ppm): 4.24-4.20; 4.15-4.09] compared to respect those of **40** [δ (ppm): 4.23-4.19; 4.10-4.06] with a $\Delta\ \delta^{RS}$ **L₂** equal to +0.01 and +0.04 ppm. (Figure 19)

The variations in chemical shift corresponding to the same protons were not appreciable in **39** and **41**. Instead they showed a slightly variation of the signals of the proton close the MTPA esters with a calculated difference of + 0.01 ppm.
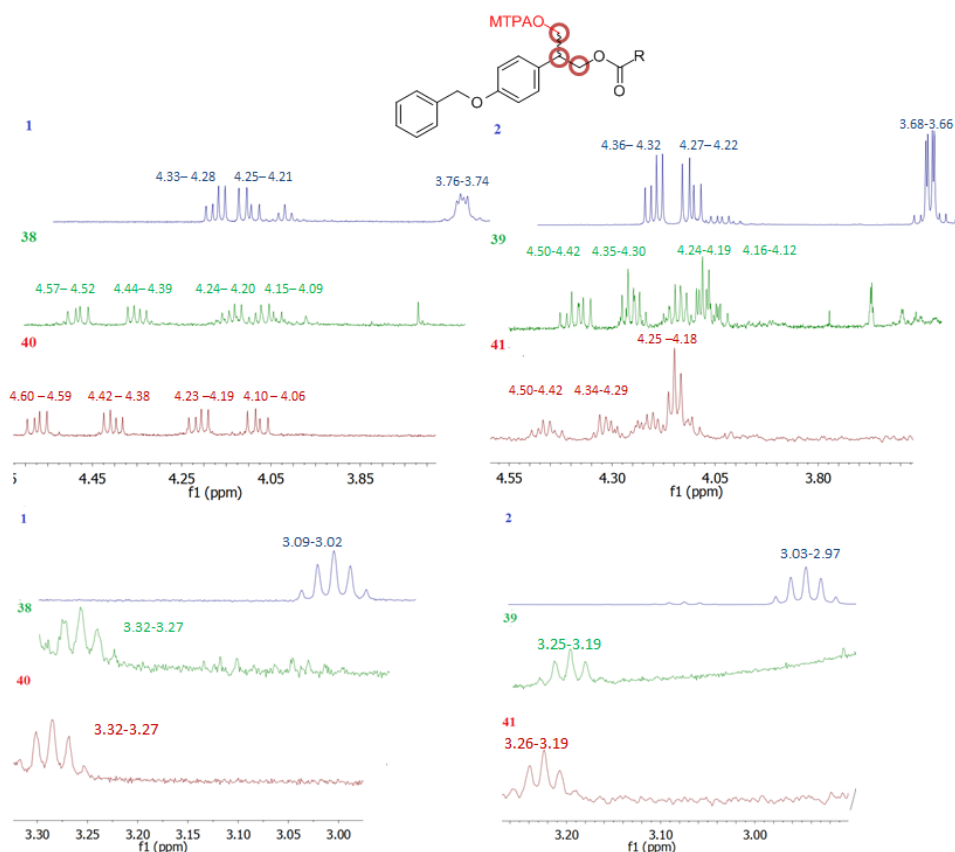
Figure 19 Partial ^{1}H NMR spectra of **L2** moiety of diastereomeric esters of **1** and **2** second eluted in CDCI3 at 400 MHz

In order to predict the absolute configuration, we employed the model drawn in Figure 5, with the expectative to correlate the model for secondary alcohol to primary one with the assumption that two models can be comparable.

Substituents **L1** and **L2** were placed in the correct position of the model described, taking the experimental values into consideration. On the basis of the models constructed, we were confident that we could assign *(R)* as the absolute configuration of second eluted of both **1** and **2.** (Figure 20)
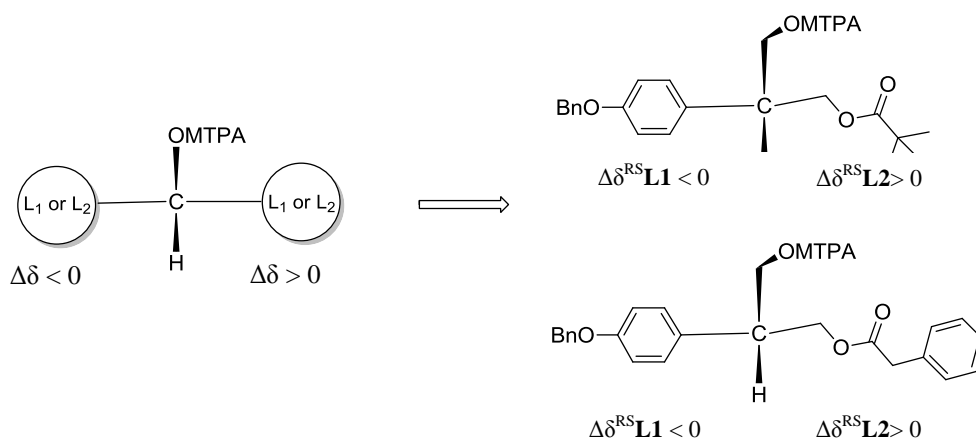

Figure 20. ACA of **1** and **2** second eluted

To exclude artefact values due to either the solvent or the instrumentation and to back up this result, a further derivation was conducted with both *R* and *S*-MTPA on the first eluted of compound **1,** applying the same procedure as shown in the previous Scheme 6. Once again the difference in terms of chemical shifts between esters **42** and **43** were small and difficult to detect especially for **L2** moiety. In general, the calculated differences in value of **L1** and **L2** in **42** and **43** were opposite compared to **38** and **40** ($\Delta \delta^{RS}$ **L₁**= + 0.01 ppm both for the aromatic proton and OCH_2Ar; $\Delta \delta^{RS}$ **L₂**= -0.01 ppm as regards the proton close to the chiral center) (Figure 21).
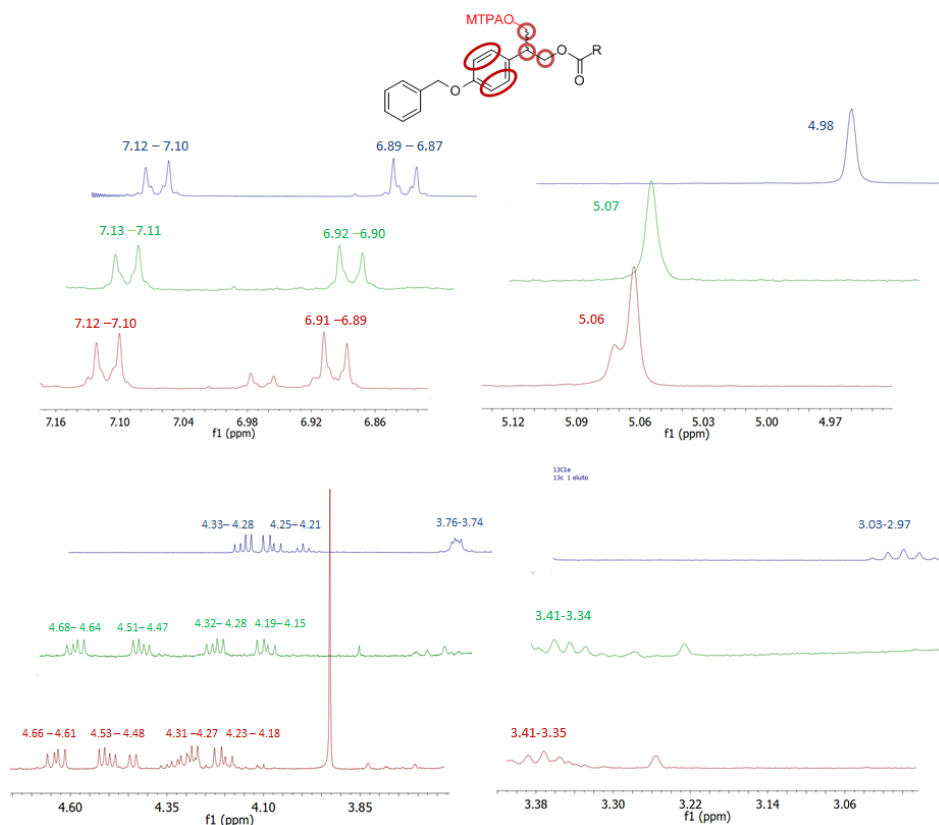
Figure 21 Partial ^{1}H NMR spectra of **L1** and **L2** moiety of diastereomeric esters of **1** first eluted in CDCI3 at 400 MHz

Building a new Mosher model on the basis of the calculated values, we were confident to assign (S) absolute configuration on the first eluted of **1**.(Figure 22) In order to back up our experimental results further , the same elution of enantiomers of **1** and **2** order was obtained on Chiralpak IC column.
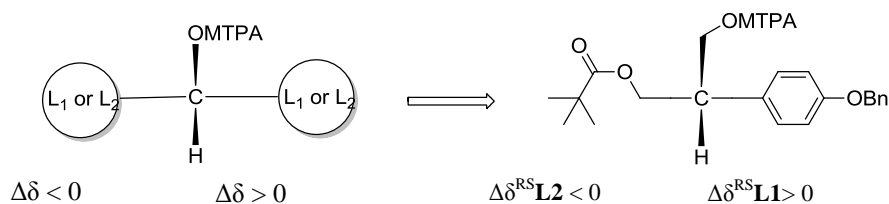
Figure 22. ACA of **1** first eluted

In summary, our work clearly shows that:

- chiral chromatography is a viable route for straightforward and rapid access to both enantiomers with high optical purity and yields in accordance with our previous experience.
- chiral spectroscopic techniques (VCD, ECD, ORD) do not seem suitable for the configurational study of molecules characterized by an high degree of flexibility.
- the combination of chiral chromatography with NMR represents a simple, powerful method to approach the configurational study of flexible organic molecules.
- MTPA is a suitable chiral agent for assigning the absolute configuration of primary alcohol in the beta position at the chiral center.

4. Biological investigation of 1 and 2

In the last part of my PhD attempts were made to draw the activator/inhibitor profile of **1** and **2** on PKCs. For this purpose, preliminary experiments aimed at evaluating the traslocation of PKCα from the cytosol to other cellular compartments, such as membranes and cytoskeleton, of human SH-SY5Y cells were planned and carried out in close collaboration with the research group of Prof. Marialaura Amadio and Alesisa Pascale of the Pharmacological section of the Department of Drug Sciences.

Firstly, a series of experiments were carried out on both racemic **1** and **2** to evaluate their ability to induce PKCα protein translocation from the cytosol (soluble fraction) to other cellular compartments (membranes, cytoskeleton) of human SH-SY5Y cells, varying the concentration of the tested compounds and exposure time. In brief, the cells were exposed to increasing concentrations (1μM-300μM) of the compounds for different times (15-120 min.) and Western blotting analysis for PKCα was performed in all the fractions. The best results were observed applying the following experimental conditions: concentration 25 μM combined with an exposure time of 15 min. for **1**, and concentration 1 μM combined with an exposure time of 60 min. for **2**. These conditions were also used for investigating the effect on PKCα translocation of **1** and **2** in their enantiopure forms with the final aim of studying whether or not chirality may play a key role

in the biological activity. Results obtained clearly proved that following treatment with each molecule, a decrease in the PKCα protein level in the soluble fraction can be observed, although a statistically significant difference respect the control is reached only with **2** in their racemic form (Figure 23, panel A). No significant changes in PKCα levels were observed in the membrane fractions (not shown). Instead, a trend towards an increase in PKCα protein content in the cytoskeleton was found, which was statistically significant for racemic **2** (**rac-2**) and its first eluted enantiomer (**2A**) (Figure 23, panel B).
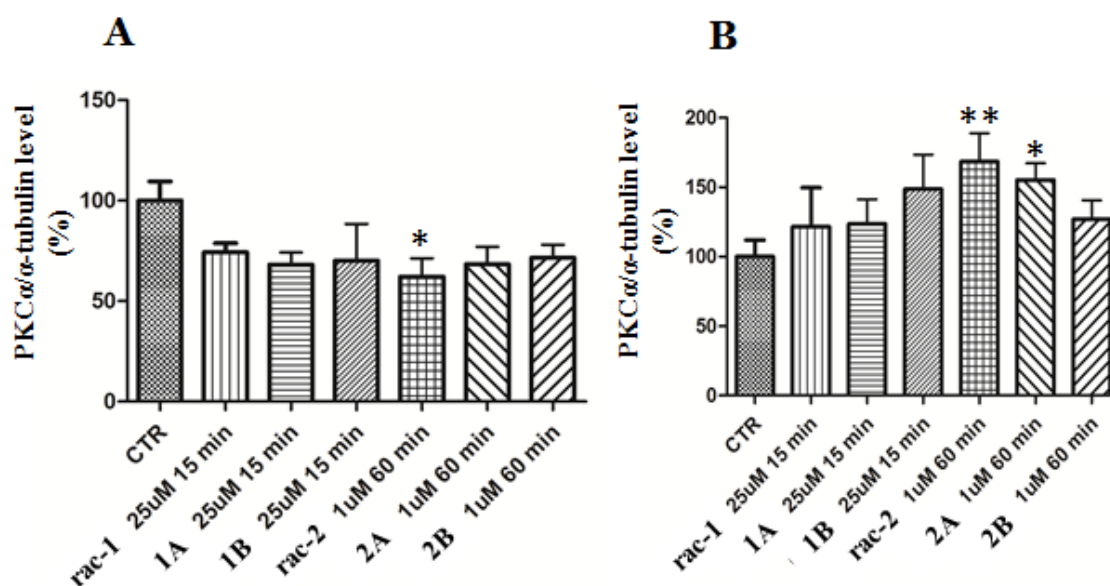

Figure 23. Figure 23. Densitometric analysis of PKCα/α-tubulin in the soluble (**A**) and cytoskeletal (**B**) fractions of human SH-SY5Y cells after exposure to vehicle (control; CTR), **1** [25 μM racemic mixture (rac) or one of its enantiomers (**1A**, **1B**) for 15 min.], or to **2** [1 μM rac or **2A**, **2B** for 60 min.]. Results are expressed as mean percentages ± S.E.M. with respect to control (100%). *$p<0.05$, **$p<0.005$, Dunnett's multiple comparisons test, n=3-6.

In summary, based on the results obtained so far, it is reasonable to state that compounds **1** and **2** act as activators of PKCα inducing a translocation of the protein from cytosol to cytoskeleton. As regards the role of chirality in this biological activity, it emerged from our results that for both the compounds studied the enantiopure forms seem to have a very similar biological behavior to that of the corresponding racemate. Further experiments are already planned to further addressed this issue.

5. Conclusion and perspectives

In an attempt to study the impact of modifying template IV on the affinity for the C1 domain of PKC, we designed and prepared thirteen new analouges of compound **1** characterized by different functionalities at the carbonyl group as well as different aromatic substitutions. In contrast with our

molecular modeling predictions, the results of PKC binding assays suggested that replacing the ester group with the amide group determines the total loss of affinity. We can thus postulate that the presence of the ester function is essential for ligand-target interaction. Furthermore, it can be seen from our study that in order to preserve the C1 domain affinity only few structural modifications at the ester group are allowed. Indeed, only the normal ester derivative **2** showed affinity to the PKC C1 domain comparable to that of the reference compound **1**, while the retro-ester derivatives **3-5** bound to the target more loosely, thus suggesting that the impact on medicinal chemistry of modifying the normal ester functional group is very high independently of the aromatic moiety of the molecules. Finally, as regards the role chirality in the ligand-target interaction, we showed that the PKC C1 domain of does not exhibit enantiopreference for the pure stereoisomers of compounds **1** and **2**.

6. Sperimental section

6.1 General

Reagents and solvents for synthesis were obtained from Aldrich (Italy). Unless otherwise specified, the commercially available reagents were used as received from the supplier. Solvents were purified according to the guidelines in Purification of Laboratory Chemicals.6 Microwave dielectric heating was performed in a Discover® LabMate instrument (CEM Corporation) specifically designed for organic synthesis and following an appropriate microwave program. Melting points were measured on SMP3 Stuart Scientific apparatus and are uncorrected. Analytical thin-layer-chromatography (TLC) was carried out on silica gel pre-coated glass-backed plates (Fluka Kieselgel 60 F254, Merck) and visualized by ultra-violet (UV) radiation, acidic ammonium molybdate (IV), or potassium permanganate. Flash chromatography (FC) was performed with Silica Gel 60 (particle size 230–400 mesh, purchased from Nova Chimica). IR spectra were recorded on a Jasco FT/IR-4100 spectrophotometer with ATR module; only noteworthy absorptions are given. Proton nuclea magnetic resonance (NMR) spectra were recorded on a Bruker Avance 400 spectrometer operating at 400.13 MHz or JEOL JNM-LA 300 at 300 MHz. Proton chemical shifts (δ) are reported in ppm with the solvent reference relative to tetramethylsilane (TMS) employed as the internal standard (CDCl3, δ = 7.26 ppm; CD2Cl2, δ = 5.32 ppm; [D6]acetone, δ = 2.05 ppm). The following abbreviations are used to describe spin multiplicity: s = singlet, d = doublet, t = triplet, q = quartet, m = multiplet, br = broad signal, dd = doublet-doublet, td = triplet-doublet. The coupling constant values are reported in Hz. 13C NMR spectra were recorded on a 400 MHz spectrometer operating at 100.56 MHz, with complete proton decoupling. Carbon chemical shifts (δ) are reported in ppm relative to TMS with the respective solvent resonance as the internal standard (CDCl3, δ = 77.23 ppm; CD2Cl2, δ = 54.00 ppm; [D6]acetone, δ = 29.84 ppm). HPLC-UV-ESI/MS analyses were

28

carried out on a Thermo Scientific LCQ FLEET system (LCQ FLEET ion trap mass spectrometer, Surveyor MS Pump/Autosampler/PDA Detector) using an ESI source operating in positive ion mode, controlled by Xcalibur software 1.4 (Thermo Finnigan). Analyses were run on a Synergi Fusion-RP 80A (0.2 cm diameter $\times$ 5 cm length, 4 μ m) column, at room temperature, with gradient elution (solvent A: acetonitrile containing 0.1% of formic acid; solvent B: water containing 0.1% of formic acid; gradient: 10% A in B to 100% A in 4 min, followed by isocratic elution 100% A for 3 min) at a flow rate of 0.3 mL min-1. All of the final compounds had 95% or greater purity. Chiral HPLC runs were conducted on a Jasco HPLC system equipped with a Jasco AS-2055 plus autosampler, a PU-2089 plus quaternary gradient pump, and an MD-2010 plus multi-wavelength detector. Experimental data were acquired and processed by Jasco Borwin PDA and Borwin Chromatograph Software. Solvents used were HPLC grade and supplied by Carlo Erba. Optical rotation values were measured on a Jasco photoelectric polarimeter DIP 1000 using a 0.5 dm cell and a mercury lamp (λ =405 nm); sample concentration values (c) are given in 10-2g mL-.

6.3 Synthesis of compounds 36 and 37

To a solution of **1** or **2** (0.02 g, 1 equiv.) in absolute ethanol (3 mL), ammonium formate (5 equiv.) and 10% Pd/C (0.07 equiv.) were added. The reaction mixture was irradiated with a microwave power of 100 W, at 100 °C for 180 s, then filtered on paper with DCM and concentrated in *vacuo*. The residue was dissolved in ethyl acetate and washed with water. The organic phase was then dried over sodium sulfate and evaporated to dryness.

3-hydroxy-2-(4-hydroxyphenyl)propyl pivalate (36): uncolorless oil, 0.014 g (95%), ^{1}H-NMR (CDCl$_3$, 400 MHz): δ 1.10 (s, 9H), 3.09 – 3.00 (m, 1H), 3.75 (dd, J = 6.3, 3.6 Hz, 2H), 4.23 (dd, J = 11.1, 7.2 Hz, 1H), 4.29 (dd, J = 11.1, 6.0 Hz, 1H), 6.72 (d, J = 8.6 Hz, 2H), 7.05 (d, J = 8.5 Hz, 2H). ^{13}C-NMR (CDCl$_3$, 100 MHz): δ, 27.56, 39.26, 47.03, 64.24 (t), 65.39 (t), 115.46, 129, 129.61, 137.34 (s), 158.39 (s), 134.1(s), 179.23 (s).

3-hydroxy-2-(4-hydroxyphenyl)propyl 2-phenylacetate (37): uncolorless oil, 0.016 g (95%), ^{1}H-NMR (CDCl$_3$, 400 MHz): δ 3.14 (d, J = 25.6 Hz, 1H), 3.70 (s, 2H), 3.81 (d, J = 2.3 Hz, 1H), 3.82 (d, J = 2.4 Hz, 1H), 4.39 (dd, J = 11.2, 7.1 Hz, 1H), 4.48 (dd, J = 11.1, 5.9 Hz, 1H), 5.18 (s, 1H), 6.82 (d, J = 8.6 Hz, 2H), 7.09 (d, J = 8.6 Hz, 2H), 7.32 – 7.28 (m, 2H), 7.40 (s, 3H). ^{13}C-NMR (CDCl$_3$, 400 MHz): ^{13}C-NMR (CDCl$_3$, 10 MHz): δ, 46.8 (t), 41.7, 64.0 (t), 65.9 (t), 115.9, 122.9, 127.5, 128.9, 129.6, 131.2(s), 134.1(s), 155.1(s), 172 (s).

6.4 Synthesis of compounds 39 -43

The second eluted of **1** and **2** were equally divided into two portions to undergo derivatization.

To a second eluted solution of **36** or **37** (0.002 mg, 1eq) dissolved in DCM (0.100 mL), DMAP supported on resins (0.004 mg) and *R* or *S*-MTPA-Cl (0.005 mL, 5eq) were added. The reaction mixture was stirred at room temperature for 72 hours, then was filtered on sintered glass filter eluting with DCM and concentrated *in vacuo*. The crude was purified on small silica pad eluting with DCM and then the organic solvent was evaporated *in vacuo*.

(R)-(R)-2-(4-(benzyloxy)phenyl)-3-(pivaloyloxy)propyl-3,3,3-trifluoro-2-methoxy-2-phenylpropanoate (38): light yellow oil, 0.003 mg (90%); $[\alpha]_{405}^{20}$: −7.85 (c 0.003 in chloroform) ¹H-NMR (CDCl₃, 400 MHz): ¹H NMR (400 MHz, CDCl₃) δ 7.49 (s, 2H), 7.40 − 7.36 (m, 4H), 7.27 (ddd, *J* = 10.3, 8.2, 4.7 Hz, 5H), 7.03 − 7.01 (d, *J* = 8.6 Hz 2H), 6.82-6.80 (d *J* = 8.6 Hz, 1H), 4.97 (s, 2H), 4.57-4.52 (dd, *J* = 11.0, 7.3 Hz, 1H), 4.44-4.39 (dd, *J* = 11.0, 5.8 Hz, 1H), 4.22-4.15 (dd, *J* = 11.1, 6.2 Hz, 1H), 4.14-4.09 (td, *J* = 11.0, 6.6 Hz, 1H), 3.47 (s, 3H), 3.31 − 3.25 (m, 1H), 1.07 (s, 9H).

(R)-(S)-2-(4-(benzyloxy)phenyl)-3-(pivaloyloxy)propyl-3,3,3-trifluoro-2-methoxy-2-phenylpropanoate (40): light yellow oil, 0.003 mg (90%); $[\alpha]_{405}^{20}$: + 4.54 (c 0.005 in chloroform). ¹H-NMR (CDCl₃, 400 MHz): δ 7.55 − 7.48 (m, 2H), 7.39 − 7.33 (m, 4H), 7.33 − 7.26 (m, 4H), 7.04 − 7.02 (d, *J* = 8.6 Hz 2H), 6.83 − 6.81 (d, *J* = 8.6 Hz 2H), 4.98 (s, 2H), 4.60-4.55 (dd, *J* = 11.0, 6.6 Hz, 1H), 4.42-4.30 (dd, *J* = 11.0, 5.8 Hz, 1H), 4.23-4.19 (dd, *J* = 11.1, 6.2 Hz, 1H), 4.10-4.06 (dd, *J* = 11.1, 7.3 Hz, 1H), 3.48 (s, 3H), 3.32 − 3.25 (m, 1H), 1.08 (s, 9H).

(R)-(R)-2-(4-(benzyloxy)phenyl)-3-(2-phenylacetoxy)propyl-3,3,3-trifluoro-2-methoxy-2-phenylpropanoate (39): light yellow oil, 0.003 mg (90%). $[\alpha]_{405}^{20}$: −8.17 (c 0.015 in chloroform). ¹H-NMR (CDCl₃, 400 MHz): δ 7.60–758 (m, 4H), 7.47–7.38 (m, 10H), 6.92–6.91 (d, *J* = 8.6 Hz 2H), 6.77–6.76 (d *J* = 8.6 Hz, 1H), 4.96 (s, 2H), 4.50–4.42 (dd, *J* = 11.0, 7.3 Hz, 1H), 4.35–4.30 (dd, *J* = 11.0, 5.8 Hz, 1H), 4.24–4.19 (dd, *J* = 11.1, 6.2 Hz, 1H), 4.16–4.12 (dd, *J* = 11.0, 6.6 Hz, 1H), 3.52 (s, 2H), 3.34 (s, 3H), 3.25–3.19 (m, 1H).

(R)-(S)-2-(4-(benzyloxy)phenyl)-3-(2-phenylacetoxy)propyl-3,3,3-trifluoro-2-methoxy-2-phenylpropanoate (41): light yellow oil, 0.003 mg (90%). $[\alpha]_{405}^{20}$: + 2.24 (c 0.013 in chloroform). ¹H-NMR (CDCl₃, 400 MHz): δ 7.60–758 (m, 4H), 7.47–7.38 (m, 10H), 6.93 − 6.92 (d, *J* = 8.6 Hz 2H), 6.79–6.77 (d *J* = 8.6 Hz, 1H), 4.97 (s, 2H), 4.50–4. 42 (dd, *J* = 11.0, 7.3 Hz, 1H), 4.34–4.29

(dd, J = 11.0, 5.8 Hz, 1H), 4.25–4.18 (dd, J = 11.1, 6.2 Hz, 2H), 3.52 (s, 2H), 3.32 (s, 3H), 3.26–3.19 (m, 1H).

(S)-(R)-2-(4-(benzyloxy)phenyl)-3-(pivaloyloxy)propyl-3,3,3-trifluoro-2-methoxy-2-phenylpropanoate (42): light yellow oil, 0.003 mg (90%). $[\alpha]_{405}^{20}$: –13.12 (c 0.05 in chloroform). ^{1}H-NMR (CDCl$_3$, 400 MHz): δ 7.60–758 (m, 4H), 7.47–7.38 (m, 10H), 7.13 – 7.11 (d, J = 8.6 Hz 2H), 6.92–6.90 (d J = 8.6 Hz, 1H), 5.07 (s, 2H), 4.68–4.64 (dd, J = 11.0, 7.3 Hz, 1H), 4.51–4.47 (dd, J = 11.0, 5.8 Hz, 1H), 4.32–4.28 (dd, J = 11.1, 6.2 Hz, 1H), 4.19–4.15 (dd, J = 11.0, 6.6 Hz, 1H), 3.57 (s, 3H), 3.41–3.34 (m, 1H), 1.16 (s, 9H).

(S)-(S)-2-(4-(benzyloxy)phenyl)-3-(pivaloyloxy)propyl-3,3,3-trifluoro-2-methoxy-2-phenylpropanoate (43): light yellow oil, 0.003 mg (90%). $[\alpha]_{405}^{20}$: +17.57 (c 0.072 in chloroform). ^{1}H-NMR (CDCl$_3$, 400 MHz): δ 7.54–7.42 (m, 4H), 7.45–7.36 (m, 10H), 7.12 – 7.10 (d, J = 8.6 Hz 2H), 6.91–6.89 (d, J = 8.6 Hz 2H), 5.06 (s, 2H), 4.66–4.61 (dd, J = 11.0, 6.6 Hz, 1H), 4.53–4.48 (dd, J = 11.0, 5.8 Hz, 1H), 4.31–4.27 (dd, J = 11.1, 6.2 Hz, 1H), 4.23–4.18 (dd, J = 11.1, 7.3 Hz, 1H), 3.58 (s, 3H), 3.41 – 3.35 (m, 1H), 1.17 (s, 9H).

6.5 Chiral chromatography

6.5.1 Resolution of 36 and 37 on chiralpak AD-H column

In order to identify the optimal experimental conditions for the enantioresolution of **36** and **37**, a standard screening protocol was applied to Chiralpak AD-H (0.46 cm diameter x 15 cm length, 5 μm) columns produced by Daicel Industries Ltd. (Tokyo, Japan). The elution conditions experimented include mixtures of *n*-hexane and polar modifiers (ethanol or 2-propanol) as well as alcohols (methanol, ethanol and 2-propanol). The results of the screening protocol are reported in Table3 as capacity factor (*k*), selectivity (α) and resolution (Rs) factors. The retention factor (*k*) was calculated using the equation $k = (t_R - t_0)/t_0$, where t_R is the retention time and t_0 the dead time (t_0 was considered to be equal to the peak of the solvent front and was taken from each particular run). The enantioselectivity (α) and the resolution factor (R_s) were calculated as follows: $\alpha = k_2/k_1$ and $R_s = 2(t_{R2} - t_{R1})/(w_1 + w_2)$ where t_{R2} and t_{R1} are the retention times of the second and the first eluted enantiomers, and w_1 and w_2 are the corresponding base peak widths.

The enantiomers of **36** and **37** were then completely resolved by a (semi)-preparative process using a RegisPack (1cm diameter x 25 cm length, 5μm) eluting with *n*-hexane/ 2-propanol (90/10, v/v) and *n*-hexane/ EtOH (90/10, v/v) at room temperature with a flow rate of 4 mL/min for **36** and **37**, respectively. The eluate was properly partitioned according with UV profile (detection preformed at

254 nm for compound **36** and **37**). Analytical control of the collected fractions was performed on a Chiralpack AD-H (0.46 cm diameter x 15 cm length, 5 μm), at room temperature at a flow rate of 1 mL/min and UV detection at 254 nm for compound **36** and **37**. The fractions obtained containing the enantiomers were evaporated at reduced pressure.

*(+)-3-hydroxy-2-(4-hydroxyphenyl)propyl pivalate (**36A**):* white solid, *e.e.* 95% determined by analytical chiral HPLC: tr= 10.1 min; Spectroscopic properties comply with those reported for compound **36**.

*(-)-3-hydroxy-2-(4-hydroxyphenyl)propyl pivalate (**36B**):* white solid, *e.e.* 90 % determined by analytical chiral HPLC: tr= 11.9; Spectroscopic properties comply with those reported for compound **36**.

*(+)-3-hydroxy-2-(4-hydroxyphenyl)propyl 2-phenylacetate (**37A**):* uncolorless oil, *e.e.* 99.9% determined by analytical chiral HPLC: tr= 22.6; Spectroscopic properties comply with those reported for compound **37**.

*(-)-3-hydroxy-2-(4-hydroxyphenyl)propyl 2-phenylacetate (**37B**):* uncolorless oil, *e.e.* 98% determined by analytical chiral HPLC: tr= 25.9; Spectroscopic properties comply with those reported for compound **37**.

6.6 Configurational study *via* chiroptical spectroscopies techniques

ECD spectra were taken from 350 to 185 nm on a Jasco 815SE spectropolarimeter. Solutions were ca. 0.01M/CH_3CN and were contained in 1 mm cylindrical quartz cuvettes. For each measurement, 10 scans were taken and averaged, considering both enantiomers of each compound **1, 2, 36** and **37**. ECD spectra of the solvent under the same experimental conditions were subtracted. Data are reported in Δε vs. λ (nm), from knowledge of the cell pathlength and solution concentration.

VCD spectra were taken from 900 to 1800 nm on a Jasco FVS600 FTIR spectropolarimeter. Solutions were ca. 0.1M/CD_3Cl and were contained in 200 μm BaF_2 IR cells. 5000 scans were taken for each measurement on both enantiomers of each compound **1, 2, 36** and **37**. VCD spectra of the solvent under the same experimental conditions were obtained between the measurements of the two enantiomers and were then subtracted and data are reported in Δε vs. ν (cm^{-1}), from knowledge of the cell pathlength and solution concentration.

6.7 Biological investigation

6.7.1 Cell culture and treatments

Human neuroblastoma SH-SY5Y cells (CRL-2266, ATCC, Manassas, VA, USA) were cultured in Eagle's minimum essential medium (MEM) supplemented with 10% fetal calf serum (FCS), 100 units/ml penicillin, 100 µg/ml streptomycin, 1% non-essential amino acids, 1 mM sodium pyruvate. Cells were maintained at 37°C in an atmosphere of 5% CO_2 and 95% air in 100% relative humidity, and grown to 80% confluence in petri dishes. For preliminary studies, cells were exposed to vehicle (DMSO) or increasing concentrations (from 1 µM to 300 µM) of C13 and B13 racemates for different times (from 15 to 120 min.) to find the best conditions for PKCα activation. In the experiments, the diacylglycerol (DAG) analogue phorbol-12-myristate-13-acetate (PMA, 100 nM for 15 min.) was used as a positive control of PKCα activation (not shown). For further studies, cells were exposed to vehicle, 25 µM C13 (racemate or enantiomers, for 15 min.) or 1 µM B13 (racemate or enantiomers, for 60 min.). All drug treatments were carried out in cells falling within 23 - 28 passages, in normal cell culture medium and under standard conditions.

6.7.2 Samples preparation, SDS-PAGE and Western blotting analysis

After treatment, the cells were washed twice with ice-cold Phosphate-buffered saline, harvested and homogenized in ice-cold lysis buffer [20 mM Tris (pH 7.4), 2 mM EDTA, 0.5 mM EGTA, 50 mM mercaptoethanol, 0.32 mM sucrose, protease and phosphatase inhibitors according to the manufacturer's instructions] by using a teflon/glass homogenizer. Total cell homogenates were then subjected to fractioning by ultracentrifugation, to obtain cytosol, membranes and cytoskeleton according to a published method [Talman et al., 2013]. Protein concentrations in cellular fractions were determined using Bradford's method. Samples for sodium dodecyl sulfate polyacrylamide gel electrophoresis (SDS-PAGE) and Western blotting were prepared by diluting the homogenates from each fraction in SDS loading solution, boiled for 5 min and separated on 12% SDS-PAGE, subsequently transferred to nitrocellulose membranes and processed following standard procedures. In brief, membranes were washed in 0.1% Tween 20 in Tris-buffered saline (TTBS), blocked for 1 h at room temperature (RT) with 5% non-fat milk powder in TTBS (milk–TTBS), and incubated overnight at 4°C with the primary antibody in milk–TTBS. The primary antibody dilutions were 1:500 for anti-PKCα and 1:1000 for anti-α-tubulin mouse antibodies, respectively. Membranes were then washed and incubated at RT for 1 h with an horseradish peroxidase-conjugated secondary antibody diluted at 1:3000 in milk–TTBS. After washing with TTBS, the immunoreactive bands were visualized with enhanced chemiluminescence. The α-tubulin was used to normalize the data. Statistical analysis of Western blotting data was performed on the densitometric values obtained using the NIH Image software. The data were subjected to one-way analysis of variance (ANOVA),

followed by a Dunnett's multiple comparisons test. Differences were considered statistically significant when p values were <0.05.

7. References

[1] Y. Takai, A. Kishimoto; M. Inoue, Y. Nishizuka, Studies on a Cyclic Nucleotide-independent Protein Kinase and Its Proenzyme in Mammalian Tissues. I. Purification and Characterization of an Active Enzyme from Bovine Cerebellum. *J.Biol.Chem,* 1977, *252,* 7603; Shun-ichi N., Hirokei Y., Yasutomi Nishizuka: Father of protein kinase C, *J.Biochem,* 2010, 148, 125-130

[2] House C., Kemp B.E., Protein kinase C contains a pseudosubstrate prototope in its regulatory domain, *Science,* 1987, 238, 1726-1728

[3] Newton A.C., Protein Kinase C: Structure, Function, and Regulation**,** *J. Biol. Chem.* 1995, 270, 28495-28498

[4] Steinberg S.F., Structural basis of protein kinase C isoform function. *Physiol. Rev.* 2008, 88, 1341-1378

[5] Shao X., Davletov B.A, Sutton R.B., Sudhof T. C., Rizo J., Bipartite Ca2+-binding motif in C2 domains of synaptotagmin and protein kinase C, *Science*, 1996, *273*, 248-51

[6] Palmer R.H., Dekker L.V., Woscholski R., Le Good J.A, Gigg R., Parker P.J., Activation of PRK1 by phosphatidylinositol 4,5-bisphosphate and phosphatidylinositol 3,4,5-trisphosphate. A comparison with protein kinase C isotypes, *J. Biol. Chem.* 1995, *270*, 22412-22416

[7] Jaken S., Parker P.J, Protein kinase C binding partners, *BioEssays*, 2000, 22, 245–254

[8] Choi C.H, ABC transporters as multidrug resistance mechanisms and the development of chemosensitizers for their reversal,*Cancer Cell*, 2005, 5, 30

[9] Gottesman M.M, Fojo T., Bates S.E., Multidrug resistance in cancer: role of ATP-dependent transporters, *Nat.Rev.Cancer*, 2002, 2, 48-58

[10] Martiny-Baron G., Fabbro D., Classical PKC isoforms in cancer, *Pharmacological Research*, 2007, 55, 477-486

[11] Lamark T., Perander M., Outzen H., Kristiansen K., Øvertan A., Michaelsen M., Bjørkøy G., Johansen T., Interaction codes within the family of mammalian Phox and Bem1p domain-containing proteins, *J. Biol.chem*, 2003, 278, 34568-34581

[12] Murray N.R., Kalari K.R, Fields A.P, Protein kinase Cι expression and oncogenic signaling mechanisms in cancer, *J.Cell.Physiology*, 2011, 226, 879-887

[13] Kun-Sun M., Alkon D.L, Pharmacology of protein kinase C activators: cognition-enhancing and antidementic therapeutics, *Pharmacol. Ter*, 2010, 127, 66-77

[14] Pascale A., Amadio M., Govoni S., Battaini F., The aging brain, a key target for the future: the protein kinase C involvement, *Pharmacol. Res*, 2007, 55, 560-569; Pascale A., Amadio M., Scampagnini G., Lanni C., Racchi M., Provenzani A., Govoni S., Alkon D.L., Quattrone A., Neuronal ELAV proteins enhance mRNA stability by a PKCalpha-dependent pathway, *PNAS*, 2005, 102, 12065-12070

[15] Amadio M., Bucolo C., Leggio G.M, Drago F., Govoni S., Pascale A., The PKCbeta/HuR/VEGF pathway in diabetic retinopathy, *Biochem.Pharm* 2010, 80, 1230-1237.

[16] Mura S., Iwai Y., Hirano A., Nakagawa A., Awaya J, Tsuchiya H., Takahashi Y., Masuma R, A new alkaloid AM-2282 OF Streptomyces origin. Taxonomy, fermentation, isolation and preliminary characterization, *J. Antibiot*. 1977, 30, 4, 275–282

[17] Zhang H.C, Derian C.K., McComsey D.F., White K.B., Ye H., Hecker L. R.,. Li J., Addo M.F., Croll D., Eckardt A. J., Smith C. E., Li Q., Cheung W.M, Conway B.R., Emanuel S., Demarest K.T., Andrade-Gordon P., Damiano B.P., Maryanoff B. E., Novel indolylindazolylmaleimides as inhibitors of protein kinase C-beta: synthesis, biological activity, and cardiovascular safety, *J. Med. Chem,* 2005, 48, 725-1728

[18] Pearce H. L., Miller M. A., The evolution of cancer research and drug discovery at Lilly Research Laboratories, *Adv Enzyme Regul*, 2005, 45, 229–55

[19] Smith B.D., Levis M., Beran M., Giles F., Kantarjian H., Berg K., Murphy K.M., Dauses T., Allebach J., Small D., Single-agent CEP-701, a novel FLT3 inhibitor, shows biologic and clinical activity in patients with relapsed or refractory acute myeloid leukemia, *Blood*, 2004, 103, 3669–76

[20] Stone R.M., DeAngelo D.J., Klimek V., Galinsky I., Estey E., Nimer S.D., Grandin W., Lebwohl D., Wang Y., Cohen P., Fox E.A., Neuberg D., Clark J., Gilliland D.G., Griffin J.D., Patients with acute myeloid leukemia and an activating mutation in FLT3 respond to a small-molecule FLT3 tyrosine kinase inhibitor, PKC412, *Blood* 2005, 5, 54–60.

[21] Stone R.M., Fischer T., Paquette R., Schiller G., Schiffer C.A., Ehninger G., *ASH Annual Meeting Abstracts* 2005, 106, 404.

[22] Levis M., Smith B.D., Beran M., Baer M.R., Erba H.P., Cripe L., *ASH Annual Meeting Abstracts* 2005, 106, 403.

[23] Parang K., Cole P.A., Designing bisubstrate analog inhibitors for protein kinases, *Pharmacology & Therapeutics*, 2002, 93, 145– 157

[24] Poot A. J., van Ameijde J., Slijper M., van den Berg A., Hilhorst R., Ruijtenbeek R., Rijkers D.T.S, Liskamp R.M.J., Development of selective bisubstrate-based inhibitors against protein kinase C (PKC) isozymes by using dynamic peptide microarrays**,** *Chem.Bio.Chem* 2009, 10, 2042 – 2051

[26] van Wandelen L.T.M., van Ameijde J., Mady A.S.A., Wammes A.E.M., Bode A., Poot A.J., Ruijtenbeek R., Liskamp R.M.J., Directed modulation of protein kinase C isozyme selectivity with bisubstrate-based inhibitors, *Chem.Med.Chem,* 2012, 7, 2113 – 2121

[27] Lee J.H., Nandy S.K., Lawrence D.S., A highly potent and selective PKCalpha inhibitor generated via combinatorial modification of a peptide scaffold, *J. Am. Chem. Soc*, 2004, 126, 3394-3395

[28] Cywin C.L., Dahmann G., Prokopowicz A.S., Young E.R.R., Magolda R.L., Cardozo M.G., Cogan D.A., DiSalvo D., Ginn J.D., Kashem M.A., Wolak J.P.,. Homon C.A, Farrell T.M., Grbic H., Hu H., Kaplita P.V., Liu L.H, Spero M.D, Jeanfavre D.D., O'Shea K.M., White D.M., Woska J.R. Jr., Brown M.L., Discovery of potent and selective PKC-theta inhibitors**,** *Bioorg. Med. Chem. Lett.* 2007, 17, 225–230

[29] Pettit G.R., Cherry L.H., Doubek D.L., Herald D.L., Arnold E., Clardy J., Isolation and structure of bryostatin 1, *J. Am. Chem. Soc*. 1982, 104 ,6846–6848

[30] Irie K., Yanagita R.C., Synthesis and biological activities of simplified analogs of the natural PKC ligands, bryostatin-1 and aplysiatoxin**,** *Chem. Rec.,* 2014, 14, 251–267

[31] Wender P.A., Verma V.A., Design, synthesis, and biological evaluation of a potent, PKC selective, B-ring analog of bryostatin, *Org. Lett.*, 2006, 8, 1893

[32] Hang G., Kazanietz M.G., Blumberg P.M., Hurley J.H., Crystal structure of the cys2 activator-binding domain of protein kinase C delta in complex with phorbol ester, *Cell*, 1995, 81, 917-924

[33] Baba Y., Ogoshi Y., Hirai G., Yanagisawa T., Nagamatsu K., Mayumi S., Hashimoto Y., Sodeoka M., Design, synthesis, and structure-activity relationship of new isobenzofuranone ligands of protein kinase C, *Bioorg. Med. Chem. Lett*. 2004, 14, 2963-2967.

[34] Marquez V.E., Blumberg P.M., Synthetic diacylglycerols (DAG) and DAG-lactones as activators of protein kinase C (PK-C), *Acc. Chem. Res*. 2003, 36, 434.

[35] Kang J.H., Siddiqui M.A., Lewin N.E., Pu Y., Sigano D.M., Blumberg P.M., Lee J.,

Marquez V.E., Conformationally constrained analogues of diacylglycerol. 24. Asymmetric synthesis of a chiral (R)-DAG-lactone template as a versatile precursor for highly functionalized DAG-lactones, *Org. Lett*. 2004, 6, 2413

[36] Boije af Gennas G., Talman V., Aitio O., Ekokoski E., Finel M., Tuominen R.K., Yli-Kauhaluoma J., Design, synthesis, and biological activity of isophthalic acid derivatives targeted to the C1 domain of protein kinase C, *J. Med. Chem.,* 2009, 52, 3969-3981

[37] Lee J., Lee J.H., Kim S.Y., Perry N.A., Lewin N.E., Ayres J.A., Blumberg P.M., 2-Benzyl and 2-phenyl-3-hydroxypropyl pivalates as protein kinase C ligands, *Bioorg. Med.Chem*. 2006*, 14,* 2022-31

[38] Ling L.U., Lin H., Tan K.B., Chiu G.N., The role of protein kinase C in the synergistic interaction of safingol and irinotecan in colon cancer cells, *Int J Oncol.*, 2009, 35, 1463-71

[39] Polavarapu P.L., Determination of the Absolute Configurations of Chiral Drugs Using Chiroptical Spectroscopy, *Molecules*, 2016, 21, 1056

[40] Abbate S., Ciogli A., Fioravanti S., Gasparrini F, Longhi G., Pellacani L., Rizzato E, Spinelli D., Tardella P.A., Solving the Puzzling Absolute Configuration Determination of a Flexible Molecule by Vibrational and Electronic Circular Dichroism Spectroscopies and DFT Calculations: The Case Study of a Chiral 2,2-Dinitro-2,2-biaziridine, *Eur. J. Org. Chem.,* 2010, 6193–6199

[41] Mándi A., Swamy M.M., Taniguchi T., Anetai M., Monde K, Molecular Flexibility by Cyclization for Elucidation of Absolute Configuration by CD Calculations: Daurichromenic Acid, *Chirality*, 2016, 28, 453–459

[42] Gaggeri R, Rossi D, Collina S, Mannucci B, Baierl M, Juza M. Quick development of an analytical enantioselective high performance liquid chromatography separation and preparative scale-up for the flavonoid Naringenin. *J Chromatogr A*, 2011, 1218, 5414–5422

[43] Jose´ Manuel Seco, Emilio Quin˜oa´ and Ricardo Riguera Tetrahedron: *Asymmetry* 12 (2001) 2915–2925

[44] Latypov S.K. , Ferreiro M.J., Quiñoá E., Riguera R., Assignment of the Absolute Configuration of β-Chiral Primary Alcohols by NMR: Scope and Limitations, *J. Am. Chem. Soc*. 1998, 120, 4741-4751

[45] Doesburg H. M., Petit G.H., Merckx E.M., *Acre Crysrullogr.*1982,838, 1181. Oh S.S., Butler W.H.; Koreeda M., *J. Org. Chem.* 1989, 54, 4499

[46] Yamaguchi S.; Yasuhara F.; Kabuto K. *Tetrahedron* 1976, 32, 1363.Yamaguchi S.,Yasuhara F. *Tetrahedron Lett.* 1977, 89. Yasuhara F., Yamaguchi S. *Ibid.* 1977,4085

[47] Kusumi T., Ohtani 1., Inouye Y., Ishitsuka O. M., Kakisawa H., 16th IUPAC International Symposium on the Chemistry of Natural Products, Kyoto, May-June, 1988; Abstract Pa17; Kusumi, T., Ohtani1, Inouye Y., Kakisawa H., *Tetrahedron Lett.* 1988,29,4731; Ohtani 1., Kusumi T., Ishitsuka O.M., Kakisawa H., *Ibid.* 1989, *30,* 3147

[48] Sullivan G.R., Dale J.A., Mosher H.S., Correlation of configuration and ^{19}F chemical shifts of a-methoxy-a-trifluoromethylphenylacetate derivatives. *J. Org.Chem.* 1973, 38, 2143–2147

[49] Dale J.A.; Mosher H.S., Nuclear magnetic resonance enantiomer regents. Configurational correlations via nuclear magnetic resonance chemical shifts of diastereomeric mandelate, O-methylmandelate, and .alpha.-methoxy-.alpha.-trifluoromethylphenylacetate (MTPA) esters, *J. Am. Chem. Soc*. 1973,95, 512.

[50] Latypov Sh. K., Seco J. M., Quiñoá E., Riguera R., MTPA vs MPA in the Determination of the Absolute Configuration of Chiral Alcohols by 1H NMR, *J. Org. Chem.* 1996**,** 61*,* 8569-8577

[51] I. Ohtani, Kusumi T., Kashman Y., Kakisawa H., High Field FT-NMR Application of Mosher's Method. The Absolute Configurations of Marine Terpenoids, *J. Am. Chem. Soc.*, 1991, 113, 4092-4096

MedChemComm

Broadening the field of opportunity for medicinal chemists

www.rsc.org/medchemcomm

ROYAL SOCIETY
OF CHEMISTRY

EFMC
European Federation
for Medicinal Chemistry
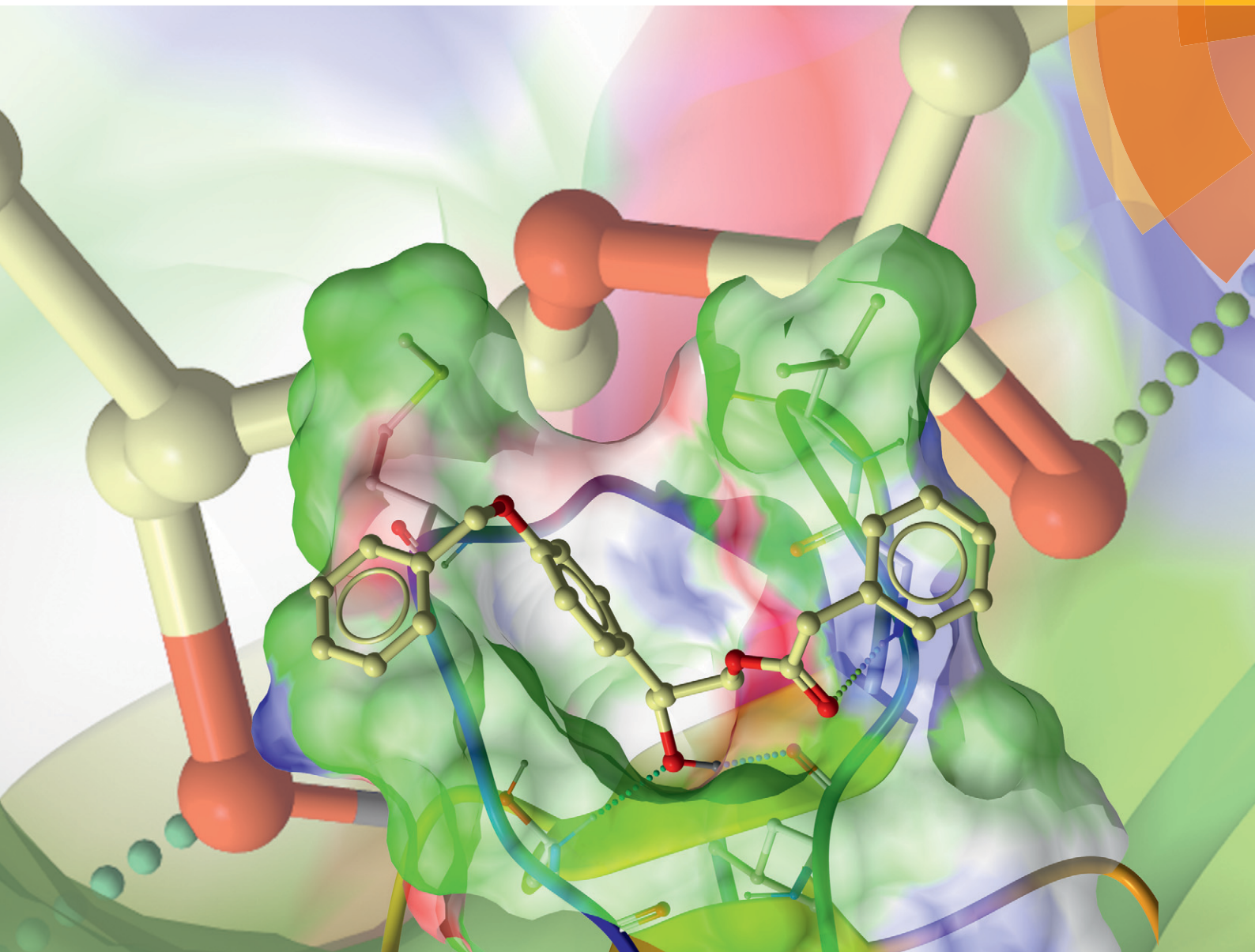
CONCISE ARTICLE
Simona Collina *et al.*
Beyond the affinity for protein kinase C: exploring 2-phenyl-3-hydroxypropyl pivalate analogues as C1 domain-targeting ligands

MedChemComm

CrossMark
click for updates

Beyond the affinity for protein kinase C: exploring 2-phenyl-3-hydroxypropyl pivalate analogues as C1 domain-targeting ligands†

Daniela Rossi,‡[a] Virpi Talman,‡[b] Gustav Boije Af Gennäs,‡[c] Annamaria Marra,‡[a] Pietro Picconi,‡[a] Rita Nasti,‡[a] Massimo Serra,‡[a] Jihyae Ann,‡[d] Marialaura Amadio,‡[e] Alessia Pascale,‡[e] Raimo K. Tuominen,‡[b] Jari Yli-Kauhaluoma,‡[c] Jeewoo Lee‡[d] and Simona Collina‡*[a]

Over the past fifteen years, we reported the design and synthesis of different series of compounds targeting the C1 domain of protein kinase C (PKC) that were based on various templates. Out of the pivalate templates, 2-[4-(benzyloxy)phenyl]-3-hydroxypropyl pivalate (compound **1**) emerged as the most potent and promising PKCα ligand, showing a K_i value of 0.7 μM. In the present contribution our efforts are aimed at better understanding which structural modifications of the pivalate template are allowed for its affinity to the C1 domain of PKC to be preserved or increased. To this aim, thirteen novel analogues of **1** were designed and their interaction with the target was evaluated *in silico*. Designed compounds were then prepared and fully characterized as well as their affinity for the α and δ isoforms of PKC evaluated. Additionally, in order to investigate the role of chirality in the ligand–target interaction, the pure enantiomers of the most interesting PKC ligands were prepared and their affinity for PKC isoforms was determined. Results from our study revealed that: i) the presence of the ester function seems to be essential for the ligand–target interaction; ii) only a few structural modifications at the ester group are allowed for the C1 domain affinity to be preserved; and iii) the [³H]PDBu replacement experiments showed that the C1 domain of PKC does not exhibit enantiopreference for the pure stereoisomers of tested compounds. Altogether our observations provide further insights into the ligand–target interactions of the PKC C1 domain and represent a step-forward in future development of more specific and effective PKC ligands.

[a] *Department of Drug Sciences, Medicinal Chemistry and Pharmaceutical Technology Section, University of Pavia, Viale Taramelli 12, 27100 Pavia, Italy. E-mail: simona.collina@unipv.it; Fax: (+39)0382 422975; Tel: (+39)0382 987379*
[b] *Division of Pharmacology and Pharmacotherapy, Faculty of Pharmacy, University of Helsinki, Viikinkaari 5 E (P.O. Box 56), FI-00014, Finland*
[c] *Division of Pharmaceutical Chemistry and Technology, Faculty of Pharmacy, University of Helsinki, Viikinkaari 5 E (P.O. Box 56), FI-00014, Finland*
[d] *Laboratory of Medicinal Chemistry, College of Pharmacy, Seoul National University, Seoul 151-742, Korea*
[e] *Department of Drug Sciences, Pharmacology Section, University of Pavia, Viale Taramelli 14, 27100 Pavia, Italy*

Introduction

Protein kinase C (PKC) is a family of ten serine/threonine kinases which can phosphorylate a large number of substrates and is thus involved in several cellular functions. Based on both sequence homology and sensitivity to activators, the isoforms are classified into: (1) calcium-dependent conventional isoforms (cPKCs; α, βI, βII and γ); (2) calcium-independent novel isoforms (nPKCs; δ ε, η and θ); and (3) atypical isoforms (aPKCs; ζ and ι/λ).[1,2] From a structural standpoint, PKCs are generally characterized by a primary amino acid sequence composed of a single polypeptide chain which includes conserved domains (named C1–C4) separated by variable sequences (Fig. 1). The N-terminal regulatory region hosts C1 and C2 domains that control the kinase activity of the enzyme and also its subcellular localization. The C1 domain presents the binding motif for the physiological activator diacylglycerol (DAG, Fig. 2) as well as for exogenous activators, such as phorbol esters (*i.e.* phorbol-13-*O*-acetate, Fig. 2). The C2 domain coordinates the binding to anionic
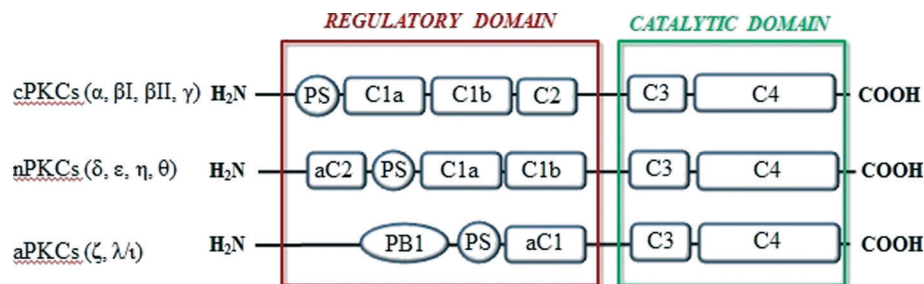
This journal is © The Royal Society of Chemistry 2015

Med. Chem. Commun., 2015, **6**, 547–554 | 547

Fig. 1 Schematic structures of PKC isoforms. aC1: atypical C1 domain of aPKCs; nC2: C2 domain of nPKCs; PS: pseudosubstrate sequence; PB1: Phox and Bem 1 domain.
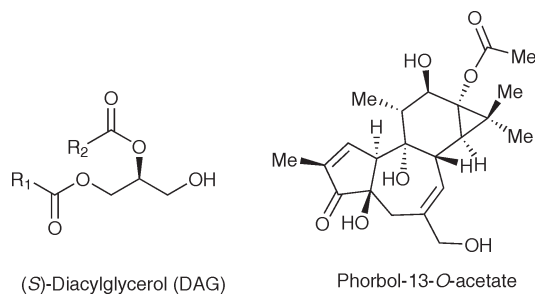

Fig. 2 Structure of the physiological PKC activator diacylglycerol (DAG) and the exogenous PKC activator phorbol-13-*O*-acetate, both targeting the C1 domain of PKC.

phospholipids on the cell membrane and in the case of cPKCs includes the binding site for Ca^{2+}.[3–5] The regulatory region also contains an auto-inhibitory pseudosubstrate sequence (PS, Fig. 1) that clamps the catalytic site in the inactive conformation and inhibits substrate binding thus preventing the activation of the enzyme in the absence of external stimuli. The C-terminal kinase domain is responsible for the phosphotransfer activity and thus contains ATP and substrate binding sites located in C3 and C4 domains, respectively (Fig. 1).

Signaling pathways mediated by DAG/phorbol ester-responsive PKCs have a pivotal role in various cellular functions, such as apoptosis, proliferation and differentiation, as well as in cognitive processes.[6,7] Accordingly, the aberrant function of PKC-mediated pathways underlies several pathological conditions, ranging from cancer to neurodegenerative diseases, especially Alzheimer's disease (AD), passing through diabetes, heart disease and autoimmune diseases.[8–13] Depending on the pathological condition, PKC isoforms may

show either increased or decreased activity and, consequently, both PKC inhibitors and activators may possess strong therapeutic potential in various pathological contexts. Particularly, the C1 domain of PKC is an intriguing pharmacological target for developing new PKC activators, which may be useful in the treatment of several diseases, including AD. Indeed, *in vivo* experiments with AD double-transgenic mice have shown that activation of PKC with C1-targeting compounds is a highly promising therapeutic strategy for AD treatment.[14]

Over the past fifteen years, we and others have reported the design and synthesis of different series of C1-targeting PKC ligands (templates I–IV, Fig. 3). First, conformationally constrained DAG analogues embedded in a variety of lactone templates (*i.e.* templates I and II) were designed to reduce part of the entropic penalty associated with the binding of the flexible glycerol backbone of DAG.[15–17] As an alternative approach, we also studied a novel group of synthetic C1 domain ligands based on the dialkyl 5-(hydroxymethyl)isophthalate template III,[18] as well as a compound series built on 2-phenyl- and 2-benzyl-3-hydroxypropyl pivalate template IV.[19]

For compounds based on template IV, both benzyl ($n = 1$) and phenyl ($n = 0$) derivatives bearing hydrogen bonding groups, such as hydroxy, benzyloxy and hexanoyl groups at different positions of the aromatic moiety, were investigated as novel PKCα ligands. Among this compound series, 2-[4-(benzyloxy)phenyl]-3-hydroxypropyl pivalate (compound **1**, Fig. 4) emerged as the most potent PKCα ligand, showing a K_i value of 0.7 μM.

As a part of our on-going research in the PKC field, the present contribution is aimed at better understanding which structural modifications of template IV are allowed for the affinity for the C1 domain of PKC to be preserved or
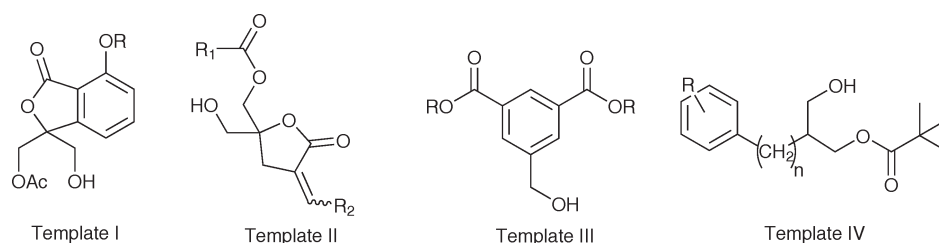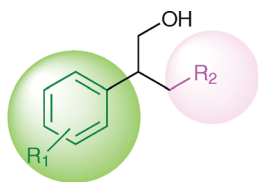

Fig. 3 Structures of the previously investigated PKC ligands.

Which structural changes are allowed?

Fig. 4 Structures of compounds **1**–**14**.

increased. To this purpose, thirteen novel analogues of compound **1** (Fig. 4) were prepared and fully characterized as well as their affinity for the α and δ isoforms of PKC evaluated. Additionally, since enantiomers of a biologically active compound may show different interactions with the target protein, the pure enantiomers of the most interesting PKC ligands were prepared and their affinity for PKC isoforms was determined.

Results and discussion

Compound design

We designed compounds **2**–**14** which are characterized by different functionalities at the carbonyl group as well as different aromatic substitutions (Fig. 4).

The crystal structure of the C1b domain of PKCδ (PDB ID: 1PTR)[20] complexed with phorbol 13-*O*-acetate reveals an approximately 50 residue-long sequence with the "bottom" third of the domain containing negatively charged amino acids. The "central" part of the domain is hydrophilic, whereas the binding site of DAG and phorbol esters can be

found in the hydrophobic "top" third of the C1 domain, where a deep, narrow and polar groove can be found between two β-sheets. To investigate if compounds **2**–**14** would bind to the binding groove of the C1 domain of PKC, we performed docking experiments using the crystal structure (Fig. 5). Compound **1** was also included in this study as the reference compound. Results suggested that *e.g.* compound (*S*)-**2** can bind to the bottom of the binding groove of the C1 domain and has the same interactions as phorbol-13-*O*-acetate in the crystal structure (Fig. 5A). These interactions include hydrogen bonds between the hydroxy group and the backbone amide proton of Thr 242 and the carbonyl of Leu 251. In addition to these interactions, the carbonyl of compound (*S*)-**2** forms a hydrogen bond with the amide proton of Gly 253. A similar interaction can be seen between the C3 carbonyl of phorbol-13-*O*-acetate and the C1 domain in the crystal structure. Even though the C13 ester carbonyl of phorbol-13-*O*-acetate is essential for the binding activity, no interaction between the carbonyl and the protein can be seen in the crystal structure, as in the case with the other carbonyl of DAG.[21] Interestingly, the docking results of the retro-esters (compounds **3**–**5**) and retro-amides (compounds **6**–**14**) suggest that these compounds can bind to the deep groove of the C1 domain of PKC similarly to **1** and **2** [*e.g.* compound (*S*)-**3**, Fig. 5B]. The docking results also suggest that some of the compounds could adapt another binding mode, similarly to the DAG-lactones.[16] In this binding mode Gly 253 does not act as a hydrogen donor to the carbonyl of *e.g.* compound **4** but instead to the oxygen of the 3-benzyloxy group. Given the considerations above, the designed compounds were considered to be suitable for the purpose of this study.

Syntheses

Compounds **1** and **2** were essentially prepared according to the methodology described in our previous work,[19] with suitable modifications (Scheme 1). Briefly, starting from the commercially available 4-(benzyloxy)benzaldehyde, the alcohol **15** was easily obtained using lithium aluminium hydride and then transformed into the corresponding benzyl chloride **16** with thionyl chloride. Compound **16**, in turn, was converted into the nitrile **17** by using sodium cyanide. Intermediate **17** was hydrolysed by refluxing it in an aqueous solution of 30% NaOH, and the resulting carboxylic acid **18** was converted into the methyl ester **19**, which in turn was acylated with dimethyl carbonate to give compound **20**. The diester groups of **20** were then reduced to the corresponding alcohols by using LiAlH$_4$, yielding **21**. Finally, one of the hydroxy groups of **21** was selectively acylated by pivaloyl chloride or 2-phenylacetyl chloride, giving the target products **1** and **2**, respectively.

The key step for the synthesis of compounds **3**–**14** was the preparation of 3-unsaturated γ-butyrolactones **28**–**30** (Scheme 2), which was easily achieved through a two-step reaction sequence.

First, the Heck reaction, performed according to our previously optimized phosphine-free protocol, gave the
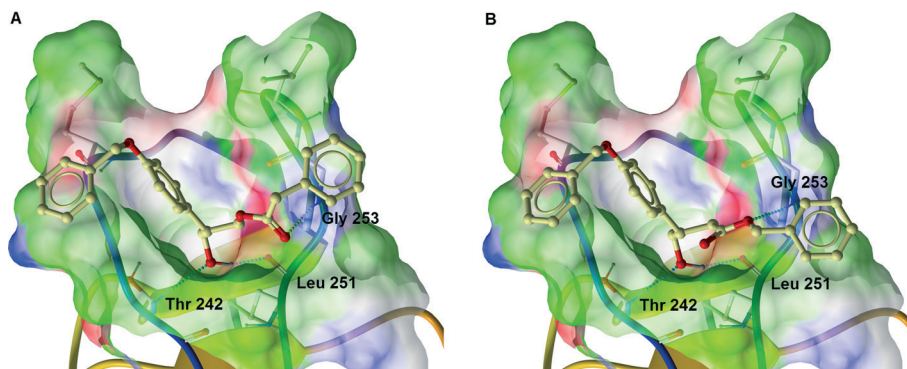
Fig. 5 (A) Compounds (S)-**2** and (B) (S)-**3** docked to the C1b domain of PKCδ (PDB ID: 1PTR).[20] Hydrogen bonds are represented as green spheres and the surface of the binding pocket of the protein is colored as follows: hydrogen bond acceptor area (red), hydrogen bond donor area (blue) and hydrophobic area (green). The figure was created using ICM-Browser (version 3.7-2a, Molsoft L.L.C.).
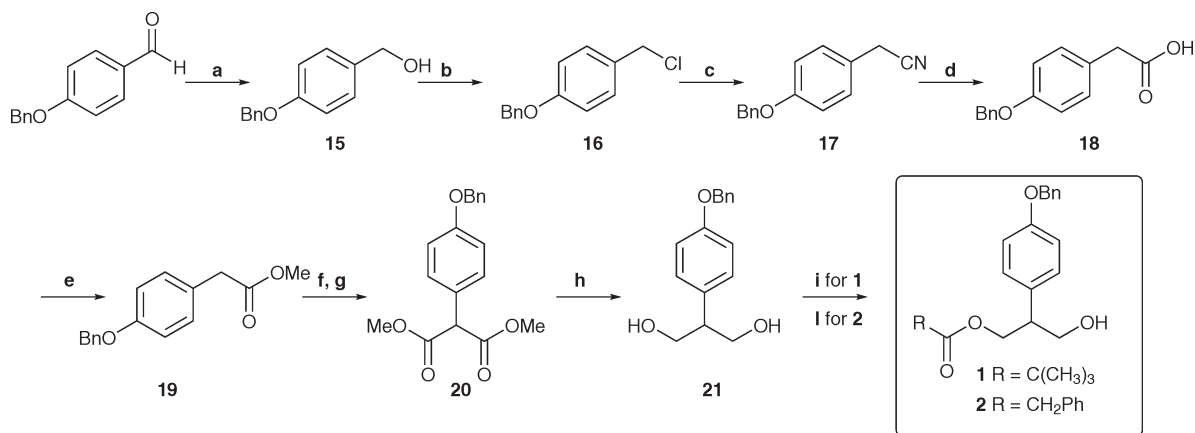
Scheme 1 Synthesis of **1** and **2**. Reagents and conditions: (a) LiAlH$_4$, diethyl ether, 0 °C, then reflux, 30 min; (b) SOCl$_2$, DCM, 0 °C, 1 h; (c) NaCN, DMF, 100 °C, 2 h; (d) 30% NaOH (aq), reflux, overnight; (e) H$_2$SO$_4$, MeOH, reflux, 2 h; (f) NaH, 1,4-dioxane, 0 °C, then rt, 30 min; g) (MeO)$_2$CO, 1,4-dioxane, 0 °C then reflux, 2 d; (h) LiAlH$_4$, THF, 0 °C, then rt, 2 h; (i) (Me$_3$)$_3$CCOCl, pyridine, DCM, 0 °C, then rt, 2 h; (l) PhCH$_2$COCl, pyridine, DCM, 0 °C, then rt, 2 h.
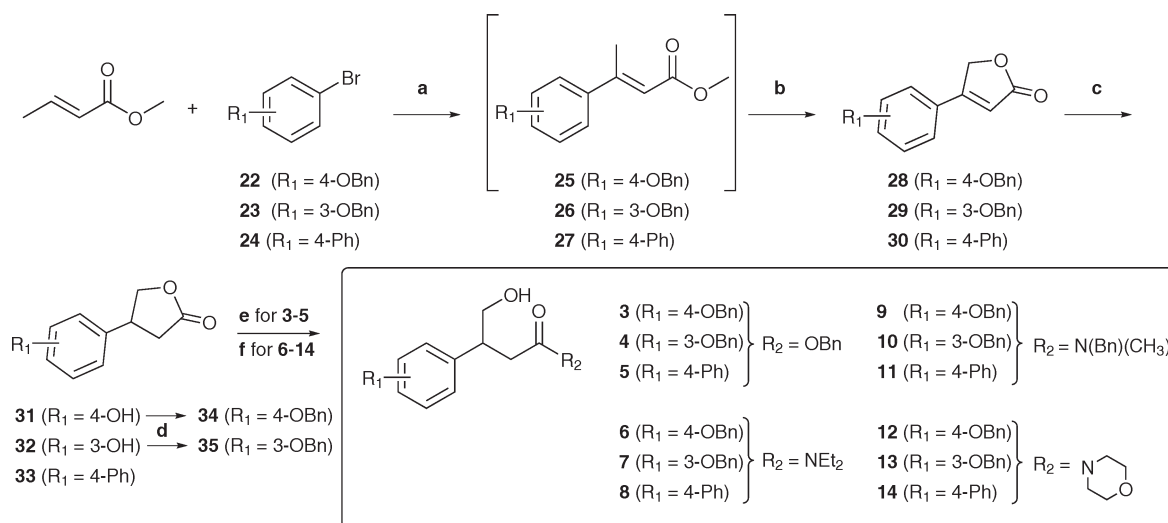
Scheme 2 Synthesis of compounds **3–14**. Reagents and conditions: (a) TBAC, AcONa, Pd(OAc)$_2$, DMF, reflux, overnight; (b) SeO$_2$, tBuOOH, DCE, reflux, overnight; (c) HCOONH$_4$, 10% Pd/C, MW conditions: 100 °C, 100 W, 180 s; (d) Cs$_2$CO$_3$, benzyl bromide, MeCN, MW conditions: 100 °C, 60 W, 40 min; (e) 10% NaOH (aq), MeOH, reflux, 3 h, then K$_2$CO$_3$, benzyl bromide, H$_2$O/DMF (1:10), rt, overnight; (f) 10% NaOH (aq), MeOH, reflux, 3 h, then AlCl$_3$, amine, DCE, MW conditions: 100 °C, 60 W, 25 min.

550 | Med. Chem. Commun., 2015, **6**, 547–554

This journal is © The Royal Society of Chemistry 2015

α,β-unsaturated esters **25–27** as mixtures of (*E*,*Z*)-isomers.[22,23] Subsequently, crude **25–27** underwent allylic oxidation with selenium dioxide and *tert*-butyl hydroperoxide without further purification,[24] furnishing the desired oxidation products **28–30**. γ-Butyrolactones **28–30** were then subjected to microwave-assisted catalytic hydrogenation under phase transfer conditions,[25] yielding intermediates **31–33**. It has to be noted that catalytic hydrogenation of **28** and **29** resulted in the simultaneous reduction of the double bond and cleavage of the benzyloxy group, thus furnishing compounds **31** and **32**, respectively. These, in turn, were fully *O*-benzylated[26] to yield the desired γ-butyrolactones **34** and **35**.

Target products **3–5** were synthesized starting from γ-butyrolactones **33–35** by a tandem hydrolysis–esterification process.[27] First, γ-butyrolactones **33–35** were converted into the corresponding sodium 3-aryl-4-hydroxybutanoates, which in turn were treated with benzyl bromide in the presence of K₂CO₃ to yield the corresponding benzyl esters **3–5**. The target products **6–14** were synthesized from the same γ-butyrolactones **33–35** using the appropriate secondary amine and AlCl₃, according to the protocol developed by Lesimple *et al.*,[28] with suitable modifications. Specifically, to speed up the synthetic procedure, we decided to take advantage of microwave irradiation instead of using conventional heating, thus obtaining the desired products in a very short reaction time.

Isolation of 1 and 2 enantiomers

The resolution of racemic **1** and **2** by semi-preparative HPLC using chiral stationary phases was carried out. In order to identify the optimal experimental conditions for the enantioresolution of **1** and **2**, a standard screening protocol[29] was applied to both Chiralcel OJ-H (0.46 cm diameter × 15 cm length, 5 μm) and Chiralpak IC (0.46 cm diameter × 25 cm

length, 5 μm) columns (for details see Table S2, ESI†). As presented in Fig. 6, for both compounds, baseline resolution was achieved on the Chiralpak IC column eluted with *n*-hexane/2-propanol (90/10, v/v) at a flow rate of 1 mL min⁻¹ [t_{r1} 19.9 min, t_{r2} 22.5 min, α 1.16 and R_s 2.00 for **1**, Fig. 6A; t_{r1} 36.7 min, t_{r2} 47.1 min, α 1.31 and R_s 4.16 for **2**, Fig. 6B]. Hence, these experimental conditions were selected to be properly scaled-up to the semipreparative scale. Briefly, 48 mg of **1** was processed in 24 cycles according to the conditions reported in Table 1, yielding 20.0 mg of the first eluted enantiomer **1A** (ee 99.9%, $[\alpha]_{405}^{20}$ = + 37.7, *c* 0.6 in methanol) and 19.3 mg of the second eluted enantiomer **1B** (ee 99.9%, $[\alpha]_{405}^{20}$ = − 37.2, *c* 0.6 in methanol), together with 7.5 mg of an intermediate fraction which was a mixture of the two enantiomers. As regards **2**, 30 mg of the racemate was processed in 5 cycles following the conditions summarized in Table 1, furnishing 14.2 mg of the first eluted enantiomer **2A** (ee 99.9%, $[\alpha]_{405}^{20}$ = + 37.5, *c* 0.4 in methanol) and 13.1 mg of the second eluted enantiomer **2B** (ee 99.9%, $[\alpha]_{405}^{20}$ = − 37.4, *c* 0.4 in methanol), together with 1.1 mg of the intermediate fraction.

Biological activity

After synthesis and chemical characterization, compounds **1–14**, **1A–B** and **2A–B** were subjected to biological assays to determine their binding affinity for PKCα and PKCδ. Compounds **1–14** were used in the concentration range of 0.1–100 μM to displace [³H]-phorbol 12,13-dibutyrate ([³H]PDBu) from the C1 domain of PKCα and PKCδ using a 96-well plate filtration method as previously described.[18] The percentages of residual [³H]PDBu binding after exposure to **1–14** at 100 μM concentration are presented in Table 2. As regards the affinity to PKCα, the novel compound **2** displaced [³H]PDBu in a concentration-dependent manner with an IC₅₀ value of 73.9 μM
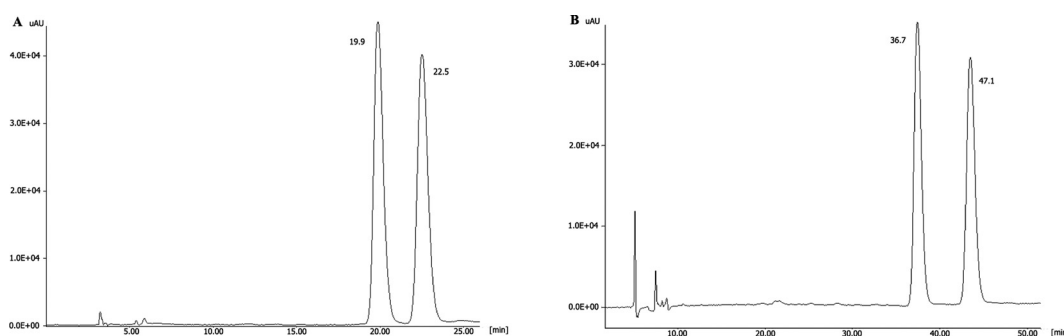
Fig. 6 Analytical separation of (A) compound **1** (detection at 274 nm) and (B) compound **2** (detection at 254 nm) on a Chiralpak IC column (0.46 cm diameter × 25 cm length, 5 μm), mobile phase: *n*-hexane/2-propanol (90/10, v/v), flow rate: 1 mL min⁻¹.

Table 1 Semi-preparative resolution of **1** and **2** on a Chiralpak IC column (10 mm diameter × 250 mm length, 5 μm), eluted with *n*-hexane/2-propanol (90/10, v/v)

Cmpd	*n*-Hexane/2-propanol	Flow rate [mL min⁻¹]	t_{r1} [min]	t_{r2} [min]	Inj. vol [mL]	Conc. [mg mL⁻¹]	λ [nm]
1	90/10	3	29.5	33.5	0.2	10	274
2	90/10	2	48.1	63.5	1	6	254

Table 2 Binding affinity of compounds **1–14** to PKCα and PKCδ[a]

Cmpd	Residual [³H]PDBu binding to PKCα (% of control)	Residual [³H]PDBu binding to PKCδ (% of control)
1	41.6 ± 2.7 (4)	29.3 ± 2.1 (4)
2	51.3 ± 5.8 (4)	34.8 ± 2.2 (4)
3	73.9 ± 8.0 (2)	61.6 ± 0.4 (2)
4	67.4 ± 2.1 (2)	52.5 ± 1.3 (2)
5	64.4 ± 11.5 (2)	56.7 ± 3.5 (2)
6	100.5 ± 12.2 (2)	n.d.
7	90.0 ± 11.6 (2)	n.d.
8	84.4 ± 4.9 (3)	n.d.
9	80.6 ± 10.3 (3)	n.d.
10	72.4 ± 10.7 (3)	n.d.
11	76.1 ± 7.7 (3)	n.d.
12	106.7 ± 7.8 (3)	n.d.
13	99.7 ± 0.9 (2)	n.d.
14	86.6 ± 11.9 (3)	n.d.

[a] The binding affinities were studied as described in the ESI[1] and are expressed as mean ± SEM of residual [³H]PDBu binding (% of control) with 100 μM ligand concentration. The number of independent experiments is presented in brackets for each value. n.d. – not determined.

(Fig. 7A), showing a binding profile very similar to that of the reference compound **1** (IC_{50} = 37.5 μM). The retro-ester derivatives **3–5** also exhibited clear concentration-dependent binding to the C1 domain of PKCα (Fig. 7B), although they were less potent than compounds **1** and **2** in displacing [³H]PDBu. However, no significant displacement of [³H]PDBu was observed for the retro-amides **6–14**, not even at the highest concentration (100 μM) tested (Table 2). Only compounds **10–11** displaced 27.6% and 23.9% of [³H]PDBu at 100 μM concentration, respectively, but exhibited no clear concentration–response (data not shown). The poor affinities of the retro-amides were contradictory to our molecular modeling predictions, in which their affinities were expected to be similar to those of the ester derivatives. However, this is in line with our observations with the isophthalate derivatives, in which the substitution of the esters with the respective amides diminished the binding affinity.[19]

For PKCδ, the results were consistent with those obtained from the PKCα binding assays: compounds **1** and **2** exhibited the highest affinity (IC_{50} values of 33.2 μM and 39.9 μM, respectively; Fig. 8A), while compounds **3–5** displaced
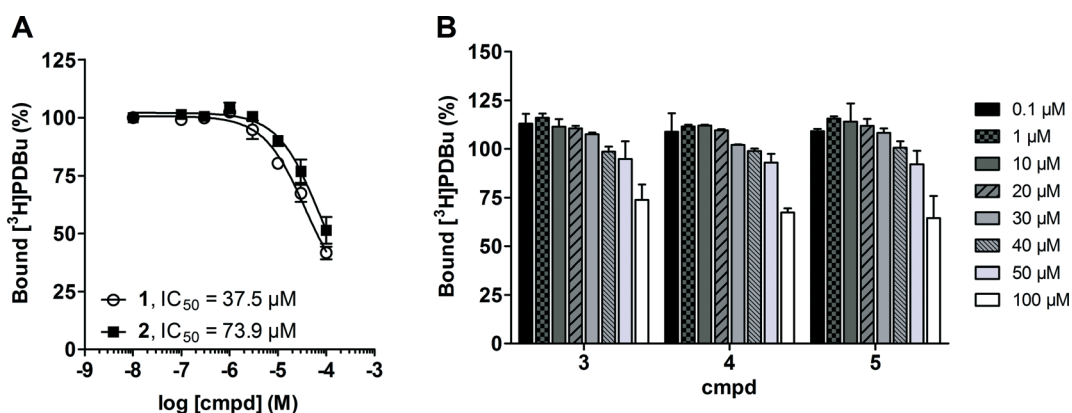
Fig. 7 Binding of compounds **1–5** to PKCα. Affinities of **1**, **2** and **3–5** for PKCα were determined as described in the ESI† and are presented as percentage of control (DMSO). (A) Results are expressed as mean ± SEM of 4 independent experiments. IC_{50} values were calculated with GraphPad Prism 5 software. (B) Results are expressed as mean ± SEM of 2 independent experiments.

Fig. 8 Binding of compounds **1–5** to PKCδ. Affinities of **1**, **2** and **3–5** for PKCδ were determined as described in the ESI† and are presented as percentage of control (DMSO). (A) Results are expressed as mean ± SEM of 4 independent experiments. IC_{50} values were calculated with GraphPad Prism 5 software. (B) Results are expressed as mean ± SEM of 2 independent experiments.

552 | *Med. Chem. Commun.*, 2015, **6**, 547–554

This journal is © The Royal Society of Chemistry 2015

[³H]PDBu from PKCδ in a concentration-dependent manner (Fig. 8B), but with lower potency.

Based on the biological results discussed so far, **1** and **2** were selected to be further investigated. Since the enantiomers of a biologically active molecule may behave differently under physiological conditions (*i.e.*, they can exhibit different pharmacodynamic and/or pharmacokinetic properties as well as different toxicological profiles), the investigation of enantiopure forms is a key step in the drug discovery process.[30] Accordingly, we evaluated the ability of the pure enantiomers of **1** and **2** to displace [³H]PDBu from the C1 domain of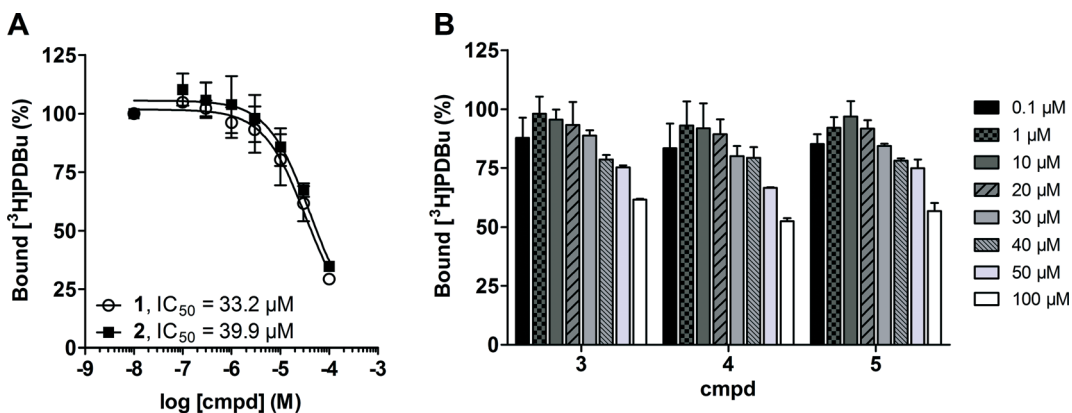 PKC, according to the methodology described above. Results showed that, for both compounds **1** and **2**, the *dextro* (**1A** and **2A**) and the *levo* (**1B** and **2B**) isomers possess almost the same binding profile as the corresponding racemates (displacement at 100 μM equal to: 34.6% for **1A**, 36.3% for **1B**, 27.3 for **2A** and 26.3 for **2B**), thus suggesting that chirality does not seem to play a significant role in the ligand–target interaction.

Conclusion

In an attempt to study the impact of modifying template IV on the affinity for the C1 domain of PKC, we designed and prepared thirteen novel analogues of compound **1**, characterized by different functionalities at the carbonyl group as well as different aromatic substitutions. In contrast to our molecular modeling predictions, the results of PKC binding assays suggested that replacing the ester group with the amide one determines the total loss of affinity. This experimental evidence is consistent with the SAR consideration previously drawn for compounds belonging to the template III series.[18] Indeed, also for the isophthalate derivatives, moving from esters to amides led to a dramatic decrease in the binding affinity for the C1 domain of PKC,[18] even though molecular modeling suggested that the amides should interact similarly with the target. Moreover, the results obtained in our study clearly revealed that the presence of the ester function is essential for the ligand–target interaction, as widely demonstrated by numerous studies (for an overview see the reviews in bibliography[31,32]). Furthermore, it can be seen from our study that to preserve the C1 domain affinity only a few structural modifications at the ester group are allowed. Indeed, only the normal ester derivative **2** showed affinity for the C1 domain of PKC comparable to that of the reference compound **1**, while the retro-ester derivatives **3–5** bound to the target more loosely, thus suggesting that the medicinal chemistry impact of modifying the normal ester functional group is very high, independently of the aromatic moiety of the molecules.

Finally, as regards the role of chirality in the ligand–target interaction, we showed that the C1 domain of PKC does not exhibit enantiopreference for the pure stereoisomers of compounds **1** and **2**.

Collectively, our observations provide further insights into the ligand–target interactions of the PKC C1 domain and represent a step-forward in future development of more specific and effective PKC ligands. Particularly, the most interesting feature of the results presented herein appears to be the observation that, at least for ligands belonging to the template IV series, only a few structural modifications are tolerated by the C1 domain of PKC.

Abbreviations

AD	Alzheimer's disease
Bn	Benzyl
Cmpd	Compound
DAG	Diacylglycerol
DCE	1,2-Dichloroethane
DCM	Dichloromethane
DMF	*N,N*-Dimethylformamide
MW	Microwave
[³H]PDBu	[³H]-Phorbol 12,13-dibutyrate
PKC	Protein kinase C
THF	Tetrahydrofuran
TBAC	Tetrabutylammonium chloride

Acknowledgements

References

1 A. C. Newton, *Chem. Rev.*, 2001, **101**, 2353–2364.

2 F. Battaini and D. Mochly-Rosen, *Pharmacol. Res.*, 2007, **55**, 461–466.

3 C. House and B. E. Kemp, *Science*, 1987, **238**, 1726–1728.

4 A. C. Newton, *J. Biol. Chem.*, 1995, **270**, 28495–28498.

5 S. F. Steinberg, *Physiol. Rev.*, 2008, **88**, 1341–1378.

6 E. A. Van der Zee, P. G. Luiten and J. F. Disterhoft, *Prog. Neuropsychopharmacol. Biol. Psychiatry*, 1997, **21**, 531–572.

7 A. Pascale, X. Noguès, A. Marighetto, J. Micheau, F. Battaini, S. Govoni and R. Jaffard, *NeuroReport*, 1998, **9**, 725–729.

8 S. Govoni, M. Amadio, F. Battaini and A. Pascale, *Curr. Pharm. Des.*, 2010, **16**, 660–671.

9 F. Battaini, *Pharmacol. Res.*, 2001, **44**, 353–361.

10 J. Hofmann, *Curr. Cancer Drug Targets*, 2004, **4**, 125–146.

11 P. M. Blumberg, N. Kedei, N. E. Lewin, D. Yang, G. Czifra, Y. Pu, M. L. Peach and V. E. Marquez, *Curr. Drug Targets*, 2008, **9**, 641–652.

12 Y. S. Bynagari-Settipalli, R. Chari, L. Kilpatrick and S. P. Kunapuli, *Cardiovasc. Hematol. Disord.: Drug Targets*, 2010, **10**, 292–308.

13 D. Mochly-Rosen, K. Das and K. V. Grimes, *Nat. Rev. Drug Discovery*, 2012, **11**, 937–957.

14 R. Etcheberrigaray, M. Tan, I. Dewachter, C. Kuiperi, I. Van der Auwera, S. Wera, L. Qiao, B. Bank, T. J. Nelson,

This journal is © The Royal Society of Chemistry 2015

Med. Chem. Commun., 2015, **6**, 547–554 | **553**

A. P. Kozikowski, F. Van Leuven and D. L. Alkon, *Proc. Natl. Acad. Sci. U. S. A.*, 2004, **101**, 11141–11146.

15 Y. Baba, Y. Ogoshi, G. Hirai, T. Yanagisawa, K. Nagamatsu, S. Mayumi, Y. Hashimoto and M. Sodeoka, *Bioorg. Med. Chem. Lett.*, 2004, **14**, 2963–2967.

16 V. E. Marquez and P. M. Blumberg, *Acc. Chem. Res.*, 2003, **36**, 434.

17 J. H. Kang, M. A. Siddiqui, N. E. Lewin, Y. Pu, D. M. Sigano, P. M. Blumberg, J. Lee and V. E. Marquez, *Org. Lett.*, 2004, **6**, 2413.

18 G. Boije af Gennäs, V. Talman, O. Aitio, E. Ekokoski, M. Finel, R. K. Tuominen and J. Yli-Kauhaluoma, *J. Med. Chem.*, 2009, **52**, 3969–3981.

19 J. Lee, J. H. Lee, S. Y. Kim, N. A. Perry, N. E. Lewin, J. A. Ayres and P. M. Blumberg, *Bioorg. Med. Chem.*, 2006, **14**, 2022–2031.

20 G. Zhang, M. G. Kazanietz, P. M. Blumberg and J. H. Hurley, *Cell*, 1995, **81**, 917–924.

21 (*a*) K. Sugita, C. F. Neville, M. Sodeoka, H. Sasai and M. Shibasaki, *Tetrahedron Lett.*, 1995, **36**, 1067–1070; (*b*) M. Sodeoka, K. Uotsu and M. Shibasaki, *Tetrahedron Lett.*, 1995, **36**, 8795–8798; (*c*) M. G. Kazanietz, J. J. Barchi, J. G. Omichinski and P. M. Blumberg, *J. Biol. Chem.*, 1995, **270**, 14679–14684.

22 S. Collina, M. Urbano, A. Magnani, G. Loddo and O. Azzolina, *Lett. Org. Chem.*, 2006, **3**, 16.

23 D. Rossi, A. Marra, P. Picconi, M. Serra, L. Catenacci, M. Sorrenti, E. Laurini, M. Fermeglia, S. Pricl, S. Brambilla, N. Almirante, M. Peviani, D. Curti and S. Collina, *Bioorg. Med. Chem.*, 2013, **21**, 2577–2586.

24 M. A. Umbreit and K. B. Sharpless, *J. Am. Chem. Soc.*, 1977, **99**, 5526–5528.

25 S. Collina, G. Loddo, M. Urbano, L. Linati, A. Callegari, F. Ortuso, S. Alcaro, C. Laggner, T. Langer, O. Prezzavento, G. Ronsisvalle and O. Azzolina, *Bioorg. Med. Chem.*, 2007, **15**, 771–783.

26 G. Keglevich, E. Balint, E. Karsai, J. Varga, A. Grun, M. Balint and I. Greiner, *Lett. Org. Chem.*, 2009, **6**, 535–539.

27 J. Xia, J. Song, L. Zhen, X. Zhang, X. Lei, L. Zheng, Q. Wang and H. Sun, *Bioorg. Med. Chem.*, 2011, **21**, 3894–3897.

28 P. Lesimple and D. C. H. Bigg, *Synthesis*, 1991, 306–309.

29 R. Gaggeri, D. Rossi, S. Collina, B. Mannucci, M. Baierl and M. Juza, *J. Chromatogr. A*, 2011, **1218**, 5414–5422.

30 (*a*) I. Agranat, H. Caner and J. Cadwell, *Nat. Rev. Drug Discovery*, 2002, **1**, 753–768; (*b*) T. Andersson, *Clin. Pharmacokinet.*, 2004, **43**, 279–285.

31 P. M. Blumberg, N. Kedei, N. E. Lewin, D. Yang, G. Czifra, Y. Pu, M. L. Peach and V. E. Marquez, *Curr. Drug Targets*, 2008, **9**, 641–652.

32 J. Das and G. M. Rahman, *Chem. Rev.*, 2014, **114**, 12108–12131.

BEYOND THE AFFINITY FOR PROTEIN KINASE C: EXPLORING 2-PHENYL-3-HYDROXYPROPYL PIVALATE ANALOGUES AS C1 DOMAIN-TARGETING LIGANDS.

DANIELA ROSSI,[1] VIRPI TALMAN,[2] GUSTAV BOIJE AF GENNÄS,[3] ANNAMARIA MARRA,[1] PIETRO PICCONI,[1] RITA NASTI,[1] MASSIMO SERRA,[1] JIHYAE ANN,[4] MARIALAURA AMADIO,[5] ALESSIA PASCALE,[5] RAIMO K. TUOMINEN,[2] JARI YLI-KAUHALUOMA,[3] JEEWOO LEE,[4] SIMONA COLLINA[1]

[1]*Department of Drug Sciences, Medicinal Chemistry and Pharmaceutical Technology Section, University of Pavia, Viale Taramelli 12, 27100 Pavia, Italy*
[2]*Division of Pharmacology and Pharmacotherapy, Faculty of Pharmacy, Viikinkaari 5 E (P.O. Box 56), FI-00014 University of Helsinki, Finland*
[3]*Division of Pharmaceutical Chemistry and Technology, Faculty of Pharmacy, Viikinkaari 5 E (P.O. Box 56), FI-00014 University of Helsinki, Finland*
[4]*Laboratory of Medicinal Chemistry, College of Pharmacy, Seoul National University, Seoul 151-742, Korea*
[5]*Department of Drug Sciences, Pharmacology Section, University of Pavia, Viale Taramelli 14, 27100 Pavia, Italy*

Table of contents
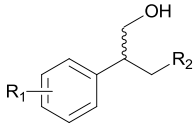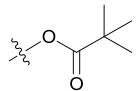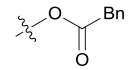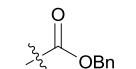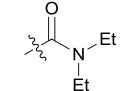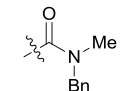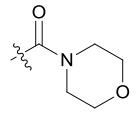
1. Molecular Simulations

The docking studies were performed with the crystal structure of PKCδ C1b domain complexed with phorbol-13-O-acetate (Protein Data Bank code: 1PTR).[1] The crystal structure was modified as previously described.[2] Briefly, phorbol-13-O-acetate was removed from the crystal structure, and the hydrogens and the side chains of Lys 234, Arg 273, and Glu 274 were added to the protein. The structure was then energy minimized and used for ligand docking.

SOMA$_2$, the Open Source Molecular Modelling Workflow Environment of the Finnish Center for Scientific Computing,[3] was used in the ligand geometry optimization and ligand docking studies. Firstly, the structures of the ligands were cleaned and the hydrogens added to the compounds. CORINA v3.2 [4] was used in the 2D to 3D optimization of the ligands and the basic settings were utilized, except that CORINA was forced to generate stereoisomeric compounds from the input files. Next, the docking simulations were performed with GOLD v5.1 [5] where the binding cavity of the protein was set to the carbonyl oxygen atom of Leu 251 (atom number 168) with an active site radius of 10 Å. With the predefined settings in GOLD, eight docking runs of each ligand were executed. The docking scores can be found in Table 1.

Table 1. Docking scores of PKCδ C1b domain for the enantiomers of the designed compounds.

Compound	R₁	R₂	Docking score
1	4-BnO		57.02 (*S*) / 62.45 (*R*)
2	4-BnO		66.54 (*S*) / 68.34 (*R*)
3	4-BnO		67.24 (*S*) / 69.19 (*R*)
4	3-BnO		69.09 (*S*) / 66.29 (*R*)
5	biphen-4-yl		57.86 (*S*) / 60.69 (*R*)
6	4-BnO		56.09 (*S*) / 64.42 (*R*)
7	3-BnO		59.95 (*S*) / 61.16 (*R*)
8	biphen-4-yl		48.29 (*S*) / 56.31 (*R*)
9	4-BnO		64.76 (*S*) / 65.16 (*R*)
10	3-BnO		68.54 (*S*) / 64.88 (*R*)
11	biphen-4-yl		54.92 (*S*) / 59.26 (*R*)
12	4-BnO		56.15 (*S*) / 64.69 (*R*)
13	3-BnO		61.90 (*S*) / 62.09 (*R*)
14	biphen-4-yl		47.89 (*S*) / 55.93 (*R*)

2. Chemistry

2.1 General

Reagents and solvents for synthesis were obtained from Aldrich (Italy). Unless otherwise specified, the commercially available reagents were used as received from the supplier. Solvents were purified according to the guidelines in Purification of Laboratory Chemicals.[6] Microwave dielectric heating

was performed in a Discover® LabMate instrument (CEM Corporation) specifically designed for organic synthesis and following an appropriate microwave program. Melting points were measured on SMP3 Stuart Scientific apparatus and are uncorrected. Analytical thin-layer-chromatography (TLC) was carried out on silica gel precoated glass-backed plates (Fluka Kieselgel 60 F254, Merck) and visualized by ultra-violet (UV) radiation, acidic ammonium molybdate (IV), or potassium permanganate. Flash chromatography (FC) was performed with Silica Gel 60 (particle size 230–400 mesh, purchased from Nova Chimica). IR spectra were recorded on a Jasco FT/IR-4100 spectrophotometer with ATR module; only noteworthy absorptions are given. Proton nuclear magnetic resonance (NMR) spectra were recorded on a Bruker Avance 400 spectrometer operating at 400.13 MHz or JEOL JNM-LA 300 at 300 MHz. Proton chemical shifts (δ) are reported in ppm with the solvent reference relative to tetramethylsilane (TMS) employed as the internal standard (CDCl$_3$, δ = 7.26 ppm; CD$_2$Cl$_2$, δ = 5.32 ppm; [D$_6$]acetone, δ = 2.05 ppm). The following abbreviations are used to describe spin multiplicity: s = singlet, d = doublet, t = triplet, q = quartet, m = multiplet, br = broad signal, dd = doublet-doublet, td = triplet-doublet. The coupling constant values are reported in Hz. ^{13}C NMR spectra were recorded on a 400 MHz spectrometer operating at 100.56 MHz, with complete proton decoupling. Carbon chemical shifts (δ) are reported in ppm relative to TMS with the respective solvent resonance as the internal standard (CDCl$_3$, δ = 77.23 ppm; CD$_2$Cl$_2$, δ = 54.00 ppm; [D$_6$]acetone, δ = 29.84 ppm).

HPLC-UV-ESI/MS analyses were carried out on a Thermo Scientific LCQ FLEET system (LCQ FLEET ion trap mass spectrometer, Surveyor MS Pump/Autosampler/PDA Detector) using an ESI source operating in positive ion mode, controlled by Xcalibur software 1.4 (Thermo Finnigan). Analyses were run on a Synergi Fusion-RP 80A (0.2 cm diameter × 5 cm length, 4 μm) column, at room temperature, with gradient elution (solvent A: acetonitrile containing 0.1% of formic acid; solvent B: water containing 0.1% of formic acid; gradient: 10% A in B to 100% A in 4 min, followed by isocratic elution 100% A for 3 min) at a flow rate of 0.3 mL min^{-1}. All of the final compounds had 95% or greater purity.

Chiral HPLC runs were conducted on a Jasco HPLC system equipped with a Jasco AS-2055 plus autosampler, a PU-2089 plus quaternary gradient pump, and an MD-2010 plus multi-wavelength detector. Experimental data were acquired and processed by Jasco Borwin PDA and Borwin Chromatograph Software. Solvents used were HPLC grade and supplied by Carlo Erba.

Optical rotation values were measured on a Jasco photoelectric polarimeter DIP 1000 using a 0.5 dm cell and a mercury lamp (λ=405 nm); sample concentration values (c) are given in 10^{-2}g mL^{-1}

2.2 Synthesis of 1 and 2

*Synthesis of 4-(benzyloxy)benzyl alcohol (**15**)*

A solution of 4-benzyloxy benzaldehyde (1.5 g, 7.1 mmol) in diethyl ether was treated with lithium aluminum hydride (0.794 g, 21.2 mmol) at 0 ºC and then refluxed for 30 min. The reaction mixture was allowed to reach room temperature, cooled at 0 ºC, carefully quenched with ice-water followed by 15% aqueous sodium hydroxide and finally extracted with diethyl ether. The organic phase was washed with water, dried over magnesium sulfate, and concentrated *in vacuo*. The residue was purified by FC on silica gel eluting with ethyl acetate/*n*-hexane (30/70, v/v), yielding **15** as a white solid, 1.36 g (90%). ^{1}H NMR (CDCl$_3$, 300 MHz) δ 4.62 (d, 2H, J = 5.88 Hz, CH_2OH), 5.07 (s, 2H, OCH_2Ph), 6.95 (d, 2H, J = 8.58 Hz, ArH), 7.24-7.45 (m, 7H).

*Synthesis of 4-(benzyloxy)benzyl chloride (**16**)*

A solution of **15** (1.20 g, 5.6 mmol) in dichloromethane (DCM) was treated with thionyl chloride (0.911 mL, 11.2 mmol, 2 equiv.) at 0 ºC and stirred for 1 h at the same temperature. The reaction mixture was then concentrated *in vacuo*. The residue was diluted in DCM and the resulting solution was washed with water, dried over magnesium sulfate and concentrated *in vacuo*, yielding compound **16**, as a white solid, 1.18 g (91%), that was used for the next step without further purification. ^{1}H NMR (CDCl$_3$, 300 MHz) δ 4.60 (s, 2H, CH_2Cl), 5.07 (s, 2H, OCH_2Ph), 6.95 (d, 2H, J = 8.58 Hz, ArH), 7.24-7.45 (m, 7H).

*Synthesis of 2-[4-(benzyloxy)phenyl]acetonitrile (**17**)*

A mixture of **16** (1.0 g, 4.3 mmol) and sodium cyanide (0.526 g, 10.8 mmol, 2.5 equiv.) in *N,N*-dimethylformamide (DMF) was heated at 100 °C for 2 h. The reaction mixture was allowed to reach room temperature, diluted with water and then extracted with ethyl acetate. The combined organic layers were washed with water, dried over magnesium sulfate and concentrated *in vacuo*. The residue was purified by FC on silica gel eluting with ethyl acetate/*n*-hexane (20/80, v/v), furnishing **17** as a white solid, 0.940 g (98%). ^{1}H NMR (CDCl$_3$, 400 MHz) δ 3.66 (s, 2H, CH_2CN), 5.05 (s, 2H, OCH_2Ph), 6.95 (d, 2H, J = 8.60 Hz, ArH), 7.21 (d, 2H, J = 8.60 Hz, ArH), 7.31-7.41 (m, 5H).

*Synthesis of 2-[4-(benzyloxy)phenyl]acetic acid (**18**)*

A solution of **17** (0.92 g, 4.1 mmol) in 30% aq. sodium hydroxide (19 mL) was refluxed overnight. The reaction mixture was allowed to reach room temperature, neutralized with 1N aqueous hydrochloric acid, added with 1N aqueous sodium hydroxide (pH~10) and then extracted with ethyl

acetate. The aqueous layer was made acidic by adding 1N aqueous hydrochloric acid (pH~1) and the resulting mixture was then extracted with ethyl acetate. The organic layer was washed with water, dried over magnesium sulfate and concentrated in *vacuo*, yielding **18** as pale yellow solid, 0.898 g (90%). ^{1}H NMR (CDCl$_3$, 300 MHz) δ 3.60 (s, 2H, C*H$_2$*CN), 5.05 (s, 2H, OC*H$_2$*Ph), 6.94 (d, 2H, *J* = 8.79 Hz, Ar*H*), 7.21 (d, 2H, *J* = 8.79 Hz, Ar*H*), 7.31-7.41 (m, 5H).

Synthesis of methyl 2-[4-(benzyloxy)phenyl]acetate (19)

The carboxylic acid **18** (0.88 g, 3.6 mmol) was dissolved in methanol and the resulting solution was treated with sulfuric acid (a couple of drops) at 0 ℃. The mixture was refluxed for 2 h and then allowed to reach room temperature. The reaction mixture was concentrated in *vacuo*, diluted with water and extracted with ethyl acetate. The organic layer was washed with water, dried over magnesium sulfate and evaporated. The residue was purified by FC on silica gel eluting with ethyl acetate/*n*-hexane (30/70, v/v) to furnish **19** as yellow oil, 0.763 g (82%). ^{1}H NMR (CDCl$_3$, 300 MHz) δ 3.56 (s, 2H, C*H$_2$*CO$_2$CH$_3$), 3.69 (s, 3H, CO$_2$C*H$_3$*), 5.05 (s, 2H, OC*H$_2$*Ph), 6.94 (d, 2H, *J* = 8.61 Hz, Ar*H*), 7.20 (d, 2H, *J* = 8.61 Hz, Ar*H*), 7.31-7.44 (m, 5H).

Synthesis of dimethyl 2-[4-(benzyloxy)pheny]malonate (20)

A solution of **19** (0.750 g, 2.9 mmol) in 1,4-dioxane was treated with sodium hydride (0.210 g, 8.7 mmol, 3equiv.) at 0 ℃ and stirred at room temperature for 30 min. Dimethyl carbonate (29.4 ml) was then added at 0 ℃ and the resulting mixture was refluxed for 2 days. The reaction mixture was then diluted with water at 0 ℃ and extracted with ethyl acetate. The organic layer was washed with water, dried over magnesium sulfate and concentrated in *vacuo*. The residue was purified by FC on silica gel eluting with ethyl acetate/*n*-hexane (20/80, v/v), yielding **20** as pale yellow solid, 0.559 g (61%). ^{1}H NMR (CDCl$_3$, 300 MHz) δ 3.75 (s, 6H, 2x CO$_2$C*H$_3$*), 4.59 (s, 1H, ArC*H*), 5.05 (s, 2H, OC*H$_2$*Ph), 6.96 (d, 2H, *J* = 8.61 Hz, Ar*H*), 7.29-7.44 (m, 7H).

Synthesis of 2-(4-(benzyloxy)phenyl)propane-1,3-diol (21)

A solution of lithium aluminium hydride (0.170 g, 5.1 mmol, 3 equiv.) in tetrahydrofuran (THF) was cooled at 0 ℃. A solution of **20** (0.540 g, 1.71 mmol) in THF was then added dropwise to the reaction mixture. The resulting mixture was stirred at room temperature for 2 h, cooled at 0 ℃ and then carefully diluted with water. A 15% aqueous solution of sodium hydroxide was then added dropwise and the resulting mixture was stirred for 1 h, filtrated and concentrated in *vacuo*. The residue was purified by FC eluting with ethyl acetate/*n*-hexane (50/50, v/v), furnishing **21** as white solid, 0.310 g (70%). ^{1}H NMR (CDCl$_3$, 400 MHz) δ 3.07 (m, 1H, ArC*H*), 3.80 (m, 4H, 2x C*H$_2$*OH),

5.04 (s, 2H, OCH_2Ph), 6.88 (d, 2H, J = 8.60 Hz, ArH), 7.05 (d, 2H, J = 8.60 Hz, ArH), 7.29-7.44 (m, 5H).

General procedure for synthesis of 1 and 2

A solution of **21** (0.150 g, 0.6 mmol) in DCM was cooled at 0 °C and pyridine (0.045 mL, 0.6 mmol, 1 equiv.) was added to this solution. The resulting solution was stirred for 10 min. Pivaloyl chloride (0.067 mL, 0.6 mmol, 1 equiv., for **1**) or 2-phenylacetyl chloride (0.75 mL, 0.6 mmol, 1 equiv., for **2**) was then added to the solution at 0 °C and the resulting mixture was stirred for 2 h at room temperature. The reaction mixture was washed with water and brine, dried over magnesium sulfate and concentrated in *vacuo*. The residue was purified by FC eluting with ethyl acetate/*n*-hexane (20/80, v/v) for compound **1** or ethyl acetate/hexane (50/50, v/v) for compound **2.**

2-[4-(Benzyloxy)phenyl]-3-hydroxypropyl pivalate (1). White solid, 0.127 g (64%). Mp 49.7-53.0 °C; IR (v_{max}/cm^{-1}): 1725 (m s C=O$_{ester}$), 3435 (m b OH $_{alcohol}$). ^{1}H-NMR data comply with those reported in the literature. [7] ^{13}C NMR (CDCl$_3$, 100 MHz) δ 27.6, 39.3 (s), 47.1, 64.3 (t), 65.4 (t), 70.4 (t), 115.5, 127.9, 128.4, 129.0, 129.6, 131.6 (s), 137.4 (s), 158.4 (s), 179.3 (s). t_R 3.50 min, λ: 254 nm. MS (ESI) m/z 343.01 [M+H]$^+$, m/z 704.26 [4M+NH$_4^+$+Na$^+$]$^{m/2}$.

2-[4-(Benzyloxy)phenyl]-3-hydroxypropyl 2-phenylacetate (2). White solid, 0.111 g (51%)**.** Mp 42.6-44.5 °C. IR (v_{max}/cm^{-1}): 1732 (m s C=O$_{ester}$), 3469 (m b OH $_{alcohol}$). ^{1}H NMR (CDCl$_3$, 400 MHz) δ 1.72–1.91 (br s, 1H, *OH, exchanges with D$_2$O*), 3.10 (quin, J = 6.3 Hz, 1H, –CHCH$_2$OCO), 3.65 (s, 2H, PhCH_2CO), 3.72–3.81 (m, 2H, –CHCH_2OH), 4.34 (dd, J = 7.0, 11.1 Hz, 1H, –CHCH_2OCO), 4.44 (dd, J = 5.9, 11.1 Hz, 1H, –CHCH_2OCO), 5.07 (s, 2H, –OCH_2Ph), 6.93 (d, J = 8.7 Hz, 2H, ArH), 7.10 (d, J = 8.6 Hz, 2H, ArH), 7.22–7.50 (m, 10H, ArH) ^{13}C NMR (CDCl$_3$, 100 MHz) δ 41.9 (t), 46.9, 64.3 (t), 66.0 (t), 70.4 (t), 115.5, 127.6, 127.9, 128.5, 129.1 (2C), 129.6, 129.7, 131.4 (s), 134.2 (s), 137.4 (s), 158.4 (s), 172.2 (s). t_R : 3.47min, λ: 274 nm. MS (ESI) m/z 377.01 [M+H]$^+$, m/z 772.51 [4M+NH$_4^+$+Na$^+$]$^{m/2}$

2.3 Synthesis of compounds 3-14

General procedure for synthesis of 28-30.

To a solution of the appropriate aryl bromide (**22**, **23** or **24**, 2.5 g, 1 equiv.) in DMF (40 mL), tetra-*n*-butylammonium chloride (TBAC, 2 equiv.), anhydrous sodium acetate (2 equiv.), palladium (II) acetate (0.05 equiv.) and methyl but-2-enoate (1.5 equiv.) were sequentially added. The reaction

mixture was refluxed overnight under stirring, filtered through Celite eluting with DCM, concentrated in *vacuo* and finally extracted with water. The organic layer was dried over sodium sulfate and evaporated in *vacuo*. The residue was dissolved in 1,2-dichloroethane (120 mL, DCE) and to this solution was added selenium dioxide (0.8 equiv.) and *tert*-butyl hydroperoxide (4 equiv.). The resulting mixture was refluxed overnight under stirring, filtered, concentrated under *vacuo* (~ 40 mL) and extracted with water. The organic layer was dried over sodium sulfate and evaporated to dryness. The residue was purified with FC eluting with *n*-hexane/ethylacetate (70/30, v/v).

4-(4-Benzyloxyphenyl)-5H-furan-2-one (28).

Compound **28** was synthesized according to the general procedure using **22** (2.5 g, 9.5 mmol) to yield 1.02 g (41%), white powder, mp 146.6-149.1 °C. ^{1}H NMR (CDCl$_3$, 400 MHz) δ 5.15 (s, 2H, -OC*H*$_2$Ph), 5.21 (d, *J* = 1.6 Hz, 2H, O-CH*H*), 6.27 (t, *J* = 1.6 Hz, 1H, -C(O)-C*H*=C), 7.06 (d, *J* = 8.8 Hz, 2H, ArH), 7.35-7.51 (m, 7H, ArH).

4-(3-Benzyloxyphenyl)-5H-furan-2-one (29).

Compound **29** was synthesized according to the general procedure using **23** (2.5 g, 9.5 mmol) to yield 0.834 g (33%), yellow powder, mp 108.7-110.2 °C.^{1}H-NMR (CDCl$_3$, 400 MHz) δ 5.14 (s, 2H, -OC*H*$_2$Ph), 5.21 (d, *J* = 1.6 Hz, 2H, O-CH*H*), 6.37 (t, *J* = 1.6 Hz, 1H, -C(O)-C*H*=C), 7.09-7.16 (m, 3H, ArH), 7.35-7.53 (m, 6H, ArH).

4-Biphenyl-4-yl-5H-furan-2-one (30).

Compound **30** was synthesized according to the general procedure using **24** (2.5 g, 10.7 mmol) to yield 1.36 g (54%), yellow powder, mp 164.6-165.8 °C (lit.,[8] 176 °C).^{1}H NMR (CDCl$_3$, 400 MHz) δ 5.30 (d, *J* =1.5 Hz, 2H, O-CH*H*), 6.44 (t, *J* =1,5 Hz, 1H, -C(O)-C*H*=C), 7.39-7.47 (m, 1H, ArH), 7.51 (t, *J* = 7.7 Hz, 2H, ArH), 7.58–7.68 (m, 4H, ArH), 7.73 (d, *J* = 8.3 Hz, 2H, ArH).

*General procedure for synthesis of **31-33**.*

To a solution of the appropriate α,β-unsaturated γ-butyrolactone (**28**, **29** or **30**, 0.4 g, 1 equiv.) in absolute ethanol (40 mL), ammonium formate (5 equiv.) and 10% Pd/C (0.07 equiv.) were added. The reaction mixture was irradiated with a microwave power of 100 W, at 100 °C for 180 s, then filtered through Celite eluting with DCM and concentrated in *vacuo*. The residue was dissolved in ethyl acetate and washed with water. The organic phase was then dried over sodium sulfate and evaporated to dryness.

4-(4-Hydroxyphenyl)dihydrofuran-2-one (31).

Compound **31** was synthesized according to the general procedure using **28** (0.4 g, 1.5 mmol) to yield 0.253 g (95%), yellow powder, mp 119.4-121 °C (lit.,[9] 120-121 °C). ^{1}H NMR (CDCl$_3$, 400 MHz) δ 2.65 (dd, J = 9.2, 17.5 Hz, 1H, -C(O)-CHH); 2.92 (dd, J = 8.6, 17.5 Hz, 1H, -C(O)-CHH), 3.70-3.80 (m, 1H, ArCH), 4.21-4.28 (m, 1H, O-CHH), 4.63-4.70 (m, 1H, , O-CHH), 4.80-5.96 (brs, 1H, ArH), 6.85 (d, J = 8.5 Hz, 2H, ArH), 7.12 (d, J = 8.6 Hz , 2H, ArH).

4-(3-Hydroxyphenyl)dihydrofuran-2-one (32).

Compound **32** was synthesized according to the general procedure using **29** (0.4 g, 1.5 mmol) to yield 0.253 g (95%), yellow oil. ^{1}H NMR (CDCl$_3$, 400 MHz) δ 2.69 (dd, J = 8.7, 17.6 Hz, 1H, -C(O)-CHH), 2.94 (dd, J = 8.7, 17.6, 1H, -C(O)-CHH), 3.69–3.82 (m, 1H, ArCH), 4.25–4.34 (m, 1H, O-CHH), 4.63–4.73 (m, 1H, O-CHH), 5.80–6.46 (brs, 1H, ArH), 6.73–6.76 (m, 1H, ArH), 6.76–6.83 (m, 2H, ArH), 7.24 (t, J = 7.9 Hz, 1H, ArH).

4-Biphenyl-4-yldihydrofuran-2-one (33).

Compound **33** was synthesized according to the general procedure using **30** (0.4 g, 1.7 mmol) to yield 0.384 g (95%), white powder, mp 164.6-165.3 °C. ^{1}H NMR (CDCl$_3$, 400 MHz) δ 2.70 (dd, J = 9.1, 17.5 Hz, 1H, -C(O)-CHH); 2.94 (dd, J = 8.7, 17.5 Hz, 1H, -C(O)-CHH), 3.76-3.88 (m, 1H, ArCH), 4.25-4.33 (m, 1H, O-CHH), 4.65-4.72 (m, 1H, O-CHH), 7.27-7.37 (m, 3H, ArH), 7.43 (t, J = 7.3 Hz, 2H, ArH), 7.53-7.61 (m, 4H, ArH).

*General procedure for the synthesis of **34**-**35***

To a solution of the appropriate precursor (**31** or **32**, 0.240 g, 1 equiv.) in acetonitrile (25 mL), caesium carbonate (1 equiv.) and benzyl bromide (1.2 equiv.) were subsequently added. The reaction mixture was irradiated with a microwave power of 60 W, at 100 °C for 40 min, then filtered and evaporated to dryness. The residue was purified by FC eluting with *n*-hexane to *n*-hexane/ethylacetate (70/30, v/v).

4-(4-Benzyloxyphenyl)dihydrofuran-2-one (34).

Compound **34** was synthesized according to the general procedure using **31** (0.240 g, 1.34 mmol) to yield 0.344 g (95%), white powder, mp 131.0-132.3 °C. ^{1}H-NMR (CDCl$_3$, 400 MHz) δ 2.65 (dd, J = 9.3, 17.5 Hz, 1H, -C(O)-CHH), 2.92 (dd, J = 8.6, 17.5 Hz, 1H, -C(O)-CHH), 3.70-3.81 (m, 1H, O-CHH), 4.21-4.28 (m, 1H, O-CHH), 4.63-4.69 (m, 1H, ArCH), 5.09 (s, 2H, -OCH_2Ph), 6.99 (d, J = 8.7 Hz, 2H, ArH), 7.17 (d, J = 8.6 Hz, 2H, ArH), 7.34-7.38 (m, 1H, ArH), 7.38-7.47 (m, 4H, ArH).

4-(3-Benzyloxy-phenyl)-dihydro-furan-2-one (35).

Compound **35** was synthesized according to the general procedure using **32** (0.240 g, 1.34 mmol) to yield 0.344 g (95%), brown oil. ^{1}H NMR (CDCl$_3$, 400 MHz) δ 2.68 (dd, *J* = 9.1, 17.4 Hz, 1H, -C(O)-C*H*H); 2.93 (dd, *J* = 8.7, 17.4 Hz, 1H, -C(O)-C*H*H), 3.73-3.83 (m, 1H, O-CH*H*), 4.24-4.31 (m, 1H, O-CH*H*), 4.64-4.70 (m, 1H, ArC*H*), 5.09 (s, 2H, -OC*H*$_2$Ph), 6.83-6.88 (m, 2H, ArH), 6.91-6.95 (m, 1H, ArH), 7.30-7.49 (m, 6H, ArH).

General procedure for synthesis of retro-ester derivatives 3-5

To a solution of the appropriate γ-butyrolactone (**33**, **34** or **35,** 0.1 g, 1 equiv.) in methanol (18 mL), a 10% aqueous solution of sodium hydroxide (0.420 mL) was added. The mixture was refluxed for 3 h and then evaporated *in vacuo.* The residue was dissolved in water/DMF (1/10, v/v, 10 mL) and potassium carbonate (1 equiv.) and benzyl bromide (5 equiv.) were then sequentially added to the solution. The resulting mixtures was stirred at room temperature overnight, filtered and evaporated to dryness in *vacuo* at room temperature. The residue was dissolved in diethyl ether and washed with water. The organic layer was dried over sodium sulfate and evaporated to dryness in *vacuo* at room temperature. The residue was purified by FC eluting with DCM/methanol/diethylamine (99/1/0.1, v/v/v). The final products were stored at -20 °C under nitrogen.

3-(4-Benzyloxyphenyl)-4-hydroxybutyric acid benzyl ester (3)

Compound **3** was synthesized according to the general procedure using **34** (0.1 g, 0.37 mmol) to yield 0.048 g (34%), yellow oil. IR (ν$_{max}$/cm^{-1}): 1156 (m s C-C(=O)-O), 1729 (m s C=O$_{ester}$), 2871 and 2920 (w C-H$_{arom}$), 3421(m b OH). ^{1}H-NMR (CDCl$_3$, 400 MHz) δ 1.63–1.93 (br s, *OH*, partially overlapped with H$_2$O signal, *exchanges with D$_2$O*), 2.70 (dd, *J* = 8.0, 15.5 Hz, 1H, –CH*CH$_2$*CO), 2.87 (dd, *J* = 7.0, 15.5 Hz, 1H, –CH*CH$_2$*CO), 3.35 (quin, *J* = 6.9 Hz, 1H, –*CH*CH$_2$CO), 3.73 (dd, *J* = 6.9, 10.9 Hz, 1H, –CH*CH$_2$*OH), 3.78 (dd, *J* = 6.6, 10.9 Hz, 1H, –CH*CH$_2$*OH), 5.06 (s, 2H, –*CH$_2$*O), 5.08 (s, 2H, –*CH$_2$*OCO), 6.95 (d, *J* = 8.7 Hz, 2H, ArH), 7.16 (d, *J* = 8.7 Hz, 2H, ArH), 7.23–7.28 (m, 2H, ArH), 7.32–7.48 (m, 8H, ArH). *t$_R$*: 3.51 min, λ: 273 nm. MS (ESI): *m/z* 376.93 [M+H]$^+$, *m/z* 772.40 [4M+NH$_4$$^+$+Na$^+$]$^{m/2}$.

3-(3-Benzyloxyphenyl)-4-hydroxybutyric acid benzyl ester (4)

Compound **4** was synthesized according to the general procedure using **35** (0.1 g, 0.37 mmol) to yield 0.041 g (29%), white oil. IR (ν$_{max}$/cm^{-1}): 694, 736, 1024, 1151 (m s C-C(=O)-O), 1729 (m s C=O$_{ester}$), 2870 and 2924 (w C-H$_{arom}$), 3426 (m b OH). ^{1}H-NMR (CDCl$_3$, 400 MHz) δ 2.73 (dd, *J* = 7.6, 15.7 Hz, 1H, –CH*CH$_2$*CO), 2.87 (dd, *J* = 7.6, 15.7 Hz, 1H, –CH*CH$_2$*CO), 3.37 (quin, *J* = 6.9

Hz, 1H, –*CH*CH$_2$CO), 3.76 (dd, J = 6.5, 10.9 Hz, 1H, –CH*CH$_2$*OH), 3.81 (dd, J = 6.5, 10.9 Hz, 1H, –CH*CH$_2$*OH), 5.04 (s, 2H, –*CH$_2$*O), 5.09 (s, 2H, –*CH$_2$*OCO), 6.83–6.92 (m, 3H, ArH), 7.23–7.30 (m, 3H, ArH), 7.31–7.48 (m, 8H, ArH). ^{13}C NMR (CDCl$_3$, 100 MHz) δ 37.6 (t), 44.9, 66.9 (t), 67.3 (t), 70.4 (t), 113.7, 115.0, 120.7, 128.0, 128.4, 128.6 (2C), 128.9, 129.0, 130.2, 136.2 (s), 137.3 (s), 142.9 (s), 159.5 (s), 172.7 (s). t_R: 3.47 min, λ: 273 nm. MS (ESI): m/z 377.02 [M+ H]$^+$, m/z 772.78 [4M+NH$_4^+$+Na$^+$]$^{m/2}$.

3-Biphenyl-4-yl-4-hydroxy-butyric acid benzyl ester (5)

Compound **5** was synthesized according to the general procedure using **33** (0.1 g, 0.41 mmol) to yield 0.123 g (84%), yellow oil. IR (v_{max}/cm^{-1}): 1149 (m s C-C(=O)-O), 1727 (m s C=O$_{ester}$), 2942 (w C-H$_{arom}$), 3402 (m b OH). ^{1}H NMR (DMSO-d_6, 400 MHz) δ 2.68 (dd, J = 9.8, 15.6 Hz, 1H, –CH*CH$_2$*CO), 2.95 (dd, J = 5.3, 15.6 Hz, 1H, –CH*CH$_2$*CO), 3.16–3.26 (m, 1H, –*CH*CH$_2$CO), 3.47–3.55 (m, 1H, –CH*CH$_2$*OH, dd after exchange with D$_2$O, J = 7.6, 10.5 Hz), 3.55–3.62 (m, 1H, –CH*CH$_2$*OH, dd after exchange with D$_2$O, J = 6.0, 10.5 Hz), 4.85 (t, J = 5.3 Hz, 1H, *OH*, exchanges with D$_2$O), 5.00 (s, 2H, –*CH$_2$*OCO), 7.14–7.21 (m, 2H, ArH), 7.25–7.39 (m, 6H, ArH), 7.47 (t, J = 7.5 Hz, 2H, ArH), 7.57 (d, J = 8.3 Hz, 2H, ArH), 7.62–7.68 (m, 2H, ArH). t_R: 3.46 min, λ: 254 nm. MS (ESI): m/z 346.98 [M+H]$^+$, m/z 712.75 [4M+NH$_4^+$+Na$^+$]$^{m/2}$.

General procedure for synthesis of retro-amide derivatives 6-14

To a suspension of aluminium chloride (1.3 equiv.) in DCE (1 mL) a solution of the appropriate amine (5 equiv.) in DCE (1 mL) and a solution of the appropriate γ-butyrolactone (**33**, **34** or **35,** 0.05 g, 1 equiv.) in DCE (1 mL) were sequentially added. The reaction mixture was irradiated with a microwave power of 60 W, at 100 °C for 25 min, and evaporated to dryness. The residue was dissolved in ethyl acetate and washed with 0.1 M hydrochloric acid. The organic layer was dried over sodium sulfate and evaporated *in vacuo*. The residue was purified by FC eluting with ethyl acetate/methanol (95/5, v/v).

3-(4-Benzyloxy-phenyl)-4-hydroxy-but-2-enoic acid diethylamide (6).

Compound **6** was synthesized according to the general procedure using **34** (0.07 g, 0.29 mmol) to yield 0.056 g (61%), white powder, mp: 83.6-85.5 °C. IR (v_{max}/cm^{-1}): 1240 (w C-N-H), 1608 (n C=O$_{amide}$), 2929 (m NH), 3443 (m b OH). ^{1}H NMR (DMSO-d_6, 400 MHz), a mixture of rotamers, δ 0.91 (t, J = 7.0 Hz, 3H, –NCH$_2$*CH$_3$*), 1.02 (t, J = 7.0 Hz, 3H, –NCH$_2$*CH$_3$*), 2.48 (dd, J = 8.4, 15.4 Hz, 1H, –CH*CH$_2$*CO), 2.68 (dd, J = 5.7, 15.4 Hz, 1H, –CH*CH$_2$*CO), 3.10–3.27 (m, 5H, –N(*CH$_2$*CH$_3$)$_2$ + –*CH*CH$_2$CO), 3.48 (t, J = 6.1 Hz, 2H, –CH*CH$_2$*OH), 4.65 (t, J = 5.3 Hz, 1H, OH,

exchanges with D_2O), 5.06 (s, 2H, $-OCH_2Ph$), 6.89 (d, $J = 8.6$ Hz, 2H, ArH), 7.13 (d, $J = 8.6$ Hz, 2H, ArH), 7.29–7.47 (m, 5H, ArH). ^{13}C NMR (DMSO-d_6, 100 MHz), a mixture of rotamers, δ 13.9, 15.2, 36.1 (t), 39.8 (t), 42.1 (t), 44.6, 66.1 (t), 69.9 (t), 115.1, 128.4, 128.6, 129.3, 129.7, 136.3 (s), 138.2 (s), 157.5 (s), 170.9 (s). t_R: 3.08 min, λ: 273 nm. MS (ESI): m/z 342.28 [M+H]$^+$, m/z 683.08 [2M+H]$^+$.

3-(3-Benzyloxyphenyl)-4-hydroxybut-2-enoic acid diethylamide (7).

Compound **7** was synthesized according to the general procedure using **35** (0.05 g, 0.19 mmol) to yield 0.039 g (60%), yellow oil. IR (v_{max}/cm^{-1}): 1258 (w C-N-H), , 1607 (n C=O$_{amide}$), 2870, 2931 and 2972 (m N-H) , 3366 (m b O-H) ; ^1H NMR (DMSO-d_6, 400 MHz). a mixture of rotamers, δ 0.92 (t, $J = 7.0$ Hz, 3H, $-NCH_2CH_3$), 1.02 (t, $J = 7.0$ Hz, 3H, $-NCH_2CH_3$), 2.52 (dd, $J = 8.2$, 15.6 Hz, 1H, $-CHCH_2CO$), 2.70 (dd, $J = 5.8$, 15.6 Hz, 1H, $-CHCH_2CO$), 3.13–3.29 (m, 5H, $-N(CH_2CH_3)_2 + -CHCH_2CO$), 3.52 (t, $J = 6.0$ Hz, 2H, $-CHCH_2OH$), 4.70 (t, $J = 5.3$ Hz, 1H, OH, exchanges with D_2O), 5.06 (s, 2H, $-OCH_2Ph$), 6.78–6.85 (m, 2H, ArH), 6.86–6.90 (m, 1H, ArH), 7.17 (t, $J = 7.9$ Hz, 1H, ArH), 7.30–7.36 (m, 1H, ArH), 7.40 (t, $J = 7.2$ Hz, 2H, ArH), 7.45 (d, $J = 7.2$ Hz, 2H, ArH). ^{13}C NMR (DMSO-d_6, 100 MHz), a mixture of rotamers, δ 13.9, 15.2, 35.8 (t), 40.2 (t), 42.1 (t), 45.4, 65.9 (t), 69.9 (t), 112.9, 115.5, 121.4, 128.5, 128.6, 129.3, 129.8, 138.1 (s), 145.9 (s), 159.0 (s), 170.8 (s). t_R: 3.08 min, λ: 273 nm. MS (ESI): m/z 342.31 [M+H]$^+$, m/z 682.51 [2M+ H]$^+$.

3-Biphenyl-4-yl-N,N-diethyl-4-hydroxybutyramide (8).

Compound **8** was synthesized according to the general procedure using **33** (0.1 g, 0.37 mmol) to yield 0.034 g (27%), white powder, mp 100.6-101.7 °C. IR (v_{max}/cm^{-1}): 1490 (m C-N), 1617 (n C=O), 2870 and 2918 (m NH), 3349 (m b OH). ^1H-NMR (DMSO-d_6, 400 MHz), a mixture of rotamers, δ 0.92 (t, $J = 7.0$ Hz, 3H, $-NCH_2CH_3$), 1.05 (t, $J = 7.0$ Hz, 3H, $-NCH_2CH_3$), 2.58 (dd, $J = 8.3$, 15.6 Hz, 1H, $-CHCH_2CO$), 2.76 (dd, $J = 5.8$, 15.6 Hz, 1H, $-CHCH_2CO$), 3.11–3.32 (m, 5H, $-N(CH_2CH_3)_2 + -CHCH_2CO$), 3.56 (t, $J = 6.1$ Hz, 2H, $-CHCH_2OH$), 4.76 (t, $J = 5.3$ Hz, 1H, OH, exchanges with D_2O), 7.29–7.38 (m, 3H, ArH), 7.45 (t, $J = 7.6$ Hz, 2H, ArH), 7.55 (d, $J = 8.1$ Hz, 2H, ArH), 7.63 (t, $J = 7.4$ Hz, 2H, ArH). ^{13}C NMR (DMSO-d_6, 100 MHz), a mixture of rotamers, δ 13.8, 15.1, 35.8 (t), 40.2 (t), 42.2 (t), 45.0 (2C), 65.8 (t), 65.9 (t), 127.1, 127.3, 128.0, 129.4, 129.8, 138.8 (s), 141.0 (s), 143.4 (s), 170.9 (s). t_R: 3.11 min, λ: 254 nm, MS (ESI): m/z 312.28 [M+H]$^+$, m/z 622.89 [2M+H]$^+$.

3-(4-Benzyloxyphenyl)-4-hydroxybut-2-enoic acid N-benzyl-N-methylamide (9).

Compound **9** was synthesized according to the general procedure using **34** (0.05 g, 0.19 mmol) to yield 0.039 g (54%), yellow oil. IR (v_{max}/cm^{-1}): 1238 (w C-N-H), 1609 (n C=O$_{amide}$), 2922 and 3030 (m N-H), 3405 (m b O-H). ^{1}H NMR (DMSO-d_6, 400 MHz), a mixture of rotamers, δ 2.58–2.71 (m, 1H, –CH*CH₂*CO), 2.72 (s, 1H, –N*CH₃*), 2.78 (dd, J = 5.5, 15.6 Hz, 1H, –CH*CH₂*CO), 2.85 (s, 2H, –N*CH₃*), 3.14–3.24 (m, 1H, –*CH*CH₂CO), 3.37–3.57 (m, 2H, –CH*CH₂*OH), 4.34 (d, J = 15.0 Hz, 0.65H, –N*CH₂*Ph), 4.51 (d, J = 15.0 Hz, 0.65H, –N*CH₂*Ph), 4.53–4.57 (m, 0.7H, –N*CH₂*Ph), 4.65 (t, J = 5.3 Hz, 0.35 H, OH, exchanges with D₂O), 4.70 (t, J = 5.3 Hz, 0.65 H, OH, exchanges with D₂O), 5.02–5.12 (m, 2H, –O*CH₂*Ph), 6.86–6.94 (m, 2H, ArH), 6.94–7.00 (m, 1.4H, ArH), 7.05–7.12 (m, 1.4H, ArH), 7.14–7.30 (m, 3.7H, ArH), 7.33 (t, J = 7.1 Hz, 1.6 H, ArH), 7.40 (t, J= 7.1 Hz, 2H, ArH), 7.45 (d, J= 7.8 Hz, 1.9H, ArH). ^{13}C NMR (DMSO-d_6, 100 MHz). a mixture of rotamers, δ 34.3, 35.8, 35.9 (t), 36.1 (t), 44.5, 44.8, 50.7 (t), 53.2 (t), 66.2 (t), 66.4 (t), 70.0 (t), 115.2, 127.3, 127.7, 128.0, 128.1, 128.5, 128.6, 129.1, 129.3, 129.5, 129.7, 129.8, 136.0 (s), 136.1 (s), 138.2 (s), 138.4 (s), 138.6 (s), 157.6 (s), 157.7 (s), 172.2 (s), 172.3 (s). t_R: 3.26 min, λ: 273 nm, MS (ESI): *m/z* 390.30 [M+H]$^+$, *m/z* 779.01 [2M+H]$^+$.

*3-(3-Benzyloxyphenyl)-4-hydroxybut-2-enoic acid N-benzyl-N-methylamide (**10**).*

Compound **10** was synthesized according to the general procedure using **35** (0.05 g, 0.19 mmol) to yield 0.046 g (63%), yellow oil. IR (v_{max}/cm^{-1}): 1255 (w C-N-H), 1607 (n C=O$_{amide}$), 2867 and 2921 (m N-H), 3374 (m b O-H). ^{1}H NMR (DMSO-d_6, 120 °C, 400 MHz), a mixture of rotamers, δ 2.67 (dd, J = 7.8, 15.5 Hz, 1H, –CH*CH₂*CO), 2.79–2.86 (m, 4H, –CH*CH₂*CO + –N*CH₃*), 3.29 (quint, J = 6.3 Hz, 1H, –*CH*CH₂CO), 3.57–3.67 (m, 2H, –CH*CH₂*OH), 4.15–4.25 (br s, 1H, OH, exchanges with D₂O), 4.47 (d, J = 15.5 Hz, 1H, –N*CH₂*Ph), 4.52 (d, J = 15.5 Hz, 1H, –N*CH₂*Ph), 5.09 (s, 2H, –O*CH₂*Ph), 6.81–6.88 (m, 2H, ArH), 6.90–6.95 (m, 1H, ArH), 7.11 (d, J = 7.2 Hz, 2H, ArH), 7.18 (t, J = 7.9 Hz, 1H, ArH), 7.20–7.34 (m, 4H, ArH), 7.35–7.41 (m, 2H, ArH), 7.42–7.47 (m, 2H, ArH).^{13}C NMR (DMSO-d_6, 100 MHz), a mixture of rotamers, δ 34.3, 35.6 (t), 35.7, 35.8 (t), 45.3, 45.6, 50.7 (t), 53.2 (t), 66.0 (t), 66.2 (t), 70.0 (t, 2C), 112.9, 113.0, 115.4, 115.5, 121.5, 121.6, 127.3, 127.7, 128.0, 128.1, 128.6 (2C), 128.7, 129.2, 129.3, 129.5, 129.8, 129.9, 136.0 (s), 138.1 (s), 138.4 (s), 138.6 (s), 145.6 (s), 145.7 (s), 159.1 (s, 2C), 172.1 (s), 172.2 (s). t_R: 3.13 min, λ: 273 nm, MS (ESI): *m/z* 390.30 [M+H]$^+$, *m/z* 779.01 [2M+H]$^+$.

*N-Benzyl-3-biphenyl-4-yl-4-hydroxy-N-methylbutyramide (**11**).*

Compound **11** was synthesized according to the general procedure using **33** (0.05 g, 0.21 mmol) to yield 0.032 g (42 %), yellow powder, mp 81.6-83.7 °C. IR (v_{max}/cm^{-1}): 1263 (w C-N-H), 1415 (m C-N), 1617(n C=O$_{amide}$), 2854 and 2921 (m NH), 3326 (m b OH). ^{1}H NMR (DMSO-d_6, 120°C, 400

MHz), a mixture of rotamers, δ 2.73 (dd, *J* = 7.9, 15.5 Hz, 1H, –CH*CH₂*CO), 2.86–2.94 (m, 4H, –CH*CH₂*CO + –N*CH₃*), 3.36 (quint, *J* = 6.5 Hz, 1H, –*CH*CH₂CO), 3.67 (br s, 2H, –CH*CH₂*OH), 4.26 (br s, 1H, OH, exchanges with D_2O), 4.49 (d, *J* = 15.5 Hz, 1H, –*CH₂*Ph), 4.54 (d, *J* = 15.5 Hz, 1H, –*CH₂*Ph), 7.12 (d, *J* = 7.1 Hz, 2H, ArH), 7.19–7.38 (m, 6H, ArH), 7.45 (t, *J* = 7.5 Hz, 2H, ArH), 7.54 (d, *J* = 8.1 Hz, 2H, ArH), 7.63 (d, *J* = 8.1 Hz, 2H, ArH). ^{13}C NMR (DMSO-d_6, 100 MHz), a mixture of rotamers, δ 34.3, 35.6 (t), 35.8, 35.9 (t), 45.0, 45.3, 50.7 (t), 53.2 (t), 66.1 (t), 66.2 (t), 127.2, 127.3, 127.4, 127.7, 128.0, 128.1, 129.2, 129.4, 129.5, 129.8, 138.4 (s), 138.6 (s), 138.9 (s, 2C), 141.1 (s), 143.3 (s), 143.4 (s), 172.1 (s, 2C). t_R: 3.23 min, λ: 254 nm, MS (ESI): *m/z* 360.30 [M+H]$^+$, *m/z* 718.85 [2M+H]$^+$.

*3-(4-Benzyloxyphenyl)-4-hydroxy-1-morpholin-4-ylbut-2-en-1-one (**12**).*
Compound **12** was synthesized according to the general procedure using **34** (0.05 g, 0.19 mmol) to yield 0.038 g (57.1%), white powder, mp 134.5-135.8 °C. IR (v_{max}/cm^{-1}) 1240 (w C-N-H), 1604 (n C=O$_{amide}$), 2862, 2925 and 3259 (m N-H), 3462 (m b O-H); ^{1}H NMR (DMSO-d_6, 400 MHz), a mixture of rotamers, δ 2.55 (dd, *J* = 8.7, 15.3 Hz, 1H, –CH*CH₂*CO), 2.72 (dd, *J* = 5.5, 15.3 Hz, 1H, –CH*CH₂*CO), 3.10 (quint, *J* = 6.7 Hz, 1H, –*CH*CH₂CO), 3.24–3.43 (m, 6H, MorH), 3.43–3.53 (m, 4H, –CH*CH₂*OH + MorH), 4.68 (t, *J* = 5.3 Hz, 1H, OH, exchanges with D_2O), 5.07 (s, 2H, –O*CH₂*Ph), 6.90 (d, *J* = 8.6 Hz, 2H, ArH), 7.14 (d, *J* = 8.6 Hz, 2H, ArH), 7.22–7.48 (m, 5H, ArH). ^{13}C NMR (DMSO-d_6, 100 MHz), a mixture of rotamers, δ 35.8 (t), 42.3 (t), 44.7, 46.5 (t), 66.2 (t), 66.9 (t), 67.0 (t), 70.0 (t), 115.2, 128.4, 128.6, 129.3, 129.8, 136.0 (s), 138.2 (s), 157.6 (s), 170.8 (s). t_R: 2.75 min, λ: 273 nm, MS (ESI): *m/z* 356.27 [M+H]$^+$, *m/z* 710.89 [2M+H]$^+$.

*3-(3-Benzyloxyphenyl)-4-hydroxy-1-morpholin-4-ylbut-2-en-1-one (**13**).*
Compound **13** was synthesized according to the general procedure using **35** (0.1 g, 0.38 mmol) to yield 0.058 g (44%), white powder, mp 119.8-120.8 °C. IR (v_{max}/cm^{-1}): 1247 (w C-N-H) , 1601(n C=O$_{amide}$) , 2855 and 2926 (m N-H), 3257(m b O-H). ^{1}H NMR (DMSO-d_6, 400 MHz), a mixture of rotamers, δ 2.60 (dd, *J* = 8.5, 15.4 Hz, 1H, –CH*CH₂*CO), 2.73 (dd, *J* = 5.7, 15.4 Hz, 1H, –CH*CH₂*CO), 3.09–3.19 (m, 1H, –*CH*CH₂CO), 3.25–3.45 (m, 6H, MorH), 3.45–3.57 (m, 4H,–CH*CH₂*OH + MorH), 4.72 (t, *J* = 5.3 Hz, 1H, OH, exchanges with D_2O), 5.07 (s, 2H, –O*CH₂*Ph), 6.79–6.86 (m, 2H, ArH), 6.87–6.91 (m, 1H, ArH), 7.18 (t, *J* = 7.9 Hz, 1H, ArH), 7.30–7.36 (m, 1H, ArH), 7.37–7.43 (m, 2H, ArH), 7.43–7.49 (m, 2H, ArH). ^{13}C NMR (DMSO-d_6, 100 MHz), a mixture of rotamers, δ 35.2 (t), 42.3 (t), 45.6, 46.5 (t), 66.0 (t), 66.9 (t), 67.0 (t), 70.0 (t), 113.0, 115.5, 121.5, 128.6, 128.7, 129.3, 129.9, 138.1 (s), 145.6 (s), 159.1 (s), 170.7 (s). t_R: 2.74 min, λ: 273 nm, MS (ESI): *m/z* 356.28 [M+H]$^+$, *m/z* 710.86 [2M+H]$^+$.

*3-Biphenyl-4-yl-4-hydroxy-1-morpholin-4-ylbutan-1-one (**14**).*

Compound **14** was synthesized according to the general procedure using **33** (0.05 g, 0.21 mmol) to yield 0.035 g (51%), white powder, mp 135-136.4 °C. IR (v_{max}/cm^{-1}): 1262 (w C-N-H), 1609 (n C=O$_{amide}$), 2856 and 2964 (m NH), 3361(m b OH). ^{1}H NMR (DMSO-d_6, 400 MHz), a mixture of rotamers, δ 2.66 (dd, J = 8.6, 15.5 Hz, 1H, –CH*CH$_2$*CO), 2.79 (dd, J = 5.5, 15.5 Hz, 1H, –CH*CH$_2$*CO), 3.17–3.27 (m, 1H, –*CH*CH$_2$CO), 3.29–3.54 (m, 8H, MorH), 3.57 (app t, J = 5.9 Hz, 2H, –CH*CH$_2$*OH), 4.76 (t, J = 5.3 Hz, 1H, OH, exchanges with D$_2$O), 7.30–7.38 (m, 3H, ArH), 7.46 (t, J = 7.6 Hz, 2H, ArH), 7.56 (d, J = 8.1 Hz, 2H, ArH), 7.63 (t, J = 7.7 Hz, 2H, ArH). ^{13}C NMR (DMSO-d_6, 100 MHz), a mixture of rotamers, δ 35.6 (t), 42.4 (t), 45.1, 46.4 (t), 66.0 (t), 66.9 (t), 67.0 (t), 127.2, 127.4, 128.0, 129.5, 129.8, 139.0 (s), 141.1 (s), 143.2 (s), 170.7 (s). t_R: 2.73 min, λ: 254 nm, MS (ESI): m/z 326.28 [M+H]$^{+}$, m/z 650.91 [2M+H]$^{+}$.

2.4 Chiral chromatography

In order to identify the optimal experimental conditions for the enantioresolution of **1** and **2**, a standard screening protocol [10] was applied to both Chiralcel OJ-H (0.46 cm diameter × 15 cm length, 5 µm) and Chiralpak IC (0.46 cm diameter × 25 cm length, 5 µm) columns produced by Daicel Industries Ltd. (Tokyo, Japan). Elution conditions experimented include mixtures of *n*-hexane and polar modifiers (ethanol or 2-propanol) as well as alcohols (methanol, ethanol and 2-propanol). Results of the screening protocol are reported in Table 1 as capacity factor (*k*), selectivity (α) and resolution (*Rs*) factors. The retention factor (*k*) was calculated using the equation

$$k = (t_R - t_0)/ t_0$$

where t_R is the retention time and t_0 the dead time (t_0 was considered to be equal to the peak of the solvent front and was taken from each particular run). The enantioselectivity (α) and the resolution factor (R_s) were calculated as follows:

$$\alpha = k_2 / k_1 \text{ and } R_s = 2 (t_{R2} - t_{R1}) / (w_1 + w_2)$$

where t_{R2} and t_{R1} are the retention times of the second and the first eluted enantiomers, and w_1 and w_2 are the corresponding base peak widths.

The enantiomers of **1** and **2** were then completely resolved by a (semi)-preparative process using a Chiralpak^{TM} IC (1cm diameter × 25 cm length, 5 µm), eluting with *n*-hexane/2-propanol (90/10, v/v) at room temperature with a flow rate of 3 mL min^{-1} and 2 mL min^{-1} for **1** and **2**, respectively. The eluate was properly partitioned according with UV profile (detection preformed at 274 nm for compound **1** and 254 nm for compound **2**). Analytical control of collected fractions was performed on a Daicel Chiralpak IC (0.46 cm diameter × 25 cm length, 5 µm) column eluting with *n*-hexane/2-

propanol (90/10, v/v), at room temperature at a flow rate of 1 mL min^{-1} and UV detection at 274 nm for compound **1** and 254 nm for compound **2**. The fractions obtained containing the enantiomers were evaporated at reduced pressure.

*(+)-2-[4-(Benzyloxy)pheny]-3-hydroxypropyl pivalate (**1A**).*

White solid, mp 49.7-53.0 ºC; *e.e.* 99.9% determined by analytical chiral HPLC: t_R: 19.9 min; $[\alpha]_{405}^{20}$: +37.7 (c 0.6 in methanol). Spectroscopic properties comply with those reported for compound **1**.

*(-)-2-[4-(Benzyloxy)phenyl]-3-hydroxypropyl pivalate (**1B**)*

White solid, mp 49.7-53.0 ºC; *e.e.* 99.9% determined by analytical chiral HPLC: t_R: 22.5 min; $[\alpha]_{405}^{20}$: -37.2 (c 0.6 in methanol). Spectroscopic properties comply with those reported for compound **1**.

*(+)-2-[4-(Benzyloxy)phenyl]-3-hydroxypropyl 2-phenylacetate (**2A**)*

White solid, mp 42.6-44.5 ºC; *e.e.* 99.9% determined by analytical chiral HPLC: t_R: 36.7 min; $[\alpha]_{405}^{20}$: +37.5 (c 0.4 in methanol). Spectroscopic properties comply with those reported for compound **2**.

*(-)-2-[4-(Benzyloxy)phenyl]-3-hydroxypropyl 2-phenylacetate (**2B**)*

White solid**,** mp 42.6-44.5 ºC; *e.e.* 99.9% determined by analytical chiral HPLC: t_R: 47.1 min min; $[\alpha]_{405}^{20}$: -37.4 (c 0.4 in methanol). Spectroscopic properties comply with those reported for compound **2**.

Table 2 Screening results for the enantiomer separation of 1 and 2

1

Eluent[a]	Chiracel® OJ-H[b]				Chiralpak® IC[b]			
	k_1	k_2	α	R_s	k_1	k_2	α	R_s
A	1.37		-	-	n.t.	n.t.	n.t.	n.t.
B	0.90		-	-	n.t.	n.t.	n.t.	n.t.
C	0.80		-	-	0.09		-	-
D[c]	0.80		-	-	0.46		-	-
E	7.14	7.45	-	-	2.16		-	-
F	n.t.	n.t.	n.t.	n.t.	8.15	8.33	-	-
G	n.t	n.t	n.t	n.t	n.t.	n.t.	n.t.	n.t.
H	n.t	n.t	n.t	n.t	n.t.	n.t.	n.t.	n.t
I	n.t	n.t	n.t	n.t	n.t	n.t	n.t	n.t
L	3.19	3.43	-	-	n.t	n.t	n.t	n.t
M	7.65	8.27	1.08	0.75	**5.18**	**6.00**	**1.16**	**2.00**
N	19.06	20.75	1.09	1.06	13.25	15.37	1.16	2.50
O	n.t	n.t	n.t	n.t	n.t	n.t	n.t	n.t

2

Eluent[a]	Chiralcel® OJ-H[b]				Chiralpak® IC[b]			
	k_1	k_2	α	R_s	k_1	k_2	α	R_s
A	19.67		-	-	n.t.	n.t.	n.t.	n.t.
B	12.05		-	-	n.t.	n.t.	n.t.	n.t.
C	8.12	9.01	1.11	1.00	0.17		-	-
D[c]	7.85	8.94	1.14	0.93	0.76	0.91	-	-
E	n.t.	n.t	n.t	n.t	3.95	4.60	-	-
F	n.t.	n.t.	n.t.	n.t.	9.57	11.36	1.19	3.09
G	n.t	n.t	n.t	n.t	5.13	5.96	1.16	1.50
H	8.34	9.27	1.11	0.92	n.t	n.t	n.t	n.t
I	8.37.	9.33	1.12	0.92	n.t.	n.t.	n.t.	n.t.
L	-	-	-	-	n.t	n.t	n.t	n.t
M	n.t.	n.t.	n.t.	n.t.	**10.36**	**13.59**	**1.31**	**4.16**
N	n.t	n.t	n.t	n.t	n.t	n.t	n.t	n.t
O	6.63	7.29	-	-	n.t	n.t	n.t	n.t

Bold type indicates the best result obtained

[a] Eluent composition: A: methanol (100); B: methanol/ethanol (50/50,v/v); C: ethanol (100); D: 2-propanol (100); E: *n*-hexane/ethanol (90/10, v/v); F: *n*-hexane/ethanol (95/5, v/v); G: *n*-hexane/ethanol (92/8, v/v); H: *n*-hexane/ethanol (10/90, v/v); I: *n*-hexane ethanol (5/95, v/v); L: *n*-hexane/ 2-propanol (80/20, v/v); M: *n*-hexane/ 2-propanol (90/10, v/v); N: *n*-hexane/ 2-propanol (95/5, v/v); O: *n*-hexane/2-propanol (10/90, v/v). Sample dissolved in 2-propanol; conc. 1mg mL^{-1}, injection volume 10 µL. Detection: λ= 274 nm (compound **1**) - 254 nm (compound **2**).

[b] Flow rate: 1 mL min^{-1}.

[c] Flow rate: 0.5 mL min^{-1}. n.t: not tested

3. Biological Assays

3.1 Materials

[20-^{3}H]Phorbol-12,13-dibutyrate ([^{3}H]PDBu) was custom-labeled by Amersham Radiolabeling Service (GE Healthcare, Little Chalfont, UK). Bovine immunoglobulin G (IgG) and phosphatidyl-L-serine (PS) were acquired from Sigma-Aldrich (Steinheim, Germany) and protease inhibitors (Complete Protease Inhibitor Cocktail Tablets) from Roche (Mannheim, Germany).

3.2 Production of recombinant human PKCα and PKCδ in insect cells.

The cloning of the expression vectors for full-length human recombinant PKCα and PKCδ has been described previously[11,12]. The proteins were produced in baculovirus-infected Sf9 insect cells as described. Briefly, Sf9 cells were infected with an optimized amount of recombinant baculovirus and harvested 2 days postinfection. Cells were then washed with PBS and cell pellets were frozen. Crude cell lysates were prepared by suspending the cells in buffer containing 25 mM Tris-HCl (pH 7.5), 0.5 mM EGTA, 0.1% Triton-X 100, and protease inhibitors according to the manufacturer's instructions. Suspensions were incubated on ice for 30 min and subsequently centrifuged at $16000g$ for 15 min at 4 °C, whereafter the supernatant was collected. The protein concentration was determined and the supernatant was used for [^{3}H]PDBu binding experiments.

3.3 [3H]PDBu binding assay for assessment of binding affinity

The affinity of the synthesized compounds to the C1 domains of PKCα and PKCδ was determined as their ability to compete with radioactively labeled phorbol ester [^{3}H]PDBu for binding to PKC using a filtration-based method as described previously.[2] Briefly, 20 μg of protein/well from the supernatant of Sf9 cell was incubated with the test compound and [^{3}H]PDBu for 10 min at room temperature (RT) in a 96-well filter plate (Millipore, cat. no. MSHVN4B50, Bedford, MA) in a total volume of 125 μL. The reaction buffer consisted of 20 mM Tris-HCl (pH 7.5), 40 μM $CaCl_2$, 10 mM $MgCl_2$, 400 μg mL^{-1} bovine IgG, 50 nM [^{3}H]PDBu, and 0.1 mg/ml phosphatidyl-L-serine. To precipitate the proteins, 125 μL of ice-cold 20% poly(ethylene glycol) 6000 was added, and the plates were shaken rigorously for 15 min at RT, whereafter the filters were washed six times with washing buffer (20 mM Tris-HCl (pH 7.5), 100 μM $CaCl_2$, 5 mM $MgCl_2$). The plates were then dried, liquid scintillant (Optiphase SuperMix; PerkinElmer, Groningen, The Netherlands) was added, plates were equilibrated for at least two hours, and radioactivity was measured with Wallac Microbeta Trilux microplate liquid scintillation counter (PerkinElmer, Waltham, MA). All the test

compounds were diluted into DMSO so that the final DMSO concentration in the assay was 4%, and the results were calculated as percentage of control (DMSO) on the same plate.

4. References

1. G. Zhang, M.G. Kazanietz, P.M. Blumberg, J. H. Hurley, *Cell*,1995, *81*, 917–924.

2. G. Boije af Gennäs, V. Talman, O. Aitio, E. Ekokoski, M. Finel, R. K. Tuominen, J. Yli-Kauhaluoma, *J. Med. Chem.,* 2009*, 52,* 3969-3981.

3. a) T. Kinnunen, T. Nyrönen, P .Lehtovuori, *Chem. Cent. J.*, 2008, *2*, P4, b) P. Lehtovuori, T. Nyrönen, *J. Chem. Inf. Model.,* 2006, *46*, 620-625.

4. a) J. Sadowski, J. Gasteiger, *Chem. Rev.,* 1993, *93*, 2567-2581, b) J. Sadowski, J. Gasteiger, G. Klebe, *J. Chem. Inf. Comput. Sci.,* 1994, *34*, 1000-1008.

5. M.L. Verdonk, J.C. Cole, M.J. Hartshorn, C.W. Murray, R.D. Taylor, *Proteins*, 2003, *52*, 609-623.

6. D.D. Perrin, W.L.F. Armarego, *Purification of Laboratory Chemicals*, Pergamon, Oxford, 3 rd. ed.,1988.

7. J. Lee, J.H. Lee , S.Y. Kim, N.A. Perry , N.E. Lewin, J.A. Ayres, P.M. Blumberg, *Bioorg. Med. Chem.,* 2006*, 14,* 6, 2022-31.

8. P. Thombare, J. Desai, A. Argade, S. Gite, K. Shah, L. Pavase, P. Patel, *Synthetic. Commun.* 2009, *13*, 2423-2429.

9. S. Protti, M. Fagnoni, A. Albini, *J. Am. Chem. Soc.,* 2006, *33*, 10670-10671.

10. a) D. Rossi, A. Pedrali, A. Marra, L. Pignataro, D. Schepmann, B. Wünsch, L. Ye, K. Leuner, M. Peviani, D. Curti, O.Azzolina, S.Collina, *Chirality*, 2013, *25*, 11, 814-22, b) R. Gaggeri, D. Rossi, S. Collina, B. Mannucci, M. Baierl, M. Juza, *J. Chromatogr. A.*, 2011, *1218*, 32, 5414-22.

11. C. Sandler, E. Ekokoski, K.A. Lindstedt, P.J. Vainio, M. Finel, T. Sorsa, P.T. Kovanen, L.M. Golub, K.K. Eklund, *Inflamm. Res.,* 2005, *54*, 304-312.

12. P. Tammela, E. Ekokoski, A. García-Horsman, V. Talman, M.Finel, R.K.Tuominen, P. Vuorela, *Drug. Dev. Res.,* 2004, *63*, 76-87.

Chapter II

1.Introduction

In recent years the role of post-transcriptional processes has become crucial for controlling gene expression. It has been demonstrated that cellular Ribo Nucleic Acids (RNAs) contain more than a hundred structurally distinct post-transcriptional modifications [1] and that some RNA modifications are dynamic and may have critical regulatory roles no less relevant then protein and DNA modifications. There has been evidence of dysfunctional RNA processing in several pathologies such as neurodegenerative diseases [2], and some tumors, like acute myeloid leukemia [3]. In particular, severe neurological disorders are associated with defects at the post-transcriptional level of the brain, thus highlighting the central importance of these mechanisms for neuronal plasticity. Indeed, neurons in particular need to adapt their proteome quickly to modulate synaptic strength according to changing environmental inputs. These findings were possible thanks to the expansion of genome-wide experimental and computational techniques in the last decade that allow the study of protein-RNA and miRNA-RNA interactions with high specificity and resolution (microRNA: a small non-coding RNA also involved in the control of gene expression) [4]. Moreover, the development of experimental methods useful for RNA and ribosome profiling have enabled studies on RNA alternative splicing, editing, methylation, stability and translation [5]. In this way, the study of post-transcriptional modifications occurring on both coding RNAs (mRNA, rRNA, tRNA) and non-coding-RNAs (long non-coding RNA, short non-coding RNA) has been possible.

In the past decade a lot of interest has also been directed toward the role of small RNAs (sRNAs) in bacterial post-transcriptional regulation [6], while more recently attention has been especially focused on RNA-binding proteins (RBPs). RBPs are a large family of proteins able to affect, at different levels, the fate of target mRNAs whose corresponding proteins are fundamental for a number of key cellular functions. Some of them are ubiquitously expressed, while others are localized in specific subcellular compartments (i.e. cytoplasm or nucleus) and/or tissues, mainly in the nervous system. To date, several hundred RBPs have been identified (the most important ones are reported in Table 1), which are all involved in regulating the fate of RNA which has a key role in the post-transcriptional process albeit at distinct levels [7]. Any dysregulation within these pathways may have consequences on gene expression, and hence contribute to the pathogenesis of several neurological diseases such as Alzheimers disease (AD), paraneoplastic neurologic disorder [8,9], Paraneoplastic Opsoclonus Myoclonus Ataxia [10] and cognitive disorders [11-14].

Moreover, a derangement in post-transcriptional mechanisms may also modify the expression of tumor promoters and oncogenes that favor cell proliferation and angiogenesis, thus resulting in cancer growth and development [15].

RBP		localization	role	Rif
Name	**acronym**			
Cytoplasmic Polyadenylation Element binding protein	CPEB	Neuronal dendrites	Regulation of mRNA transcription	[16]
Embryonic Lethal Abnormal Vision proteins	ELAVs	Ubiquitous (HuR) Neuron (HuB, HuC, HuD), gonadis (HuB),	Regulation of mRNA stability and translation, splicing, polyadenylation	[15, 17]
Fragile-X Mental Retardation protein	FMRP	brain	Control of mRNA transport and translation at synapse level	[19]
Fused in sarcoma/Translocated in LipoSarcoma	FUS/ TLS	nucleus	Regulation of RNA biogenesis	[20]
Neuro-Oncological Ventral Antigen	NOVA-1 NOVA-2	differentiated neuron; spinal cord and hindbrain (NOVA-1), neocortex (NOVA-2)	Regulation of alternative splicing of RNA	[21-23]
Polypyrimidine Tract Binding Protein 2	PTBP-2	early post-mitotic neurons, muscle and testis	Repression of alternative splicing	[24]
Transactive Response DNA-Binding Protein 43	TDP-43	nucleus	Involvement in pre-mRNA splicing, mRNA trafficking and turnover	[25]

Table 1: role and localization of the best known RBPs

Embrionic Lethal Abnormal Vision (ELAVs) or Hu proteins in particular have been known to play pivotal roles in neural development and maintenance. In mammals, four ELAV-like proteins are known; these are: HuR (a.k.a ELAVL1), HuB (a.k.a ELAVL2), HuC (a.k.a ELAVL3) and HuD (a.k.a ELAVL4) [26]. HuR is ubiquitously expressed while the other proteins are prevalently expressed in the nervous system and are classified as neuronal ELAV (nELAV). Mammalian ELAVs are characterized by a high degree of sequence homology (70-85%) and are about 40 kDa in size. They contain three RNA Recognition Motif-type (RRM) domains each approximately 90 amino acids long [27]. Their main role is to improve the stability and/or rate of translation of the target mRNAs through the binding to Adenine Uracil Rich elements (ARE sequence) localized in their 3'untranslated region.[28] Indeed, within the RRM1/2 domains is present a specific sequence

able to recognize the ARE-sequence known as RNA recognition sequence. Specific ELAV post-translational modifications, such as phosphorylation mediated by protein kinase C (PKC), represent the final step of signaling cascades capable of affecting the various functions of the ELAVs themselves (see Table 1), with consequences on the downstream expression of the targeted mRNAs. [29] Going into the detail of their functions, literature data has evidenced that the ELAV-like-mediated mRNA stabilization is a mechanism relevant to AD, cancer and cell homeostasis. An overview of the most important targets of four ELAVs is summarized in Table 2.

ELAV	mRNA target	Rif
HuR	TNFα, VEGF, IL-8, COX-2, GM-CFS, cfos, p21, cyclinA, cyclinB1, cyclinD1, INOS, ATF2, p53, p21	[30-41]
HuB	GAP-43	[42, 43]
HuC	MEPC2	[43, 44]
HuD	TNFa, IL-10, GAP-43	[45]

Table 2:ELAVs and their targets

Specifically, HuB and HuC are promoters of neuronal development in both central and peripheral nervous system [46]; HuD plays a key role in the synaptic plasticity processes [47, 48]. Within this context, by activating ELAV cascade PKC activators show potential as disease-modifying drugs in neurodegenerative pathologies such as AD [29]

Furthermore, the activity of HuR has been linked to the development of inflammatory processes. [49] and different studies have also established its importance in promoting cancer pathways which are tightly associated with inflammatory processes [50, 51]. In this regard, HuR may indeed be considered a prognostic factor for different types of cancer.[52]

In conclusion, the relevance of ELAV proteins in the etiology of various pathologies and, as a consequence, their high potential as pharmacological targets is clearly evident. Accordingly, finding small molecules (*i.e.* synthetic organic compounds) able to interact with such a family of proteins can be considered an important challenge for medicinal chemistry.

1.1 Discovery of new Hu's modulators by High Throughput Screening (HTS)

As stated above, research in the field of ELAV protein modulators and RNB modulators in general, is still considered to be a pioneering challenge for medicinal chemists. To date, only a few research groups have approached the ELAVs-mRNA system in their search for novel potential therapeutic agents. Related research studies have been conducted through screenings of a wide number (or extensive database) of commercial compounds on a specific "protein–RNA complex" following the High Throughput Screening (HTS) approach.

Moreover, compounds have been screened using different biological assays based on various detection technologies characterized by a different sensitivity, homogeneity and influence factors. The HTS approaches used for studying the ELAV–mRNA complexes are illustrated in Figure 1. By applying this method, some *hit* compounds characterized by different structural features have been discovered, although no information about the binding mode could be deduced. A brief overview of the recent results in this field are disclosed in the next paragraph, starting from the pioneering work of Meisner [53] until today.
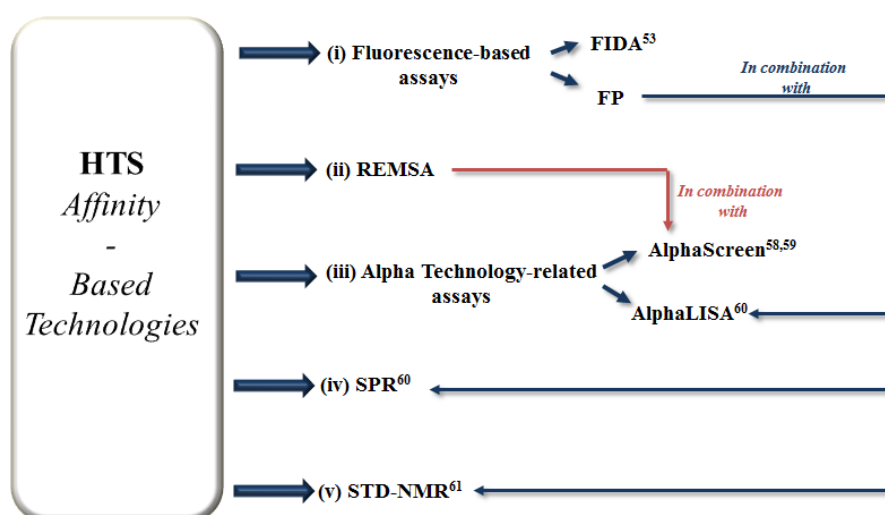

Figure 1

1.2 Dehydromutactin, okicenone and compound MS-444

In 2007, N.C. Meisner and coworkers first approached ELAV-mRNA system from a medicinal chemistry standpoint, particularly focusing on HuR.[53] Within a nature-aided drug discovery program, 50000 different extracts derived from microbial, mycological and plants sources, were screened using a FIDA assay on a shortened variant of recombinant HuR (HuR$_{12}$: amino acids 2–189 equivalent to RRM1/2 domains). The extracts which showed an inhibitory effect on the protein-mRNA interaction were then purified, thus allowing to the isolation of five compounds which were successively fully characterized. Three of the molecules whose relative structures are reported in

Figure 2) evidenced an *in vitro* inhibitory activity of the HuR–mRNA complex in a concentration-dependent manner. More specifically, the experiments were conducted on both full-length protein HuR and the fragment HuR_{12} employing ARE-RNA sequences of TNFα, IL-2, Cox-2 of equal length. (Figure 2) Given the inhibition exerted by **1–3** to the formation of complexes constituted by both the full-length protein and the HuR fragment, the Authors supported the hypothesis that these compounds share the same binding site placed within the RRM1 and RRM2 domains. In light of the positive results obtained and with the purpose of supporting the *in vitro* results, these researchers exploited a mathematical approach for studying the HuR_{12}–RNA interaction mechanism to clarify the mechanism of interaction.

In accordance with previous studies and their experimental data [54, 55] the Authors postulated that ì) HuR exists as homodimer; ii) HuR binds the mRNA in stoichiometric ratio (HuR:RNA, 2:1 and 2:2) and iii) RRM domains could mediate homodimerization. Moreover the *in silico* studies confirmed that compounds **1** and **2** are able to interfere with HuR homodimerization. Taken as a whole, these observations partially clarify the mechanism of interaction among ligands and ELAV protein, highlighting the engagement of RRM sequences in the interaction. More precisely, the binding region may be localized within the RRM sequences or in their proximity. Therefore, the binding of compounds **1** and **2** to the RRM sequences may prevent homodimerization of the protein and, thus to impede the interaction with the ARE-sequence of the mRNA.

In light of this disclosure, this study could be considered a milestone in this field, displaying initial evidence of the chemical druggability of the ELAV protein family.
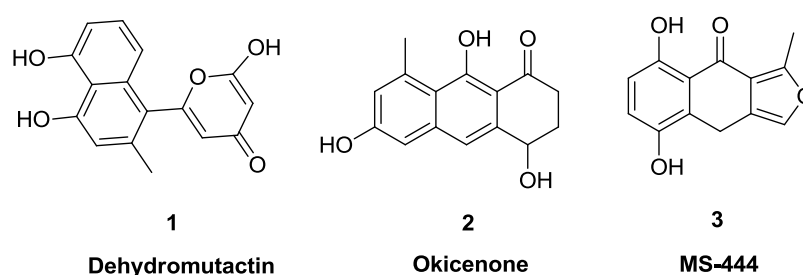

1
Dehydromutactin

2
Okicenone

3
MS-444

Figure 2. Compounds isolated from microbial extract and identified as first HuR inhibitors

1.3 Flavonoids

At the same time W.Y. Park and coworkers identified some flavonoids able to inhibit the HuC–mRNA complex.[56] They screened a library of 52 natural compounds with certain anti-inflammatory and anti- tumorigenic activity (source not reported) employing a non-radioactive RNA electrophoretic mobility gel shift assay (REMSA). Only compounds with drug-like properties, i.e high membrane permeability, low toxicity and suitable size of the molecules (MW<500), have

been screened. The authors used artificial AU-rich ARE sequence recognised by HuC. The compounds library was initially tested at a concentration of 100 μM and the most effective compounds were assayed at low doses thus evidencing 14 molecules able to be effective at low concentration (20, 4 μM). For the most active compounds (Figure 3, Box A), the IC_{50} values were determined. In synthesis, flavonoids **4–9** showed an IC_{50} ranging from 0.2 to 1.4 μM. Starting from these results, W.Y Park and coworkers [57] studied the complex HuR–ARE-mRNA^{TNFα} in order to find new compounds potentially useful in inflammatory diseases. Firstly, an HTS has been applied using a chemical library at the Korea Research Institute of Technology (KRICT). 179 compounds were screened by REMSA at a concentration of 100 μM with recombinant HuR using a cloned-ARE-mRNA^{TNFα}. Thereafter nine candidates were selected on the basis of cut-off >25% indicative of inhibitory effect and the IC_{50} was evaluated by binding filter assay leading the authors to select compounds **9–11** (Figure 3, Box A-B). Interestingly the IC_{50} of compound **9** (1.4 μM) was in line with the previous experiment thus proving the reliability of the protocol. The capability to prevent HuR–mRNAs complex formation of compounds **9–11** were successively evaluated using other cloned-ARE sequences of different mRNAs (IL-6, Cox-2, c-*fos*). Encouraging results showed that compound **9** inhibited only the complex HuR–ARE^{TNFα} at 0.5 μM, whereas compound **10** inhibited both complexes HuR–ARE^{TNFα} and HuR–ARE^{cfos} at low doses (0.25 μM). In addition, HuR–ARE^{IL-6} and ARE^{Cox-2} complexes studied in this work are not affected by **9–11**. Taking into account these experimental data, compounds **9–11** seem to preferentially bind to specific complexes, exerting their activity at different concentrations depending on the complex studied.
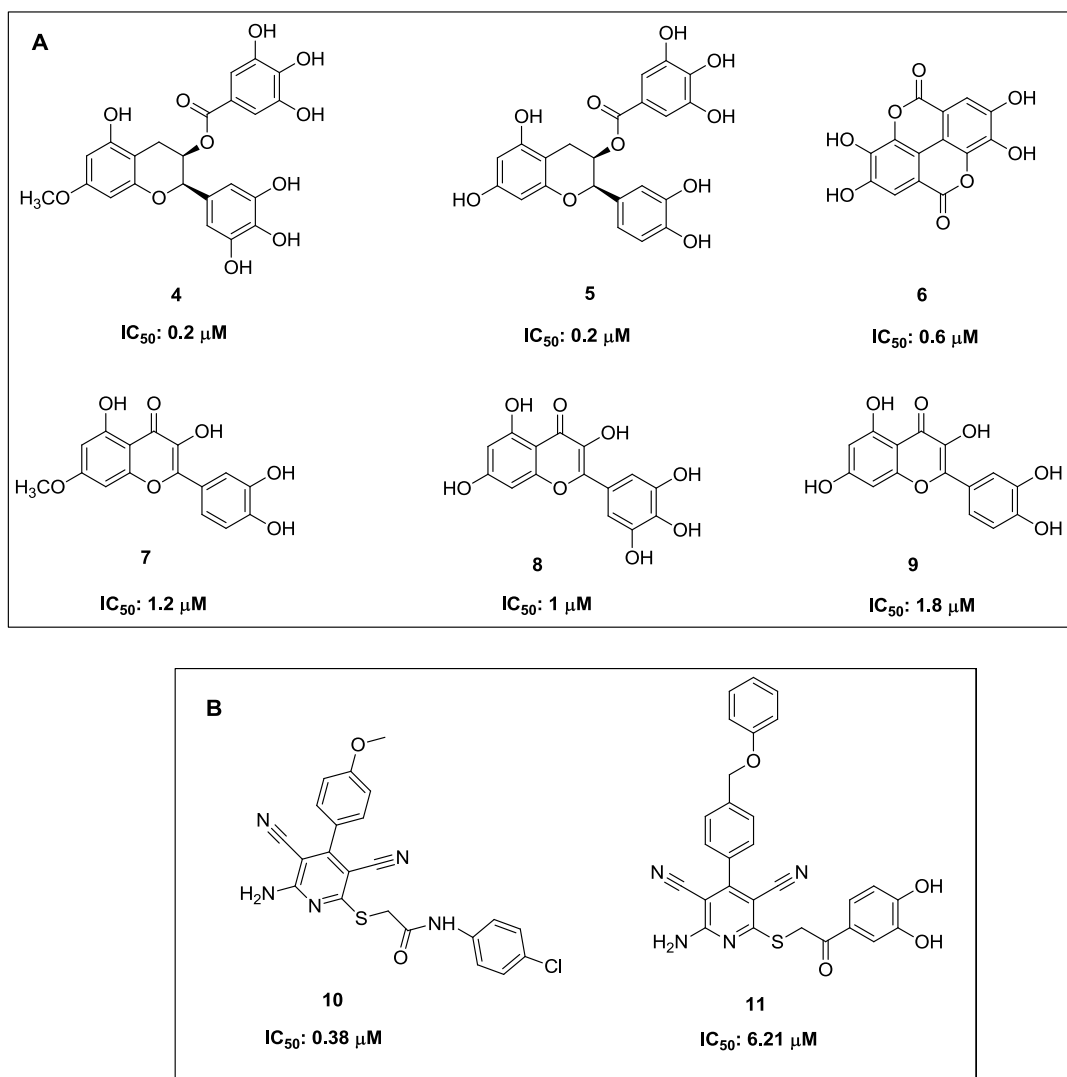
Figure 3. Candidate inhibitors of HuR–ARE[TNFα] complex and related IC$_{50}$ values. Box A: natural compounds from first screening tested on HuC; Box B: compounds from second screening tested on HuR.

1.4 Dihydrotanshinones

A. Provenzani and coworkers [58] recently proposed the AlphaScreen assay as new biochemical tool for HTS useful for identifying new compounds able to interfere with the HuR-RNA complex formation. At the first step, they confirmed the need for HuR dimerization before binding RNA with a stoichiometry of 2:1 (HuR:RNA), fitting the experimental data (AlphaScreen) with a mathematical model. Applying AlphaScreen technology they successfully screened a library of 2000 molecules (source not described) on recombinant HuR (rHuR) in the presence of a biotinylated single-stranded TNFα (Bi-TNF) thus selecting 16 compounds (about 10% of the hits) for an in depth investigation. To this aim and particularly to exclude false-positive results due to technical artifacts as well as to better discriminate between interfering compounds and real inhibitors, the selected compounds were tested by the REMSA assay. Interestingly, mitoxantrone

(**12**) (Figure 4) resulted able to disrupt the HuR–RNA complex, in agreement with the results previously reported, thus confirming the reliability of the assays. Indeed, Meisner *et al.* [53] already evidenced that compounds characterized by anthracenedione scaffolds, might inhibit HuR function. Once the proposed approach has been validated, the authors screened a library of 107 anti-inflammatory agents on the HuR–mRNA$^{TNF\alpha}$ complex, again using Alphascreen assay for selecting hits and REMSA for identifying the most interesting compounds.[59] Among the eight *hits* identified, compound **12** (Figure 4) emerged as the most potent in preventing the complex formation. To test its potential selectivity, the DHTS interaction with other RBPs such as Lin28b, TTP, TDP-43 (Table 2) and HuD was then investigated. As expected in virtue of the high degree of structural similarity with HuR, only the HuD–RNA complex was altered by **12** at the reference dose (5μM). Additionally, the author replicated the experiments using the different combinations of HuR's domains (RRM1 and RRM2; RRM2 and RRM3) in presence of **12** and RNA. As expected, **12** bound the domain RRM1 and RRM2 with an affinity similar to the full-lenght HuR, inhibiting the RRM1 and RRM2-RNA complex formation. Notably, a limited effect of **12** was observed on the binding to RRM2 and RRM3 constructs. For better understand the interaction mechanism, the authors tested the binding of a single RRM domain of HuR (M1, M2 and M3) with RNA in presence of **12**. Compound **12** affects the interaction between M1 and the protein only marginally at a concentration of 5μM. On the light of these results, the author did not exclude the possibility for **12** to interact with the complex at a different site from the RNA-recognition domain.
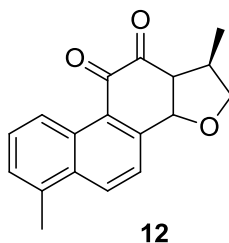
12

IC$_{50}$: **149 ± 34 nM** (REMSA)
68 ±16 nM (AlphaScreen)

Figure 4. Compound **12** (Experimental IC$_{50}$ values was determined by REMSA and AlphaScreen assays)

1.5 Coumarines

Very recently, in 2015, L. Xu and coworkers [60] screened 6,000 molecules present in the KU Chemical Methodologies and Library Development Center and in a library of FDA-approved drugs, through fluorescent polarization (FP) binding assay using a full-length HuR and the ARE sequence from mRNA^{Msi1}. In this way, they selected 38 candidate compounds successively analyzed using ChemMine, a free database which divides compounds into several groups based on structural similarities and physicochemical properties. To compare the different clusters and choose the best

one, the authors selected atom pairs as structural descriptors and Tanimoto coefficients as similarity coefficients. Applying this approach, they identified six coumarine derivatives (compounds **13–18**) able to disrupt the HuR–ARE complex (Figure 5). To evaluate the reliability of the methodology applied compounds **13–18** were further investigated employing the AlphaLISA assay using RRM1/2 domains of HuR and ARE sequence from mRNA[Msi1]. The ability of compounds **13–18** to interfer with the complexes HuR(full length)−ARE[Msi]- mRNA and HuR (RRM1/RRM2 domains)−ARE[Msi] mRNA has been evaluated, using respectively FP and AlphaLISA. Results reported in Table 4 clearly show that lower IC_{50} and K_i values were observed assaying the full-length protein, respect to the truncated protein. To gain further insight into the interaction of HuR with mRNA, the author employed an exploited the Surface Plasmon Resonance (SPR) assay. Again, the experimental data showed that all compounds gave rise to an higher response in the presence of the full-length protein respect the corresponding RRM1 and RRM2 domains. The same experiments conducted on ARE[Bcl-2] and ARE[XIAP] mRNA sequences led to similar results (data not shown). Taken together these data suggest a direct binding of the compounds **13–18** with the protein, but do not without provide information about the binding region involved.

This study is of particular interest since it is the first one to focus deeply on the HuR−mRNA interaction mechanism.
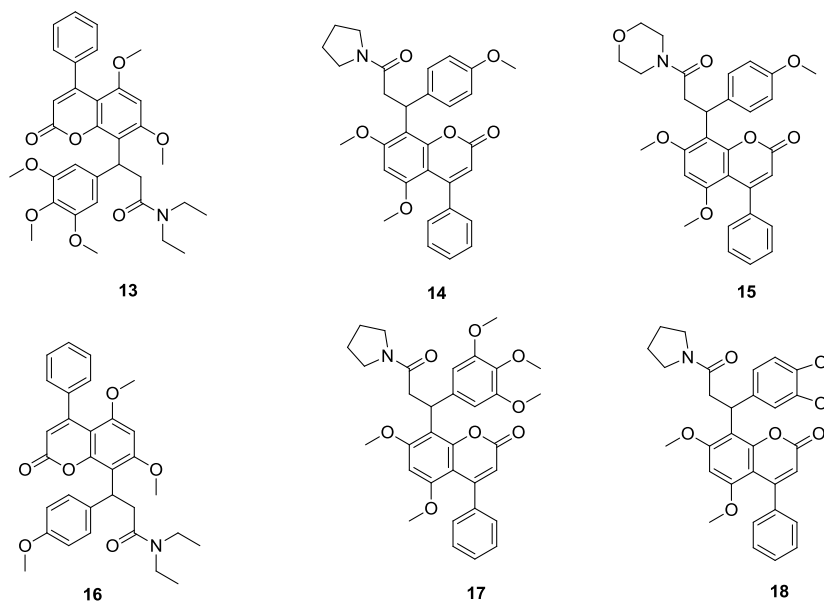

Figure 5. Inhibitors of HuR–ARE[Msi1] interaction with coumarin-derived core

Cmpd	Assay			
	FP[a]: HuR + ARE^{Msi} mRNA		AlphaLISA[b]: RRM1/RRM2+ ARE^{Msi} mRNA	
	IC$_{50}$ (µM)	K$_i$ (µM)	IC$_{50}$ (µM)	K$_i$ (µM)
13	4 ± 1.5	0.59 ± 0.13	12.2 ± 2.4	5.1 ± 0.9
14	2.4 ± 0.5	0.35 ± 0.03	8.2 ±1.0	3.4 ± 0.4
15	5.1 ± 1.5	0.80 ± 0.12	15.7 ± 0.5	6.5 ± 0.2
16	3.7 ± 0.9	0.57 ± 0.07	11.0 ± 0.8	4.6 ± 0.3
17	6.7 ± 2.2	1.10 ± 0.21	17.6 ± 1.3	7.3 ± 0.5
18	6.6 ± 1.8	1.05 ± 0.18	16.5 ± 1.3	6.9 ± 0.5

[a]: experiments performed with 10 nM HuR protein and 2nM fluorescein-labeled Msi-1mRNA
[b]: experiments performed with 100 nM HuR RRM1/RRM2 protein and 25 nM biotin-labeled Msi-1mRNA
Table 3. IC$_{50}$ and K$_i$ values calculated in presence of full-length protein or RRM1/RRM2 HuR domains

1.6 Other compounds

During the same year Z. Wang and coworkers [61] screened 1597 compounds belonging to the "*NCI diversity set V library*" by Fluorescent Polarization (FP) to evaluate their ability to inhibit the HuR–mRNA^{cfos} complex. Based on the results obtained, the authors identified 12 compounds (Figure 6) with IC$_{50}$ values ranging from 2.7 to 97.4 μM. Nevertheless, only the structures of 4 compounds are shown (**19–22**). To remove false-positive results, they optimized a secondary screening by Saturation Transfer Difference-NMR (STD-NMR). The study was conducted initially on **20** and **22** and then extended to the other compounds. Surprisingly, for the other data published previously, 10 μM of HuR was used despite its low solubility (< 3μM). The ^{1}H-^{15}N HSQC spectrum of the ^{15}N-labeled full-length protein showed that very few signals were visible and they displayed poor spectral dispersion. These signals are only due to the flexible portions of the protein given that the folded domains could be involved in the oligomerization process. The successive addition of **22** to this solution in a ratio of 2:1 (**22**:HuR) involved a change of HSQC spectrum, probably due to the disruption of protein oligomerization. Indeed, the improvement of the protein spectrum confirmed direct interaction. In contrast, the same screening applied on the other compounds did not show a particular effect on the HSQC spectrum. Even though **20** did not have significant impact on the spectrum, it appeared to have an effect on the formation of dimer/oligomer of HuR. Successively, the authors investigated the effects of the compounds on RRM1/RRM2 domains. These additional experiments showed the capability of only **20** to act on two domains as well as in the presence of unlabeled 11-mer single stranded RNA. The interference caused by **20** was significant by the reinstatement of peaks usually broadened by the interaction of the protein with the RNA. In

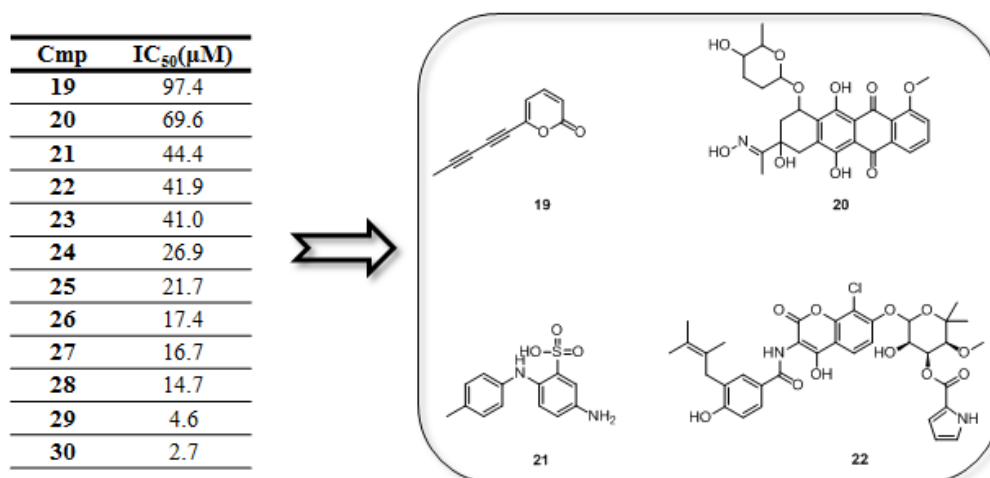particular, this last experiment might reveal the presence of the ligand binding site between RRM domains.

Cmp	IC$_{50}$(µM)
19	97.4
20	69.6
21	44.4
22	41.9
23	41.0
24	26.9
25	21.7
26	17.4
27	16.7
28	14.7
29	4.6
30	2.7

Figure 6. Inhibitors of HuR-mRNA complex (Experimental IC$_{50}$ values determinate by FP)

2. Remarks

Applying HTS approaches, thirty not-structurally related compounds able to interfere with the activity ELAV–ARE-mRNA complexes have been identified, but the comparison of the results obtained is a very critical issue especially considering that different techniques have been employed for screening (see Table 4). Moreover, in almost all the experiments the HuR protein has been considered sometimes using the full length protein or the RRM1 and RRM2 domains. In addition, the ARE-mRNA used for the experiments, selected in function of the genic expression of proteins involved in several pathologies, was different (TNFα, IL-2, IL-6, Cox-2, c-fos and Msi1); even if the ARE-mRNA^{TNFα} is the most frequently studied.

Nevertheless, some important considerations can be drawn:

1. compounds **1–3** confirmed the hypothesis that HuR exists in a dimeric form on the basis of theoretical and experimental data. Additionally, they are able to interfere with the complex RRM1/2–ARE-mRNA demonstrating the engagement of RRM domains in the interaction with ARE–mRNA;

2. compounds **9–11** may have a binding preference towards ARE sequences, as evidenced in the case of ARE–mRNA^{TNFα};

3. compounds **13–18** are active on both full length protein and RRM domains;

4. compound **20** seems to act on RRM domains also in the presence of ARE sequence but not on full length protein; contrarily, compound **22** interacts with the full protein but not with RRM domains. These data are difficult to rationalize, taking into account that they have both

been selected using the same HTS assay where full length protein and ARE sequence were used. On the basis of our experience, we can suppose that **20** and **22** bind a binding site localized in a different region of the protein.

In summary, considering the recently discovered molecules and their structural variability, outlining a SAR still represents a challenge. Indeed, compounds interferring with the HuR-mRNA complexes discovered so far are not structurally related and new efforts should be addressed to discover an efficient, alternative approach. (*manuscript submitted*)

cmpd	Complex		Assay	Ref
	HuR	**ARE-mRNA**		
1–3	RRM1/2	TNFα, IL-2, Cox-2	FIDA	53
9–11	Full-length protein	TNFα, IL-6, Cox-2, c-*fos*	REMSA - Filter binding assay	57
13	Full-length protein	TNFα	REMSA - Alpha screen	59
13–18	Full-length protein - RRM1/2	Msi1, Bcl$_2$, XIAP	FP - Alpha LISA	60
19 –30	Full-length protein - RRM1/2	c-*fos*	FP - STD-NMR	61

[a] Interaction with RRM1/2 domains in STD-NMR assay
[b] Interaction with full length-protein in STD-NMR assay

Table 4. Summary of the HTS techniques, ARE-.mRNA sequences and ELAV used for discovering **1–30**.

3. Rational approach for designing new Hu-mRNA interfering compounds

In the previous section, we have widely discussed how RBPs are still generally considered "undruggable targets" due to the lack of well-defined binding pockets for target mRNA. This can explain the difficult to find new chemical entities (NCE) able to interfere with mRNA-protein complex. In the case of ELAV proteins, during last year, studies lay the foundations for their druggability assessment. Briefly here below the most important milestones are reported.

1) The primary sequence of all ELAVs is known. In detail, the four vertebrate ELAV proteins are characterized by a high degree of sequence homology (70 – 85%). They are about 40 kDa in size and contain three ~90 amino acid-long RNA Recognition Motif-type (RRM) domains. The first two RRMs, positioned at the N-terminal end, are separated from the third one at the C-terminus by a hinge segment. Sequence alignment studies of the different ELAV proteins clearly evidenced that the first two RRM domains contain two highly conserved sequences, each of 8 and 6 amino acids, named RNP1 and RNP2 respectively (RNP stands for RiboNucleoProteic). [62, 63]

2) The 3D-structure of HuD in complex with a target transcript has been resolved. X-ray crystallography revealed that the four RNPs (RNP1 and RNP2 sequences of both RRM1 and RRM2 domains) are directly involved in the mRNA binding. [62]

3) The profile of the RNA recognition sequence was predicted using the RRM1 and RRM2 domains of HuD bound to ARE-mRNA cfos and TNFα long 11 nucleotides. The analysis of steric restriction and the availability of hydrogen-bonding partners permitted to identify it in AUUUA nucleotide repeat sequence. [62] Further studies on HuR showed consistent results with those reported so far. More in details, the sequence necessary for high-affinity binding by HuR corresponding to a two stretches of eight-nine nucleotides composed by uracile and adenine whose substitution with cytosine and guanine led to a dramatic reduce binding to HuR [64]

4) In 2008 Collina's team synthetized the four peptides corresponding to the highly RNP1-2 sequences placed in RRM of HuD (Table 5). The capability of the four peptides P1-P4 (assayed in mixture) to stabilize mRNA^{NOVA1} and mRNA^{VEGF} was then demonstrated.[65] Successive *in vitro* studies combined with molecular modeling experiments (MM/PBSA methodology) highlighted that the peptide sequences **P1** and **P2** play a major role in binding the nucleic acid to their **P3** and **P4** counterparts.[66] Further confirmation was provided by NMR studies (DOSY and STD-NMR). Interestingly, NMR experiments confirmed that each peptide is not able to bind the biological target on its own and that the peptide mixture **P1**+**P2** is the most effective in stabilizing mRNA. [67] Data obtained are in agreement with molecular modeling studies and with the biological tests.

Domain	Peptides	Amino acid sequences
RRM1_RNP1	P1	LGYGFVNY
RRM1_RNP2	P2	LIVNYL
RRM2_RNP1	P3	RGVGFIRF
RRM2_RNP2	P4	LYVSGL

Table 5. Amino acid sequences of peptide P1-P4 and their RNA recognition motif (RRM)

Results obtained so far can provide a contribution in understanding the region mainly involved in stabilizing mRNA and could be the starting point for the development of new small molecules able to interact with mRNA and for finding new drugs characterized by an innovative mechanism of action.

Taken together, the above considerations suggest that a rational approach could be adopted for designing ELAVs-mRNA interfering compounds. We decided to take advantage of Computer-Aided Drug Design techniques (CADD) with the purpose of predicting the binding mode. This part of the project was conducted in collaboration with Prof. Anna K.H. Hirsch at the University of Groningen where I spent seven months on an international Erasmus program. Contrary to the other research groups, we focused on HuD proteins already studied by us as described in the introduction. In brief, the work consists in (i) the identification of a binding pocket *via* molecular modelling studies; (ii) the design of new ligands;(iii) the synthesis of selected molecules and (iv) the evaluation of their biochemical activity through biological assay. The latter step will be accomplished in collaboration with Dr. Alessandro Provenzani at University of Trento who has already studied the ELAV–mRNA complex (see introduction section). (*manuscript in preparation*) The workflow is summarized in Figure 7.
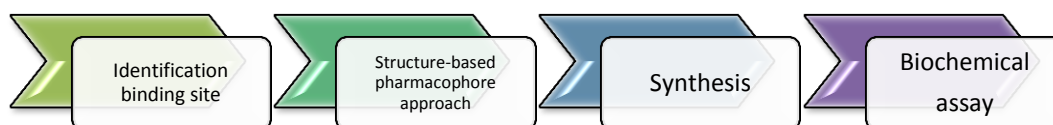

Figure 7: workflow

3.1 Identification of binding site (Step I)

The avaiability in the Protein Data Bank (PDB) of HuD structure co-crystallized with $mRNA^{TNF\alpha}$ (code:1G2E)[62] enabled the study of the interactions between the protein and its endogenous ligand. As previously described, HuD is a 40 kDa protein that comprises three RRM: the first two are involved in the interaction with the ARE sequence while the third one displays terminal adenosyl transferasy activity. Each RRM domain is composed of 90 amino acids forming two α -helices and four double-stranded ß-sheets with a ß1-α1-ß2-ß3-α2-ß4 topology.[62] (Figure 8)
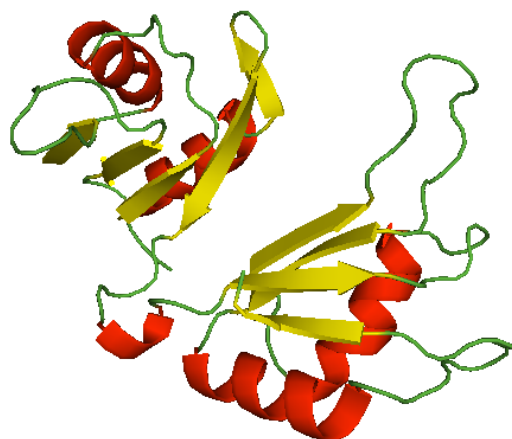
Figure 8: Crystal structure of ELAVL4 (PDB: 1G2E). Color code: protein (show as cartoon): loop: green, ß -sheet: yellow, α -helix: red

In order to discover new chemical entities that can act on this post-transcriptional level, we initially considered which part of this protein would represent the most druggable binding pocket for new ligands. We focused our attention on the part of protein involved in binding with 8-uracil and 9-uracil (U8-U9). In particular, visual inspection using the programs MOLOC and PyMol [68, 69] highlighted that the two asymmetric units of the protein are in proximity providing a deeper, narrower pocket, which should lend itself well to host small ligands. Moreover, the presence of arginines and asparagines left this cleft partially basic (Figure 9). It is interesting to note that the consensus RNA recognition sequence was identified exactly in this region (AUUUA). On the contrary, the rest of the ARE sequence is solvent–exposed, mainly involved in electrostatic interactions with the surface of the protein.
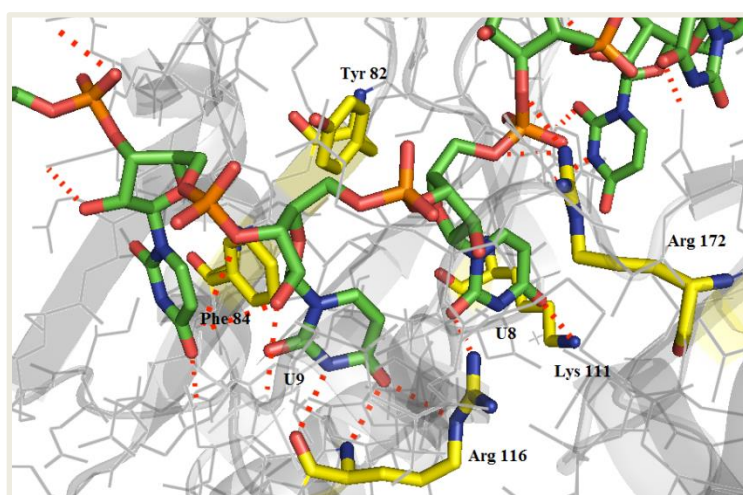

Figure 9: hypothesised binding pocket. Colour code: protein (shown as cartoon): gray. Amino acids: C: yellow, O: red, N: Blue. Nucleotides (shown as stick): C:green, O: red, N: blue, P: orange. Hydrogen bonds below 3.5 Å shown as red dashed lines.

Going into further detail, U8 and U9 are involved in the following interactions:

- U8: one carbonyl moiety forms a H bond with K111, while the other carbonyl moiety forms H bonds with R116

- U9: the carbonyl moiety and nitrogen atom form a H bond with R116.

On these bases, we built our pharmacophoric model.

3.2 Structure-based approach (Step II)

Given that the X-ray crystal structure of the protein in complex with its endogenous ligand is shown [62], we decided to generate new ligands employing structure–based techniques. In particular, Virtual Screening (VS) was taken into consideration as a suitable tool due to the lack of time and costs.

3.2.1 Nucleo Query

VS was performed using *NucleoQuery*: it is a free web-based virtual screening platform targeting proteins using a nucleotide-containing cofactor in which the nucleotide moiety is known as an "anchor". [70] The features of the anchor and the receptor can be defined through filters present in the "query"user interface. Every compound identified using this program can be synthesised by multi-component reactions (MCRs). U8 and U9 both were selected as anchors with the aim of investigating which of the two nucleotide may be a pharmacophore, in terms of occupied position and interactions. In order to increase the probability of discovering selective ligands with high affinity, U9 was modified so as to bear an additional phenyl group in order to establish a π-π-stacking interaction with Tyr82, not normally present between mRNA and ELAV. (Figure 10)
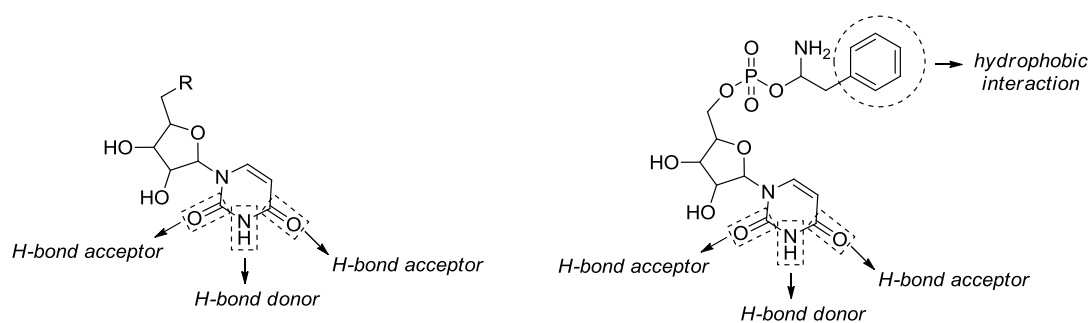
Figure 10: selected anchor on the left; anchor with additional modification on the right.

Each run in NucleoQUERY has allowed us to obtain a library of 200 molecules as a result. Thereafter a total of four runs were performed in total. The resulting 800 molecules derived from NucleoQuery were screened by PyMol examination and the best interactions and conformations within the binding pocket were compared to U8-U9. Before proceeding with docking studies, only the most interesting molecules were submitted to energy minimization using the force field implemented in the MOLOC programme.

Afterwards, a docking study was performed using the FlexX module in the LeadIT [71] suite as well as SeeSAR.[72] The choice of pharmacophore points was based on the important interactions previously observed with mRNA to be maintained by the new ligands. 30 Docked poses were generated for each m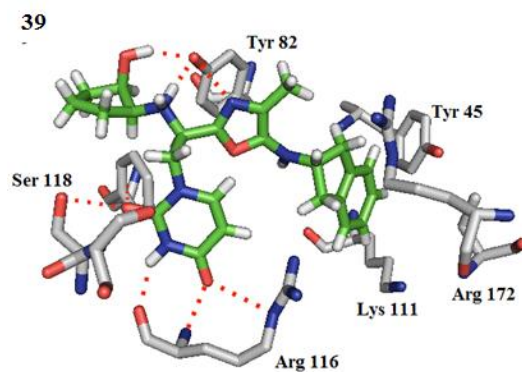olecule and analysed in SeeSAR in order to identify the best poses adopting similar binding modes and conformations as the U8-U9 fragment and featuring a highly predictable free energy of binding. Among 800 compounds, only nine were considered suitable candidates to be considered for synthesis (**1–9**) (Figure 11).

Figure 11. Selected compounds. The anchors are colored in blue, red, green and purple.

In all docked poses, the binding pocket was fully occupied by the selected molecules (Figure 12). The anchor perfectly overlapped with the corresponding uracil preserving the same Hbonds with Arg 116 and Lys 111. Compound **31** is engaged in additional Hbonds with the side chain of Ser 118 and the hydroxyl group of Tyr 82. Moreover the lateral chain of ligand **34** is involved in additional Hbond with the Arg 172. Furthemore, the phenyl group of compounds **35–37** formed a π-π-stacking interaction with Tyr 82 (3.5 Å). In compound **38**, additional Hbond was formed between the imidazolyl group and the side chain of Tyr 82. Interestingly, the main interactions of **39** are present between the oxazolyl group and the hydroxyl group of Tyr 82.

Figure 12. Docked poses of **31–39**. Color code: Amino acids: C: grey, O: red, N: Blue. Cmpd **1–8** (shown as stick): C:green, O: red, N: blue, Cl: green, F: cyano, S: yellow. Hydrogen bonds below 3.5 Å shown as red dashed lines.

All the results obtained have been grouped according to the corresponding MCR by which they could be synthesized. Looking at the structures, it was immediately possible to intuit the clustering of the molecules in function of several MCR: the Castagnoli–Cushman reaction for **31–33**, the Groebke reactions for **34**, the Reductive amination reactions for **35–37** the Van Leusen reaction for **38**, and the Zhu reaction for **39**.

In order to simplify the synthesis and taking into account the availability of starting materials, some small structural modifications were made; and just for one compound (**39**) it was decided not to synthesize it given that it is not accessible using the suggested Zhu MCR (Figure 13). Indeed, Zhu reaction is very sensitive to the reactivity of building blocks which can influence the yield of the final result. In particular, two factors influence the course of the reaction: the nucleophilicity of isocyanide and the choice of amine. Optimization of the reaction could require time not indicated in this early phase of the work. [73]
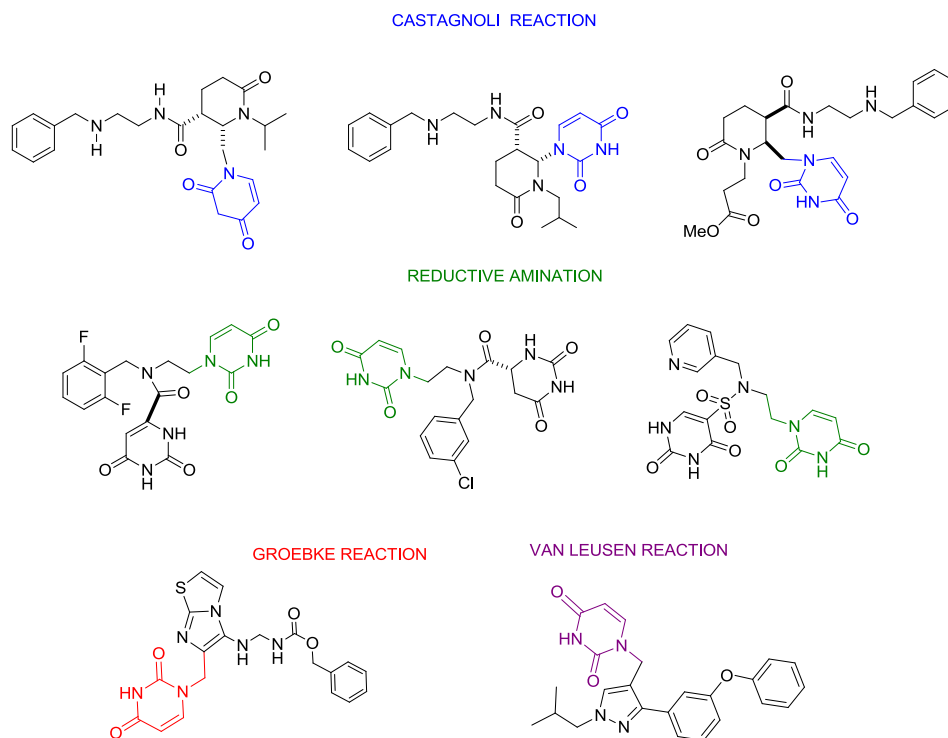
Figure 13. Structural optimization of **31–38**

The modified molecules were again submitted to energy minimization by MOLOC and docked in order to verify if the structural modifications could influence the binding modes. Fortunately, they did not alter the interaction with the binding site.

4 Synthesis (Step III)

To prepare our target compounds **31-38** we decided to follow a MCR approach also thanks to the collaboration with the research group of prof. Alex Dömling.

On the basis of the retrosynthetic analysis (Scheme 1) the appropriate starting materials have been selected. Most of them are commercially available, while compounds **41** [74], **47** and **59** [75] were previously synthetized according to literature procedures (Scheme 2). Aldehyde **42** was furnished by the Domling's group. Only the intermediate **56** is not commercially available and was never been prepared before and therefore we decided to postpone the synthesis of **37** .
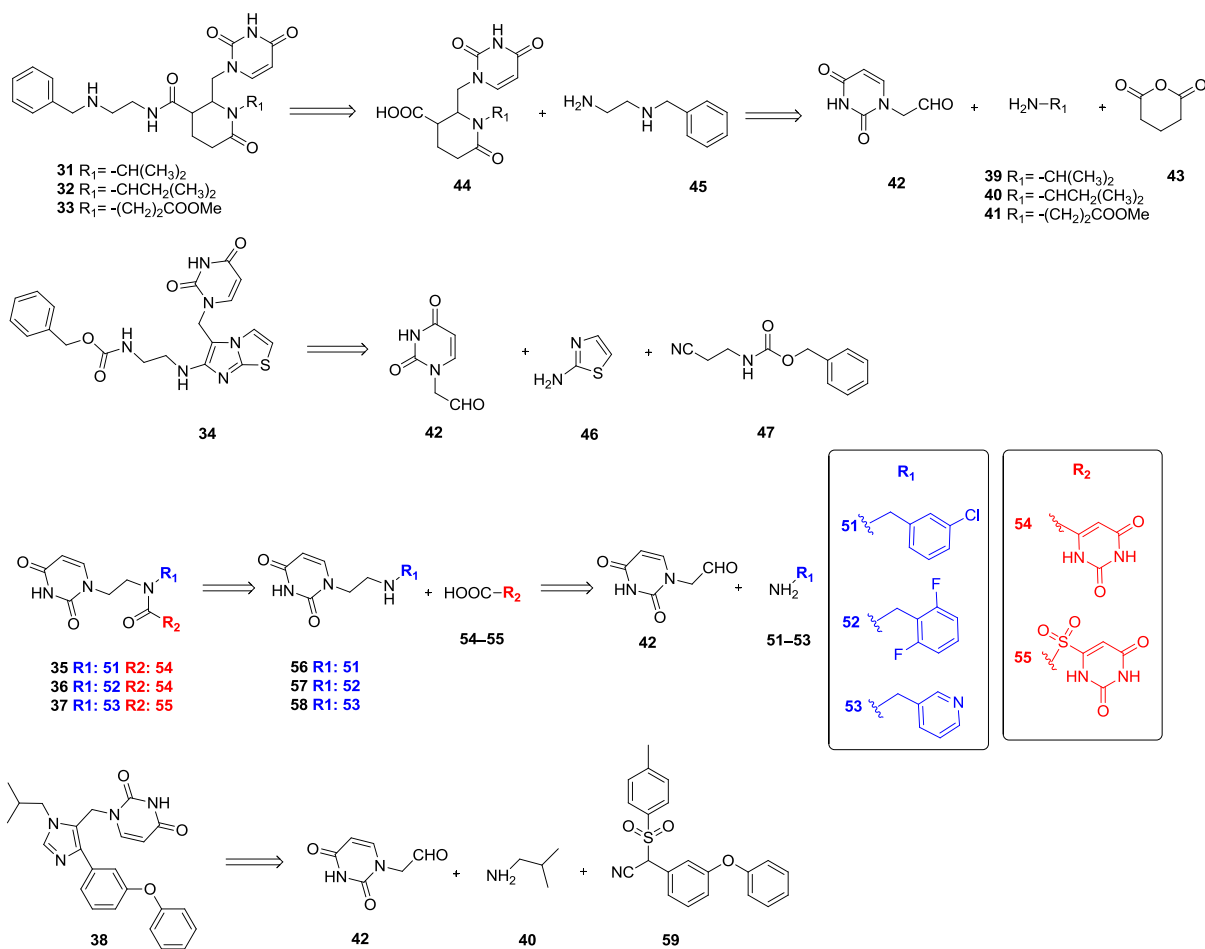
Scheme 1. Retrosynthetic analysis of **31–38**
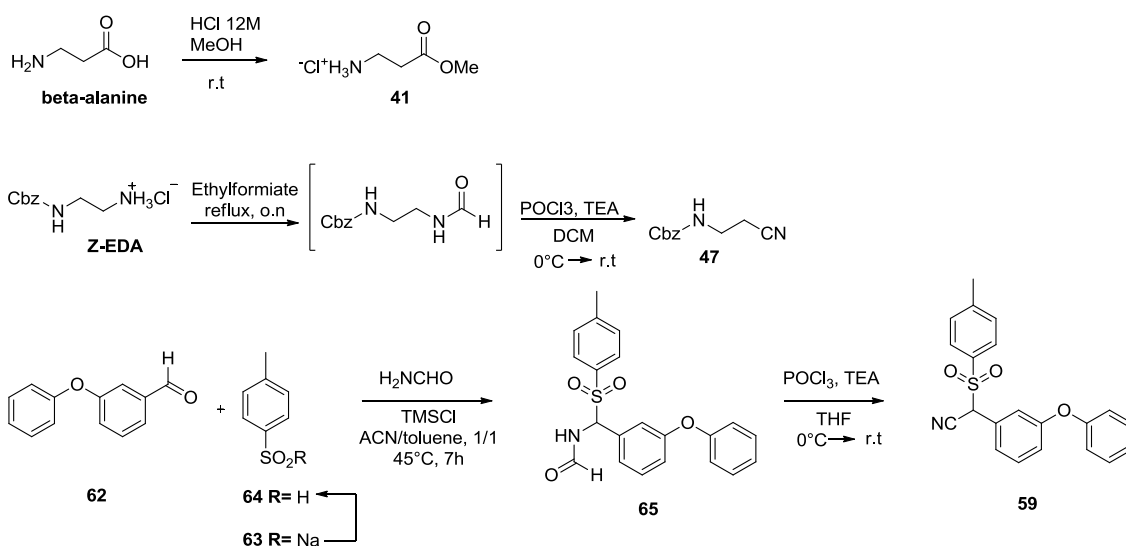
Scheme 2. Synthesis of building blocks **41**, **47** and **59**

Once the starting materials have been identified, the synthesis of **31–36** and **38** was experimented, following the synthetic approach, according with literature procedures.

The study regarding the synthesis of **31-36** and **38** and related compounds is widely described in the following paragraphs 4.1–4.6.

4.1 Synthesis of 31–33 *via* Castagnoli-Cushman (CC) reaction

This reaction was described for the first time by Castagnoli in 1969 and subsequently optimised by Cushman. It consists in the cycloaddition of a cyclic-anhydride to an imine, thus leading to the formation of a lactam bearing various substituents (Scheme 3). [76–77] Along the years the reaction was further investigated, expanding the scope to heterocyclic anhydrides.

Scheme 3. The Castagnoli-Cushman reaction
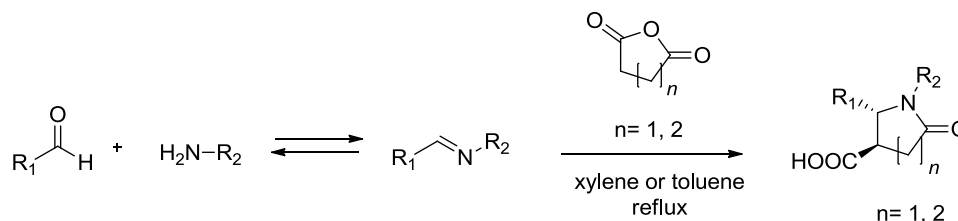
Owing to its versatility, the CC reaction has found several interesting application in medicinal chemistry and natural- product synthesis.[78] Moreover it not requires neither exotic reagents or particular conditions regarding temperature and pressure. The only apparent disadvantage is the prolonged heating in high boiling point hydrocarbon solvents (often leading to tar formation) required. The prolonged heating at high temperature somewhat limited scope, particularly with respect to the dicarboxylic anhydride component.

To obtain compounds **31–33** we follow the general procedure shown in Scheme 4, consisting in the two steps: the CC to obtain lactams 44a-c, which subsequent undergoes the amidation reactions. To obtain lactames we initially applied the reaction reported in the literature [79]. The reactants **42** and amine (**39–41**) were suspended in methanol in the presence of acetic acid as a catalyst for carrying out the corresponding imine. Then the reaction mixtures were then added of a solution of glutaric acid (**43**) in p-xylene and heated under reflux for 12 hours. Unfortunately, no reaction occurs in these conditions.
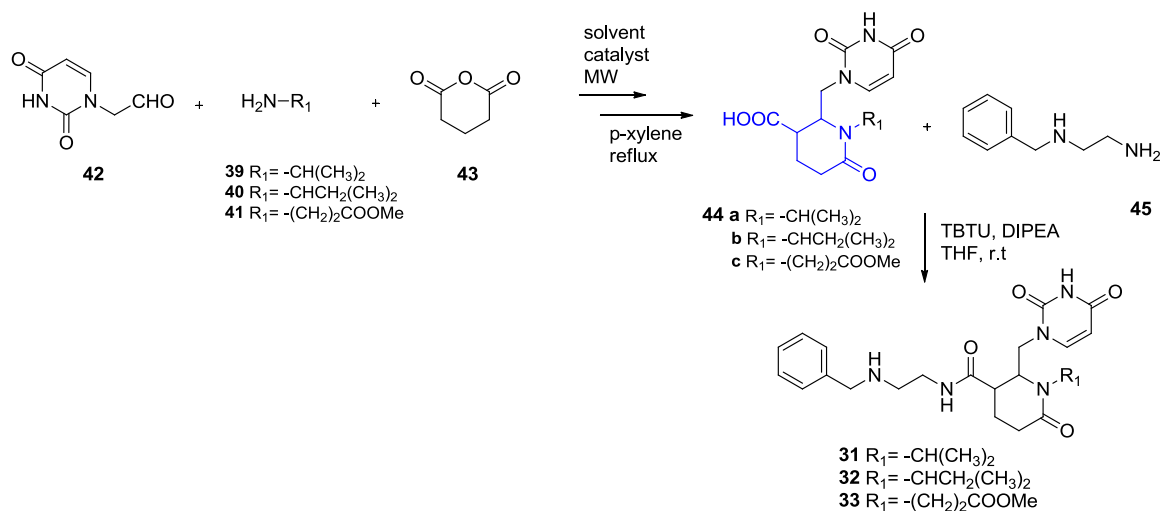
Scheme 4. Synthesis of **31–33**

On the bases of our previous experiences, we decided to experiment the microwave irradiation heating instead of the conventional one attempting the reaction in methanol (Table1, entry 1)The TLC analysis showed a reduction in the intensity of the spots due to the starting materials and the formation of a new spot, probably due to the corresponding imine. Encouraged from these results, the solvent was evaporated, glutaric anhydride in p-xylene added and the reaction mixture was refluxed for 12 hours. Nevertheless, no product formation was observed after at reflux.

We hypothesized that the low solubility of aldehyde **42** in MeOH could have a negative impact in the imine formation. Accordingly, we screened different conditions in terms of solvent and heating as reported in Table 6. Nevertheless, we isolated the by-product corresponding to the aliphatic chain/opened lactam ring (Figure 14). These experimental results reinforced our hypothesis that the key intermediate **42** is not suitable for such reactions. Indeed, the use of aliphatic aldehydes is not suggested in MCRs synthesis due to their poor electrophilic behaviour, leading to the formation of relatively unstable imines that could not be involved in the cycloaddition. We then completely revised our strategy, and come back to the design of new compounds.

Entry	Aldehyde (eq)	Amine (eq)	solvent	MW conditions (cycle/time/temperature)
1	1	1	MetOH	2 /20 min /120 °C
2	1	1	MeOH/DMF	2/20 min/120 °C
3	1	1	trifluoroethanol	1/120 min/120 °C
4	1	1	ACN	1/90 min/120 °C
5	1	1	DCM	1/90 min/120 °C

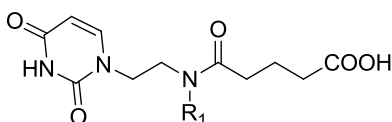Table 6. Screening of several conditions for imine formation

Figure 14. Isolated by-product

4.1.2 Structural optimization of 31–33

We changed the uracil portion in order to use building blocks with a better reactivity in the CC reaction. Accordingly, compounds **31–33** were virtually modified by MOLOC with several hydrophobic/aromatic portions that can replace uracil moiety, able to maintain the interactions with Arg116 in the binding site. The 3,4-dimethoxybenzaldehyde (**66**) seems to meet these criterions. Moreover it is commercially available. To prove the synthetic feasibility, we attempted to synthetize one random molecule of this class (**68**). Compound **68** was obtained applying the same protocol experimented for **31–33** (Scheme 5), by MW heating and using ACN as solvent. After evaporation of the solvent, the crude product was immediately used for the cycloaddition in presence of glutaric anhydride in p-xylene at reflux. Finally, after a light work-up, the identity of **67** was confirmed by NMR spectroscopy (^{1}H-NMR, COSY). Subsequently, amidation step was performed using TBTU as coupling agent in THF afforded **68** in high yield (71%)[80]. The success in the synthesis of 67 reinforced our original hypothesis regarding the low reactivity of compounds 42. We propose the optimized protocol for the synthesis of the other analogues.
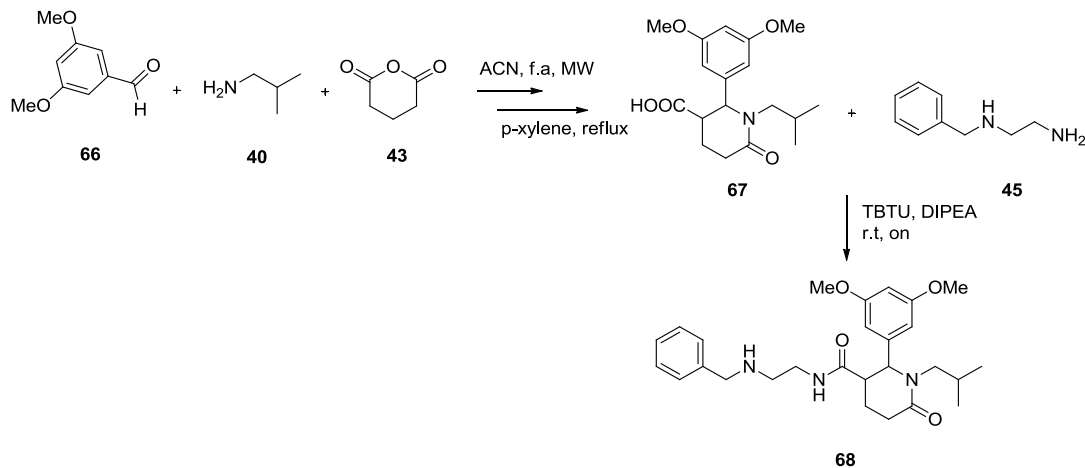
Scheme 5. Synthesis of **68**

## 4.2 Synthesis of 34 *via* Groebke–Blackburn–Bienaymé (GBB) reaction

The Groebke–Blackburn–Bienaymé reaction (GBBR) was first reported in 1998 as a variant of the Ugi reaction.[81-83] It is a three-component reaction that proceeds *via* an intramolecular no-concerted mechanism. Indeed, the *in situ* formation of the iminium species is followed by a no-concerted [4+1] cycloaddition with the isocyanide to give the corresponding fused imidazoles (Scheme 6). In general, the reaction is conducted in the presence of a catalyst such as Lewis, Brønsted and solid acids under mild conditions in polar and protic solvents (i.e, MeOH, trifluoroethanol etc).
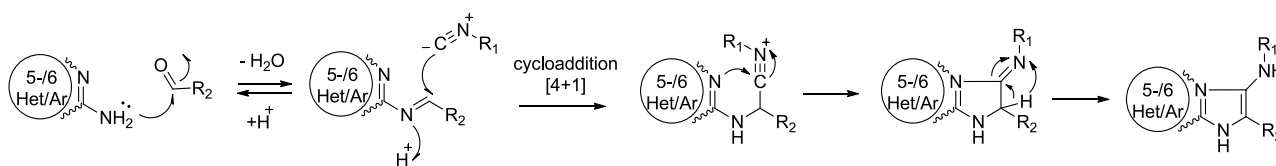
Scheme 6. GBB reaction

This type of MCR has found wide application in medicinal-chemistry projects especially in antiviral, antibacterial and anti-inflammatory drug synthesis.[84-85 ~~86, 87~~]

We attempted the synthesis of **34** via GBB reaction, as outlined in Scheme 7 in accordance with the literature. To pre-form the imine intermediate, compounds **42** and **49** allowed to react in MeOH under MW heating. Then the catalyst Zirconium Chloride IV (ZrCl$_4$, 10%) and isocyanide were added to the reaction mixture and the again heated by MW. Unfortunately, the product of interest was not isolated. Not discouraged by this first attempt, other reaction conditions were screened as summarized in Table 7.
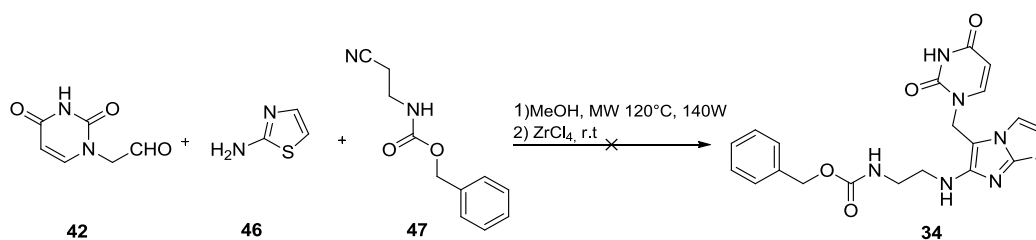
Scheme 7. Attempted synthesis of **34**

In the case of entries 3–5, we carried out the imine pre-formation by reflux followed by the addition of **47** and acid catalyst, heating by MW and increasing the amount of acid catalyst from 0.1 eq to 1.5 eq in order to promote the isocyanide attack. Again, in none of these conditions, compound **34** was obtained. This finding is not surprising: as previously observed for the synthesis of **31-33**, the use of aliphatic aldehyde led to the formation of unstable imine that could not be involved in [4+1]

cycloaddition. The fact that there is no reference regarding the use of aliphatic aldehyde in GBB in the literature supports our experimental results.

Entry	Solvent	Catalyst (eq)	Conditions (cycle/time/temperature)
1	MetOH	ZrCl$_4$ (0.1)	2 /20 min /120 °C
2	trifluoroethanol	ZrCl$_4$ (1)	2/20 min/120 °C
3	THF	ZrCl$_4$ (1.5)	Reflux, 20 h
4	THF	Zinc triflate (1.5)	Reflux, 20 h
5	toluene	Zinc triflate (1.5)	reflux (2h) followed by MW (30 min/120°C)

Table 7. Screening and conditions for the synthesis of **34**

4.2.1 Structural optimization of 34

To dispose of compounds able to interfere with the ELAV-mRNA complex, and keeping in our mind the synthetic problems, we decided to modified the structure of **34**changed the uracil portion in order to use building blocks with a better reactivity in the CC reaction. Accordingly, the optimization of the aldehyde moiety, and then of the final compound, was performed virtually led to the identification of **69** as a potential hit. To obtain **69**, compound **66** seems to be a suitable electron-poor aldehyde intermediate. (Scheme 8).
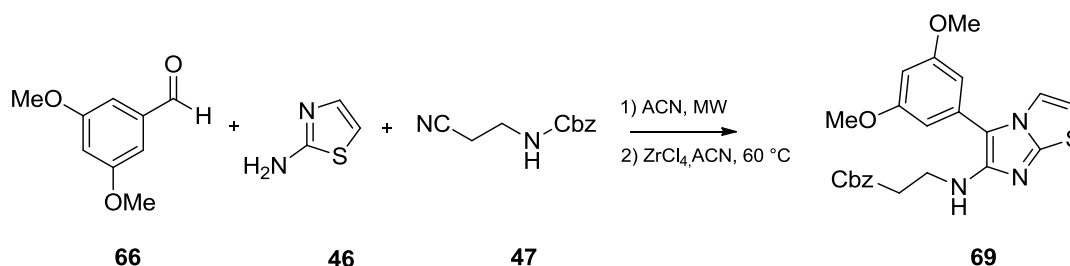
Scheme 8. Synthesis of **69**

We carried out the pre-formation of the imine in ACN, heating by MW at 120°C for 30 mins. The addition of ZrCl$_4$ in catalytic amount (0.1 eq) and the isocyanide to the reaction mixture led to the formation of compound **69** in low yield (21%) (^{1}H-NMR). The low yield could be explained by the incomplete conversion of **46** and **47** to the iminium species; both **46** and **49** were recovered, calling for the optimization of this reaction.

4.3 Synthesis of 35–37 *via* reductive amination

The reductive amination proceeds via iminium species formation followed by reduction of the double bond, leading it to the formation of a secondary or tertiary amine. The reaction usually occurs sequentially in one-pot. The carbonyl groups involved in this reaction can be both ketones or aldehydes. The reductive amination using sodium cyanoborohydride ($NaBH_3CN$) as reducing agent is called Borch reaction. [86] $NaBH_3CN$ is a relatively weak reductant which works under mildly acidic conditions. Correlated reactions are: Eschweiler–Clarke, Leuckart–Wallach and Mannich reactions.[87–90]

As a first step, we carried out the reductive amination for obtaining compounds **56** and **57** (Scheme 9), key intermediates for the synthesis of **36** and **37**.

The reaction for obtaining the iminic intermediate was performed in anhydrous THF under a nitrogen atmosphere at reflux. After 15 minutes, a large excess of sodium triacetoxyborohydride [$NaBH(OCOCH_3)_3$] (3eq.) was added [91]. After 20 hours the TLC analysis showed the formation of the desired compounds wich was isolated in reasonable yield (54% yield). The reaction was then optimised with the addition of molecular sieves to the reaction (4 Å) (Scheme 12).
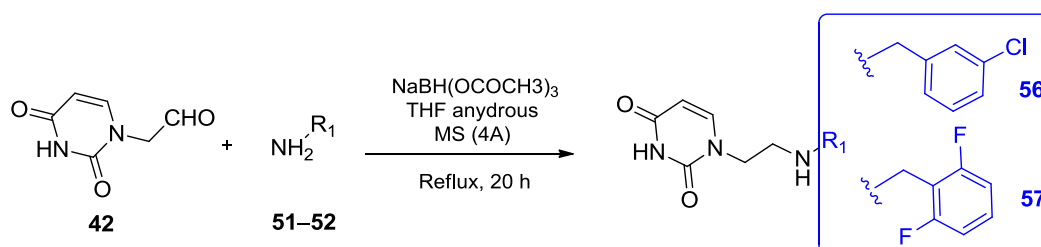
Scheme 9. Synthesis of **56** and **57**

To attempt the synthesis of **35–36**, different strategies were pursued (Scheme 10): (i) we converted the orotic acid (**54**) in the corresponding acyl chloride (**70**)[92], but the reaction did not lead to the desired product (Table 3, entry 1); (ii) we experimented the use of different coupling agents in accordance with literature [93–95] (Table 3, entries 2–7), but . the formation of the desired products was not evidenced; (iii) we converted the orotic acid **54** into the corresponding methyl ester (**71**) [96–100] and performed the reaction (Table 3 entry 8–9) again without observing product formation In conclusion, no reaction occurs when orotic acid **54** was used, as such or suitably derivatized and we hypothesized that it is not the right reactant for this reaction. In line with our previous approach, we decided to modify the carboxylic moiety involved in the reaction and to revise the compound design.
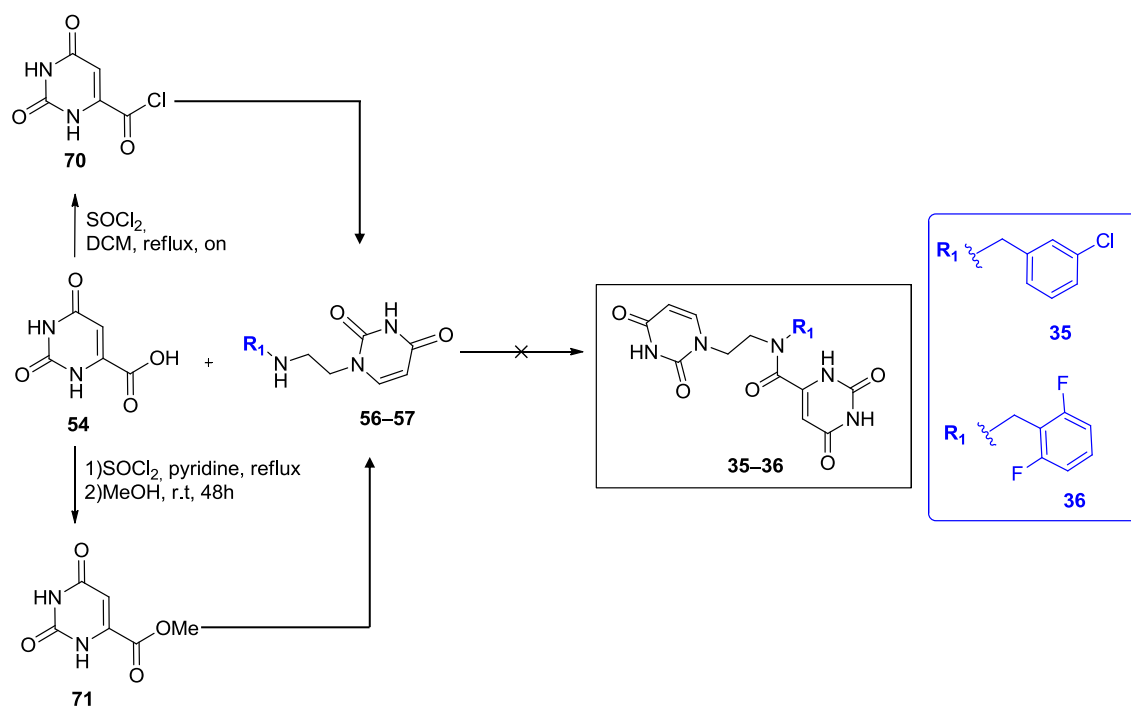
Scheme 10. Attempted synthesis of **35** and **36**

Entry	Compound (eq)	Amine (eq)	Condition
1	**70** (1)	**56** or **57** (3)	0 °C → r.t, o.n
2	**54** (1)	**56** or **57** (3.3)	TBTU (3.3 eq) DIPEA (3.3 eq) THF, MW
3	**54** (1)	**56** or **57** (1.2)	CDI (1.2 eq) DBU (0.5 eq) THF, r.t/MW
4	**54** (1)	**56** or **57** (1.2)	CDI (1.2 eq) DBU (0.5 eq) 2-methyl-THF, reflux
5	**54** (1)	**56** or **57** (0.6)	DCI (1.2 eq) Pyridinium chloride (1.2 eq) ACN, r.t
6	**54** (1)	**56** or **57** (1.2)	EDC (1.3 eq) HOBt (1.3 eq) DIPEA (7 eq) DMF, r.t/MW
7	**54** (1)	**56** or **57** (1.2)	DBAL-Me$_3$ (0.8 eq), THF, MW
8	**71** (1)	**56** or **57** (2)	TBD (30%), THF dry

| 9 | **71**
(1) | **56** or **57**
(1) | DBAL-Me3 (0.8 eq),
THF, MW |

Table 8. Attempted amidation conditions for the synthesis of **35** and **36**

4.3.1 Structural optimization of 35–36

Applying the same approach described before, we screened several carboxylic acids able to maintain the same interactions with the binding pocket. The design was performed using MOLOC. The most promising molecules **72** and **73** (Figure 15) are characterized by the presence of an aromatic p-hydroxy substituted moiety instead of the orotic one. As shown in Figure 15, compound **72** partially lacked the π-π stacking interaction with the side chain of Tyr 82 as well as the two Hbonds with lateral chain of Arg 116. Instead, **73** has maintained the same interactions with the amino acids of the cavity.
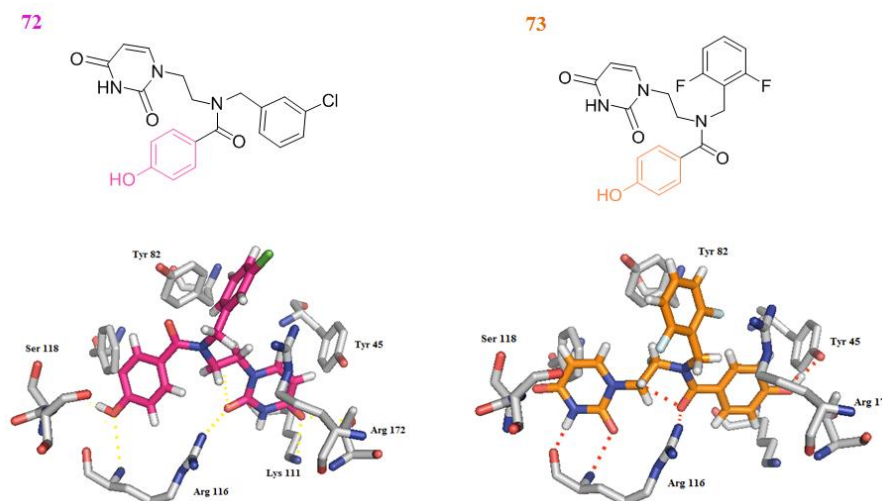
Figure 15: Docked poses of **72–73**. Color code: Amino acids: C: grey, O: red, N: Blue. Cmpd **72** (shown as stick): C: magenta, O: red, N: blue, Cl: green. Hydrogen bonds below 3.5 Å shown as yellow dashed lines. Cmpd **73** (shown as stick): C: orange, O: red, N: blue, F: cyano. Hydrogen bonds below 3.5 Å shown as yellow and red dashed lines, for **72** and **73** respectively.

Compounds **72** and **73** seem to be easy to synthetize, starting from the commercially available p-hydroxy benzoic acid (**74**).To prevent the formation of by-products, the hydroxyl group of **74** was protected with a benzyl group, which can be easily removed in the presence Pd/C 10% and ammonium formiate (Scheme 11).[101]
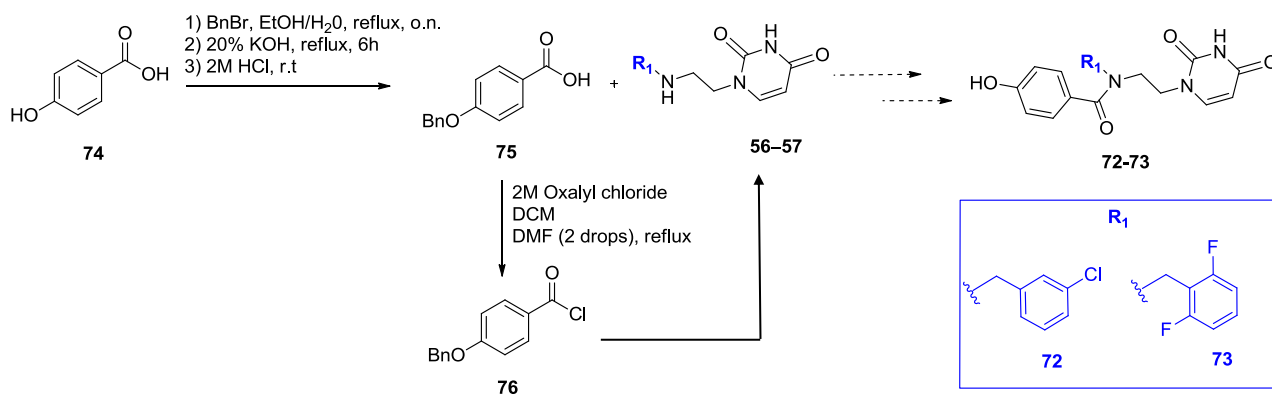
Scheme 11. Attempted synthesis of **72** and **73**

For optimizing the amidation reaction, the conditions reported in Table 9 have been experimented, always employing **56** as a test amine.

Entry	Compound (eq)	Amine (eq)	Conditions
1	**76** (1)	**56** (0.3)	0°C → r.t, o.n DMAP (0.01 eq)
2	**75** (1)	**56** (1)	HBTU (1.2 eq) TEA (2.5 eq) DMF, r.t
3	**75** (1)	**56** (1)	TBTU (1.2 eq) DIPEA (2 eq) THF, MW
4	**75** (1)	**56** (1)	HATU (1.2 eq) DIPEA (2.4 eq) THF, reflux
5	**75** (1)	**56** (1)	EDC (1.2 eq) HOBt (1.2 eq) DIPEA (3 eq) DMF, r.t

Table 9. Reagents and conditions screened for the synthesis of **72**

The TLC analysis clearly showed the formation of the adduct between the carboxylic acid and the coupling reagent was observed, indicating that the reactivity of the acid is acceptable, but its addition to the reactant did not lead to product formation, despite its disappearance in TLC. We can speculate that this might be due to the high flexibility of the lateral chains that constrain the secondary amine to assume a structural conformation not suitable for attacking the adduct or that thetautomerization of the anchor moiety under basic condition hydroxyl groups with the secondary amine in the amidation reaction (this second hypothesis was not supported by the isolation of by-products).

On the basis of these last negative results, we revised again the compound structure of the target compounds (using MOLOC), replacing the uracil moiety with another hydrophobic portion. We hypothesized that compound **77**, could be a valid alternative. Indeed, the hydroxyl groups maintain the same role of H-donor/acceptor engaged in the interaction with Arg 116.

For preparing **77**, the synthetic route outlined in Scheme 12 can be proposed. The aldehyde intermediate is not commercially available, but it can be prepared starting from the corresponding ester (**78**), protecting pre-emptively the hydroxyl groups. This precaution is necessary to guarantee the success of the reduction in presence of the reductive agent DIBAL-H.[102]
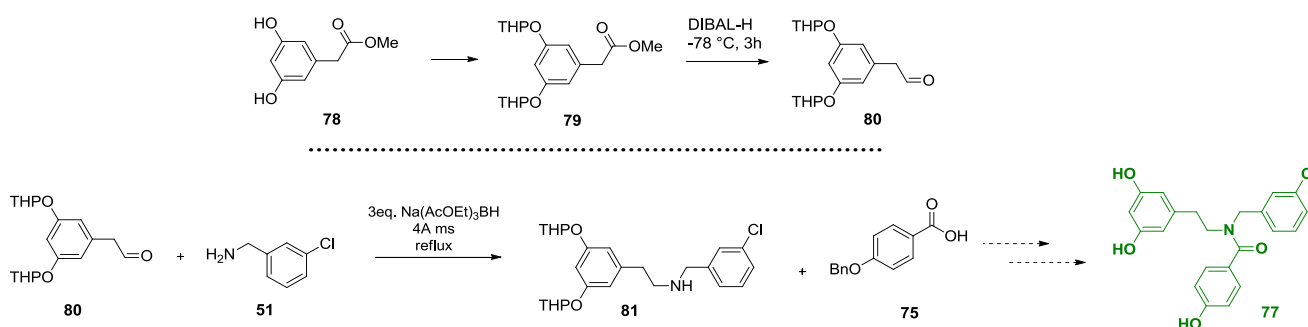
Scheme 12. Proposed synthesis of **77**

Because of time constraints, the synthesis of compound **77** has not been experimented and it must be set-up and then extended to analogue.

4.4 Synthesis of 38 *via* Van Leusen reaction

The van Leusen reaction represents the most straightforward methodology to access functionally rich imidazoles known to date. It allows for the preparation of polysubstituted imidazoles in a single pot and in a completely regioselective manner compared to TosMIC reagents and imines generated *in situ* from an aldehyde and an amine under mild conditions (Scheme 13) [103]. Usually the reaction takes places in presence of a base (K_2CO_3, piperazine, morpholine, *t*BuOK, etc) for promoting the cycloaddition.
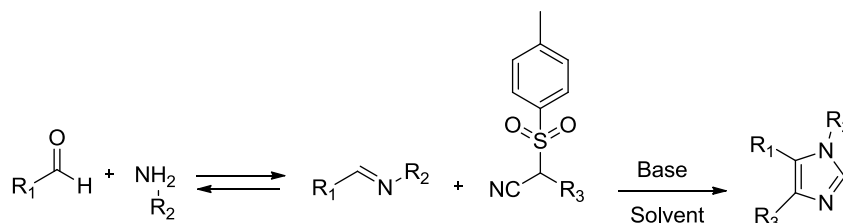
Scheme 13. General scheme of Van Leusen reaction

The imidazole synthesis was performed according to the classical condition using MeOH as solvent and K_2CO_3 as shown in Scheme 14. The reaction was left to under stirring for 3 days.
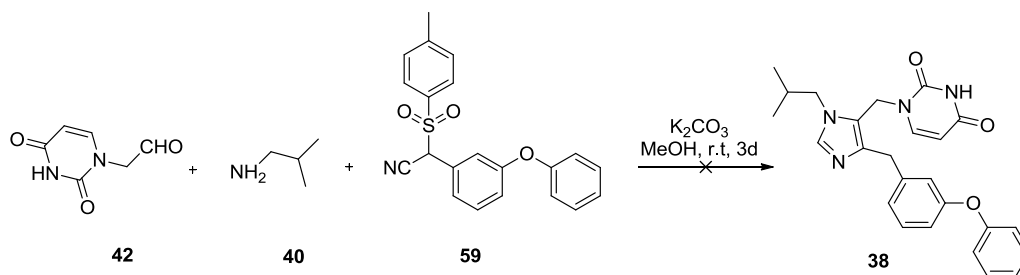
Scheme 14. Attempted synthesis of **38**

Unfortunately these conditions did not lead to product formation. It is probable, as observed in other scaffolds, that the unstable imine intermediate limited the progress of the reaction. Moreover, the use of heat to push the conversion of **42** and **40** to imine was limited by the degradation of **59** at high temperature.

On the basis of these experimental data, a structural optimisation of **38** was made with the purpose of challenging the aldehyde portion as well as optimising the method of synthesis .Therefore, we decide to replace the uracil moiety with another scaffold. Compound **38** was then virtually modified with several aromatic portions, bearing different substituents, paying attention to preserve the interactions with the side chain of Arg 116 in the binding pocket. The most promising compound seems to be compound **82** (designed using MOLOC) which can be synthesised starting from aldehyde **83** (commercially available). At this point, the reaction conditions should be set up (Scheme 15).
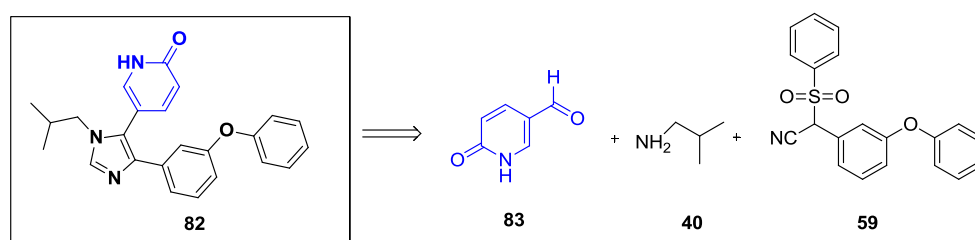
Scheme 15. Proposed retro-synthesis of **82**

5. Discussion

Multi-components reactions (MCRs) involve three or more reactants added together in one vessel to synthetize a new product characterized by the presence of moieties deriving from all reactant. If compared to traditional synthesis, MCRs allow to synthesise molecules with high structural complexity in one-pot, thus reducing time and costs.[104–106] The possibility to rapidly obtain molecules with different scaffolds can easily lead to the identification of new hits and can speed up

the hit-to-lead optimization process. Keeping these considerations in mind, to identify new compounds able to interfere with ELAV-mRNA complexes, I followed a MCR approach, in collaboration with the research group of prof. Alex Dömling.

A previously discussed, our target compounds were **31-38** which have been designed as potential ELAV-mRNA complex modulators. Nevertheless, as commonly occurs in synthetic chemistry, several drawbacks have been evidenced and some reactions steps were found to be optimized.

First of all, aldehyde **42** is characterized by poor electrophilic behaviour and for this reason led to the formation of relatively unstable imines that could not be involved in the cycloaddition a key step of the Castagnoli-Cushman (**31–33**), Groebke–Blackburn–Bienaymé (**34**) and Van Leusen reactions (**38**). To promote the imine formation, we experimented the use of the Microwave (MW) heating, but no successful results have been obtained. Moreover, the formation of lactame **44** (Scheme 4), intermediate of compounds **31–33**, was not observed even if different reaction conditions (*i.e* room temperature, reflux, MW) and solvents (*i.e* methanol, acetonitrile, tetrahydrofurane) were experimented. A similar situation took place in the synthesis of compounds **34** and **38**. It has to be underlined that there is no literature evidences regarding the use of electron-poor aldehyde in CC, GBB and Van Leusen reactions and therefore our results are not so surprisingly.

Interestingly, using **42** as building block and *via* reductive amination, we isolated the amines **56-57** . We supposed that in this case imine intermediate rapidly reacted with the reductive agent (sodium triacetoxyborohydride [NaBH(OCOCH$_3$)$_3$]), thus being subtracted to the equilibrium. In the case of the synthesis of **35** and **36** the amidation step (scheme 1) constituted the bottle neck of the reaction and the synthesis do not proceed. A lot of attempts have been performed using the orotic acid (**54**) or its corresponding acyl chloride (**70**) and ester derivatives (**71**), but the final compounds **35-36** have never been isolated.

In light of the difficulties in obtaining the compounds and strengthened by our synthetic experience, we revised the drug design performing a structural optimization of **31–38**. In particular, we decided to replace **42** with a similar one that presents electron-withdrawing groups and that could lead to final compounds able to maintain the main interactions in the binding site and preserve the initial scaffolds. Compounds **31–38** were then virtually modified by MOLOC with several hydrophobic/aromatic portions that can replace in particular the uracil moiety (Scheme 5, 8, 11–12, 15). Afterward the new designed compounds were docked in the putative pharmacophoric model by LeadIT. Most of them maintained the fundamental interactions with the amino acids of the binding site, only **72** partially lacked the π-π stacking interaction with the side chain of Tyr 82 as well as the two Hbonds with lateral chain of Arg 116.

To be sure of the synthetic feasibility, an attempt was proved on one molecule representative of each class. The synthetic procedure previously suggested for **31–34** was successful applied for the synthesis of **68** and **69**. In light of these results, the procedure has been extended to the other compounds. Instead, different synthetic routes were proposed for compounds **72–73** and **82**, as outlined in Scheme 12 and15. In this case the procedures will be necessary set-up and eventually apply to the synthesis of the other derivatives.

In conclusion, this research work has been permitted not only to achieve new synthetic compounds of ELAV-mRNA complex but also to highlight some limitations of MCR. Especially in this last aspect we made our efforts to in depth study the causes of our synthetic failures.

6. Conclusion and outlooks

Recently it has been demonstrated that ELAV proteins are involved in the etiology of several pathologies and they are considered a promising pharmacological target. An important challenge to face is to discover small molecules (*i.e.* synthetic organic compounds) able to interact with such family of proteins.

To this aim, we firstly recognized the literature for assessing the druggability of the target. On the basis of this preliminary information, we then postulate the binding site of the protein. To validate our hypothesis, we design and synthesize new compounds with different scaffolds. To this aim, We approached the synthesis *via* MCRs, which represent a powerful and attractive alternative to traditional synthesis, especially during the early phase of the drug discovery process. Although it is subject to the reactivity of the building block employed, it may considerably limit the production of interesting compounds. In the work described, we found several limitations to carry out our goals. Although some negative results represented a challenge for obtaining the molecules. In particular, they gave us the opportunity to thoroughly investigate these particular reactions and to study in detail which other structural modifications are allowed on the molecules for maintaining the same interactions within the binding pocket. All this information might prove to be useful in the hit-to-lead process. Before attempting this step, the completion of the compounds library will be necessary to enforce the synthesis of the latest compounds attempting the new synthetic strategy.

Successively, the capability of molecules presented to interact with the complex HuR–mRNA will be assessed through biochemical assays. The Provenzani's procedure provides for the combination of REMSA and Alpha screen assays in order to evaluate the ability of compounds to compete with ARE-sequence of mRNA in the binding with HuR. The experimental results could provide important indications regarding the pharmacophoric elements in accordance or not with docking

results. Therefore, these preliminary results will be the starting point for investigating the real interaction between the hit and the target protein through NMR techniques.

7.Sperimental Section

7.1 General

Reagents and solvents for synthesis were obtained from Aldrich (Italy, The Netherland). Unless otherwise specified, the commercially available reagents were used as received from the supplier. Solvents were purified according to the guidelines in Purification of Laboratory Chemicals.6 Microwave dielectric heating was performed in a Discover® LabMate instrµMent (CEM Corporation) specifically designed for organic synthesis and following an appropriate microwave program. Melting points were measured on SMP3 Stuart Scientific apparatus and are uncorrected. Analytical thin-layer-chromatography (TLC) was carried out on silica gel precoated glass-backed plates (Fluka Kieselgel 60 F254, Merck) and visualized by ultra-violet (UV) radiation, acidic ammoniµM molybdate (IV), or potassium permanganate. Flash chromatography (FC) was performed with Silica Gel 60 (particle size 230–400 mesh, purchased from Nova Chimica). IR spectra were recorded on a Jasco FT/IR-4100 spectrophotometer with ATR module; only noteworthy absorptions are given. Proton nuclear magnetic resonance (NMR) spectra were recorded on a Bruker Avance 400 spectrometer operating at 400.13 MHz and Bruker Avance 500 spectrometer operating at 500.13 MHz

Proton chemical shifts (δ) are reported in ppm with the solvent reference relative to tetramethylsilane (TMS) employed as the internal standard (CDCl3, δ = 7.26 ppm; CD2Cl2, δ = 5.32 ppm; [D6]acetone, δ = 2.05 ppm). The following abbreviations are used to describe spin multiplicity: s = singlet, d = doublet, t = triplet, q = quartet, m = multiplet, br = broad signal, dd = doublet-doublet, td = triplet-doublet. The coupling constant values are reported in Hz. 13C NMR spectra were recorded on a 400 MHz spectrometer operating at 100.56 MHz, with complete proton decoupling. Carbon chemical shifts (δ) are reported in ppm relative to TMS with the respective solvent resonance as the internal standard (CDCl3, δ = 77.23 ppm; CD2Cl2, δ = 54.00 ppm; [D6]acetone, δ = 29.84 ppm).

Compounds **60[74]**,**70[92]**, **71[96]**, **75[100]**, were synthesized according to literature procedures and the spectral data are consistent with those reported in the literature.

Synthesis of 2-(3,5-dimethoxyphenyl)-1-isobutyl-6-oxopiperidine-3-carboxylic acid (67)

To a solution of **68** (100 mg, 1eq) in acetonitrile (2 mL) at room temperature, **40** (0.048 mL, 1 eq) and two drops of formic acid were sequentially added. The reaction mixture was irradiated with a

microwave power of 140 W, at 120 °C for 30 min. After that the yellow solution was immediately evaporated to dryness, dissolved in p-xylene (2 mL) and then **43** (55 mg, 1eq) was added. The suspension was refluxed overnight under stirring. The solvent was picked up and the remain brown solid was washed with ether affording a beige solid. The recovery crude was further purified by flash chromatography eluting with DCM/MeOH (90/10, v/v) giving **47** as white solid (125 mg, 62%,), mp= 176-179 °C. ^{1}H-NMR (400 MHz, CDCl$_3$) = δ 9.76 (s, 1H), 6.31 (t, J = 2.2 Hz, 1H), 6.24 (d, J = 2.2 Hz, 2H), 5.02 (d, J = 2.9 Hz, 1H), 3.88 (dd, J = 13.6, 8.8 Hz, 1H), 3.71 (s, 6H), 2.80 (dd, J = 7.5, 4.2 Hz, 1H), 2.64 (ddd, J = 17.7, 10.5, 6.9 Hz, 1H), 2.48 (ddd, J = 18.1, 6.0, 3.4 Hz, 1H), 2.19 (dd, J = 13.5, 6.1 Hz, 1H), 1.96 (t, J = 22.9 Hz, 2H), 1.85 (d, J = 35.1 Hz, 1H), 0.80 (d, J = 6.7 Hz, 3H), 0.76 (d, J = 6.6 Hz, 3H). ^{13}C NMR (101 MHz, CDCl$_3$) δ 175.26, 171.13, 161.21, 142.42, 104.53, 99.23, 61.68, 55.31, 52.91, 45.75, 28.78, 26.41, 20.18, 19.97, 18.50. IR (vmax/cm-1): 838.88, 875.52, 901.55, 925.66, 991.23, 1596.77, 1711.51, 1968, 2900.41, 2958.27, 3487.63.

Synthesis of N-(2-(benzylamino)ethyl)-2-(3,5-dimethoxyphenyl)-1-isobutyl-6-oxopiperidine-3-carboxamide (68)

To a solution of **67** (100 mg, 1eq dissolved in THF (3mL), TBTU (115,3 mg, 1.2 eq) and DIPEA (0.109 mL, 2 eq) were sub sequentially added. The reaction mixture was stirred at room temperature for 30 minutes. After this time, **45** (0.045 mL, 1 eq) was added and the solution was stirred at room temperature overnight. The reaction mixture was concentrated *in vacuo*, dissolved in DCM (10 mL) and washed with water (20 mL). The organic layer was dried on Na$_2$SO$_4$, filtrated and the solvent evaporated *in vacuo*. The crude was purified by FC eluting with DCM/MeOH (80/20, v/v) giving **68** as yellow oil (99.6 mg, 71%). ^{1}H NMR (400 MHz, CDCl$_3$) δ 7.25 (ddd, J = 7.4, 4.5, 1.5 Hz, 2H), 7.22 – 7.15 (m, 3H), 6.30 – 6.27 (m, 1H), 6.25 (d, J = 2.2 Hz, 2H), 5.96 (s, 1H), 4.75 (d, J = 7.5 Hz, 1H), 3.87 – 3.80 (m, 1H), 3.67 (d, J = 3.0 Hz, 6H), 3.62 (d, J = 4.5 Hz, 2H), 3.23 (ddd, J = 16.9, 11.9, 5.1 Hz, 1H), 3.18 – 3.08 (m, 1H), 2.61 (dq, J = 8.7, 4.9 Hz, 1H), 2.57 – 2.49 (m, 2H), 2.46 – 2.34 (m, 2H), 2.15 (dd, J = 13.6, 6.2 Hz, 1H), 2.02 – 1.83 (m, 5H), 0.78 (d, J = 5.4 Hz, 3H), 0.76 (s, 3H). ^{13}C NMR (101 MHz, CDCl$_3$) δ 175.26, 171.13, 161.21, 142.42, 104.53, 99.23, 61.68, 55.31, 52.91, 45.75, 28.78, 26.41, 20.18, 19.97, 18.50.IR (vmax/cm^{-1}): 836.9, 910.4, 991, 1061.62, 1156.12, 1203.36, 1607.38, 1746.23, 3002.62, 3027.69, 3381.57.

Synthesis of benzyl (cyanomethyl)carbamate (47)

Benzyl (aminomethyl) carbamate (500 mg) was dissolved in ethyl formiate and the suspension was refluxed overnight. The reaction mixture was concentrated *in vacuo* giving the benzyl (formamidomethyl) carbamate as white solid without further purification. Subsequentially, a

solution of benzyl (formamidomethyl) carbamate (530 mg, 1 eq) and TEA (2mL, 5eq) in DCM (10 mL) was cooled to 0°C under stirring, then POCl$_3$ (0.250 mL, 0.9 eq) was added dropwise keeping the internal reaction temperature below 5°C. After the POCl$_3$ addition is complete, the reaction was left a room temperature for 4 hours. The variation of color reaction, from yellow to dark brown was indicative of the end of the reaction, checked as well by TLC. After the described time, the reaction was purged in NaHCO$_3$ aq. solution (5%) and icy-water, then it is extracted with DCM (40 mL) and the organic layer washed with NaHCO$_3$ aq. solution (5%). The collected organic layers were dried on MgSO$_4$, filtrated and the solvent evaporated *in vacuo*. The crude was re-dissolved in DCM and filtred on silica pad. The filtrate was one more time evaporated *in vacuo* yelding **47** as brown oil. (271.1 mg, 56%). ^{1}H NMR (500 MHz, CDCl$_3$) δ 7.43 – 7.28 (m, 5H), 5.35 (s, 1H), 5.14 (s, 2H), 3.52 (d, *J* = 10.6 Hz, 2H), 3.47 – 3.36 (m, 2H). IR (ν max/cm^{-1}): 774.279, 921.807, 1016.3, 1077.05, 1142.62, 1666.2, 1713.44, 1965.11, 2149.28, 2683.46, 2812.67, 2893.66, 2947.66

Synthesis of Benzyl-2-((5-(3,5-dimethoxyphenyl)-7,7a-dihydroimidazo[2,1-b]thiazol-6-yl)amino)acetate (69)

Compounds **68** (100 mg, 1eq) and **46** (49 mg, 1 eq) were placed in a microwave vessel and dissolved in ACN (2mL) then two drops of formic acid was added. The reaction mixture was irradiated with a microwave power of 200 W, at 120 °C for 30 min. Then Zirconium chloride (10 mg, 10%) and **47** (100 mg, 1eq) were sequentially added. The reaction mixture was warmed in an oil bath at 70-80°C under stirring overnight. The reaction was concentrated *in vacuo,* dissolved in DCM (25 mL) and washed with HCl aq. solution (1M). The aqueous layer was alkalined with a NaOH aq. solution (1M) and then was extracted with EtOAc (40 mL). The organic layers were collected, dried on Na$_2$SO$_4$ and then filtrate. The solvent was evaporated *in vacuo*. The crude was purified by flash chromatography eluting with DCM/MeOH (97/3, v/v) afforded **61** as yellow oil (57.5 mg, 21 %). ^{1}H NMR (400 MHz, CDCl3) δ 7.37 (m, 5H), 7.34 (d, J = 4.6 Hz, 2H), 7.06 (d, J = 2.2 Hz, 2H), 6.76 (d, J = 4.5 Hz, 1H), 6.41 (t, J = 2.1 Hz, 1H), 5.11 (s, 2H), 5.04 (d, J = 7.3 Hz, 6H), 3.82 (s, 6H), 3.30 (dd, J = 11.3, 5.6 Hz, 2H), 3.21 (s, 2H), 3.13 – 3.05 (m, 1H).. ^{13}C NMR (101 MHz, DMSO $_{d6}$) δ 165.30, 165.30, 157.78, 138.35, 137.09, 135.42, 128.32, 128.32, 128.17, 128.17, 128.16, 124.60, 114.15, 112.65, 112.65, 105.80, 101.23, 66.69, 56.04, 56.04, 43.82, 40.21. IR (ν max/cm^{-1}): 926.62, 992.19, 1204.33, 1295.93, 1318.111510.95, 1596.77, 1738.51, 2837.74, 2935.13, 3001.66, 3181.01, 3333.36.

General procedure for the synthesis of 56–57

In two necked round-bottom flask **42** (1000 mg, 1eq) was dissolved in anhydrous THF in presence of molecular sieves (4Å). Then the amine (1.3 eq) and two drops of formic acid were sequentially added. After 15 minutes sodium triacetoxyborohydride [NaBH(OCOCH$_3$)$_3$] (1333 mg, 3 eq) was added to the reaction mixture. The suspension was refluxed overnight under stirring in nitrogen inert atmosphere. The reaction mixture was quenched with NaOH aqueous solution (5%) and concentrated *in vacuo*. The crude was dissolved in EtOAc (20 mL) and washed with NaOH aqueous solution (5%) (40 mL) then the aqueous layer was treated with HCl aqueous solution (1M) and extracted with DCM (40 mL). The organic layers were collected and dried over Na$_2$SO$_4$, filtrated and the solvent evaporated *in vacuo*. The crude was further purified by flash chromatography eluting with AcOEt/MeOH (98/2 to 85/15, v/v) and DCM/MeOH (95/5, v/v) for **56** and **57,** respectively.

1-(2-((3-chlorobenzyl)amino)ethyl)pyrimidine-2,4(1H,3H)-dione (56)

White solid (875.5 mg, 54 %).^{1}H NMR (400 MHz, CD$_3$OD) δ 7.61 − 7.55 (m, 1H), 7.38 − 7.35 (d, 1H), 7.30 − 7.23 (m, 3H), 5.68 − 5.62 (d, 1H), 3.86 (t, *J* = 6.1 Hz, 2H), 3.78 (s, 2H), 2.86 (t, *J* = 6.8 Hz, 2H). ^{13}C NMR (101.13, CD$_3$OD) δ 171.77, 165.27, 151.54, 146.04, 141.74, 134.15, 134.08, 129.79, 129.62, 128.01, 127.28, 127.03, 126.95, 126.28, 125.44, 101.13, 60.43, 52.41, 48.92, 48.71, 48.49, 48.28, 48.18, 48.07, 47.85, 47.64, 46.85. IR (vmax/cm^{-1}): 736.67, 784.88, 908.31, 1460.81, 1573.63, 1598.7, 1680.66, 2925.48, 3053.73, 3564.77

1-(2-((2,6-difluorobenzyl)amino)ethyl)pyrimidine-2,4(1H,3H)-dione (57)

Light yellow solid (857.7mg, 47 %).^{1}H NMR (400 MHz, CDCl$_3$) 7.37-7.24 (m, 1H), 7.08-7.06 (d, J= 7.9 Hz), 6.99-6.96 (m, 2H), 5.67-5.65 (d, J= 7.9 Hz, 1H), 3.92 (s, 2H), 3.85-3.82 (t, J=5.7 Hz, 1H), 3.71-3.68 (t, J=5.7 Hz, 1H), 2.93-2.90 (t, J=5.7 Hz, 1H),2.38-2.35 (t, J=6.8 Hz, 1H). ^{13}C NMR (101.13 MHz, CDCl$_3$) δ 164.92, 162.99, 162.86, 151.60, 143.99, 128.97, 121.15, 111.76, 111.76, 104.72, 47.65, 46.96, 44.27. IR (vmax/cm^{-1}): 786.815, 1024.98, 1155.15 1201.43, 1469.49, 1517.7, 1593.88, 1625.7, 1678.73, 1771.3, 2349.84, 2847.38, 2919.7, 3049.87, 3108.69, 3202.22, 3257.18, 3306.36.

Synthesis of 2-(3-phenoxyphenyl)-2-tosylacetonitrile (59)

A dry flask was charged with **62** (300 mg, 1.92 mmol) and **64** (408 mg, 1.92 mmol). Anhydrous CH$_3$CN (0.85 mL) and anhydrous toluene (0.85 mL) were added, followed by formamide (0.190 mL, 4.88 mmol) and chlorotrimethyl silane (0.207 mL, 2.12 mmol). The mixture was stirred at 45 ºC for 4.5 h, MeOH (4 mL) was added, and the white precipitate was filtered over a Buchner filter,

washed with MeOH (20 mL) and dried with an oil vacuum pump for 10 h to afford **65** as a crude product, which was used in the next step without any further purification.

Successively, **65** (500 mg, 1.3 mmol) was charged in dry flask and dissolved in anhydrous THF (4 mL), then POCl$_3$ (0.25 mL, 2.6 mmol) was added at room temperature. The solution was left to stir for 15 min. The reaction mixture was cooled down to 0 $^{\circ}$C, Et$_3$N (1 mL, 7.80 mmol) was added dropwise, and the reaction mixture was left to warm gradually to room temperature. After 2 h 30 min, the conversion was complete (according to TLC), and EtOAc (10 mL) and H$_2$O (10 mL) were added. After stirring for 5 min, the reaction mixture was transferred to a separatory funnel, the aqueous layers were discarded, and the organic layers were washed with water (2 x 20 mL), sat. aq. NaHCO$_3$ solution (20 mL) and sat. aq. NaCl solution (20 mL). The organic layers were concentrated *in vacuo*, keeping the temperature of the bath below 40 $^{\circ}$C to avoid product decomposition (closely related isocyanides are known to be thermally unstable at temperatures above 80 $^{\circ}$C). Purification by filtration over silica pad eluting with DCM, afforded **59** as an brown amorphous solid (335 mg, 48% over two steps). ^{1}H NMR (500 MHz, CDCl3) δ 7.64 (d, *J* = 8.2 Hz, 2H), 7.36 (ddd, *J* = 12.4, 6.8, 4.3 Hz, 4H), 7.15 (td, *J* = 10.0, 3.5 Hz, 2H), 7.11 − 7.01 (m, 3H), 6.97 (d, *J* = 8.7 Hz, 2H), 5.56 (s, 1H), 2.48 (d, *J* = 10.0 Hz, 3H).

7. References

[1] Wang X., He C., Dynamic RNA modifications in posttranscriptional regulation, *Mol Cell*. 2014 56, 5-12

[2] Tang A. Y. , RNA processing-associated molecular mechanisms of neurodegenerative diseases, *J Appl Genetics* , 2016, 57, 323–333

[3] Beghini A., B. Ripamonti C., Peterlongo P., Roversi G., Cairoli R., Morra E., Larizza L., RNA hyperediting and alternative splicing of hematopoietic cell phosphatase (PTPN6) gene in acute myeloid leukemia, *Hum. Mol. Genet.* 2000, 9, 2297–2304

[4] Gascon E., Gao F.B., Cause or Effect: Misregulation of microRNA Pathways in Neurodegeneration, *Front Neurosci*. 2012, 9, 48; König J., Zarnack K., Luscombe NM., Ule J., Protein-RNA interactions: new genomic technologies and perspectives. *Nat Rev Genet.* 2012 18, 77-83

[5] Ingolia N. T., Ghaemmaghami S., Newman J.R , Weissman J.S, Genome-wide analysis in vivo of translation with nucleotide resolution using ribosome profiling, *Science*. 2009, 324, 218-23; Norris A.D, Calarco J.A, Emerging Roles of Alternative Pre-mRNA Splicing Regulation in

Neuronal Development and Function. *Front Neurosci.* 2012, 21, 122; Tariq A., Jantsch M.F, Transcript diversification in the nervous system: a to I RNA editing in CNS function and disease development. *Front Neurosci.* 2012, 9, 99

[6] G. Desnoyers, M. P Bouchard, E. Massé New insights into small RNA-dependent translational regulation in prokaryotes *Trends Genet.* 2013, 29, 92–98

[7] Doxakis E., RNA binding proteins: a common denominator of neuronal function and dysfunction. *Neurosci Bull,* 2014, 1, 610–626 .

[8] Szabo A., Dalmau J., Manley G., Rosenfeld M., Wong E., Henson J., Posner, J.B., Furneaux H.M., ELAVL4, a paraneoplastic encephalomyelitis antigen, contains RNA-binding domains and is homologous to elav and sex-lethal. *Cell* 1991, 67, 325–333.

[9] Pignolet B.S., Gebauer C.M., Liblau R.S. Immunopathogenesis of paraneoplastic neurological syndromes associated with anti-Hu antibodies: A beneficial antitμMor immune response going awry. *Oncoimmunology,* 2013, 2

[10] Darnell R.B, Posner J.B., Paraneoplastic syndromes involving the nervous system. *N. Engl. J. Med.* 2003, 349, 1543–1554

[11] Yeo G., Holste D., Kreiman G., Burge C.B., Variation in alternative splicing across human tissues. *Genome Biol.* 2004, 5, 1-15.

[12] Pascale A., Govoni S., The complex world of posttranscriptional mechanisms: Is their deregulation a common link for diseases? Focus on ELAV-like RNA-binding proteins. *Cell Mol Life Sci* 2012, 69, 501-517.

[13] Perrone-Bizzozero N., Bird C.W, Role of HuD in nervous system function and pathology. *Front Biosci* 2013, 5, 554-563.

[14] Lenzken S.C, Achsel T., Carr`ı M.T, Barabino S.M.L, NeuronalRNA-binding proteins in health and disease.*Wiley Interdiscip Rev RNA* 2014, 5, 565-576.

[15] Kim M.Y, Hur J., Jeong S., Emerging roles of RNA and RNA-binding protein network in cancer cells. *BMB Rep.* 2009, 42, 125–130

[16] Udagawa T., Swanger S.A, Takeuchi K., Kim J.H, Nalavadi V., Shin J., Lorenz L.J, Zukin R.S, Bassell G.J, Richter J.D, Bidirectional control of mRNA translation and synaptic plasticity by the cytoplasmic polyadenylation complex. *Mol Cell.* 2012, 47, 253-66.

[17] Pascale A., Amadio M., Quattrone A., Defining a neuron: neuronal ELAV proteins, *Cell. Mol. Life. Sci* 2008, 65, 128–140

[19] Christie S.B, Akins M.R, Schwob J.E, Fallon J.R, The FXG: a presynaptic fragile X granule expressed in a subset of developing brain circuits. *J Neurosci* 2009, 29: 1514–1524

[20] Ishigaki S., Masuda A., Fujioka Y., Iguchi Y., Katsuno M., Shibata A., Urano F., Sobue G., Ohno K., Position-dependent FUS-RNA interactions regulate alternative splicing events and transcriptions. *Sci. Rep.,* 2012, 2, 529

[21] Jensen K.B, Dredge B.K, Stefani G., Zhong R., Buckanovich R.J, Okano H.J, Yang Y.Y, Darnell R.B, Nova-1 regulates neuron-specific alternative splicing and is essential for neuronal viability. *Neuron* 2000, 25, 359–371.

[22] Yano M., Hayakawa-Yano Y., Mele A., Darnell R.B, Nova2 regulates neuronal migration through an RNA switch in disabled-1 signaling. *Neuron* 2010, 66, 848–858.

[23] Jensen K.B, Musunuru K., Lewis H.A, Burley S.K, Darnell R.B, The tetranucleotide UCAY directs the specific recognition of RNA by the Nova K-homology 3 domain**.** *Proc Natl Acad Sci U S A*, 2000, 97, 5740–5745.

[24] Licatalosi D.D, Yano M., Fak J.J, Mele A., Grabinski S.E, Zhang C., Darnell R.B Ptbp2 represses adult-specific splicing to regulate the generation of neuronal precursors in the embryonic brain, *Genes Dev*, 2012, 26, 1626–1642 25; Ayala Y.M, Pantano S., D'Ambrogio A., Buratti E., Brindisi A., Marchetti C., Romano M., Baralle F.E, Human, Drosophila, and C.elegans TDP43: nucleic acid binding properties and splicing regulatory function. *J Mol Biol*, 2005, 348, 575–588.

[26] Antic D., Keene J.D., Embryonic lethal abnormal visual RNA-binding proteins involved in growth, differentiation, and posttranscriptional gene expression. *Am. J. Hum. Genet.*, 1997, *61*, 273

[27] Query C.C.; Bentley, R.C., Keene, J.D., A common RNA recognition motif identified within a defined U1 RNA binding domain of the 70K U1 snRNP protein, *Cell* 1989, 57, 89

[28] Wang X., Tanaka Hall T. M. Structural basis for recognition of AU-rich element RNA by the HuD protein. *Nat. Struc. Biol* 2001, 8, 141-145

[29] Talman V., Pascale A., Jäntti M., Amadio M., Tuominen R.K., Protein Kinase C Activation as a Potential Therapeutic Strategy in Alzheimer's Disease: Is there a Role for Embryonic Lethal Abnormal Vision-like Proteins? *Basic Clin Pharmacol Toxicol.*, 2016, 119, 149-160

[30] Lal A., Mazan-Mamczarz K., Kawai T., Yang X., Martindale J.L, Gorospe M. Concurrent versus individual binding of ELAVL1 and AUF1 to common labile target mRNAs. *Embo J*., 2004, 23, 3092–3102.

[31] Dean J,L, Wait R,, Mahtani K,R, Sully G,, Clark A,R, Saklatvala J,, The 3′ untranslated region of tumor necrosis factor alpha mRNA is a target of the mRNA-stabilizing factor ELAVL1. *Mol Cell Biol.* 2001, 21, 721–730.

[32] Levy N.S, Chung S., Furneaux H., Levy A.P., Hypoxic stabilization of vascular endothelial growth factor mRNA by the RNA-binding protein ELAVL1. *J Biol Chem*. 1998, 273, 6417–6423.

[33]. Nabors L.B., Suswam E., Huang Y., Yang X., Johnson M.J, King P.H., Tumor necrosis factor alpha induces angiogenic factor up-regulation in malignant glioma cells: a role for RNA stabilization and ELAVL1. *Cancer Res*., 2003, 63, 4181–4187

[34] Dixon D.A, Tolley N.D, King P.H, Nabors L.B, McIntyre T.M, Zimmerman G.A, Prescott S.M, Altered expression of the mRNA stability factor ELAVL1 promotes cyclooxygenase-2 expression in colon cancer cells. *J Clin Invest*., 2001, 108, 1657–1665

[35] Peng S.S, Chen C.Y, Xu N, Shyu A.B., RNA stabilization by the AU-rich element binding protein, ELAVL1, an ELAV protein. *Embo J.,* 1998, 17, 3461–3470

[36] Fan X.C, Steitz J.A. Overexpression of ELAVL1, a nuclear-cytoplasmic shuttling protein, increases the in vivo stability of ARE-containing mRNAs. *Embo J.,*1998, 17, 3448–3460

[37] Yang X, Wang W., Fan J., Lal A., Yang D., Cheng H., Gorospe M., Prostaglandin A2-mediated stabilization of p21 mRNA through an ERK-dependent pathway requiring the RNA-binding protein ELAVL1. *J Biol Chem*. 2004, 279, 49298–49306

[38] Wang W., Caldwell M.C, Lin S., Furneaux H., Gorospe M. ELAVL1 regulates cyclin A and cyclin B1 mRNA stability during cell proliferation. *Embo J*. 2000, 19, 2340–2350

[39] Rodriguez-Pascual F., Hausding M., Ihrig-Biedert I., Furneaux H., Levy A.P, Forstermann U., Kleinert H., Complex contribution of the 3′-untranslated region to the expressional regulation of the human inducible nitric-oxide synthase gene. Involvement of the RNA-binding protein ELAVL1. *J. Biol. Chem.* 2000, 275, 26040–26049

[40] Xiao L, Rao JN, Zou T, Liu L, Marasa BS, Chen J, Turner DJ, Zhou H, Gorospe M, Wang JY. Polyamines regulate the stability of activating transcription factor-2 mRNA through RNAbinding protein ELAVL1 in intestinal epithelial cells. *Mol Biol Cell.* 2007, 18, 4579–4590

[41] Zhang X., Zou T., Rao J.N, Liu L., Xiao L., Wang P.Y, Cui Y.H, Gorospe M., Wang J.Y., Stabilization of XIAP mRNA through the RNA binding protein ELAVL1 regulated by cellular polyamines. *Nucleic Acids Res.,*2009, 37, 7623-37

[42] Ohtsuka T., Yano M., Okano H. Acute reduction of neuronal RNA binding Elavl2 protein and Gap43 mRNA in mouse hippocampus after kainic acid treatment. *Biochem Biophys Res Commun*, 2015, 466, 46-51

[43] Akamatsu W., Okano H.J, Osumi N., Inoue T., Nakamura S., Sakakibara S., Miura M., Matsuo N., Darnell R.B, Okano H., Mammalian ELAV-like neuronal RNA-binding proteins HuB and HuC promote neuronal development in both the central and the peripheral nervous systems. *Proc Natl Acad Sci U S A.* 1999, 96, 9885-90

[44] Rodrigues D.C, Kim D.S, Yang G., Zaslavsky K., Ha K.C, Mok R.S, Ross P.J, Zhao M., Piekna A., Wei W., Blencowe B.J, Morris Q., Ellis J., MECP2 Is Post-transcriptionally Regulated during Human Neurodevelopment by Combinatorial Action of RNA-Binding Proteins and miRNAs. *Cell Rep.* 2016, 17, 720-734

[45] Bolognani F., Qiu S., Tanner D.C, Paik J, Perrone-Bizzozero N.I, Weeber E.J:, Associative and spatial learning and memory deficits in transgenic mice overexpressing the RNA-binding protein ELAVL4. *Neurobiol. Learn. Mem,* 2007, 87, 635-643

[46] Gantt K.R, Jain R.G, Dudek R.W, Pekala P.H. HuB localizes to polysomes and alters C/EBP-beta expression in 3T3-L1 adipocytes. *Biochem. Biophys.res.comm,* 2004, 313, 619-622

[47] Deschênes-Furry J., Perrone-Bizzozero N., Jasmin B. J, The RNA-binding protein HuD: a regulator of neuronal differentiation, maintenance and plasticity. *Bioessays,* 2006, 28, 822-823

[48] Beckel-Mitchener A.C., Miera A., Keller R., Perrone-Bizzozero N., Poly(A) tail length-dependent stabilization of GAP-43 mRNA by the RNA-binding protein ELAVL4. *J. Biol. Chem.* 2002, 277, 27996-8002

[49] Denkert C., Koch I., von Keyserling N., Noske A., Niesporek S., Dietel M., Weichert W. *Modern Pathology*, 2006, 19, 1261–1269

[50] Dong R., Yang G.D, Luo N.A, Qu Y.Q, ELAVL1: a promising therapeutic target for angiogenesis. *Gland Surg.*, 2014, 3, 203-206

[51] Khabar K.S, Post-transcriptional control during chronic inflammation and cancer: a focus on AU-rich elements. *Cell Mol Life Sci.,* 2010, 67, 17, 2937-2955

[52] Abdelmohsen K., Gorospe M. *Advanced Review*, 2010, 1, 214–229

[53] Meisner N.C, Hintersteiner M., Mueller K., Bauer R., Seifert J.M, Naegeli H.U., Ottl J., Oberer L., Guenat C., Moss S., Harrer N., Woisetschlaeger M., C. Buehler1, V. Uhl, M. Auer, Identification and mechanistic characterization of low-molecular-weight inhibitors for HuR. *Nat. Chem. Biol.* 2007, 3, 503-515

[54] Kasashima K., Sakashita E., Saito K., Sakamoto H. Complex formation of the neuron-specific ELAV-like Hu RNA-binding proteins. *Nucleic Acids Res*. 2002, 30, 4519–4526

[55]. Huang C.Y. Determination of binding stoichiometry by the continuous variation method: the Job plot. Methods *Enzymol*. 1982, 87, 509–525

[56] Hojoong K., Kyung-Chae J., Min-Ju C., Soo-Youl K., Woong-Yang P., Flavonoids inhibit the AU-rich element binding of HuC. *BmB Rep,* 2009, 42, 41-46

[57] Min-Ju C., Hye Youn S., Eun-Hye K., Mira L., Hojoong K., Chong Hak C., Sunwoo K., Woong-Yang P., Chemical inhibitors destabilize HuR binding to the AU-rich element of TNF-α mRNA. *Exp.Mol.Med* 2009, 41, 824-831

[58] D'Agostino V. G, Adami V., Provenzani A., A Novel High Throughput Biochemical Assay to Evaluate the HuR Protein-RNA Complex Formation. *PlosOne* 2013, 8, 8

[59] D'Agostino V.G, Lal P., Mantelli B., Tiedje C., Zucal C., Thongon N., Gaestel M., Latorre E., Marinelli L., Seneci P., Amadio M., Provenzani A., Dihydrotanshinone-I interferes with the RNA-binding activity of HuR affecting its posttranscriptional function. *Nature*, 2015, 5, 16478

[60] Wu X., Lan L., Wilson D. M., Marquez R. T., Tsao W., Gao P., Roy A, Turner B. A., McDonald P., Tunge J. A, Rogers S. A, Dixon D. A., Aubé J., Xu L., Identification and Validation of Novel Small Molecule Disruptors of HuR-mRNA Interaction. *ACS chemical biology*, 2015, 10, 1476-1484

[61] Wang Z., Bhattacharya A., Ivanov D. N., Identification of Small-Molecule Inhibitors of the HuR/RNA Interaction Using a Fluorescence Polarization Screening Assay Followed by NMR Validation. *PLOSone*, 21, 2015, 1-13

[62] Wang X., Tanaka Hall T. M., Structural basis for recognition of AU-rich element RNA by the HuD protein. *Nat. Struc. Biol.* 2001, 8, 141-145

[63] Chung S., Eckrich M., Perrone-Bizzozero N., Kohn D.T., Furneaux H., The Elav-like proteins bind to a conserved regulatory element in the 3′-untranslated region of GAP-43 mRNA. *J.Biol.Chem.* 1997, 272, 6593-6598

[64] Barker A., Epis M.R., Porter C.J., Hopkins B.R., Wilce M.C., Wilce, J.A., Giles K.M., Leedman P.J. Sequence requirements for RNA binding by HuR and AUF1. *J. Biochem.* 2012 *151*, 423-37

[65] Rossi D., Amadio M., Carnevale Baraglia A., Azzolina O., Ratti A., Govoni S., Pascale A., Collina S. Discovery of small peptides derived from embryonic lethal abnormal vision proteins structure showing RNA-stabilizing properties. *J. Med. Chem.* 2009, *52* , 5017–5019

[66] Amadio M., Pascale A., Govoni S., Laurini E., Pricl S., Gaggeri R., Rossi D., Collina S. Identification of peptides with ELAV-like mRNA-stabilizing effect: an integrated in vitro/in silico approach. *Chem. Biol. Drug Des.* 2013, 81, 707–714

[67] Vasile F., Rossi D., Collina S., Potenza D.**,** Diffusion-Ordered Spectroscopy and Saturation Transfer Difference NMR Spectroscopy Studies of Selective Interactions between ELAV ProteinFragments and an mRNA Target *Eur. J. Org. Chem.* **2014**, 6399–6404

[68] Gerber P. R., Mìller K., MAB, a generally applicable molecular force field for structure modelling in medicinal chemistry. *J. Comput.-Aided Mol. Des.* 1995, 9, 251– 268.

[69] De Lano W.L, the PyMOl molecular graphic system, (2012). Http://www.pymol.org.

[70] Meireles L. M. C., Dömling A. S., Camacho C., ANCHOR: a web server and database for analysis of protein–protein interaction binding pockets for drug discovery. *J. Nucl. Acids Res*. 2010, 1; 38

[71] Reulecke G., Lange J., Albrecht R., Klein M., Rarey M., Towards an Integrated Description of Hydrogen Bonding and Dehydration: Decreasing False Positives in Virtual Screening with the HYDE Scoring Function, *ChemMedChem* 2008, 3, 885 – 897; Schneider N., Hindle S., Lange G., Klein R., Albrecht J., Briem H., Beyer K., Claußen H., Gastreich M., Lemmen C., Rarey M.,

Substantial improvements in large-scale redocking and screening using the novel HYDE scoring function. *J. Comput.-Aided Mol. Des*. 2012, 26, 701– 723.

[72] SeeSAR (vers 3.0) Biosolveit. Gmbh. 2014

[73] Elders N.; Ruijter E.; de Kanter F. J. J.; Groen M. B.; Orru R. V. A. Selective formation of 2-imidazolines and 2-substituted oxazoles by using a three-component reaction., *Chem. Eur. J.* 2008, *14*, 4961–4973; Bonne D., Dekhane M., Zhu J. Modulating the reactivity of α-isocyanoacetates: multicomponent synthesis of 5-methoxyoxazoles and furopyrrolones. *Angew. Chem. Int. Ed.* 2007, *46*, 2485-2488.

[74] Bornstein J.J., Eckroat T.J., Houghton J.L., Jones C.K. , Green K.D., Garneau-Tsodikova S., Tacrine-mefenamic acid hybrids for inhibition of acetylcholinesterase**, *Med.Chem.Comm***, 2011, 2, 406-412; Dekker F.J., Ghizzoni M., van der Meer N., Wisastra R., Haisma H.J., Inhibition of the PCAF histone acetyl transferase and cell proliferation by isothiazolones. *Bioorg. Med. Chem*, 2009, 17, 460-466

[75] Organic Syntheses, Coll. Vol. 10, p.692 (2004); Vol. 77, p.198 (2000)

[76] Castagnoli N. J., Condensation of succinic anhydride with N-benzylidene-N-methylamine. Stereoselective synthesis of trans- and cis-1-methyl-4-carboxy-5-phenyl-2-pyrrolidinone. *J. Org. Chem.* 1969, 34, 3187.

[77] Castagnoli N., Cushman M., Condensation of succinic anhydrides with Schiff bases. Scope and mechanism. *J. Org. Chem*. 1971, 36, 3404.

[78] Krasavin M., Dar'in D., Current diversity of cyclic anhydrides for the Castagnoli‑Cushman-type formal cycloaddition reactions: prospects and challenges. *Tetrahedron Letters,* 2016, 57, 1635–1640

[79] Kroon E., Schulze J. O., Süß E., Camacho C. J., Biondi R. M., A. Dömling, Discovery of a Potent Allosteric Kinase Modulator by Combining Computational and Synthetic Methods. *Angew. Chem Int Ed*, 2015, 54, 13933–13936

[80] Rossi D, Marra A, Picconi P, Serra M, Catenacci L, Sorrenti M, Laurini E, Fermeglia M, Pricl S, Brambilla S, Almirante N, Peviani M, Curti D, Collina S. Identification of RC-33 as a potent and selective σ_1 receptor agonist potentiating NGF-induced neurite outgrowth in PC12 cells. Part 2: g-

Scale synthesis, physicochemical characterization and in vitro metabolic stability. *Bioorg. Med. Chem.* 2013, 21, 2577-2586

[81] Blackburn C., Guan B., Fleming P., Shiosaki K., Tsai S., Parallel synthesis of 3 aminoimidazo[1,2-a]pyridines and pyrazines by a new three-component condensation. *Tetrahedron Lett.*, 1998, 39, 3635–3638

[82] Bienaymé H., Bouzid K., A new heterocyclic multicomponent reaction for the combinatorial synthesis of fused 3-aminoimidazoles. *Angew. Chem Int Ed* , 1998, 37, 2234–2237.

[83] Groebke K.,Weber L., Mehlin F., Synthesis of imidazo[1,2-a] annulated pyridines, pyrazines and pyrimidines by a novel threecomponent condensation. *Synlett*, 1998, 6, 661–663.

[84] Groebcke K., Weber L., Mehlin F., A fast heterocyclic three component synthesis of imidazo[1,2-a]annulated pyridines, pyrazines, pyrimidines and thiazoles under microwave conditions. *Synlett.* 1998, 661−663.47

[85] Starrett J. E., Montzka T. A., Crosswell A. R., Cavanagh R. L., Synthesis and biologicalactivity of 3-substituted imidazo[1,2-a]pyridines as antiulcer agents. *J. Med. Chem.* 1989, *32*, 2204−2210.

[86] Rival Y., Grassy G., Michel G., Synthesis and antibacterial activity of some imidazo[1,2-a]pyrimidine derivatives. *Chem. Pharm. Bull.,* 1992, *40*, 1170−1176; Shaaban S., Abdel-Wahab, B. F., Groebke–Blackburn–Bienaymé multicomponent reaction: emerging chemistry for drug discovery. *Mol Divers*, 2016, 20, 233–254,

[87] Borch, R. F.; Bernstein, M. D.; Durst, H. D., Cyanohydridoborate anion as a selective reducing agent. *J. Am. Chem. Soc.* 1971, *93*, 2897

[88] Eschweiler W., Ersatz von an Stickstoff gebundenen Wasserstoffatomen durch die Methylgruppe mit Hülfe von Formaldehyd, *Ber.*, 1905, 38, 880.

[89] Elliot A., Bowman Wildman R., Studies on the Mechanism of the Leuckart Reaction. *J.of the Am. Chem.Soc*. 1948, 70, 1187–1189

[90] Mannich C., Krösche W., Ueber ein Kondensationsprodukt aus Formaldehyd, Ammoniak und Antipyrin, *Archiv der Pharmazie*. 1912, 250, 647–667.

[91] Abdel-Magid A. F., Carson K. G., Harris B. D., Maryanoff C. A., Shah R. D., Reductive Amination of Aldehydes and Ketones with Sodium Triacetoxyborohydride. Studies on Direct and Indirect Reductive Amination Procedures. *J. Org. Chem.* 1996, 61, 3849–3862

[92] Gersho H., Pyrimidines. II. Chlorinated Pyrimidines Derived from Orotic Acid, *J. Org. Chem*, 1962, 27, 3507-10

[93] Turner J.J., Meeuwenoord N.J., Rood A., Borst P., van der Marel G.A., van Boom J.H., Reinvestigation into the Synthesis of Oligonucleotides Containing 5-(β-D-Glucopyranosyloxymethyl)-2′-deoxyuridine. *Eur. J. Org. Chem*, 2003, 2003, 3832–3839

[94] WO2013/151877; WO2015/025164A1.

[95] Prabakaran K., Nawaz Kha F., Sung Jin J., An efficient 2-(1*H*-benzotriazole-1-yl)-1,1,3,3-tetramethyluronium tetrafluoroborate (TBTU)-mediated synthesis of 5-(trifluoromethyl)-*N*-alkyl-1-(3-phenylisoquinoline-1-yl)-1*H*-pyrazole-4-carboxamides. *Res Chem Intermed*, 2012, 38, 615–627

[96] Hudson R. H. E., Wojciechowski, F., The detrimental effect of orotic acid substitution in the peptide nucleic acid strand on the stability of PNA2:NA triple helices. *Canad. J. Chem.*, 2005, 83, 1731-1740

[97] Carpino L. A., 1-Hydroxy-7-azabenzotriazole. An efficient peptide coupling additive. *J. Am. Chem. Soc.*, 1993, 115, 4397

[98] Albericio F., Bofill J. M., El-Faham A., Kates S. A., Use of Onium Salt-Based Coupling Reagents in Peptide Synthesis. *J. Org. Chem.*, 1998, 63, 9678

[99] Dubois N., Glynn D., McInally T., Rhodes B., Woodward S. , Irvine D.J., Dodds C. , On DABAL-Me$_3$ promoted formation of amides. *Tetrahedron*, 2013, 69, 9890-9897

[100] Vigante B., Rucins M., Plotniece A., Pajuste K., Luntena I., Cekavicus B., Bisenieks E., Smits R., Duburs G., Sobolev A., Direct Aminolysis of Ethoxycarbonylmethyl 1,4 Dihydropyridine-3-carboxylates. *Molecules*, 2015, *20*, 20341-20354

[101] Zhang M., Zhu W., Li Y., Discovery of novel inhibitors of signal transducer and activator of transcription 3 (STAT3) signaling pathway by virtual screening. *Eur. J. Med. Chem* 2013, 62, 301-310

[102] J. Narayanan, Y. Hayakawa, J.Fan, K. L. Kirk, Convenient syntheses of biogenic aldehydes, 3,4-dihydroxyphenylacetaldehyde and 3,4-dihydroxyphenylglycolaldehyde, *Bioorg. Chem.* **2003**, *31*, 191-197

[103] Van Leusen A. M; Wildeman, J.; Oldenziel, O. H. Chemistry of sulfonylmethyl isocyanides. 12. Base-induced cycloaddition of sulfonylmethyl isocyanides to carbon,nitrogen double bonds. Synthesis of 1, 5-disubstituted and 1,4,5-trisubstituted imidazoles from aldimines and imidoyl chlorides. *J. Org. Chem.* **1977**, *42*, 1153-1159.

[104] Ugi I., Recent progress in the chemistry of multicomponent reactions. *Pure Appl. Chem.,* 2001, *73*, 187-191.

[105] Ruijter E.; Orru R. V. A. Multicomponent reactions – opportunities for the pharmaceutical industry. *Drug Discov. Today,* 2013, *10*, e15–e20.

[106] Dömling A.; Wang W.; Wang K. Chemistry and biology of multicomponent reactions. *Chem. Rev.* 2012, 112, 3083–3135.

Chapter III

1. Introduction

Over the last two decades chirality has become a key issue in pharmaceutical research. The human body is a chiral environment due to the presence of molecules (i.e. enzymes, receptors, etc.) in their homochiral forms; therefore the enantiomers of a biologically active compound may show different interactions to the target and, more generally, different behaviour in the biological environment thus generating different responses. For this reason, the investigation (i.e pharmacokinetics, pharmacodynamics, metabolic stability and toxicological properties) of the chiral molecule in its enantiopure forms is a key issue to be addressed during the drug discovery and development process Nowadays an in depth investigation of pure enantiomers is a requirement for a chiral molecule to enter clinical trials, as stated by different regulatory agencies.[1, 2]

Different paths can be followed to obtain enantiopure compounds, including asymmetric synthesis, conversion of chiral starting materials into the desired homochiral molecule, and chiral resolution of racemates.

More specifically, asymmetric synthesis represents the most commonly employed approach to obtain homochiral compounds in large quantities, even though it presents some drawbacks mainly related to the time necessary to set-up and optimize the experimental conditions.[3] Moreover, in many cases only one enantiomer can be easily prepared, due to the commercial availability of only one stereoisomeric form of the chiral reagent used. Beside asymmetric synthesis, the chiral resolution of racemates using different methodologies, such as enzymatic kinetic resolution,[4] fractional crystallization of diasteroisomeric salts or enantioselective chromatography [5,6] has also been successfully employed for the isolation of homochiral compounds. Among these methodologies, enantioselective high performance liquid chromatography (HPLC) resolution on chiral stationary phases (CSPs) is widely used, being a viable route in order to quickly obtain both enantiomers with high optical purity and yields, and also due to the commercial availability of a wide variety of efficient and selective CSPs.[7]

As regards the assignment of the absolute configuration of enantiopure compounds, different methodologies have been successfully experimented. Among these, X-ray crystallography is the most reliable method for the assignment of the absolute configuration. [8] To apply this technique, various criteria, mainly related to the sample characteristics (i.e. presence of an element heavier than oxygen, adequate resonant scattering properties), should be respected and can not often be easily satisfied. Another interesting approach considers the involvement of Nuclear Magnetic Resonance (NMR) to assign the stereochemistry of organic compounds. This strategy involves the derivatization of the substrate with unknown configuration with an *R* and *S* chiral auxiliary reagent. Thereafter, the identification of the correct stereochemistry is based on the measurement of the

difference in terms of chemical shifts of protons in the NMR spectra of the diastereoisomeric derivatives.[9]

Finally, various chiroptical spectroscopic techniques, such as Electronic circular dichroism (ECD) and vibrational circular dichroism (VCD), have also been successfully applied to the absolute configurational assignment of biologically active molecules.[10, 11]

Interestingly, the combination of enantioselective chromatography with chiroptical spectroscopy recently emerged as a powerful tool for the isolation of pure enantiomer and the assessment of their absolute configuration. The chiroptical spectroscopic techniques most frequently employed for this purpose include (ECD), Optical Rotatory Dispersion (ORD) and (VCD), that can be combined with *ab initio* and DFT calculations in order to theoretically predict both ECD and VCD spectra, to be then compared with experimental ones.

As part of my research for my PhD, the combination of enantioselective chromatography with chiroptical spectroscopic techniques has been successfully experimented for the isolation and configurational assignment of the enantiomers of two different classes of compounds, such as γ-butyrolactones (D. Rossi, R. Nasti, *J.Pharm.Biom.Anal* Accepted, 2017, doi:10.1016/j.jpba.2017.01.007) and A_3 adenosine receptor antagonists (D. Rossi, R. Nasti, *Chirality*, 2016). The results are described in detail in the enclosed papers 2-3 and briefly summarized in the following paragraphs. Both researches were conducted in tight collaboration with Prof. Sergio Abbate, Prof. Giovanna Longhi and Dr. Giuseppe Mazzeo of University of Brescia, for the configurational study by chiroptical spectroscopy.

2. Chiral separation and configurational study of a four chiral 3-aryl-substituted-γ-butyrolactones

The γ-butyrolactone ring is a five-membered cyclic scaffold widely distributed in bioactive natural products (i.e. Helenalin, Parthenolide) [12], as well as in synthetic molecules of pharmaceutical interest (i.e antifungal [12], anticancer [13] and antifeedant compounds [14). From a synthetic standpoint, the γ-butyrolactone can be considered a versatile key intermediate for the preparation of various compound classes, including the PKC ligands studied by us (see Chapter I, scheme 2).[15] Specifically, being γ-butyrolactone **1-3** (Figure 1) the first chiral intermediates of the synthetic route, they emerged as the optimal candidates for the preparation of enantiopure forms to be then used as homochiral building blocks for the asymmetric synthesis of the target compounds. [16-18]
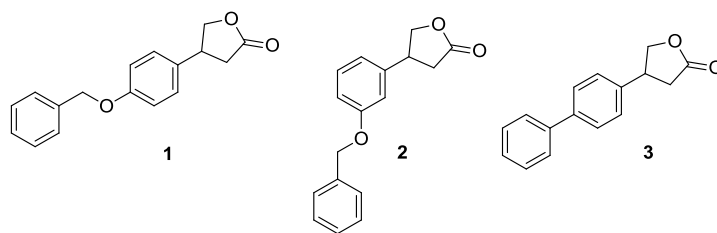
Figure 1. studied γ-butyrolactones (**1-3**)

In this context, my PhD research focused on the preparation of the enantiomers of γ-butyrolactones **1-3** followed by the assignment of their absolute configuration by a full set of chiroptical techniques (VCD, ECD and ORD) in combination with DTF calculations, as reported in *paper 2*. The enantiomers of the γ-butyrolactone **4** were also prepared and characterized as reference compounds for configurational assignment (AC) purposes.[19]. The enantioselctive synthesis of *(R)* and *(S)*-**4** have been described in literature *via* asymmetric addition of phenil boronic acid catalyzed by Rhodium (Figure 2).[19]
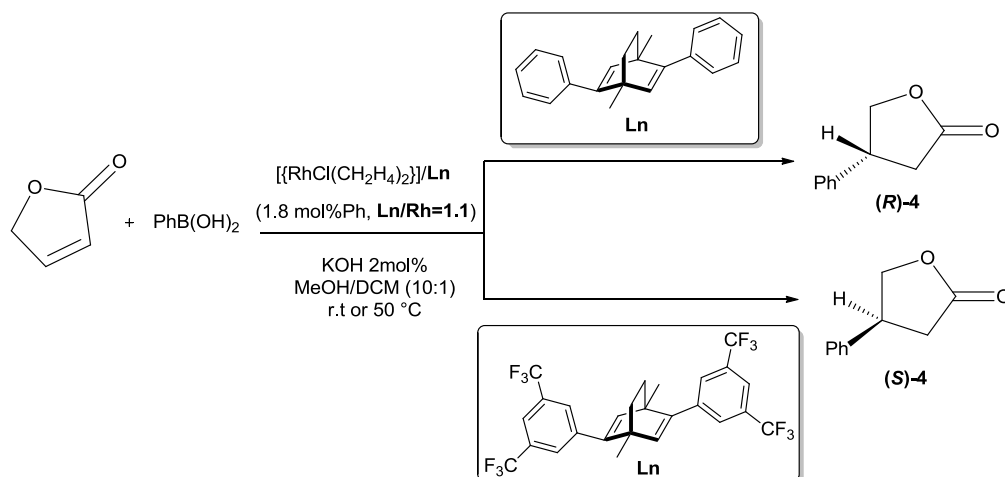
Figure 2: asymmetric synthesis of **4**

In the first step of our study, in order to identify the optimal experimental conditions for the enantioseparation of (*R/S*)-**1-3**, a primary standard screening protocol for cellulose and amylose derived CSPs was applied to Chiralcel OJ-H and Chiralpak IC (cellulose derivatives) as well as to Chiralpak AD-H (amylose derivative). Elution conditions included alcohols, such as methanol (MeOH), ethanol (EtOH) and 2-propanol (IPA), as pure solvents or in mixtures as well as mixtures of *n*-heptane (*n*-Hep) and IPA as polar modifier.

Based on the results of our screening, we selected for the next (semi)-preparative scale-up the Chiralpack AD-H CSP, combined with pure MeOH [for (*R/S*)-**1** and (*R/S*)-**3**] or *n*-Hep/EtOH 85/15 (v/v) [for (*R/S*)-**2**] as eluent (Figure 2).

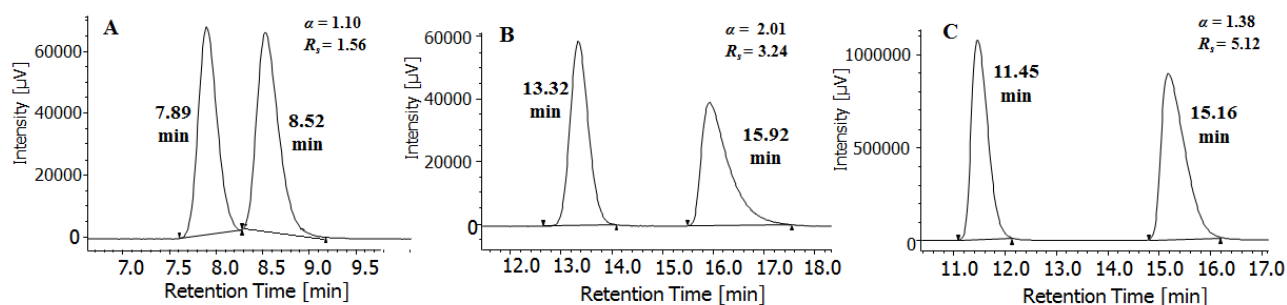**Figure 2:** Analytical separation on Chiralpack AD-H (150 mm x 4.6 mm, 5 µm) of (A) (*R/S*)-**1**, mobile phase: MeOH, detection at 274 nm; (B) (*R/S*)-**2**, mobile phase *n*-Hep/EtOH 85/15 (v/v), detection at 274 nm; (C) (*R/S*)-**3**, mobile phase: MeOH, detection at 254 nm. For all: Injection volume 10 µL, flow rate: 1 mL min^{-1}

The separation of **1-3**-enantiomers in (semi)preparative scale was accomplished using a RegisPack column (250 mm × 10 mm, 5 µm) under the conditions summarized in Table 1, providing the desired enantiomers in the amount and optical purity suitable for the configurational study, as stated in Table 2. As regards compound 4, its enantiomers were isolated applying the elution conditions previously described by Luo et *al*, with suitable modifications (Table 1). It is worth noting that, using the Chiralpak AD-H (an amylose derived CSP column) the *dextro* isomers are the first eluted enantiomers for all the studied γ-butyrolactones.

Cmpd	Mobile Phase (v/v)	Flow rate (mL min^{-1})	Tr_A (min)	Tr_B (min)	Injection volume (mL)	Concentration (mg mL^{-1})
1	MeOH	4	11.63	12.44	1	4
2	*n*-Hep/EtOH 85/15	4	20.75	24.02	1	4
3	MeOH	4	16.48	21.29	2.5	3
4	*n*-Hep/EtOH 95/5	4	25.28	30.13	5	2

Table 1 (Semi)-preparative resolution of (*R/S*)-**1-4** on a RegisPack column (250 mm × 10 mm, 5 µm).

Cmpd	t_R (min)	$[\alpha]_D^{20\ a}$	e.e [%]	Isolated amount (mg)	Yield [%]
(+)-1	7.84	29.2	99.4	7.2	32.7
(-)-1	8.39	-27.42	97.7	7.8	35.4
(+)-2	13.12	29.2	99.1	3.7	31.5
(-)-2	15.51	-28.6	99.3	3.8	32.2
(+)-3	11.84	33.8	98.8	10.3	34.5
(-)-3	15.27	-33.3	98.3	9.5	31.6
(+)-4	14.04	47.4	99.9	8.8	43.7
(-)-4	16.56	-45.6	95.1	7.1	35.3

Table 2: Chiroptical properties and isolated amounts of **1-4-** enantiomers.

The assignment of the absolute configuration of the pure enantiomers was then accomplished by VCD, EDC, ORD combined with DFT calculations. All the isomers from **1–4** have shown a good response to the three techniques employed. In particular, an excellent mirror image aspect was observed in the data of each couple of enantiomers, evidencing a correspondence between the chiroptical data and the elution order of the enantiomers on Chiralpak AD-H CSP, as summarized in Figure 3.
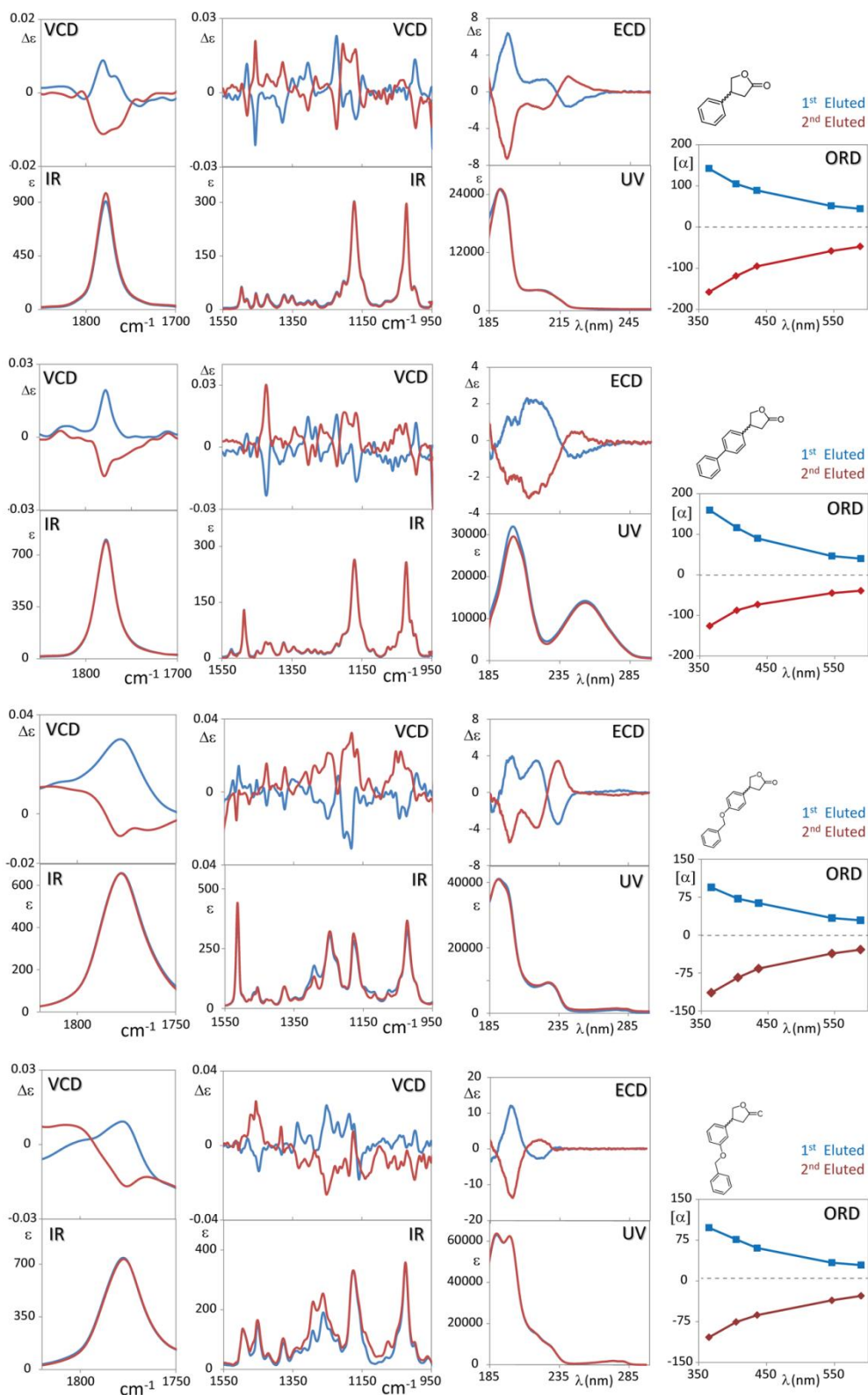
Figure 3: Superimposed VCD spectra in the C=O stretching region (first column from left), in the fingerprint region (second column), ECD spectra (third column) and ORD curves for the two enantiomers of molecules **4** (top row), **3** (second row from top), **1** (third row) and **2** (bottom row). color-coded: blue, first eluted; red, second eluted.

Successively, the experimental data were supported by DFT calculations (Figure 4 and 5). A reasonable number of conformers was found for each compound, especially for **3** and **4**, allowing the simplification of this step. In particular, as shown in Figure 4, the calculated VCD spectra for the (*S*) enantiomers of **4** and **3** were comparable to the first eluted enantiomers of the same compounds (left), whereas the calculated VCD spectra for the (*R*) enantiomers of **1** and **2** were very similar to the experimental VCD spectra of the second eluted enantiomers of these compounds (right). In addition the ECD spectra and ORD curves are excellently predicted by DFT calculations, as clearly reported in Figure 5. Overall, based on the results obtained so far, the (*S*) configuration was assigned to the first eluted enantiomers of all compounds and the (*R*) configuration to the second eluted ones, with high degree of confidence.
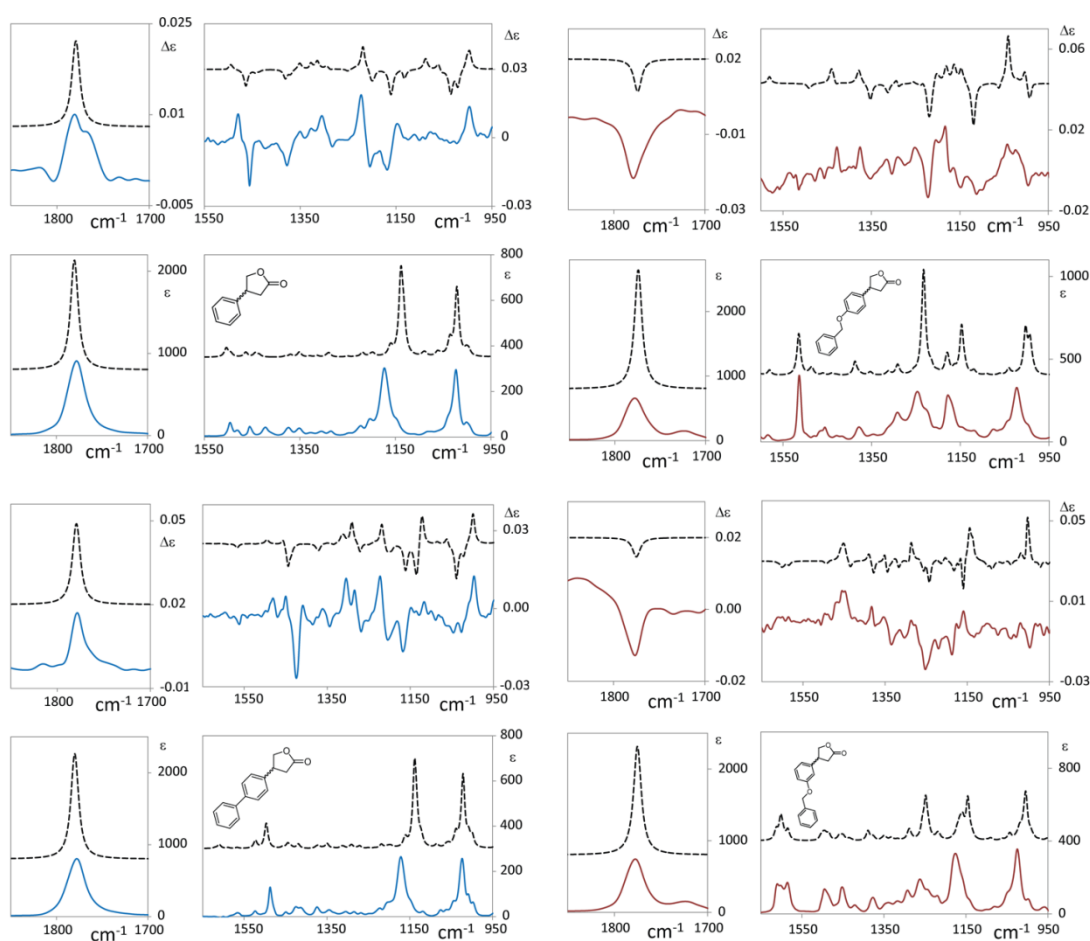

Figure 4. Comparison of experimental data (color, solid lines) with calculated data (black, dashed lines) VCD spectra of molecules **4** and **3** (left columns, top and lower respectively) and of molecules **1** and **2** (right columns, top and lower respectively). Color coding as in Figure 3.
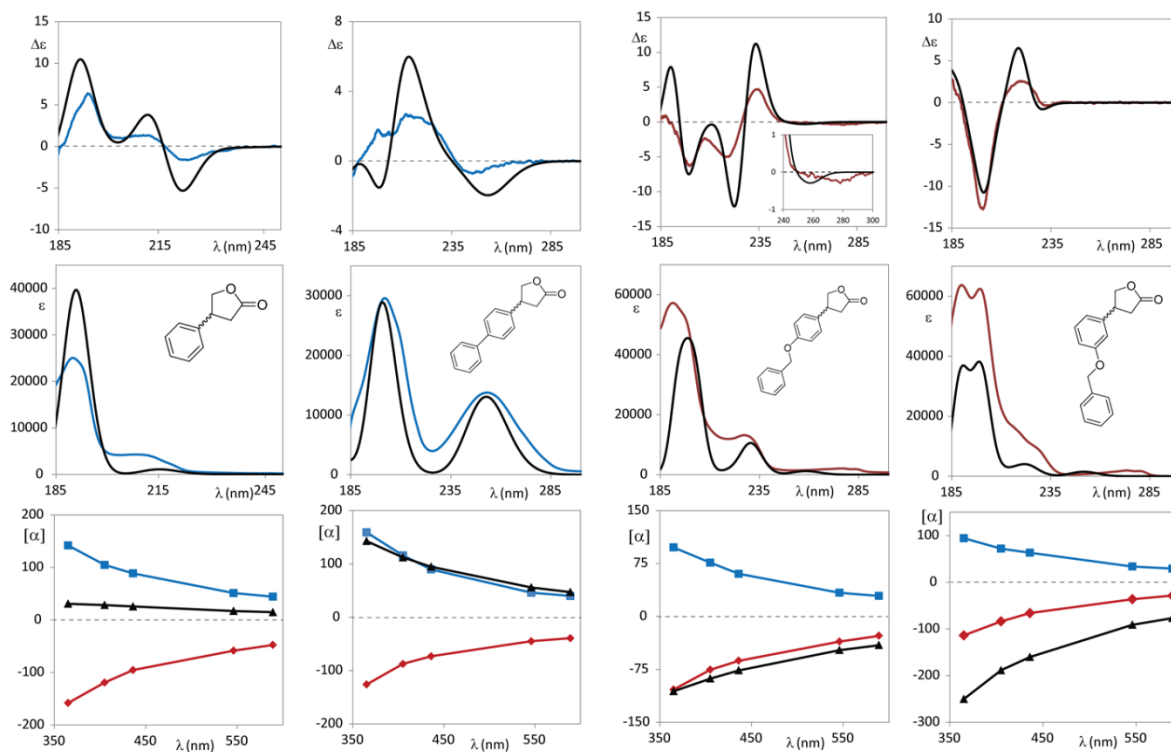
Figure 5. Comparison of experimental data (color, solid lines) with calculated data(black, solid lines) ECD spectra and ORD curves of molecules **4** and **3** (first left two columns) and of molecules **1** and **2** (right columns, top and lower respectively). Color coding as in Figure 3.

Lastly, the most populated conformers of **1-4** were selected for the docking studies onto the AD-H CSP, with the final aim of demonstrating a putative correlation between the elution order and the absolute configuration of the enantiomers The enantiopreference in the elution order can be easily explained with the mean docking scores. More specifically, in each evaluated case, the (*S*)-first eluted enantiomer presents a slightly higher binding energy correlated with shorter retention time in relation to the corresponding (*R*)-second eluted (Table 3).

Cmpd	t_R (min)	Mean Binding Energy (Kcal/mol)
(*S*)-**1**	7.84	-7.42
(*R*)-**1**	8.39	-7.58
(*S*)-**2**	13.12	-7.56
(*R*)-**2**	15.51	-7.70
(*S*)-**3**	11.84	-7.91
(*R*)-**3**	15.27	-8.19
(*S*)-**4**	14.04	-5.80
(*R*)-**4**	16.56	-5.93

Table 3. Measured elution times and calculated binding energies for the two enantiomers of **1–4**

3. Chiral resolution and configurational study of A₃ adenosine receptor (A₃AR) antagonists

Recently, the research group of prof. Giovanni Greco of University of Naples, has designed and synthetised a series of chiral 4-acylamino-6-alkyloxy-2-alkylthiopyrimidines as new adenosine receptors ligands (ARs) (Figure 6), In particular, compounds (*R/S*)-**5-7**, have been identified as the most promising A₃ receptors ligands.[20-23] In collaboration with Prof. Greco's research group, we made available our expertise in the "chirality field" to prepare enantiopure **5-7** and to assign the absolute configuration to pure enantiomers, the final aim of which was to investigate the role of chirality in the interaction with the A₃AR.

Ia= R: CH₃CH₂CH₂, R': C₆H₅CH₂
Ib= R: C₆H₅CH₂, R': CH₃CH₂CH₂

5   **6**   **7**

Figure 6. Structures of the Ia, Ib, **5-7**

In addition, the combination of enantioselective HPLC with chiroptical spectroscopies (VCD, ECD, ORD), matched with DFT calculations, was successfully experimented, as reported in paper 3.

To perform a successful analytical screening, we attempted a standard screening protocol on several polysaccharide-based CSPs, eluting with mobile phase of various composition of alkane and alcohol. Following the first screening with pure methanol, it was found that Chiralcel OJ-H (4.6 mm × 150 mm, 5 μm) lead to relatively short retention times, high enantioselectivity and high resolution for (*R/S*)-**6** ($\alpha = 6.7$, $R_s = 3.3$) and (*R/S*)-**7** ($\alpha = 1.9$, $R_s = 4.1$) (Figure 7). As regards (*R/S*)-**5,** the best enantioseparation was obtained eluting with *n*-hep/EtOH 95/5 (v/v) ($\alpha = 1.5$, $R_s = 2.4$) (Figure 7).
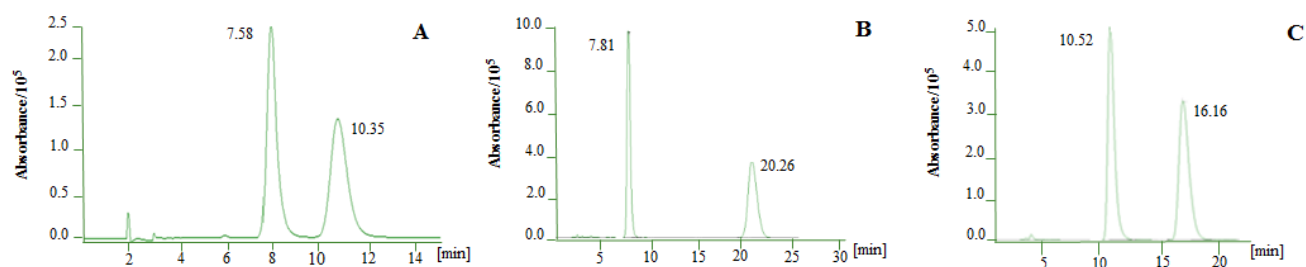
Figure 7. Analytical chromatographic profiles for *(R/S)*-**5** (A)**,** *(R/S)*-**6** (B) and *(R/S)*-**7** (C) (from left to right) obtained with Chiralcel OJ-H (4.6 mm × 150 mm, 5 µm); eluent *n*-hep/EtOH 95/5 (v/v) for **5** and 100% MeOH for **6** and **7**; flow rate: 1 mL/min; conc: 1mg/mL; injection volume: 10µL; detection at 250, 240 and 254 nm respectively

These analytical conditions were properly transferred on (semi)-preparative scale according to conditions reported in Table 4, affording enantiomeric **5**–**7** with good overall yields (81.8%, 93.1% and 97.2%, respectively) suitable for the chiroptical charaterisation both in terms of amount and optical purity (Table 5)

Cmpd	Eluent	t_A (min)	t_B (min)	Amount processed (mg)	Concentration (mg/mL)	Number of cycles
5	*n*-hep/EtOH (95:5 v/v)	13.87	20.25	38	2.0	10
6	MeOH	12.24	32.32	40	5.0	4
7	MeOH	12.79	22.15	25	5.0	3

Table 4. (Semi)-preparative resolution of racemic **5**–**7** on a Chiralcel OJ-H column (10mm x 250 mm, 5 µm).
Flow rate: 4.0 mL/min
Injection volume: 2.0 mL

Cmpd	t_R (min)	λ	c	$[\alpha]_\lambda^{22}$ (MeOH)	*ee*	Isolated amount (mg)	Yield (%)
(+)-**1**	7.67	435	0.1%	+40.4	99.9%[b]	15.2	40.0
(-)-**1**	10.25	435	0.1%	-40.4	99.9%[b]	15.9	41.8
(+)-**2**	8.12	589	0.2%	-214.7	99.9%[c]	18.5	46.3
(-)-**2**	21.91	589	0.2%	+214	99.9%[c]	18.7	46.8
(+)-**3**	10.57	435	0.5%	+56.2	99.9%[c]	12.0	48.0

(-)-3	17.2	435	0.5%	-56.4	99.9%[c]	12.3	49.2

Table 5. Chiroptical characteristics (OR, *ee*, and amount) of the separated enantiomers for **5**-7.

The assignment of the absolute configuration was then accomplished by VCD, ECD, ORD combined with DFT calculations. Both enantiomers **5** and **6** have been shown to be excellent mirror images to the three employed techniques and their experimental spectra were in complete accordance with the one calculated. (Figure 8 and 9) Although there was a good response of **7** to IR and UV analysis, the VCD and ECD spectra of **7** showed a poor signal to-noise. On the contrary, the experimental ORD analysis of **7** was in line with the one calculated, permitting the assignment of the absolute configuration of the enantiomers on the basis of recorded values.(Figure 10)
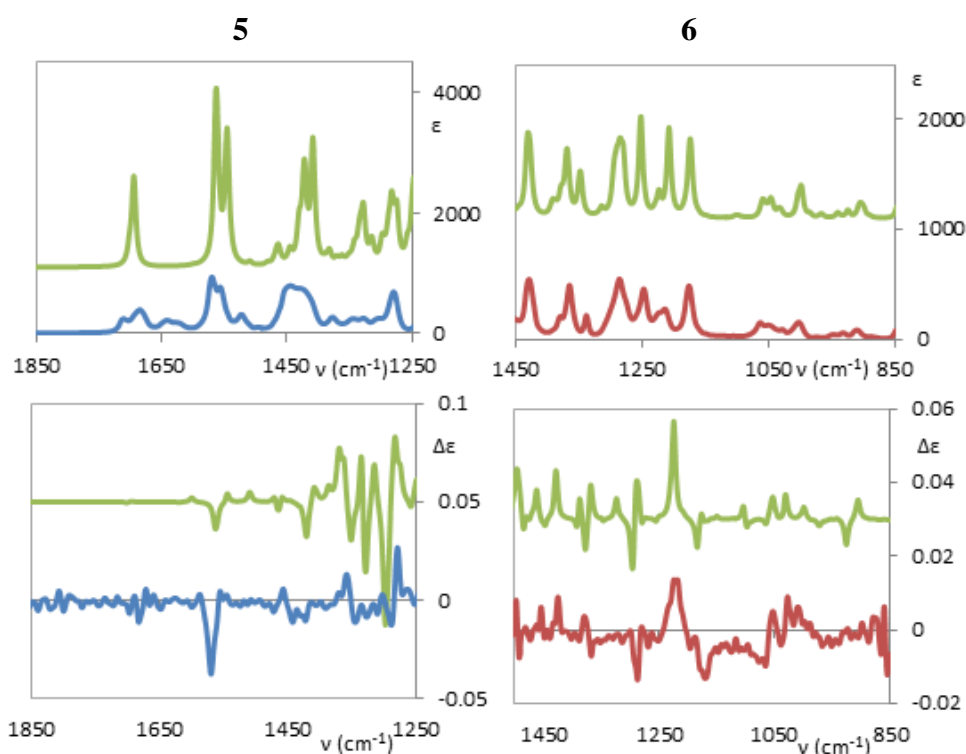
Figure 8. Comparison of experimental IR and VCD spectra (blue, first eluted enantiomer, and red, second eluted enantiomer) of **5-6** with calculated (green) IR and VCD average spectra for (*R*)-**5-6**. **5** and **6** experimental spectra are the semi-difference between enantiomers. **5** refers to solution in CD_3OD, while data for **6** was taken in CCl_4.
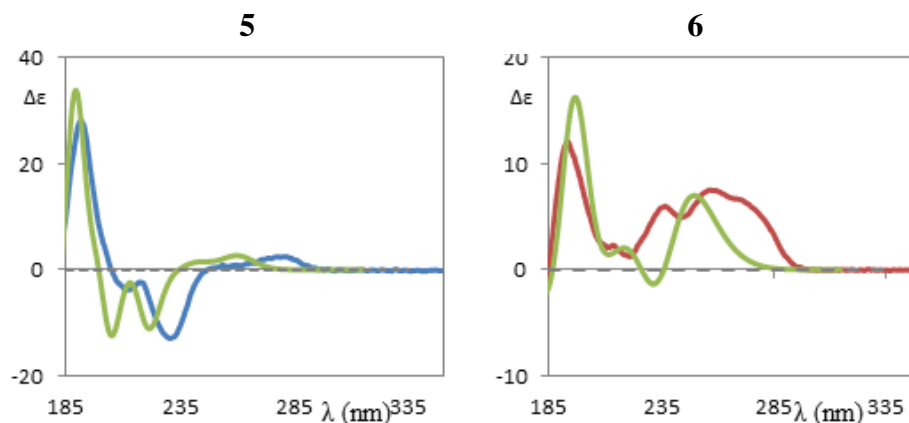
Figure 9. Comparison of average calculated (CAM-B3LYP on DFT/B3LYP/TZVP input geometries) ECD spectra for (*R*)-**5-6** (green line) and experimental ones (blue line, first eluted, and red line, second eluted).
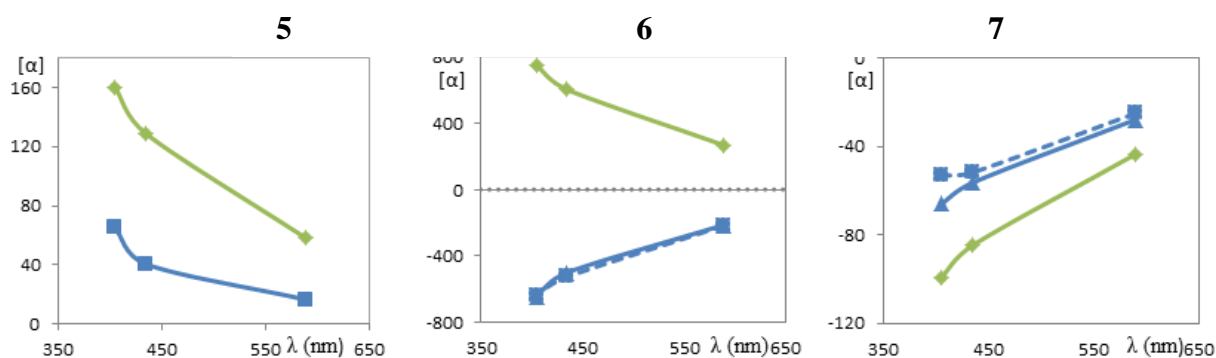

Figure 10. Comparison of average calculated (CAM-B3LYP/aug-cc-pVDZ on DFT/B3LYP/TZVP input geometries) ORD curves for (*R*)-**5-7** (green line) and experimental (solid blue line, methanol, and dotted blue line, chloroform) for the first eluted couple of compounds **5-7**.

Overall, the absolute configuration of **5** and **6** was unequivocally determined employing three chirooptical spectroscopy techniques. The experimental results in comparison with the ones calculated, have established the *(R)* absolute configuration for the first eluted enantiomer of **5** and for the second eluted enantiomer of **6**, with a high level of confidence. Although the lack of a good-response of **7** to VCD and ECD, the only ORD analysis compared with DFT calculation has without dobut permitted the assignment of the *(R)* absolute configuration to the first eluted enantiomer of **7**.

4. References

[1] Note for Guidance. Investigation of Chiral Active Substances. Brussels: Commission of the European Union, lll/3601/91 final, 1994.

[2] FDA's Policy Statement for the development of New Stereoisomeric Drugs. Chirality 1992;4:338– 40.

[3] Blaser HU, Schmidt E. Asymmetric catalysis on industrial scale.Weinheim: Wiley-VCH; 2004; Brown JM. Hydrogenation of funtionalized carbon-carbon double bonds. In: Jacobsen EN, Pfaltz A, Yamamoto Y, editors. Comprehensive asymmetric catalysis, Vol. I, Chapter 5.1. Berlin: Springer; 1999; Noyori R. Asymmetric catalysis: science and opportunities. *Angew Chem Int Ed Engl* 2002, 41, 2008–2022.

[4] Rachwalski M., Vermue N., Rutjes F.P.J.T., Recent advances in enzymatic and chemical deracemisation of racemic compounds, *Chem. Soc. Rev.*, 2013, **42**, 9268-9282

[5] Eliel E.L, Wilen S.H. Stereochemistry of organic compounds. New York: Wiley; 1994. p. 374– 81

[6] Kozma D, editor. CRC handbook of optical resolutions via diastereomeric salt formation. Boca Raton, FL:CRC Press; 2002. p. 9 –40

[7] Francotte E. Enantioselective chromatography as a powerful alternative for the preparation of drug enantiomers.*J.Chromatogr.A*, 2001, 906, 379– 97; Miller L, Orihuela C, Fronek R, Murphy J. Preparative chromatographic resolution of enantiomers using polar organic solvents with polysaccharide chiral stationary phases. *J.Chromatogr. A* 1999, 865, 211–26

[8] Flack H.D., Bernardinelli G., The use of X-ray crystallography to determine absolute configuration, *Chirality*, 2008, 20, 681–690,

[9] Jose´ Manuel Seco, Emilio Quin˜oa´, and Ricardo Riguera, The Assignment of Absolute Configuration by NMR, *Chem. Rev.* 2004**,** 104*,* 17-118

[10] Bertucci C., Pistolozzi M., De Simone A., Circular dichroism in drug discovery and development: an abridged review, *Anal. Bioanal. Chem*, 2010, 398, 155–166

[11] Freedman T.B., Cao X., Dukor R.K., Nafie L.A., Absolute configuration determination of chiral molecules in the solution state using vibrational circular dichroism**,** *Chirality,* 2003, 15, 743-

758

[12] Ghantous A., Gali-Muhtasib H., Vuorela H., Saliba N.A., Darwiche N., What made sesquiterpene lactones reach cancer clinical trials?, *Drug Discov. Today* 2010, 15, 668–679

[13] Jun-Tao F., De-Long W., Yong-Ling W., He Y., Xing Z.. New antifungal scaffold derived from a natural pharmacophore: Synthesis of a-methylene-c-butyrolactone derivatives and their antifungal activity against *Colletotrichum lagenarium*, *Bioorg. Med. Chem. Lett*., 2013, 23, 4393–4397

[14] Gladkowski W., Skrobiszewski A., Mazur M., Siepka M., Pawlak A., Obminska-Mrukowicz B., Bia1onska A., Poradowski D., Drynda A., Urbaniak M., Synthesis and anticancer activity of novel halolactones with b-aryl substituents from simple aromatic aldehydes, *Tetrahedron* 2013, 69, 10414–10423

[15] Rossi D., Talman V., Boije Af Gennas G., Marra A., Picconi P., Nasti R., Serra M., Ann J., Amadio M., Pascale A., Tuominen R. K., Yli Kauhaloma J., Lee J., Collina S., Beyond the affinity for protein kinase C: exploring 2-phenyl-3-hydroxypropyl pivalate analogues as C1 domain-targeting ligands, *Med.Chem.Comm*.,2015, 6, 547-554

[16] Skrobiszewski A., Gladkowski W., Walczak P., Gliszczyn Ska A., Maciejewska G., Klejdysz T., Nawrot J., Wawrzen Czyk C., Synthesis of β-aryl-γ -lactones and relationship: Structure – antifeedant and antifungal activity, *J. Chem. Sci.* 2015, 127, 687–699

[17] Bourguignon J.J., Schoenfelder A., Schmitt M., Wermuth C.G., Hechler V., Charlier B., Maitre M. Analogues of γ-Hydroxybutyric Acid. Synthesis and Binding Studies, *J. Med. Chem* 1988, 31, 893–897

[18] Englisch-Peters S., Synthesis of ω -hydroxy analogues of valine, leucine and isoleucine *Tetrahedron* 1989, 45, 6127–6134

[19] Luo Y., Carnell A. J., Chemoenzymatic Synthesis and Application of Bicyclo[2.2.2]octadiene Ligands: Increased Efficiency in Rhodium-Catalyzed Asymmetric Conjugate Additions by Electronic Tuning, *Angew Chem Int Ed* 2010, 49, 2750–2754

[20] Novellino E, Cosimelli B, Ehlardo M, Greco G, Iadanza M, Lavecchia A, Rimoli MG, Sala A, Da Settimo A, Primofiore G, Da Settimo F, Taliani S, La Motta C, Klotz K-N, Tuscano D, Trincavelli ML, Martini C. 2-(Benzimidazol-2-yl)quinoxalines: A novel class of selective antagonists at human A_1 and A_3 adenosine receptors designed by 3D database searching. *J Med Chem* 2005; 48, 8253–8260

[21] Da Settimo F, Primofiore G, Taliani S, Marini AM, La Motta C, Simorini F, Salerno S, Sergianni V, Tuccinardi T, Martinelli A, Cosimelli B, Greco G, Novellino E, Ciampi O, Trincavelli ML, Martini C. 5-Amino-2-phenyl[1,2,3]triazolo[1,2*a*][1,2,4]benzotriazin-1-one: A versatile scaffold to obtain potent and selective A_3 adenosine receptor antagonists. *J Med Chem* 2007, 50, 5676–5684.

[22] Cosimelli B, Greco G, Ehlardo M, Novellino E, Da Settimo F, Taliani S, La Motta C, Bellandi M, Tuccinardi T, Martinelli A, Ciampi O, Trincavelli ML, Martini C. Derivatives of 4-amino-6-hydroxy-2-mercaptopyrimidine as novel, potent, and selective A_3 adenosine receptor antagonists. *J Med Chem,* 2008, 51, 1764-1770.

[23] Taliani S, La Motta C, Mugnaini L, Simorini F, Salerno S, Marini AM, Da Settimo F, Cosconati S, Cosimelli B, Greco G, Limongelli V, Marinelli L, Novellino E, Ciampi O, Daniele S, Trincavelli ML, Martini C. Novel N^2-substituted pyrazolo[3,4-*d*]pyrimidine adenosine A_3 receptor antagonists: Inhibition of A_3-mediated human glioblastoma cell proliferation. *J Med Chem*, 2010, 53, 3954-3963

Enantiomeric 4-Acylamino-6-alkyloxy-2 Alkylthiopyrimidines As Potential A₃ Adenosine Receptor Antagonists: HPLC Chiral Resolution and Absolute Configuration Assignment by a Full Set of Chiroptical Spectroscopy

DANIELA ROSSI,[1] RITA NASTI,[1] ANNAMARIA MARRA,[1] SILVIA MENEGHINI,[1,2] GIUSEPPE MAZZEO,[2] GIOVANNA LONGHI,[2]
MAURIZIO MEMO,[2] BARBARA COSIMELLI,[3] GIOVANNI GRECO,[3] ETTORE NOVELLINO,[3] FEDERICO DA SETTIMO,[4]
CLAUDIA MARTINI,[4] SABRINA TALIANI,[4] SERGIO ABBATE,[2]* AND SIMONA COLLINA[1]**

[1]Dipartimento di Scienze del Farmaco, Università di Pavia, Pavia, Italy
[2]Dipartimento di Medicina Molecolare e Traslazionale, Università di Brescia, Brescia, Italy
[3]Dipartimento di Farmacia, Università di Napoli "Federico II", Napoli, Italy
[4]Dipartimento di Farmacia, Università di Pisa, Pisa, Italy

ABSTRACT   The chiral separation of enantiomeric couples of three potential A₃ adenosine receptor antagonists: (R/S)-N-(6-(1-phenylethoxy)-2-(propylthio)pyrimidin-4-yl)acetamide (**1**), (R/S)-N-(2-(1-phenylethylthio)-6-propoxypyrimidin-4-yl)acetamide (**2**), and (R/S)-N-(2-(benzylthio)-6-sec-butoxypyrimidin-4-yl)acetamide (**3**) was achieved by high-performance liquid chromatography (HPLC). Three types of chiroptical spectroscopies, namely, optical rotatory dispersion (ORD), electronic circular dichroism (ECD), and vibrational circular dichroism (VCD), were applied to enantiomeric compounds. Through comparison with Density Functional Theory (DFT) calculations, encompassing extensive conformational analysis, full assignment of the absolute configuration (AC) for the three sets of compounds was obtained. *Chirality 28:434–440, 2016.*   © 2016 Wiley Periodicals, Inc.

KEY WORDS: A₃ adenosine receptor antagonists; chiral HPLC; optical rotatory dispersion (ORD); electronic circular dichroism (ECD); vibrational circular dichroism (VCD); Density Functional Theory (DFT); absolute configuration assignment

In mammals, adenosine acts as a transmitter by binding to four subtypes of G-protein-coupled-receptors (GPCRs), namely, the A₁, A₂A, A₂B, and the A₃ adenosine receptors (ARs).[1,2] Activation of ARs by agonists, such as adenosine itself or synthetic ligands, leads to different intracellular events starting with inhibition (A₁ and A₃) or stimulation (A₂A and A₂B) of adenylate cyclase, stimulation of phospholipase C (A₁, A₂B, and A₃), activation of potassium channels, and inhibition of calcium channels (A₁).[2] Different from A₁, A₂A, and A₂B ARs, A₃ AR exhibits significant differences in primary amino acid sequence homology (74%) between human and rat.[3] A₃ AR can be found in human lungs, liver, kidneys, heart, brain, uterus, eyes, and testes,[4] where it is involved in a variety of physiological processes, including cell cycle regulation and cell growth.[5] Given its key role, A₃ AR is considered an attractive target for pharmacological therapies by medicinal chemists.[6,7] A₃ AR agonists may be useful as cardioprotective and cerebroprotective agents, as antiinflammatory and immunosuppressive agents, as cytostatics and chemoprotective compounds in cancer therapy. A₃ AR antagonists might be employed for the acute treatment of stroke, for glaucoma, and also as antiasthmatic and antiallergic drugs. The aforementioned potential clinical applications of A₃ AR ligands have been recently reviewed by Borea et al.[6] Recently, some of us have been involved in the synthesis and biological evaluation of novel classes of antagonists at the human A₃ AR.[8–11] Among those investigated, 4-acylamino-6-alkyloxy-2 alkylthiopyrimidines of general formula **I** stand out for ease of synthesis (Scheme 1), drug likeness, potency, and selectivity for the target receptor.[10] In this class, compounds **Ia** and **Ib** (Scheme 1) exhibit Ki values of

7.5 nM (**Ia**) and 525 nM (**Ib**) towards A₃ AR and excellent selectivity over A₁ and A₂A ARs.

Recently, we synthesized the chiral pyrimidines **1-3** (Fig. 1), formally derived from previously reported pyrimidines **Ia** and **Ib** by insertion of a methyl group on the exocyclic carbon atom attached to the oxygen or the sulfur (unpublished results). Specifically, **1** is a methyl derivative of **Ia**, whereas **2** and **3** are methyl derivatives of **Ib**. We reasoned that the new compounds, bearing branched substituents, more lipophilic, and less flexible with respect to their desmethyl counterparts, might be endowed with improved potency and selectivity as A₃ AR antagonists. As a consequence, a stereogenic center is present in compounds **1-3**.

To study the influence of chirality on the putative A₃ AR antagonist properties of structures **1-3**, we performed the chiral resolution of racemic **1-3** and assigned the absolute configuration to pure enantiomers. These tasks were achieved by using chiral high-performance liquid chromatography (HPLC) and chiroptical spectroscopy methods combined with Density Functional Theory (DFT) calculations. In detail, on the basis of our previous experience we resolved enantiomeric **1-3** via enantioselective HPLC on chiral stationary phases (CSPs), this approach being an effective way for both the analytical and the preparative separations of chiral
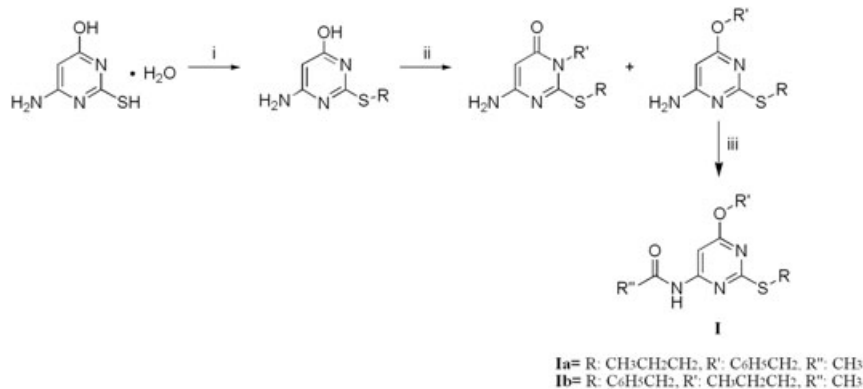
Scheme 1. Synthesis of 4-acylamino-6-alkyloxy-2-alkylthiopyrimidines (**I**). Reagents and conditions: (i)methyl iodide or (phenyl)alkylbromide, NaOH 1M; (ii) methyl iodide or (substituted-phenyl)alkyl bromide, anhydrous DMF, excess K_2CO_3; (iii) acetic or propionic anhydride, catalytic conc. H_2SO_4.
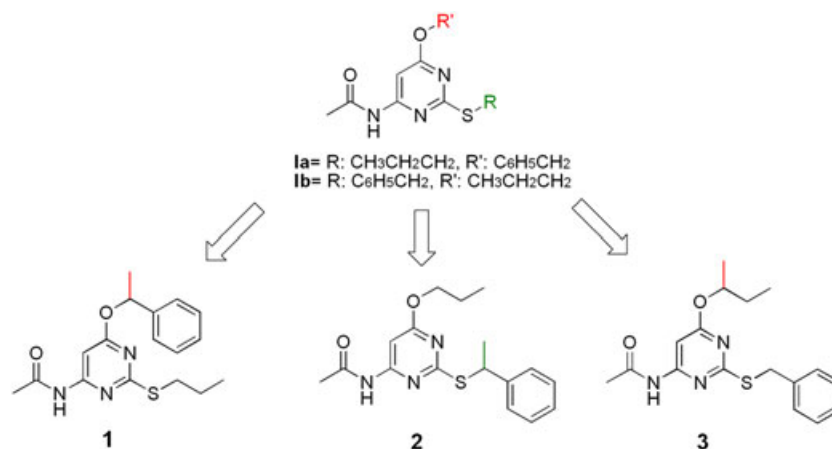

Fig. 1. Structures of the compounds studied in this work.

compounds.[12–14] We carried out the absolute configuration (AC) assignment study of **1-3** resolved enantiomers by a full set of chiroptical spectroscopies and comparison with calculated spectra obtained by ab initio methods (DFT-).[15–17] Thus, optical rotatory dispersion (ORD), electronic circular dichroism (ECD), and vibrational circular dichroism (VCD) spectra were recorded and compared to the calculated ones. The combined use of the three techniques is particularly advised for the AC assigned of flexible molecules, like drugs and natural products, which had been treated previously by the use of separate forms of chiroptical methods.[18–30] Overall, this article describes the work carried out to separate the enantiomeric couples for **1-3** and to assign their absolute configurations in order to understand how chirality may influence their interaction with human A$_3$ AR.

MATERIALS AND METHODS
Chiral Chromatographic Resolution

Chromatographic resolution was carried out at room temperature on a Jasco (Tokyo, Japan) system consisting of a PU-1580 pump, 851-AS autosampler, and MD-1510 Photo Diode Array (PDA) detector. In order to identify the best conditions to be properly scaled up, analytical screening was performed on the following columns: Chiralpak AD (250 mm × 4.6 mm, 5 µm), Chiralpak AS-H (250 mm × 4.6 mm, 5 µm), Chiralcel OD-H (150 mm × 4.6, 5 µm), and Chiralcel OJ-H (150 mm × 4.6 mm, 5 µm) from Daicel Chemical Industries (Tokyo, Japan). The chiral stationary phases of these columns were amylose tris

(3,5-dimethyl-phenylcarbamate), amylose tris[(S)-α-methylbenzylcarbamate], cellulose tris(3,5-dimethylphenyl carbamate), and cellulose tris-(4-methylbenzoate), respectively. A Hamilton (Reno, NV) syringe (syringe volume: 2.5 mL; loop: 2 mL) was employed for (semi)-preparative chiral resolutions. Chromatogram acquisitions and elaborations were performed using the Borwin PDA and Borwin Chromatograph software.

Compound Characterization

Optical rotation values were measured on a Jasco photoelectric polarimeter DIP 1000 using a 0.5 dm cell and a sodium and mercury lamp (λ = 589 nm, 435 nm, 405 nm); sample concentration values (c) are given in 10^{-2} g mL^{-1}. Optical data are reported in Supplementary Table SI-2.

Nuclear magnetic resonance spectra were recorded on a Varian (Palo Alto, CA) Inova 500 spectrometer operating at 500 MHz for the proton and 125 MHz for the carbon (compound **1**) or on a Varian Mercury 400 spectrometer operating at 400 MHz for the proton and 100 MHz for the carbon (compounds **2** and **3**) in DMSO-d_6 solution.

(+)-R-N-[6-(1-Phenylethoxy)-2-(propylsulfanyl)pyrimidin-4-yl]acetamide [(+)-R-1]: ^{1}H-NMR: 10.70 (bs, 1H, NH); 7.39–7.32 (m, 5H, H-Ar); 7.14 (s, 1H, H-5); 6.12 (q, 1H, J = 6.2, OCH) 2.96 (m, 2H, SCH$_2$); 2.07 (s, 3H, CH$_3$); 1.60-1.54 (m, 5H, CH$_2$ and CH$_3$); 0.94 (t, 3H, J = 7.3, CH$_3$).^{13}C-NMR: 170.5; 169.6; 169.1; 158.7; 142.3; 128.4; 125.6; 89.8; 73.9; 31.7; 24.0; 24.0; 22.8; 22.4; 13.2.

(-)-S-N-[6-(1-Phenylethoxy)-2-(propylsulfanyl)pyrimidin-4-yl]acetamide [(-)-S-1]: the ^{1}H-NMR spectrum is identical to that of the corresponding enantiomer.

(+)-R-N-{2-[(1-Phenylethyl)sulfanyl]-6-propoxypyrimidin-4-yl}acetamide [(+)-R-2]: ^{1}H-NMR: 10.73 (bs, 1H, NH); 7.48–7.44 (m, 2H, H-Ar); 7.36-7.31 (m, 2H, H-Ar); 7.27-7.23 (m, 1H, H-Ar); 7.08 (s, 1H, H-5); 5.00 (q,

1H, J = 7.1, SCH); 4.29–4.17 (m, 2H, OCH$_2$); 2.09 (s, 3H, CH$_3$); 1.72-1.62 (m, 5H, CH$_2$ and CH$_3$); 0.94 (t, 3H, J = 7.4, CH$_3$). ^{13}C-NMR: 170.5; 170.0; 169.1; 158.6; 143.0; 128.5; 127.2; 127.1; 89.5; 68.0; 43.5; 24.1; 22.3; 21.6; 10.3.

(-)-S-N-{2-[(1-Phenylethyl)sulfanyl]-6-propoxypyrimidin-4-yl}acetamide [(-)-S-2]: the ^{1}H-NMR spectrum is identical to that of the corresponding enantiomer.

(+)-R-N-[2-(Benzylsulfanyl)-6-(butan-2-yloxy)pyrimidin-4-yl]acetamide [(+)-R-3]: ^{1}H-NMR: 10.73 (bs, 1H, NH); 7.44–7.41 (m, 2H, H-Ar); 7.34–7.29 (m, 2H, H-Ar); 7.27-7.24 (m, 1H, H-Ar); 7.07 (s, 1H, H-5); 5.15-5.06 (m, 1H, OCH); 4.39 (s, 2H, SCH$_2$); 2.09 (s, 3H, CH$_3$); 1.70-1.52 (m, 2H, CH$_2$); 1.22 (d, 3H, J = 6.2, CH$_3$); 0.86 (t, 3H, J = 7.4, CH$_3$). ^{13}C-NMR: 170,5; 169.7; 169.1; 158.6; 137.9; 128.7; 128.4; 127.0; 89.9; 73.8; 33.9; 28.2; 24.1; 19.1; 9.5.

(-)-S-N-[2-(Benzylsulfanyl)-6-(butan-2-yloxy)pyrimidin-4-yl]acetamide [(-)-S-3]: the ^{1}H-NMR spectrum is identical to that of the corresponding enantiomer.

ORD Curves, ECD, and VCD Spectra

The DIP 1000-type photoelectric polarimeter from Jasco was used for [α] measurements, which were carried out at room temperature using sodium and mercury sources at three different wavelengths (589, 435, 405 nm) and CG3-50 cell (3.5 mm I.D. × 50 mm pathlength). ORD values were recorded both in chloroform and in methanol for **2** and **3** and just in methanol for **1**. In all cases ORD measurements were carried out for the first eluted enantiomer at all available wavelengths. The ORD and samples concentration values are reported in Table SI-2.

UV and ECD spectra were obtained with a Jasco 815SE apparatus in the range 350–180 nm, using 0.1 mm pathlength quartz cuvettes under the following conditions: 0.5 s integration time, 200 nm/min scan speed, 1 nm bandpass, 10 accumulations. UV/ECD spectra were recorded in acetonitrile for all samples ($2.4 \cdot 10^{-3}$ M and $3.6 \cdot 10^{-3}$ M for **1**, first eluted and second eluted enantiomers respectively; $3.02 \cdot 10^{-3}$ M and $3.32 \cdot 10^{-3}$ M for **2**, first eluted and second eluted enantiomer respectively; for **3** no reliable UV/ECD spectrum was taken, for paucity of compounds).

IR and VCD spectra were collected in the range from 2000 to 850 cm^{-1} with a Jasco FVS6000 FTIR instrument equipped with a liquid N$_2$-cooled MCT detector. A 200 μm pathlength BaF$_2$ cell was used with the following conditions: 2000 accumulations, 4 cm^{-1} resolution. IR/VCD spectra were recorded in CCl$_4$ solution for **2** and **3** (0.068 M and 0.070 M for **2**, first eluted and second eluted compound, respectively; for **3** no reliable VCD data were recorded, see above) and in deuterated methanol solution for **1** (0.040 M both eluted compounds).

Computational Detail

Preliminary conformational analysis was performed for (*R*)-**1-3** with the MMFF94s molecular mechanics (MM) force field: 44 conformers for **1**, 55 for **2** and 43 for **3** were found below 10 Kcal/mol. These sets of conformers were fully optimized at the B3LYP/6-31G* level using the Gaussian09 package.[31] Conformers within 2 kcal/mol in relative free energy with respect to the most stable one were treated at the B3LYP/TZVP level of theory. Calculated free energies were used to determine the Boltzmann population factor of the conformers at 298.15 K.

VCD spectra were calculated for **1** and **2** at the same B3LYP/TZVP level. The IEF-PCM approach was also employed in order to optimize and calculate VCD spectra of deuterated species of **1** (in N-H bond) in CD$_3$OD solution. For **2** no deuteration was adopted. Calculations of ORD and ECD spectra were performed by the TD-DFT approach with allowance of 30 excited states using the Gaussian Coulomb-attenuated CAM-B3LYP functional and aug-cc-pVDZ as basis set. Calculated VCD spectra were simulated with the Gaussian package[31] assigning 8 cm^{-1} Lorentzian bands shape to all vibrational transitions. ECD bands were assumed to have Gaussian line shape with 0.2 eV bandwidth. Theoretical ORD, ECD, and VCD spectra were obtained as weighted averages by the Boltzmann population factors.

RESULTS AND DISCUSSION
Chiral Resolution

The approach we followed for obtaining enantiopure **1-3** is chiral chromatographic resolution (HPLC). This methodology is suitable both for analytical and preparative purposes and is particularly useful in the early stage of the drug discovery processes, when small-scale separation is needed and both enantiomers have to be investigated.

As there is currently no way to predict which column–mobile phase combination will provide a separation of the desired product, the development process generally involves screening a number of chiral stationary phases and potential mobile phases in a systematic scheme. Based on our experience, for primary HPLC screening we normally use the sets of columns and mobile phases shown in Table SI-1. If this initial screening is not successful, typically we move to a secondary screen, where the lesser-used columns and solvents are employed, again in a similar process. Accordingly, to find a baseline separation quickly, in this work the polysaccharide-based CSPs of Table SI-1 were initially screened. Moreover, the design of the experiments took into account the good solubility of **1-3** in alcohols. For this reason the first set of experiments was performed on the considered columns, eluting with just methanol.[14]

As a result of a first screening with pure methanol, it was found that Chiralcel OJ-H (4.6 mm × 150 mm, 5 μm) lead to relatively short retention times, high enantioselectivity, and high resolution for compound **2** (α = 3.3, R_s = 6.7) and **3** (α = 1.9, R_s = 4.1). Accordingly, these experimental conditions were selected for the scale-up to (semi)-preparative scale. As regards compound **1**, a very poor resolution was obtained (α = 1.33, R_s = 0.3) and therefore it was necessary to extend the screening also to different mobile phases (Table SI-3). Baseline separation, high enantioselectivity, and resolution were obtained eluting with heptane/ethanol 95/5 (v/v) (α = 1.5, R_s = 2.4). Chromatographic profiles of racemates, together with experimental conditions, are given in Fig. 2 and Table 1.

The developed analytical methods were suitably transferred to the semipreparative scale, employing a Chiralcel OJ-H column (10 mm x 250 mm, 5 μm). In this way batches of about 40 mg of racemic **1-2** and of 25 mg of racemic **3** were processed, affording enantiomeric **1-3** in good overall yields (81.8%, 93.1%, and 97.2%, respectively) (Fig. SI-1). The optical rotatory power of the obtained enantiomers, their enantiomeric excess, determined by HPLC and recovery yields are summarized in Table 2. To assign the absolute configuration of the enantiomers of **1-3** we performed ORD analysis and for **1** and **2** we recorded ECD and VCD spectra. The identity of the resolved enantiomers **1-3** was confirmed by ^{1}H-NMR analysis.

Analysis of ORD Data

Let us begin our analysis from compound **2**, which was revealed to be simple to interpret from the computational point of view. The 13 calculated conformers of (*R*)-**2** with population factors above 2% exhibit positive OR values at three different wavelengths and show the same ORD trend (see Fig. SI-2, middle panel). The weighted average theoretical ORD curve shows the same magnitude, but opposite sign as compared with the measured curves of the first eluted enantiomer (Fig. 3, middle panel). From this we deduce that the second eluted enantiomer has (*R*)-AC. Unlike for **2**, the calculated
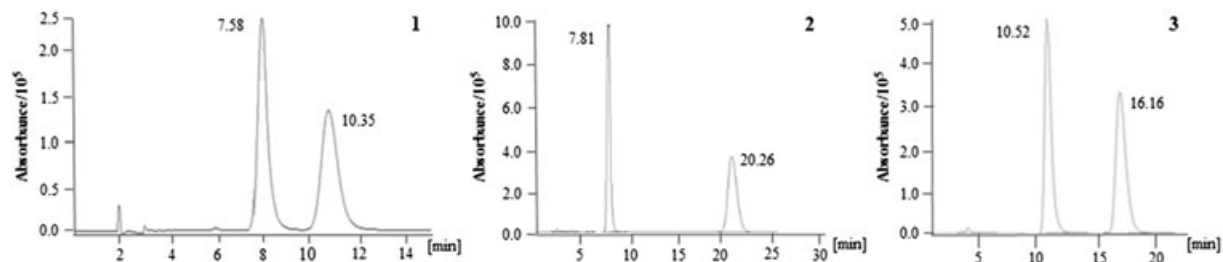
Fig. 2. Analytical chromatographic profiles for (R/S)-1, (R/S)-2, and (R/S)-3 (from left to right) obtained with Chiralcel OJ-H (4.6 mm × 150 mm, 5 μm); eluent heptane/ethanol 95/5 (v/v) for **1** and 100% MeOH for **2** and **3**; flow rate: 1 mL/min; conc.: 1 mg/mL; injection volume: 10 μL; detection at 250, 240, and 254 nm, respectively.

TABLE 1. (Semi)-preparative resolution of racemic 1-3 on a Chiralcel OJ-H column (10 mm x 250 mm, 5 μm)

Compound	Eluent	t_A (min)	t_B (min)	Amount processed (mg)	Concentration (mg/mL)	Number of cycles
1	*n*-heptane/EtOH (95:5 v/v)	13.87	20.25	38	2.0	10
2	MeOH	12.24	32.32	40	5.0	4
3	MeOH	12.79	22.15	25	5.0	3

Flow rate: 4.0 mL/min; injection volume: 2.0 mL.

TABLE 2. Chiroptical characteristics (OR, *ee*, and amount) of the separated enantiomers for 1-3

Compound	λ	C	$[a]_\lambda^{22}$ (MeOH)	ee[a]	Isolated amount(mg)	Yield (%)
(+)-1	435	0.1%	+40.4	99.9%[b]	15.2	40.0
(-)-1	435	0.1%	-40.4	99.9%[b]	15.9	41.8
(+)-2	589	0.2%	-214.7	99.9%[c]	18.5	46.3
(-)-2	589	0.2%	+214	99.9%[c]	18.7	46.8
(+)-3	435	0.5%	+56.2	99.9%[c]	12.0	48.0
(-)-3	435	0.5%	-56.4	99.9%[c]	12.3	49.2

[a]Determined on Chiralcel OJ-H (4.6 mm x 150 mm, dp 5 μm) and eluting with
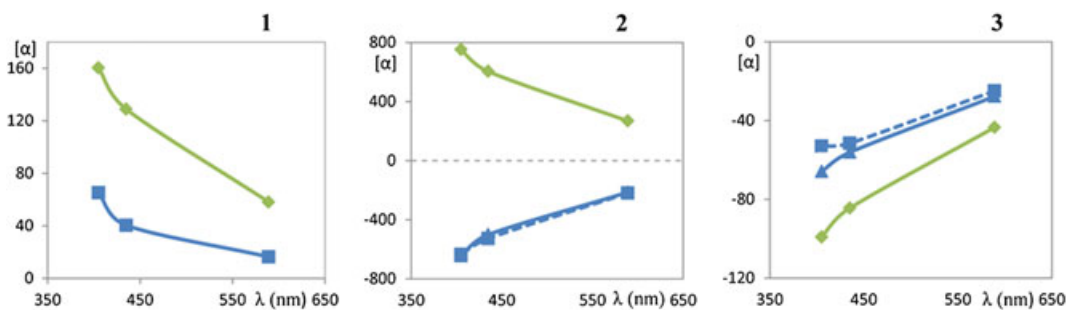[b]n-heptane 95/5 EtOH (v/v) or
[c]100% methanol.

Fig. 3. Comparison of average calculated (CAM-B3LYP/aug-cc-pVDZ on DFT/B3LYP/TZVP input geometries) ORD curves for (R)-**1-3** (green line) and experimental (solid blue line, methanol, and dotted blue line, chloroform) for the first eluted couple of compounds **1-3**. In the calculated (R)-**3** ORD curve average the conformer in Figure SI-3 is excluded (see text and Fig. SI-2).

(R)-**1** ORD curves do not present the same sign and trend for the 15 conformers above 3% population (Fig. SI-2, left panel); the calculated values appear a bit too large with respect to experiments. Anyway, the weighted average calculated ORD curve matches the trend and the sign of the experimental one, which indicates that the first eluted enantiomer has (R)-AC (Fig. 3, left panel). Figure SI-2 shows that for good prediction of the ORD curves all calculated conformers are necessary, even those with the wrong sign. For (R)-**3**, we noticed that the ORD curves of the 15 calculated conformers with population above 0.8% (Fig. SI-2, right panel) present the

same trend except for one of them reported in Figure SI-3 (conformer **3** g).

Even if its population factor is rather low (4.4%), the calculated values of [α] at three λ are very high; so this conformer negatively influences the trend of the average calculated ORD curve. If conformer **3** g is removed, the calculated ORD improves considerably as compared to experiment. Such conformer differs from the other ones by the thio-phenyl group being distorted in such a way as to be closer to the central pyrimidine moiety. However, similar to compound **1**, ORD analysis suggests that the first eluted enantiomer of **3** has (R)-configuration.
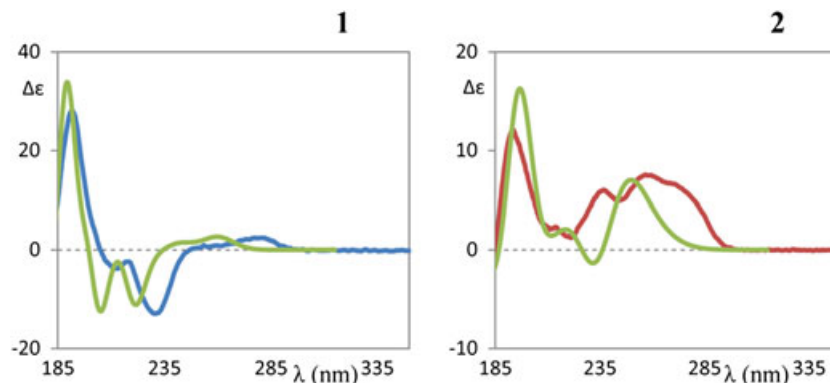
Fig. 4. Comparison of average calculated (CAM-B3LYP on DFT/B3LYP/TZVP input geometries) ECD spectra for (R)-**1-2** (green line) and experimental ones (blue line, first eluted, and red line, second eluted).

Analysis of ECD Spectra

Calculated UV absorption spectra of (R)-**1** and (R)-**2** exhibit five and, respectively, three important bands which nicely correlate with all the experimental ones (Fig. SI-4). For both **1** and **2** the experimental ECD spectra of the two pairs of enantiomers are excellent mirror images of each other (Fig. SI-5): the ECD experimental spectra of **1** and **2** are in good agreement with the calculated average ECD spectra (Fig. 4). Compared to (R)-**2**, the ECD spectrum of (R)-**1** has the same strong positive 190 nm feature, while the central broad feature at 230 nm is negative in **1**, and positive in **2**. Finally, at about 280 nm, a positive feature is present in both molecules, in **1** being weak and broad, while in **2** being a strong shoulder of a 250 nm band. For **1**, the calculated average ECD spectrum is in good agreement with the experimental one; the small features at high wavelengths are calculated at shorter wavelengths compared to those used for the experiment. For **2,** the situation is slightly worse. To improve the quality of ECD and UV calculated spectra of (R)-**2** we applied the

PCM model, which allows taking into account the solvent influence. The obtained spectra were similar to the ones calculated in gas phase. Thus, theoretical ECD spectra of (R) and (S) enantiomers of **1** and **2** are in agreement with the experimental ones of the first eluted enantiomer of **1** and **2,** respectively. These results are in agreement with those obtained performing ORD experiments and therefore the AC was undoubtedly assigned (Fig. 4). In the case of the first eluted enantiomer of **3**, the ECD spectra registered had a poor signal-to-noise ratio and therefore they were not considered.

Analysis of VCD Spectra

Since VCD for compound **1** was run in CD_3OD, where it shows good solubility, we ran a calculation for (R)-**1** with N-H replaced by N-D: the average IR calculated spectrum fits rather well the experimental one, especially for the two peaks at ~1565–1544 cm^{-1} and the two peaks at ~1435–1407 cm^{-1} (Fig. 5, left panel). VCD experimental spectra present few
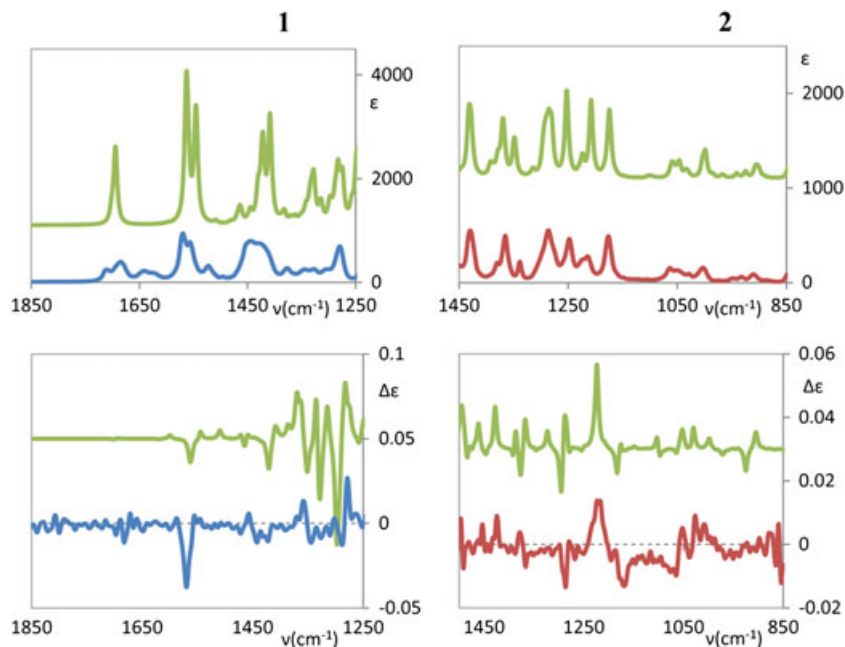

Fig. 5. Comparison of experimental IR and VCD spectra (blue, first eluted enantiomer, and red, second eluted enantiomer) of **1-2** with calculated (green) IR and VCD average spectra for (R)-**1-2. 1** and **2** experimental spectra are the semi-difference between enantiomers. **1** refers to solution in CD3OD, while data for **2** was taken in CCl_4.

1

1a (9.6%) 1b (8.7%) 1c (7.1%) 1d (7.0%) 1e (6.0%)

2

2a (34.6%) 2b (11.7%) 2c (9.8%)

3

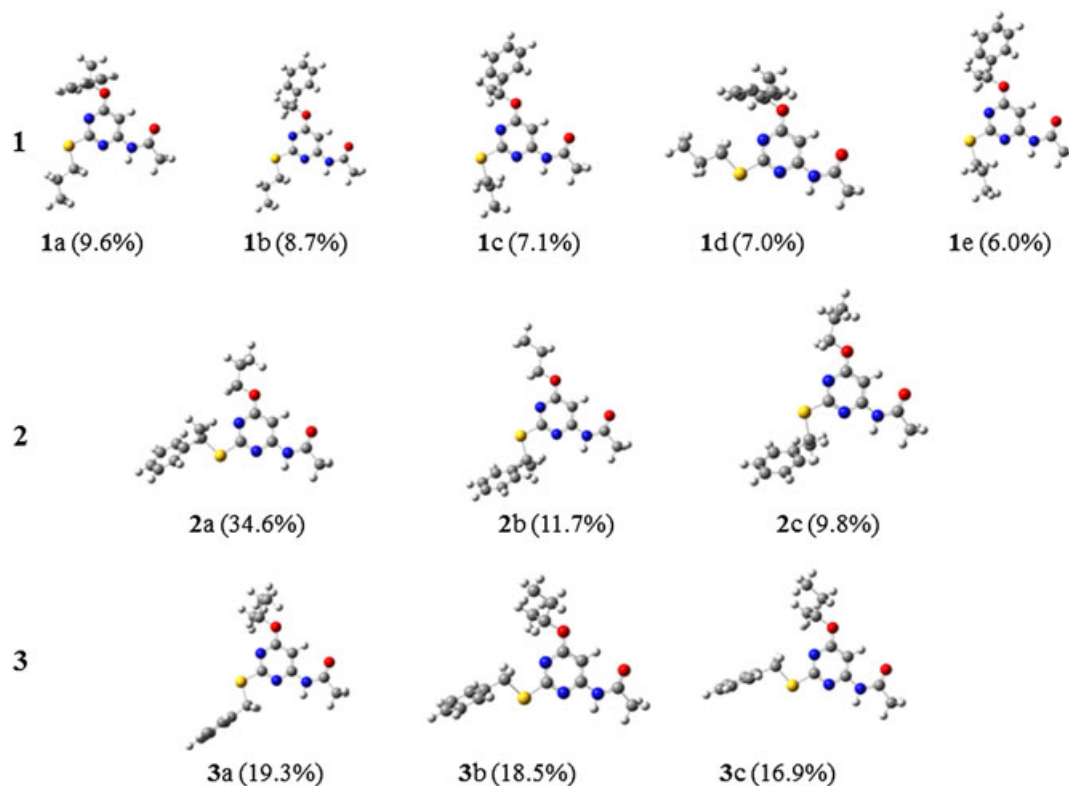3a (19.3%) 3b (18.5%) 3c (16.9%)

Fig. 6. 3D-structure of the most populated conformers for molecules **1-3** with (R)-configuration calculated in vacuo.

significant bands that are matched by calculations, in sign even if not 100% in magnitude. This may be related to the flexibility of the molecule. The negative VCD band of the first eluted enantiomer, at 1567 cm^{-1}, can be associated with the calculated one at 1558 cm^{-1}, originated by the aromatic C = C and C = N stretching (Fig. 5), while the IR peak around 1693 cm^{-1} can be related to C = O stretching. VCD confirms the same conclusion arrived at by the ORD and ECD techniques. We endeavored to measure IR and VCD spectra of **1** first eluted enantiomer in CCl$_4$ solution, getting as close as possible to the 0.04 M concentration (**1** is not very soluble in CCl$_4$). The results are given in Figure SI-6 and a CD$_3$OD solution, namely, the (R)-**1** enantiomer corresponds to the first eluted sample. For **2** the whole IR calculated spectrum provides good prediction of all the experimental peaks, while only few VCD experimental bands appear (Fig. 5, right panel) and are reproduced in sign and magnitude by the average calculated spectra of (R)-**2**. Molecular flexibility is so important that the VCD spectrum of one conformer is cancelled by the VCD of another one. The AC is the same predicted by ORD and ECD analyses. This assignment was made on the basis of the first three bands (IR peaks: 1427, 1284, and 1210 cm^{-1}, respectively), which can be attributed to CH$_2$ wagging (1422 cm^{-1}) and C* bending motions (1285 and 1220 cm^{-1}), respectively. The whole IR spectra is reported in Figure SI-7. The IR and VCD spectra recorded in other solvents (CDCl$_3$ and CS$_2$) did not give rise to results. Regarding the VCD spectra of (–)-**3**, a poor signal-to-noise ratio was obtained, as already evidenced in the case of ECD spectra.

Conformational Analysis

The previously discussed comparison of experimental and calculated ORD, ECD, and VCD spectra would not have been

feasible if a systematic investigation of possible conformers had not been conducted. Indeed, in order to establish AC, one has to carry out a detailed and reliable conformational analysis aimed at understanding the arrangement of the substituents in the different conformers. In Figure 6 we report the five most populated conformers for **1** and the three most populated conformers for **2** and **3** (see also Table SI-4). All investigated conformers present the amide group R" bound to the pyrimidine ring, always in the same position and on the same plane.

CONCLUSION

In the present article we have described the isolation of **1-3** pure enantiomers and the assignment of their absolute configuration in order to investigate the role of chirality on the potential A$_3$ AR antagonist properties of these compounds. To the best of our knowledge, pharmacological enantioselectivity of A$_3$ AR antagonists has been previously investigated only by Jacobson and colleagues.[32]

An enantioselective HPLC procedure using a Chiralcel OJ-H column was successfully applied to the enantioresolution of **1-3**, obtaining both enantiomers with an enantiomeric excess of about 99.9% and in amounts suitable for absolute configuration assignment and biological investigation. In line with emerging works, we employed a full set of chiroptical spectroscopies to determine the AC of the resolved enantiomers.[18,25,29] In detail, AC of enantiomeric **1-3** was assigned by comparing experimental and calculated ORD curves and, in the case of enantiomeric **1** and **2**, also comparing ECD and VCD spectra with the DFT calculated ones. It has to be underlined that all the applied techniques gave rise to converging conclusions. However, this behavior is not universal and VCD sometimes

arrives at safer conclusions.[18,25,33] To sum up, the first eluted enantiomers are *(R)*-**1**, *(S)*-**2,** and *(R)*-**3**, and the second eluted ones are *(S)*-**1**, *(R)*-**2,** and *(S)*-**3,** respectively. Overall, this work provided enantiomerically pure **1-3** currently being employed by us to study the influence of chirality on the interaction of this class of compounds with human A_3 AR. The results of these efforts will be reported in due course.

ACKNOWLEDGMENTS

SUPPORTING INFORMATION

Additional supporting information may be found in the online version of this article at the publisher's web-site.

LITERATURE CITED

1. Müller CE, Jacobson KA. Recent developments in adenosine receptor ligands and their potential as novel drugs. Biochim Biophys Acta 1808;2011:1290–1308.

2. Fredholm BB, IJzerman AP, Jacobson KA, Linden J, Muller CE. International union of basic and clinical pharmacology. LXXXI. Nomenclature and classification of adenosine receptors-an update. Pharmacol Rev 2011;63:1–34.

3. Salvatore CA, Jacobson MA, Taylor HE, Linden J, Johnson RG. Molecular cloning and characterization of the human A_3 adenosine receptor. Proc Natl Acad Sci U S A 1993;90:10365–10369.

4. Linden J. Cloned adenosine A_3 receptors: Pharmacological properties, species differences and receptor functions. Trends Pharmacol Sci 1994;15:298–306.

5. Brambilla R, Cattabeni F, Ceruti S, Barbieri D, Franceschi C, Kim Y-C, Jacobson KA, Klotz K-N, Lohse MJ, Abbracchio MP. Activation of the A_3 adenosine receptor affects cell cycle progression and cell growth. Naunyn Schmiedeberg's Arch Pharmacol 2000;361:225–234.

6. Borea PA, Varani K, Vincenzi F, Baraldi PG, Tabrizi MA, Merighi S, Gessi S. The A_3 adenosine receptor: history and perspectives. Pharmacol Rev 2015;67:74–102.

7. Müller CE. Medicinal chemistry of adenosine A_3 receptor ligands. Curr Top Med Chem 2003;3:445–62.

8. Novellino E, Cosimelli B, Ehlardo M, Greco G, Iadanza M, Lavecchia A, Rimoli MG, Sala A, Da Settimo A, Primofiore G, Da Settimo F, Taliani S, La Motta C, Klotz K-N, Tuscano D, Trincavelli ML, Martini C. 2-(Benzimidazol-2-yl)quinoxalines: A novel class of selective antagonists at human A_1 and A_3 adenosine receptors designed by 3D database searching. J Med Chem 2005;48:8253–8260.

9. Da Settimo F, Primofiore G, Taliani S, Marini AM, La Motta C, Simorini F, Salerno S, Sergianni V, Tuccinardi T, Martinelli A, Cosimelli B, Greco G, Novellino E, Ciampi O, Trincavelli ML, Martini C. 5-Amino-2-phenyl[1,2,3]triazolo[1,2a][1,2,4]benzotriazin-1-one: a versatile scaffold to obtain potent and selective A_3 adenosine receptor antagonists. J Med Chem 2007;50:5676–5684.

10. Cosimelli B, Greco G, Ehlardo M, Novellino E, Da Settimo F, Taliani S, La Motta C, Bellandi M, Tuccinardi T, Martinelli A, Ciampi O, Trincavelli ML, Martini C. Derivatives of 4-amino-6-hydroxy-2-mercaptopyrimidine as novel, potent, and selective A_3 adenosine receptor antagonists. J Med Chem 2008;51:1764–1770.

11. Taliani S, La Motta C, Mugnaini L, Simorini F, Salerno S, Marini AM, Da Settimo F, Cosconati S, Cosimelli B, Greco G, Limongelli V, Marinelli L, Novellino E, Ciampi O, Daniele S, Trincavelli ML, Martini C. Novel N^2-substituted pyrazolo[3,4-d]pyrimidine adenosine A_3 receptor antagonists: Inhibition of A_3-mediated human glioblastoma cell proliferation. J Med Chem 2010;53:3954–3963.

12. Lien AN, Hua H, Chuong PH. Chiral drugs. an overview. Int J Biomed Sci 2006;2:85–100.

13. Gaggeri R, Rossi D, Collina S, Mannucci B, Baierl M, Juza M. Quick development of an analytical enantioselective high performance liquid chromatography separation and preparative scale-up for the flavonoid Naringenin. J Chrom A 2011;1218:5414–5422.

14. Rossi D, Pedrali A, Marra A, Pignataro L, Schepmann D, Wünsch B, Ye L, Leuner K, Peviani M, Curti D, Azzolina O, Collina S. Studies on the enantiomers of RC-33 as neuroprotective agents: Isolation, configurational assignment, and preliminary biological profile. Chirality 2013;25:814–822.

15. Nafie LA. Vibrational optical activity, principles and applications. New York; John Wiley & Sons: 2011.

16. Polavarapu PL, Zhao C. Vibrational circular dichroism: a new spectroscopic tool for biomolecular structural determination. Fresenius J Anal Chem 2000;366:727–734.

17. Abbate S, Lebon F, Longhi G, Morelli CF, Ubiali D, Speranza G. Vibrational and electronic circular dichroism spectroscopies and DFT calculations for the assignment of the absolute configuration of hydroxysubstituted 2-tetralols. RSC Adv 2012;2:10200–10208.

18. Polavarapu PL. A single chiroptical spectroscopic method may not be able to establish the absolute configurations of diastereomers: dimethylesters of hibiscus and garcinia acids. J Phys Chem A 2011;115:5665–5673.

19. Mazzeo G, Santoro E, Andolfi A, Cimmino A, Troselj P, Petrovic AG, Superchi S, Evidente A, Berova N. Absolute configurations of fungal and plant metabolites by chiroptical methods. ORD, ECD, and VCD studies on phyllostin, scytolide, and oxysporone. J Nat Prod 2013;76:588–599.

20. Scafato P, Caprioli F, Pisani L, Padula D, Santoro F, Mazzeo G, Abbate S, Lebon F, Longhi G. Combined use of three forms of chiroptical spectroscopies in the study of the absolute configuration and conformational properties of 3-phenylcyclopentanone, 3-phenylcyclohexanone, and 3-phenylcycloheptanone. Tetrahedron 2013;69:10752–10762.

21. Górecki M. A configurational and conformational study of (-)-Oseltamivir using a multi-chiroptical approach. Org Biomol Chem 2015;13:2999–3010.

22. Polavarapu PL. Molecular structure determination using chiroptical spectroscopy: where we may go wrong? Chirality 2012;24:909–920.

23. Gordillo-Román B, Camacho-Ruiz J, Bucio MA, Joseph-Nathan P. Vibrational circular dichroism discrimination of diastereomeric cedranol acetates. Chirality 2013;25:939–951.

24. Felippe LG, Batista JM Jr, Baldoqui DC, Nascimento IR, Kato MJ, He Y, Nafie LA, Furlan M. VCD to determine absolute configuration of natural product molecules: secolignans from Peperomia blanda. Org Biomol Chem 2012;10:4208–4214.

25. Abbate S, Longhi G, Castiglioni E, Lebon F, Wood PM, Woo LWL, Potter BVL. Determination of the absolute configuration of aromatase and dual aromatase-sulfatase inhibitors by vibrational and electronic circular dichroism spectra analysis. Chirality 2009;21:802–809.

26. Brittain HG. Application of chiroptical spectroscopy in the characterization of compounds having pharmaceutical importance. In: Berova N, Nakanishi K, Woody RW editors, Circular dichroism principles and application, 2nd ed. New York: Wiley-VCH; 2000. p 819–844.

27. Keiderling TA. Peptide and protein conformational studies with vibrational circular dichroism and related spectroscopies. In: Berova N, Nakanishi K, Woody RW editors, Circular dichroism principles and application, 2nd ed. New York: Wiley-VCH; 2000. p 621–666.

28. Nakahashi A, Miura N, Monde K, Tsukamoto S. Stereochemical studies of hexylitaconic acid, an inhibitor of p53–HDM2 interaction. Bioorg Med Chem Lett 2009;19:3027–3030.

29. He Y, Wang B, Dukor RK, Nafie LA. Determination of absolute configuration of chiral molecules using vibrational optical activity: a review. Appl Spectrosc 2011;65:699–723.

30. Stephens PJ. Vibrational circular dichroism: a new tool for the stereochemical characterization of chiral molecules. In: Bultinck P, De Winter H, Langenaeker W, Tollenaere JP editors, Computational medicinal chemistry for drug discovery. New York: Marcel Dekker; 2005. p 699–726.

31. Gaussian 09, Revision A.02, Frisch MJ, Trucks GW, Schlegel HB, Scuseria GE, Robb MA, Cheeseman JR, Scalmani G, Barone V, Mennucci B, Petersson GA, Nakatsuji H, Caricato M, Li X, Hratchian HP, Izmaylov AF, Bloino J, Zheng G, Sonnenberg JL, Hada M, Ehara M, Toyota K, Fukuda R, Hasegawa J, Ishida M, Nakajima T, Honda Y, Kitao O, Nakai H, Vreven T, Montgomery JA Jr., Peralta JE, Ogliaro F, Bearpark M, Heyd JJ, Brothers E, Kudin KN, Staroverov VN, Kobayashi R, Normand J, Raghavachari K, Rendell A, Burant JC, Iyengar SS, Tomasi J, Cossi M, Rega N, Millam JM, Klene M, Knox JE, Cross JB, Bakken V, Adamo C, Jaramillo J, Gomperts R, Stratmann RE, Yazyev O, Austin AJ, Cammi R, Pomelli C, Ochterski JW, Martin RL, Morokuma K, Zakrzewski VG, Voth GA, Salvador P, Dannenberg S, Dapprich S, Daniels AD, Farkas Ö, Foresman JB, Ortiz JV, Cioslowski J, Fox DJ. Gaussian. Wallingford CT: Gaussian, Inc.; 2009.

32. Jiang J, Li AH, Jang SY, Chang L, Melman N, Moro S, Ji X, Lobkovsky EB, Clardy JC, Jacobson KA. Chiral resolution and stereospecificity of 6-phenyl-4-phenylethynyl-1,4-dihydropyridines as selective A_3 adenosine receptor antagonists. J Med Chem 1999;42:3055–3065.

33. Abbate S, Burgi LF, Castiglioni E, Lebon F, Longhi G, Toscano E, Caccamese S. Assessment of configurational and conformational properties of naringenin by vibrational circular dichroism. Chirality 2009;21:436–441.

Enantiomeric 4-Acylamino-6-alkyloxy-2 Alkylthiopyrimidines As Potential A3 Adenosine Receptor Antagonists: HPLC Chiral Resolution and Absolute Configuration Assignment by a Full Set of Chiroptical Spectroscopy

DANIELA ROSSI,[1] RITA NASTI,[1] ANNAMARIA MARRA,[1] SILVIA MENEGHINI,[1,2] GIUSEPPE MAZZEO,[2] GIOVANNA LONGHI,[2] MAURIZIO MEMO,[2] BARBARA COSIMELLI,[3] GIOVANNI GRECO,[3] ETTORE NOVELLINO,[3] FEDERICO DA SETTIMO,[4] CLAUDIA MARTINI,[4] SABRINA TALIANI,[4] SERGIO ABBATE,[2]* AND SIMONA COLLINA[1]**

[1] *DIPARTIMENTO DI SCIENZE DEL FARMACO, UNIVERSITÀ DI PAVIA, VIALE TARAMELLI 12, 27100 PAVIA, ITALY.* E-MAIL: SIMONA.COLLINA@UNIPV.IT

[2] *DIPARTIMENTO DI MEDICINA MOLECOLARE E TRASLAZIONALE, UNIVERSITÀ DI BRESCIA, VIALE EUROPA 11, 25123 BRESCIA, ITALY.* E-MAIL: SERGIO.ABBATE@UNIBS.IT

[3] *DIPARTIMENTO DI FARMACIA, UNIVERSITÀ DI NAPOLI "FEDERICO II", VIA DOMENICO MONTESANO, 49, 80131 NAPOLI, ITALY*

[4] *DIPARTIMENTO DI FARMACIA, UNIVERSITÀ DI PISA, VIA BONANNO PISANO, 56126 PISA, ITALY*
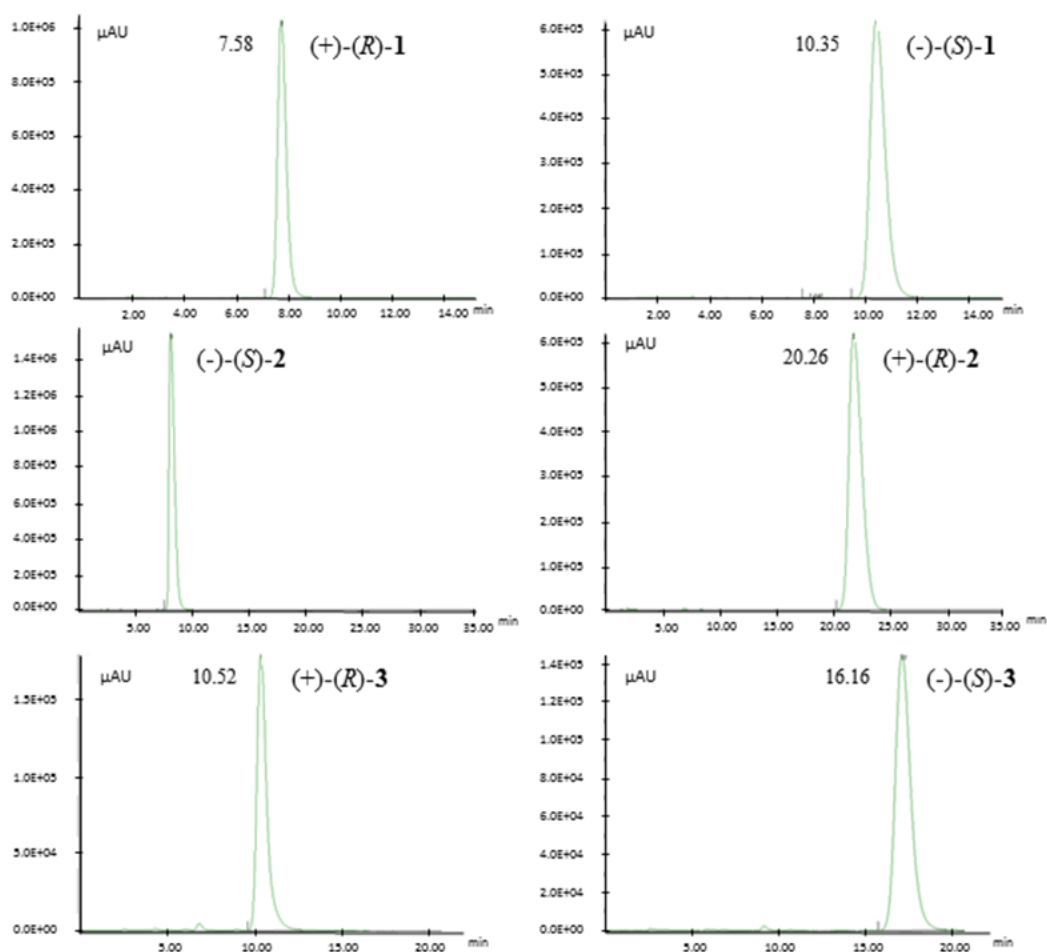
Figure SI-1 Final analysis of **1-3** enantiomers on Chiralcel OJ-H (4.6 mm x150 mm, 5 μm column). Experimental conditions: (top) mobile phase: *n*-Hep/EtOH 95/5; (middle) MeOH, detection at 250 nm; (v/v), detection at 240 nm; (bottom) MeOH, detection at 254 nm; For all: Injection volume 10 μL, flow rate: 1 mL min^{-1}
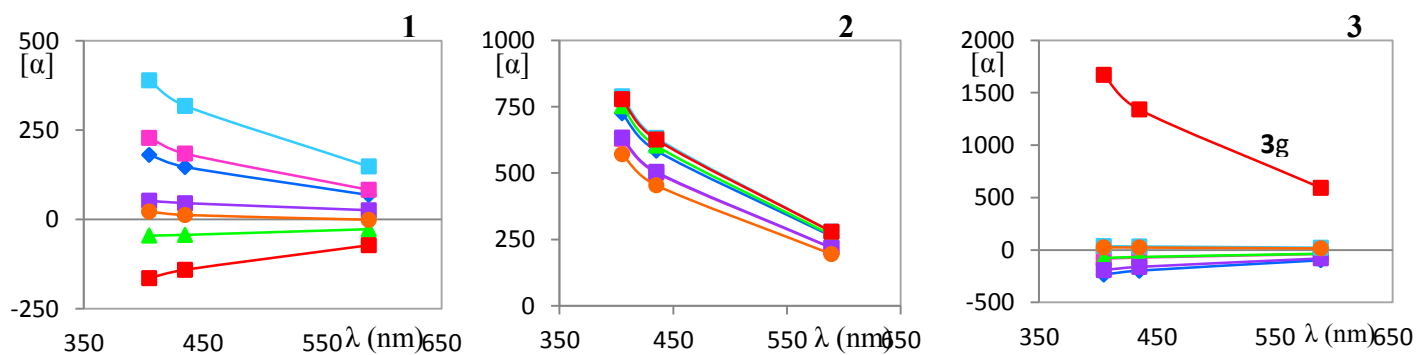

Figure SI-2. Computed ORD curves of (*R*)-**1** (left), (*R*)-**2** (middle), (*R*)-**3** (right), seven most populated conformers at DFT/B3LYP/TZVP level of theory.
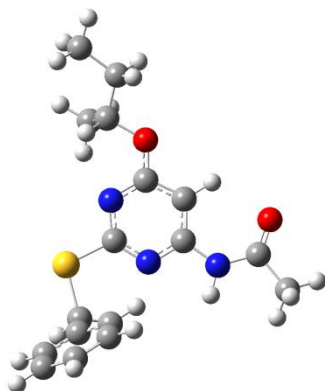
2

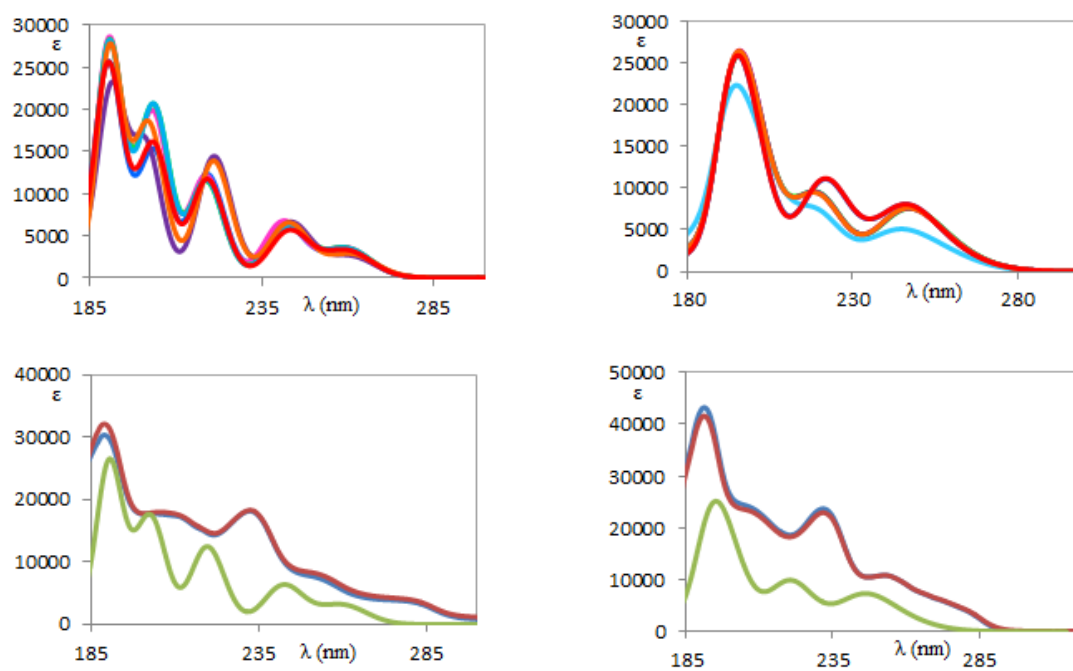**Figure SI-3.** (*R*)-**3**g

Figure SI-4. Up: UV computed spectra of (*R*)-**1** (left) and (*R*)-**2** (right) 7 most populated conformers at CAM-B3LYP/TZVP level of theory calculated in gas phase. Down: **1** (left) and **2** (right**)** first enantiomer (blue) and second enantiomer (red) experimental spectra compared to the average of all (*R*)-**1** and (*R*)-**2** calculated spectrum (green).
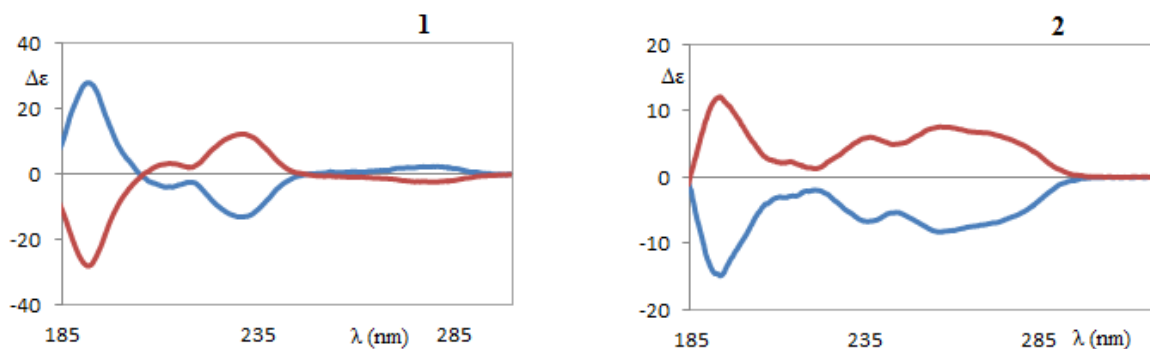
Figure SI-5. ECD experimental spectra recorded in acetonitrile for **1** (left) and **2** (right) first enantiomer (blue) and second enantiomer (red).

Figure SI-6. Comparison of experimental IR and VCD spectra recorded in CCl₄ (blue, first eluted enantiomer) of **1** with calculated (green) IR and VCD average spectra for (*R*)-**1**.

Figure SI-7. Comparison of experimental IR spectrum taken in CCl$_4$ of second eluted enantiomer of **2** (red) with calculated (green) IR average spectrum for (*R*)-**2**.

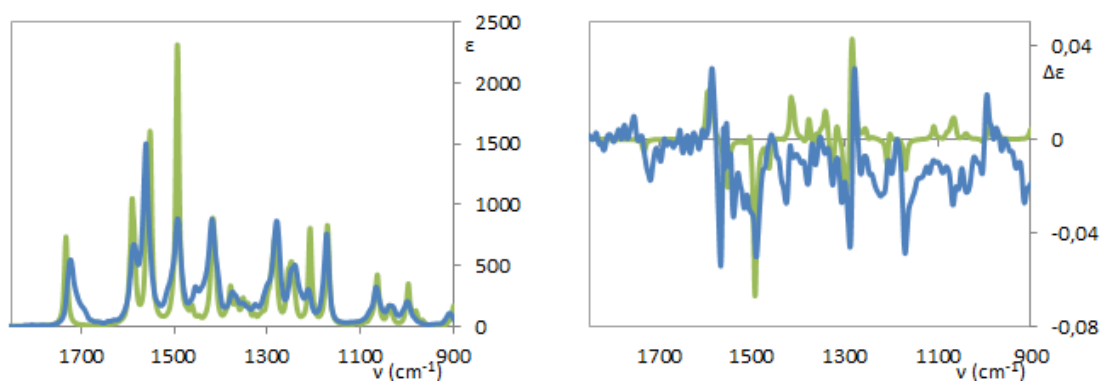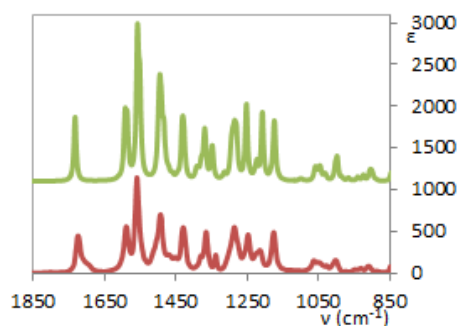**Table SI-1** Typical sets of columns and mobile phases.

CSPs *(Coated Polysaccharide-based Phase)*	
Chiralpack AD®	(amylose tris(3,5dimethylphenylcarbamate))
Chiralcel OD®	(cellulose tris(3,5-dimethylphenylcarbamate))
Chiralpack AS®	(amylose tris(*S*-α-methylbenzylcarbamate))
Chiralcel OJ-H®	(cellulose tris(4-methylbenzoate))

Mobile Phases
Methanol 100
Heptane/MeOH 90/10
Isopropanol (IPA) 100
Heptane /IPA 90/10

Table SI-2. OR first eluted values for **1-3**

λ	589		435		405	
	$[\alpha]^{22}$ Chloroform (deg cm^2 g^{-1})	$[\alpha]^{22}$ Methanol (deg cm^2 g^{-1})	$[\alpha]^{22}$ Chloroform (deg cm^2 g^{-1})	$[\alpha]^{22}$ Methanol (deg cm^2 g^{-1})	$[\alpha]^{22}$ Chloroform (deg cm^2 g^{-1})	$[\alpha]^{22}$ Methanol (deg cm^2 g^{-1})
1	- 219.24 (c. 0.560)	-214.73 (c. 0.220)	-527.39 (c. 0.560)	-501.56 (c. 0.220)	-635.68 (c. 0.224)	-644.44 (c. 0.110)
2		+ 16.35 (c. 0.108)		+40.37 (c. 0.108)		+65.18 (c. 0.108)
3	-24.96 (c. 0.630)	-27.78 (c. 0.560)	-51.52 (c. 0.630)	-56.16 (c. 0.560)	-52.97 (c. 0.252)	-65.93 (c. 0.224)

Table SI-3. Screening results for the enantiomer separation of **1**.

	Chiralcel OJ-H (0.46 cm × 15 cm, 5 μm)			
	1			
Eluent[a]	t_A (min)	t_B (min)	α	R_S
A	2.93	3.11	1.33	0.3
B	2.69	2.83	1.17	0.3
C	2.61	2.75	1.23	0.3
D[b]	5.57	6.33	1.45	0.4
E	4.88	6.07	1.40	1.8
F	**7.89**	**10.71**	**1.45**	**2.4**
G	22.73	37.13	1.70	4.0

Bold type indicates best result obtained.
[a]Eluent composition: A, MeOH (100); B, MeOH/EtOH (50:50 v/v); C, EtOH (100); D, IPA (100); E, *n*-heptane/EtOH (90:10 v/v); F, *n*-heptane/EtOH (95:5 v/v); G, *n*-heptane/EtOH (99:1 v/v).
Flow rate: 1.0 mL/min.
[b] Flow rate: 0.5 mL/min

Table SI-4. Calculated population factors of most populated (*R*)-**1**, (*R*)-**2** and (*R*)-**3** conformers at DFT/B3LYP/TZVP level of theory and values for some dihedral angle characterizing the geometries of the most populated conformers of each compound

Conf.	Pop. (%)	N(1)C(6)OC*	C(6)OC*C(benz)	N(1)C(2)SC	C(2)SCC
1a	9.6	5.3	83.2	179.5	180.0
1b	8.7	-0.6	150.7	-179.9	-179.3
1c	7.1	-0.7	151.7	178.1	-82.1
1d	7.0	4.2	82.1	-1.0	-177.0
1e	6.0	-1.0	151.2	-178.9	81.8

Conf.	Pop. (%)	N(1)C(6)OC	C(6)OCC	N(1)C(2)SC*	C(2)SC*C
2a	34.6	0.0	-178.6	-4.4	155.5
2b	11.7	0.2	179.6	178.2	155.3
2c	9.8	0.3	179.8	179.2	155.0

Conf.	Pop. (%)	N(1)C(6)OC*	C(6)OC*C	N(1)C(2)SC	C(2)SCC(benz)
3a	19.3	-0.3	154.0	179.4	-177.8
3b	18.5	-1.9	151.1	-0.6	179.8
3c	16.9	-1.9	151.1	-0.6	179.8

The role of chirality in a set of key intermediates of pharmaceutical interest, 3-aryl-substituted-γ-butyrolactones, evidenced by chiral HPLC separation and by chiroptical spectroscopies

Daniela Rossi [a], Rita Nasti [a,1], Simona Collina [a,*], Giuseppe Mazzeo [b,1], Simone Ghidinelli [b], Giovanna Longhi [b], Maurizio Memo [b], Sergio Abbate [b,*]

[a] Department of Drug Sciences, Medicinal Chemistry and Pharmaceutical Technology Section, University of Pavia, Viale Taramelli 12, 27100 Pavia, Italy
[b] Dipartimento di Medicina Molecolare e Traslazionale, Università di Brescia, Viale Europa 11, 25123 Brescia, Italy

ARTICLE INFO

ABSTRACT

The enantiomers of four chiral 3-aryl-substituted-γ-butyrolactones, key intermediates for the preparation of compounds of pharmaceutical interest, were successfully isolated by enantioselective chromatography, employing the Chiralpak AD-H chiral stationary phase. For all compounds the same elution order was observed, as monitored by a full set of chiroptical methods that we employed, namely ORD (optical rotatory dispersion), ECD (electronic circular dichroism, or CD in the UV range), and VCD (vibrational circular dichroism, or CD in the IR range). By density functional theory (DFT) calculations we were able to determine that the first eluted enantiomer has (S) absolute configuration in all four cases. We were able to justify the elution order by molecular docking calculations for all four enantiomeric pairs and suitable modeling of the stationary and mobile phases of the employed columns. The optimal performance of the chiroptical spectroscopies and of the DFT calculations allows us to formulate a lactone chirality rule out of the C=O stretching region of the VCD spectra.

© 2017 Elsevier B.V. All rights reserved.

1. Introduction

The γ-butyrolactone ring is a five-membered cyclic scaffold widely distributed in bioactive natural products (i.e. Helenalin, Parthenolide, Fig. 1) [1], as well as in synthetic molecules of pharmaceutical interest, such as antifungal [2], anticancer [3] and antifeedant compounds [4] (Fig. 1). From a synthetic standpoint, the γ-butyrolactone can be considered a versatile key intermediate for the preparation of various compound classes, including analogues of γ-hydroxybutyric acid [5] and ω-hydroxy analogues of aminoacids [6] (Fig. 1). Interestingly, γ-butyrolactones also represent key intermediates for the preparation of novel biologically active molecules identified in our recent researches [7,8]. Specifically, they are important intermediates for the synthesis of novel PKC ligands (Fig. 1) [7], which we recently identified within the

frame of researches aimed at discovering new valuable candidates for neurodegenerative diseases treatment. Additionally, the γ-butyrolactones also represent versatile intermediates for the preparation of novel sigma 1 receptor ligands (Fig. 1) [8], which we recently identified as highly promising compounds for neuropathic pain treatment basing on our long-lasting experience in the field of sigma receptor modulators [9–18]. As clearly shown in Fig. 2, the PKC and sigma 1 receptor ligands which we had studied are both characterized by the presence of one stereogenic center and therefore are chiral. Taking into account that the enantiomers of a biologically active compound may show different interactions to the target protein and, more generally, different behavior in the biological environment, the preparation and the biological investigation of its enantiopure forms represent key steps in the drug discovery process [19,20]. Accordingly, in our ongoing research projects we are approaching the preparation of our PKC and sigma1 receptor ligands as homochiral compounds in amount and purity suitable to perform an exhaustive biological investigation. As previously discussed, the 3-aryl-substituted-γ-butyrolactones **2–4** (Fig. 2) are the key intermediates for the synthesis of both the compound classes considered. Moreover, being the first chiral intermediates of the synthetic route in both cases, they emerged

* Corresponding authors.
    E-mail addresses: simona.collina@unipv.it (S. Collina), sergio.abbate@unibs.it (S. Abbate).
    [1] These two researchers contributed equally and with primary role to the present work.
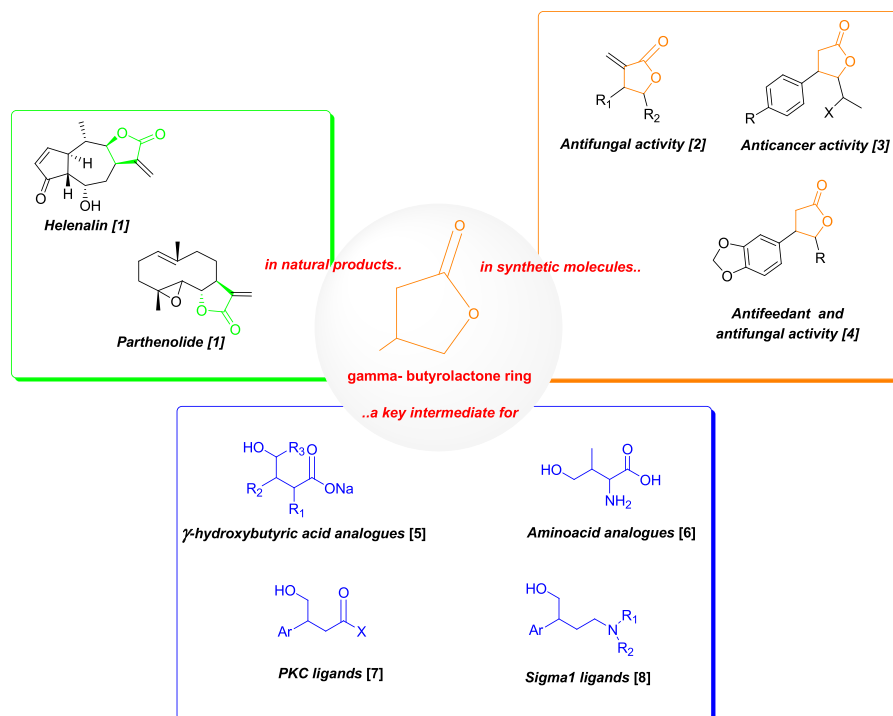
Fig. 1. Involvement of the γ-butyrolactone ring in biologically active molecules.
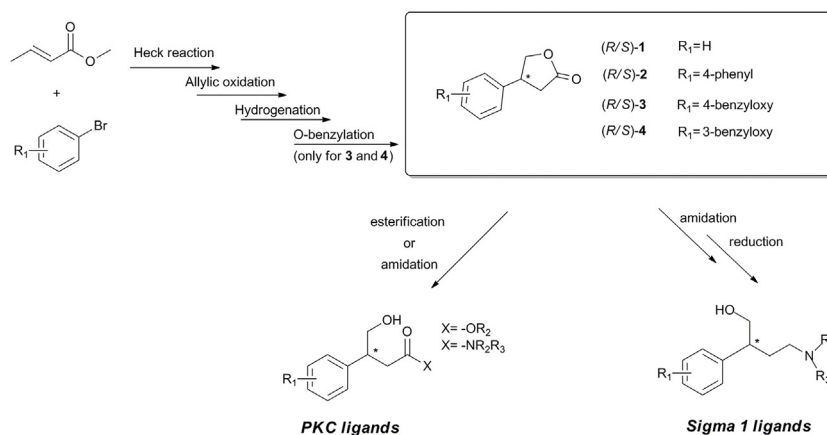

Fig. 2. Synthetic pathway of PKC and sigma 1 receptor ligands.

as the optimal candidates for the preparation of enantiopure forms to be next used as homochiral building blocks for the asymmetric synthesis of the target compounds.

Herein we report on the isolation of the enantiomers of **2–4** and the assignment of their absolute configuration (AC) by a full set of chiroptical techniques (ECD = Electronic Circular Dichroism or CD in the UV range; VCD = Vibrational Circular Dichroism or CD in the IR range; ORD = Optical Rotatory Dispersion). To isolate enantiomeric **2–4**, we select enantioselective High Performance Liquid Chromatograpy (HPLC) resolution on Chiral Stationary Phases (CSPs), as a viable route for straightforward and rapid access to both the enantiomers with high optical purity and yields [13,21–24]. Enantiomeric γ-butyrolactone **1** (Fig. 2) was also prepared and characterized as reference compound, for configurational assignment purposes [25].

In this work the employed chiroptical techniques will allow us to determine the AC; we will show that all techniques give the same answer about AC, unlike sometimes happens and as pointed out in the literature [26–31]. However we will dwell somewhat more on the VCD results [32–38], since VCD allows us, on the one hand to study in detail the conformational aspects of the molecules and since recently it has achieved success in the assignment of the absolute configuration of natural products and drug molecules [33–38]. The latter are investigated by Density Fuctional Theory (DFT) calculations, which allow one to check also the prediction of the spectroscopic data. Finally, the AC assignment will allow us to test and to rationalize the HPLC results, about the elution order of the enantiomers. This will be studied on the basis of the DFT results and Molecular Docking "experiments".

2. Materials and methods

2.1. Chemicals

Solvents used as eluents (HPLC grade) were obtained from Aldrich (Italy). (*R/S*)-**2-4** were prepared by us as already described

[7]. The same reaction procedure was applied to the preparation of the reference compound (*R/S*)-**1** (for experimental details see supplementary information).

2.2. HPLC separation

HPLC measurements were carried out on a Jasco system (JASCO Europe, Cremella, LC, Italy) consisting of PU-2089 plus pump, AS-2055 plus autosampler and MD-2010 plus detector. Data acquisition and control were performed using the Jasco Borwin Software.

Retention factors of first and second eluted enantiomer k_a and k_b, respectively, were calculated following IUPAC recommendations [39]; the dead time t_0 was considered to be equal to the peak of the solvent front for each particular run. Resolution was calculated according to Ph. Eur. 2.2.29 [40], enantioselectivity (α) was calculated according to: $\alpha = k_b/k_a$.

For a first rough characterization, optical rotation measurements were determined on a Jasco photoelectric polarimeter DIP 1000 (JASCO Europe, Cremella, LC, Italy) using a 0.5 dm cell and a sodium and mercury lamp (λ = 589 nm, 435 nm, 405 nm); sample concentration values (c) are given in 10^{-2} mL^{-1}.

2.3. Chiral chromatography

In order to identify the best conditions for the resolution of (*R/S*)-**2-4** to be properly scaled up, an analytical screening was first performed using the commercially available Chiralcel OJ-H (150 mm × 4.6 mm, 5 µm), Chiralpak IC (250 mm × 4.6 mm, 5 µm), Chiralpak AD-H (150 mm × 4.6 mm, 5 µm) columns (Daicel Industries Ltd., Tokyo, Japan). The mobile phase compositions as well as the chromatographic parameters are summarized in Table SI-1 of the Supplementary material. Sample solutions of the analyte [1 mg mL^{-1} in selected mobile phase] were filtered through 0.45 µm PTFE membranes (VWR International, Milan, Italy) before analysis. The injection volume was 10 µL, the flow rate was 1.0 mL min^{-1} and detection wavelength was 254 nm (compound **2**) and 274 nm (compounds **3** and **4**). All experiments were performed at room temperature (r.t.).

The enantiomers of (*R/S*)-**2-4** were then completely resolved by a semi-preparative process using a RegisPack column (250 mm × 10 mm, 5 µm) (Regis Technologies Inc., Morton Grove, IL, USA) according to conditions summarized in Table 1. As regards reference compound **1**, its enantiomers were resolved using the same RegisPack column (250 mm × 10 mm, 5 µm) applying the elution conditions previously described [25] with suitable modification (Table 1). The eluate was properly partitioned according to the UV profile. The collected fractions were evaporated at reduced pressure. In process control was performed using an analytical Chiralpak AD-H column.

2.4. Chiroptical measurements

Three types of chiroptical data were considered, namely ORD, ECD and VCD. Details on instrumentation and measurement conditions are briefly described below.

2.4.1. Optical rotatory dispersion (ORD)

The ORD measurements were carried out with a Jasco P-2000 Polarimeter. A 10 cm micro SiO$_2$ cuvette was employed in all cases with CHCl$_3$ solutions at ca. 0.01 M. Solutions were studied at 25 °C and five wavelengths were considered for Optical Rotations (OR), 589 nm (Na lamp), 546, 435, 405, and 365 nm (Hg lamp). OR data were obtained with ten measurements at each wavelength and proper subtraction of the OR data from the solvent at the same wavelength was carried out. Specific rotation values were obtained

from a program of the instrument. The experimental data at two adjacent wavelengths were connected through a straight line.

2.4.2. Electronic circular dichroism (ECD)

ECD spectra were taken from 350 to 185 nm on a Jasco 815SE spectropolarimeter. Solutions were measured in a range of ca. 0.002–0.003 M/CH$_3$CN and were contained in 0.1 mm quartz cylindrical cuvettes. For each measurement, 10 scans were taken and averaged, considering both enantiomers of each compound **1–4**. ECD spectra of the solvent in the same experimental conditions were subtracted. Data are reported in $\Delta\varepsilon$ vs. λ (nm), from knowledge of the cell pathlength and solution concentration.

2.4.3. Vibrational circular dichroism (VCD)

VCD spectra were taken from 950 to 1800 nm on a Jasco FVS6000 FTIR spectropolarimeter. Solutions were ca. 0.1 M/CDCl$_3$ and were contained in 200 µm BaF$_2$ IR cells. 5000 scans were taken for each measurement on both enantiomers of each compound **1–4**. A resolution of 4 and 8 cm^{-1} was used in recording 950–1500 cm^{-1} and 1600–2000 cm^{-1} region respectively. VCD spectra of the solvent in the same experimental conditions were obtained between the measurements of the two enantiomers and were then subtracted and data are reported in $\Delta\varepsilon$ vs. ν (cm^{-1}), from knowledge of the cell pathlength and solution concentration.

2.5. DFT calculations

Conformational analysis of each molecule in a given configuration (*S* for **1** and **2** and *R* for **3** and **4**) was carried out at the Molecular Mechanics (MM) level, with allowance of all conformer in the range 0–5 kcal/mol from the most stable one. All these conformers were fed to Gaussian09 [41] and DFT calculated conformers and IR and VCD spectra were obtained at B3LYP/TZVP level within the PCM approximation [42]. VCD and IR spectra simulation was obtained by assigning a Lorentzian band to each calculated transition, with assigned bandwidth of 10 cm^{-1}, for the rotational and dipole strengths calculated through Gaussian09. Scaling factors of 0.96 and 0.98 were applied to the calculated VCD bands in the C=O stretching region and fingerprint region respectively. ECD and ORD calculated spectra were obtained by Gaussian09 using respectively CAM-B3LYP/TZVP and CAM-B3LYP/6-311++G(d,p) levels of theory. ECD Spectra were simulated with 0.2 eV wide Gaussian bands. All calculated ECD and UV absorption transitions were shifted by 10 nm and were divided by 3, to facilitate comparison with experimental data.

To establish how well computed VCD and ECD spectra compare with experimental ones, beyond qualitative observation, we calculated the similarity index defined in eq. 1 [43]:

$$S.I. = \frac{\int f(x)g(x)\,dx}{\sqrt{\int |f(x)|^2 dx \int |g(x)|^2 dx}} \tag{1}$$

where $f(x)$ is the computed spectrum (VCD or ECD), $g(x)$ is the experimental one and x is the wavenumber and wavelength in the case of VCD and ECD respectively. The integral is extended over the region of interest.

3. Results and discussion

Racemic **2-4** were recently synthesized within our research projects focused on the identification of new molecules potentially useful in the treatment of neurodegenerative diseases and neuropathic pain. Indeed, they are key intermediates of the synthetic pathway of both PKC [7] and sigma 1 receptor [8] ligands recently studied by us, as already stated in the introduction section (Figs. 1 and 2). More specifically, the γ-butyrolactones **2-4**, in

Table 1
(Semi)-preparative resolution of (R/S)-**1-4** on a RegisPack column (250 mm × 10 mm, 5 μm).

Cmpd	Mobile Phase (v/v)	Flow rate (mL min^{-1})	Tr_A (min)	Tr_B (min)	Injection volume (mL)	Concentration (mg mL^{-1})
(R/S)-**1**	n-Hep/EtOH 95/5	4	25.28	30.13	5	2
(R/S)-**2**	MeOH	4	16.48	21.29	2.5	3
(R/S)-**3**	MeOH	4	11.63	12.44	1	4
(R/S)-**4**	n-Hep/EtOH 85/15	4	20.75	24.02	1	4

Table 2
Chiroptical properties and isolated amounts of **1-4** enantiomers.

Cmpd	t_R[a] (min)	$[\alpha]_D^{20}$[b]	Ee[b] [%]	Isolated amount (mg)	Yield [%]
(+)–**1**	14.04	47.4	99.9	8.8	43.7
(−)–**1**	16.56	−45.6	95.1	7.1	35.3
(+)–**2**	11.84	33.8	98.8	10.3	34.5
(−)–**2**	15.27	−33.3	98.3	9.5	31.6
(+)–**3**	7.84	29.2	99.4	7.2	32.7
(−)–**3**	8.39	−27.42	97.7	7.8	35.4
(+)–**4**	13.12	29.2	99.1	3.7	31.5
(−)–**4**	15.51	−28.6	99.3	3.8	32.2

[a] Determined by chiral HPLC using a Chiralpack AD-H column (150 mm × 4.6 mm, 5 μm). Experimental conditions: n-Hep/EtOH 95/5 (v/v) as eluent, detection at 250 nm for (R/S)-**1**; MeOH as eluent, detection at 254 nm for (R/S)-**2**; MeOH as eluent, detection at 274 nm for (R/S)-**3**; n-Hep/EtOH 85/15 (v/v) as eluent, detection at 274 nm for (R/S)-**4**. For all: Injection volume: 10 μL, flow rate: 1 mL min^{-1}.
[b] c: 0.2% in CHCl$_3$.

their enantiomeric forms, represent valuable homochiral building blocks for the asymmetric synthesis of the target compounds.

Accordingly, we developed an enantioselective HPLC methodology using CSPs suitable for ready availability of both enantiomers of **2-4** in g-scale with an enantiomeric purity adequate for the configurational study. To this aim, we followed the so called "fit-for purpose" strategy recently outlined at Pfizer and Vertex and applied in our recent researches for the isolation of the enantiomers of an interesting sigma 1 receptor agonist [24]. The enantiomers of reference compound **1**, whose absolute configuration had been already assigned [25], were also isolated for comparative purposes.

3.1. Preparation of **1-4** enantiomers via enantioselective chromatography

In the first step of our study, a primary standard screening protocol for cellulose and amylose derived CSPs [23] was applied to Chiralcel OJ-H and Chiralpak IC (cellulose derivatives) as well as to Chiralpak AD-H (amylose derivative), which employ some of the most versatile CSPs available in our laboratories. Mobile phases included alcohols, such as methanol (MeOH), ethanol (EtOH) and 2-propanol (IPA), as pure solvents or in mixtures, as well as mixtures of n-heptane (n-Hep) and IPA as polar modifier. Results of the screening protocol are reported in Table SI-1 expressed in terms of retention factor (k_A or k_B), separation factor (α), and resolution factor (R_S).

Generally, poor or no separation was observed on Chiralpak IC, with the only exception of (R/S)-**4**, for which acceptable results were obtained only eluting with mixtures of alkane and polar modifier. As regards Chiralcel OJ-H, no separation was observed for (R/S)-**3** with all tested mobile phases, almost baseline separation was obtained for (R/S)-**4** eluting with mixtures of alkane and polar modifier, while good enantioseparation was achieved for (R/S)-**2**, eluting with mixtures of alkane and IPA, pure IPA and IPA/EtOH. Unfortunately, analysis of (R/S)-**2** resulted quite time-consuming and thus do not provide enough confidence for a productive scale-up.

Interestingly, results on Chiralpak AD-H turned out to be much more effective. In details, Chiralpak AD-H was the only effective CSP in the separation of the **3**-enantiomers, for which almost baseline separation was achieved eluting with both n-Hep/IPA (90/10 v/v, α = 1.06, Rs = 1.15) and pure MeOH (α = 1.10, Rs = 1.56).

Good enantioselectivity and excellent resolution were obtained for both (R/S)-**2** and (R/S)-**4** eluting with n-Hep/IPA [90/10 v/v, α = 1.34, Rs = 5.34 for (R/S)-**2** and α = 1.20, Rs = 3.05 for (R/S)-**4**], within relatively short retention times. Moreover, retention behavior, enantioselectivity and resolution of **2**-enantiomers remained almost unvaried, when eluting with pure MeOH (α = 1.38, Rs = 5.12).

In conclusion, from our primary screening, Chiralpak AD-H clearly emerged as the optimal CSP for separating the enantiomers of (R/S)-**2-4** in (semi)preparative scale. Concerning the elution conditions, the best results in terms of both enantioresolution and shortest retention times were obtaining using pure MeOH for (R/S)-**2** and (R/S)-**3** and n-Hep/IPA (90/10 v/v) for (R/S)-**4** (Table SI-1). As previously discussed, none of the elution conditions experimented provided baseline separation of **3**-enantiomers. Therefore, we decided to change the polar modifier in the alkane/alcohol mobile phase, using EtOH instead of IPA. Indeed, it is well known that a change of the alcohol modifier often gives rise to a changed chiral selectivity. Accordingly, the mixture n-Hep/EtOH [90/10 and 85/15 (v/v)] were experimented (Table SI-1). Unfortunately, worst results were obtained for (R/S)-**3**. On the contrary, the resolution of the enantiomers of both (R/S)-**2** and (R/S)-**4** was greatly improved. Particularly: i) excellent resolution of the enantiomers of (R/S)-**2** was observed eluting with both the mobile phase compositions (Rs almost 10 or higher than 10), but analysis became time-consuming, and thus not suitable for the semi preparative scale up; and ii) good enantioselectivity and high resolution (α = 1.23, Rs = 3.24) combined with a slight decrease of the retention times was observed for (R/S)-**4** by eluting with n-Hep/EtOH 85/15 (v/v).

To recapitulate, considering that shortest retention times combined with elution using a solvent as cheap as possible are important prerequisites for an economic and productive (semi)-preparative enantiomeric separation, and based on the analytical screening results (Table SI-1), we selected for the next (semi)-preparative scale-up the Chiralpak AD-H CSP, combined with pure MeOH for R/S-**2** and (R/S)-**3** and with n-Hep/EtOH 85/15 (v/v) for (R/S)-**4** as eluent (Fig. SI-1)

The separation of **2-4**-enantiomers in (semi)preparative scale was accomplished using a RegisPack column, which employ the same Chiralpak AD-H amylose derivative CSP, according to conditions summarized in Table 1. Actually, 30 mg of (R/S)-**2** were processed in 4 cycles, yielding 10.3 mg of the first enantiomer (ee = 98.8%) and 12 mg of the second eluted one, along with 2.5 mg

of an intermediate fraction as a mixture of the two enantiomers. Unfortunately, from the analytical control of the collected fractions it emerged that the second eluted enantiomer possesses low optical purity (ee = 76.8%) and thus it was processed under the same experimental conditions ultimately giving 9.5 mg of the target compound with high optical purity (ee = 98.3%). As regard (*R/S*)-**3**, 22 mg of were processed in 6 cycles, yielding 7.2 mg of first enantiomer (*ee* = 99.4%) and 9.2 mg of the second eluted one, along with 3.4 mg of an intermediate fraction as a mixture of the two enantiomers. Again, the analytical control of the obtained fractions revealed that the second eluted enantiomer of **3** do not meet the requisites of optical purity needed for the configurational study (ee = 78.3%). Therefore it was reprocessed under the same elution conditions, providing 7.8 mg of the target compound with the desired enantiomerical purity (ee = 97.7%). Finally, 12 mg of (*R/S*)-**4**, were processed in 3 cycles, giving 3.7 mg of the first enantiomer and 3.8 mg of the second enantiomer, both with high enantiomeric excess (*ee* ≥ 99%). For the configurational study, the enantiomers of **1** were also isolated as reference compounds of known absolute configuration *via* enantioselective HPLC using a RegisPack column and applying the elution conditions previously described by Luo et al. [25], with suitable modifications (Table 1). Briefly, 20 mg of (*R/S*)-**1** were processed in two cycles yielding 8.8 mg of first enantiomer and 7.1 mg of second enantiomer with an ee higher than 95.0%.

In conclusion, by applying the recently developed "fit-for-purpose" strategy, we successfully isolated the enantiomers of **1-4** *via* enantioselective HPLC in amount and enantiomeric excess suitable for configurational study, as evidenced by the chiroptical properties and process yields reported in Table 2 as well as by the final analytical control of the enantiomers collected (Fig. SI-2). It is worth noting that, as clearly stated in Table 2, using the Chiralpak AD-H (an amylose derived CSP column) the *dextro* isomers are the first eluted enantiomers for all the studied γ-butyrolactones.

3.2. Chiroptical spectroscopies and assignment of the absolute configuration

In Fig. 3 we report the superimposed experimental VCD spectra in the C=O stretching region (1850–1700 cm^{-1}), in the so called fingerprint region (1600–950 cm^{-1}), the superimposed experimental ECD spectra and the experimental ORD traces for the two enantiomers of **1** and **2** (top part of Fig. 3) and of **3** and **4** (lower part of Fig. 3). We have decided to report the data in order of increasing molecular complexity, to better proceed in the following discussion. First of all we notice that there is an excellent mirror image aspect in the data of each couple of enantiomers. Also please notice that the color coding of the curves has always been: blue for the first eluted enantiomer and red for the second eluted enantiomer. One may also notice that the chiroptical data bear an evident correspondence with the order of elution. In particular one may observe that VCD band in the C=O stretching region and the OR data are positive for the first eluted enantiomers of all four compounds and are negative for the second eluted enantiomers (ORD data are also similar in absolute values, ranging from ca. 50 at 600 nm to 100 at 400 nm). VCD spectra of **1** and **2** are quite similar in sign and intensity for most of the VCD bands, while the VCD spectra of **3** and **4** are different; one though may recognize that three features are clearly observed between 1150 and 1250 cm^{-1} for **1** and **2**, which for the first eluted enantiomer are (−,−,+) in order of increasing wavenumbers, and are also observed for **3**. Finally, the weak VCD feature (+ for the first eluted enantiomer) in correspondence of the strong ∼1000 cm^{-1} IR band, is common to all four molecules. Also ECD spectra show strong similarities in sign and shape: one may notice that the first intense band in the range 220–230 nm is negative for the first eluted enantiomer of all molecules; for all compounds a

positive band is observed between 185 and 220 nm, which is structured differently in the four cases. While the UV spectra bear similar intensities for all four molecules (the band at ca. 200 nm has ε^{MAX} roughly varying from 24,000 to 60,000), the ECD spectra of **1** and **4** are stronger than those of **2** and **3**: in the former cases the band at ca. 200 nm has $\Delta\varepsilon^{MAX} \sim 10$, while **2** has $\Delta\varepsilon^{MAX} \sim 2$ and **4** has $\Delta\varepsilon^{MAX} \sim 4$. For the proper interpretation of phenomena underlying these variations, one needs DFT calculations which will be presented below. However, even without performing calculations, one sees that the sign of several chiroptical data are in accord with the elution order, in particular the VCD bands for the C=O stretchings and the ORD curves are all positive for the first eluted enantiomers and all negative for the second ones. Calculation will help to establish that the order of elution is related to a consistent AC, which is (*S*) for the first eluted enantiomers and (*R*) for the second ones.

In Fig. 4-left we report the comparison of DFT calculated VCD and IR spectra for the (*S*) enantiomers of **1** and **2** with the experimental VCD and IR spectra of the first eluted enantiomers of the same compounds, while in Fig. 4-right we compare DFT calculated VCD and IR spectra for the (*R*) enantiomers of **3** and **4** with the experimental VCD and IR spectra of the second eluted enantiomers of these compounds. Calculations match experiments in almost all bands, even weak ones; this allows us to conclude that the first eluted enantiomers are always (*S*), while the second eluted ones are (*R*). The best results are obtained for molecules **1** and **2**, while some minor problems are met with **3** and **4**; since also the prediction of IR spectra is very good, we conclude that the conformational population is computed in an excellent way, especially for the molecules where the number of conformers is small (**1** and **2**).

The calculated spectra are the averages through weights proportional to $e^{-(\Delta G/RT)}$; the latter weights, which are *de facto* population factors, are presented in Table 3, together with the values of three significant geometrical parameters and the values of the calculated rotational strength for the C=O stretching mode (for the definition of parameters, please see Fig. SI-3).

To assess the performance of VCD and ECD-spectra calculations with respect to VCD and ECD experiments, we computed the similarity index *S.I.*, as defined in equation (1) of the Materials and Methods section. In the case of VCD, integrals of eq. (1) were extended over the region between 950 and 1550 cm^{-1}. The ECD data will be discussed later on. If the *S.I.* number is close to +1, the assumed AC is correct; if it is close to −1 the assumed AC must be reversed. In Table 4 we report the *S.I.* values for different choices of the scaling factors and we observe that the best scaling factor is 0.98: in this case *S.I.* numbers are between 0.52–0.58 for **1**, **2** and **3**. For molecule **4** we have *S.I.* = 0.13: we noticed that this is due to the mismatch in the prediction of the negative experimental band at ca. 1000 cm^{-1} which is calculated positive. Indeed we learn from this example that the *S.I.* parameter is especially sensitive to the sign of the VCD bands and is less sensitive to their absolute values. Since qualitatively VCD spectra for **1** and **2** are excellently predicted, we conclude that a *S.I.* value of ca. +0.6 denotes unambiguous AC determination; in any case also for molecule **4** the AC is correctly determined.

The analysis of geometrical data of Table 3 allows one to appreciate the relevant features of the most populated conformers of molecules **1-4** (in Fig. SI-4 we provided the structure of the first two conformers). The relevant geometrical parameters are $\tau_1 = C(=O)CC^*H$, $\tau_2 = CC^*CC$, $\pi = C(=O)CC^*C$ (see also the graphical definition in Fig. SI-3). τ_1 is positive for (*S*) and negative for (*R*) and has higher absolute values (ca. 140°) for axial than for equatorial conformations (from ca. 60–70°); τ_2 describes the orientation of the external group; finally π describes the puckering of the lactone ring and has two values, ca. +27° for equatorial and −24° for axial conformers. One may see that, overall, the equatorial conformers dominate in population over axial conformers, being populated
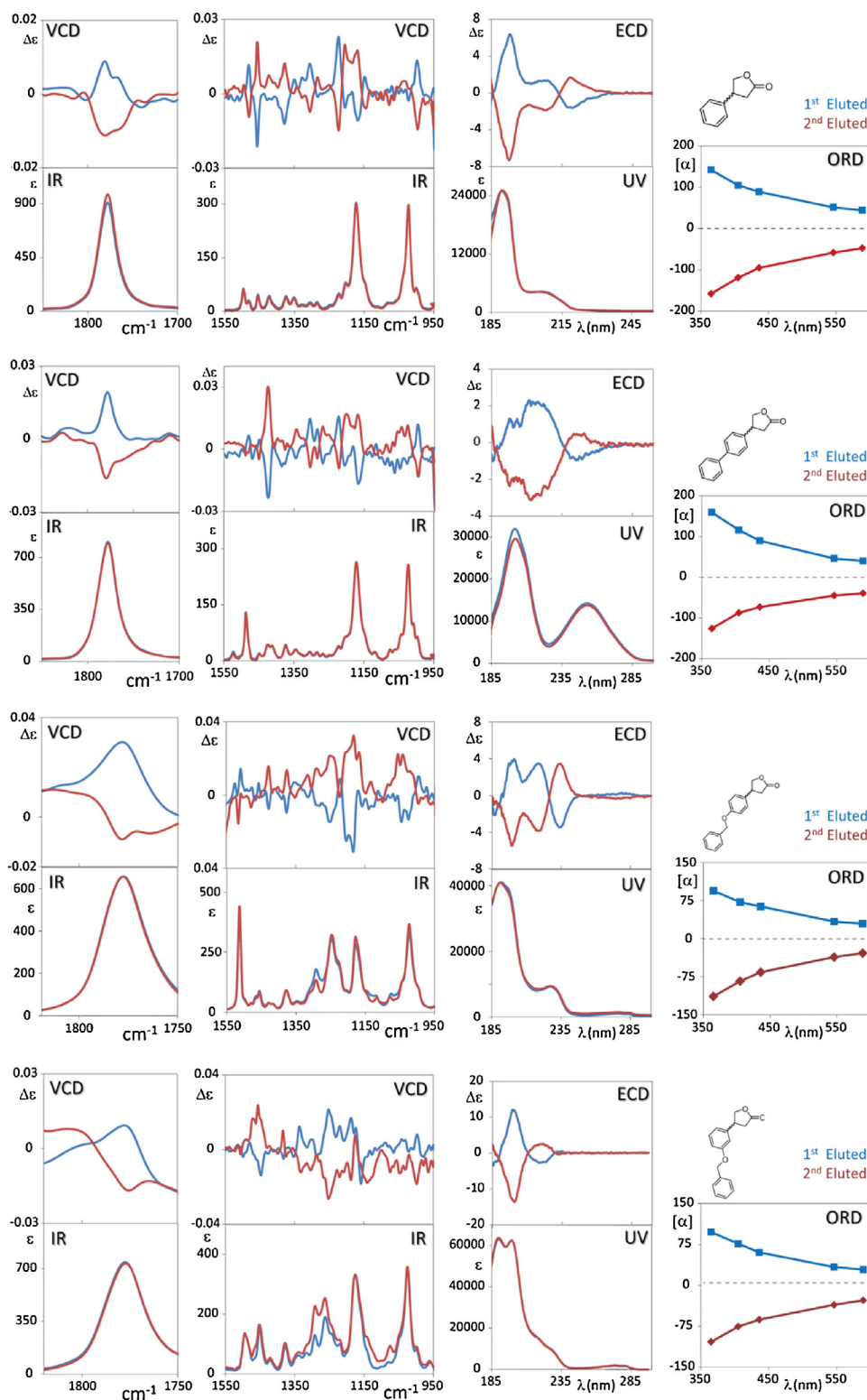
Fig. 3. Superimposed experimental VCD and IR spectra in the C=O stretching region (first column from left), in the fingerprint region (second column), ECD spectra (third column) and ORD curves for the two enantiomers of molecules **1** (top row), **2** (second row from top), **3** (third row) and **4** (bottom row). The first eluted enantiomer is color-coded blue in all graphs, and the second eluted one is color-coded red in all graphs. (For interpretation of the references to colour in this figure legend, the reader is referred to the web version of this article.)

from 70% to 80% in the various cases. Additionally one sees that the sign of the calculated rotational strengths for the C=O stretching mode correlates with the absolute configuration, irrespective on the conformation being axial or equatorial; only its absolute value depends on conformation and is larger for axial conformers than for equatorial conformers. All these facts make the sign of the C=O stretching VCD band a possible marker of AC and finds a nice explanation in the calculated APT (atomic polar tensor) and AAT (atomic axial tensor) for the C and O atoms in a reference axis system centered in the middle of the C=O bond, with the
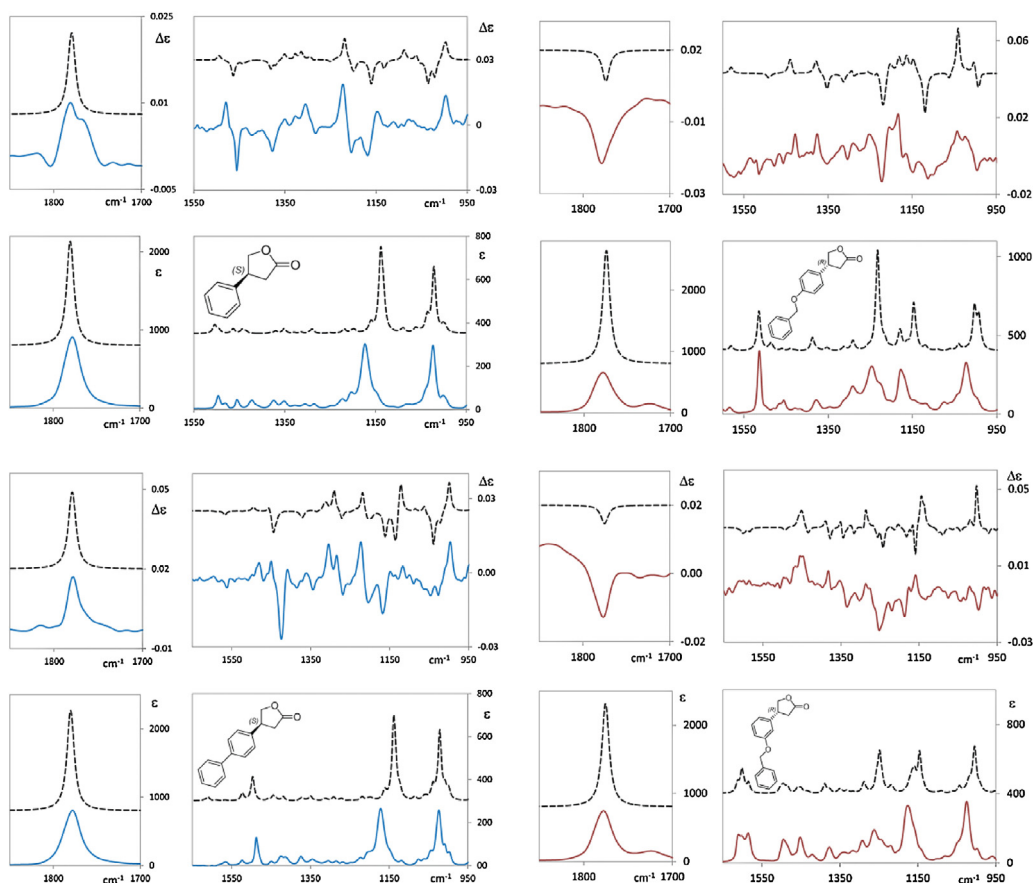
Fig. 4. Comparison of experimental VCD and IR spectra for the first eluted enantiomer (color, solid lines) with the calculated (black, dashed lines) VCD and IR spectra of the (*S*) enantiomer of molecules **1** and **2** (left columns, top and bottom respectively) and of molecules **3** and **4** (right columns, top and bottom respectively); experimental VCD spectra are semi-differences of the spectra of Fig. 3. Calculated spectra are Boltzmann averages from calculated spectra of each single conformer (see Table 3). Color coding as in Fig. 3.

Table 3
Main characteristics of the most significant populated calculated conformers of molecules **1-4**: **1** and **2** in the (*S*) configuration, and **3** and **4** in the (*R*) configuration. Dihedral angles' values $\tau_1(°)$, $\tau_2(°)$ (see text and Fig. SI-3 for definition), calculated rotational strength for the C=O stretching mode (10^{-44} esu^{2}cm^2) and Boltzmann statistical weight $\pi(°)$: lactone ring puckering.

	τ1	τ2	R	%pop	π
Compound-1 (*S*)					
1a	139.6	−111.2	60.9	25.6	23.9
1b	84.8	−124.3	17.5	74.4	−27.8
Compound-2 (*S*)					
2a	85.4	−124.4	26.4	37.3	−27.4
2b	85.2	−123.8	29.8	32.9	−27.6
2c	138.5	−111.9	77.5	17.6	23
2d	139.5	−107.8	75.1	12.3	24
Compound-3 (*R*)					
3a	−85.1	−55.5	−20.2	33.0	27.6
3b	−85.2	−56	−19.6	29.4	27.6
3c	−85.2	−57.7	−20.2	19.5	27.5
3d	−139.2	−69.4	−60	5.7	−23.9
3e	−140.2	−72.5	−59.7	3.9	−24.9
Compound-4 (*R*)					
4a	−85.3	−56.4	−20.8	17.7	27.5
4b	−85.1	122.2	−1.2	17.4	27.7
4c	−84.8	−56.6	−30.4	15.6	28
4d	−58.5	123.8	6.2	11.9	27.5
4e	−139.5	−69.3	−33	7.1	−24
4f	−84.9	120.8	3.3	3.8	27.9
4g	−139.4	106.3	−27.3	3.1	−23.8
4h	−85.1	−57.2	−24.7	3.0	27.7
4i	−139.1	−74.6	−50	2.6	−23.6
4j	−139.4	105.4	−36.2	2.4	−24
4k	−83.2	17.1	5	2.1	29.2
4l	−85.2	122.7	11.7	2.1	27.6
4m	−85.5	124.2	−16.9	1.9	27.5

Table 4
Similarity indexes (calculated as reported in eq. 1) between experimental and calculated VCD and ECD spectra. The used scaling factors for VCD and the applied red shift in nanometer for ECD maximizing similarity indexes are reported in brackets.

Compound	Enantiomer	VCD (0.985)	VCD (0.98)	VCD (0.975)	VCD (0.97)	ECD (Shift nm)
1	*S*	0.56	0.58	0.46	0.25	0.92 (10)
2	*S*	0.5	0.55	0.52	0.38	0.79 (5)
3	*R*	0.49	0.52	0.37	0.23	0.77 (15)
4	*R*	0.13	0.11	0.07	0.04	0.94 (10)

z-axis along C=O, y perpendicular to the lactone plane O=CCO and x lying on the latter plane (see Table SI-2): since the scalar product of APT and AAT defines the rotational strengths [32], one may see that, due to cancellation in the other two directions, the rotational strength is generated by the y-components of the APT and AAT of the C and O atoms defining the C=O bond. The y-component of the AAT is related to a ring current in the lactone ring initiated by the C=O stretching. In SI we also provide the three-dimensional structures for the two most populated conformers of the four molecules according to Table 3. The use of this VCD signal to monitor AC for chirally substituted lactones needs further checks. We have verified it for lactones substituted in 4 [44], while in the present case substitution is in 3. Other possible cases are from the literature [45–47]. Another possible marker of the lactone configuration is the $(-,-,+)$ triplet of bands in order of increasing wavenumbers for the (*S*) enantiomer (and $(+,+,-)$ for the (*R*) enantiomer) between 1150 and 1250 cm^{-1}; as of Fig. SI-5, top part, one sees that such bands originate from normal modes involving the C—O stretching mode coupled to CH$_2$ and C*H bending modes of the lactone moiety. This signature is observed also in refs [44–47]. Finally we considered the VCD band at ca. 1000 cm^{-1}, which is positive for (*S*) and negative for (*R*) configurations respectively. One may see that this band is associated to an intense mode for axial conformers only, and is comprised of C—O stretching mode (in larger amount than in the triplet of modes above) and some CH$_2$ rocking modes (see Fig. SI-5, bottom). Equatorial conformers do not exhibit intense VCD for that mode, and thus we are not sure that this band may be used to monitor AC.

Also the ECD spectra and ORD curves are excellently predicted by TD-DFT calculations, as one may see from Fig. 5, where results are for the (*S*) enantiomers of **1** and **2** and for the (*R*) enantiomers of **3** and **4** respectively. In all cases signs are perfectly predicted for each ECD band as well as for all four ORD curves; just one may observe that calculated ECD and UV absorption spectra of the four molecules are overall a bit too intense and we had to scale them down. Referring to Table 4 we may look at the *S.I.* parameter for judging the performance of calculated ECD spectra. The *S.I.* parameters are all above +0.75 and for **1** and **4** are above +0.90: this means that the assumed AC for **1-4** is correct. The high values for *S.I.* are due to the fact that ECD bands are less in number than in the VCD case; smaller *S.I.* values are found for **2** where the positive ECD band at high energy is incorrectly predicted in sign; similar reasons hold for the small *S.I.* value for **4**. The calculated ORD values instead do not show a unique trend; they are either exact or small in absolute value.

A last comment on the ECD spectra is that the single ECD bands are not assignable to C=O $n \rightarrow \pi^*$ or to $\pi \rightarrow \pi^*$ transitions in the aromatic moieties, which mutually influence each other; besides the $n \rightarrow \pi^*$ transition in lactones is quite different from ketones, as pointed out by Klyne [48–50] in the early days of CD spectroscopy, making it of limited use for configurational assignment. This provides the C=O stretching VCD data a potentially important value for AC assignment. Indeed the latter data may acquire the significance of a configurational marker. Additionally we may state that also the $(-,-,+)/(+,+,-)$ triplet between 1150 and 1250 cm^{-1} is marker of the absolute configuration of the lactone ring, being associated

Table 5
Measured elution times and calculated molecular docking binding energies for the two enantiomers of the four compounds studied in the present work.

Compound	Elution Times (min)	Mean Binding Energy (kcal/mol)
(*R*)-**1**	16.56	−5.93
(*S*)-**1**	14.04	−5.80
(*R*)-**2**	15.27	−8.19
(*S*)-**2**	11.84	−7.91
(*R*)-**3**	8.39	−7.58
(*S*)-**3**	7.84	−7.42
(*R*)-**4**	15.51	−7.70
(*S*)-**4**	13.12	−7.56

to C—O single bond stretching + CH bending modes: may we notice that Klyne had pointed out the special character of the C—O lactone bond in association with corresponding C=O bond [49–51]. The third possible VCD marker of lactone-AC appears associated only to one conformer, and thus appears as less robust, even though it involves the C—O stretching mode of the lactone moiety.

In any case from all the chiroptical data we conclude that the AC is unambiguously defined: indeed for all molecules **1-4** the first eluted enantiomer has (*S*) configuration and the second eluted enantiomer has (*R*) configuration. Such a unanimous conclusion from all employed chiroptical techniques is not universal for all chiral molecules [32] and especially for pharmaceutically relevant molecules [29,38,51] or for natural products [37,52]. It is noteworthy also that the same type of column determines the same order of elution in enantiomeric separation; this will be investigated in the next paragraph.

3.3. Docking numerical experiments

In the present paragraph we comment the results for the docking numerical experiments for the two enantiomers of each molecule **1-4** onto the stationary phase of the AD-H columns, namely amylose tris-(3,5-dimethylphenylcarbamate) polymer. To obtain the results presented below, the 3D-structure for the most populated conformer of Table 3 of each enantiomer of the four molecules **1-4** predicted by DFT was used as input structure. The 3D-polymer structure of amylose tris-(3,5-dimethylphenylcarbamate) in AD-H was obtained from PDB at Ref. [53]. AutoDock Tools (ADT) was downloaded free of charge from the web [54] and was used to prepare input file for docking simulations. The docking studies were carried out with AutoDock 4.2 (Scripps Research Institute, USA). The grid box was set to $70 \times 70 \times 70$ (Å) with 0.375 Å spacing. Lamarckian genetic algorithm was used with 100 runs, population size of 300, maximum number of 500,000 energy evaluations, a mutation rate of 0.02 and a crossover rate of 0.50. The mobile phase was accounted for by the use of the dielectric constant corresponding to it, namely: *i*) methanol for (*R/S*)-**3** and (*R/S*)-**2**; *ii*) weighted average of *n*-heptane/ethanol (85/15, v/v) for (*R/S*)-**4**; and *iii*) weighted average of *n*-heptane/ethanol (95/5, v/v) for (*R/S*)-**1**.

Several conformers of the enantiomers of the four molecules were obtained from the molecular docking program and were clustered in several sets, whose number and types are given in Section SI-6. The results are given in Table 5 in terms of the mean
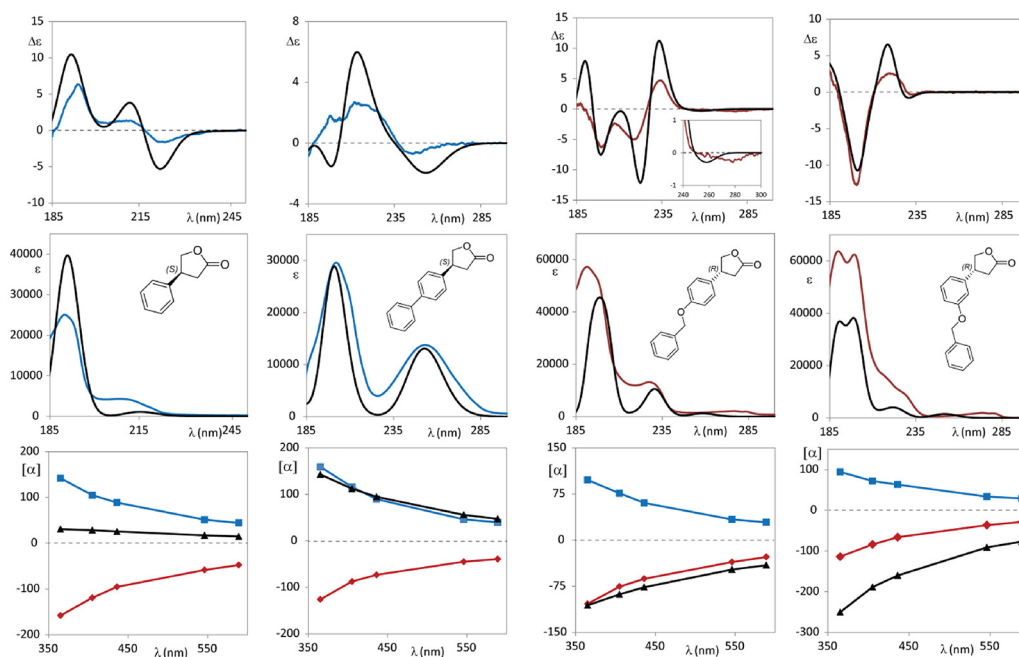
Fig. 5. Comparison of experimental (color, solid lines) with calculated (black, solid lines) ECD and UV absorption spectra and ORD curves of molecules (*R*)-**1** and (*R*)-**2** (first left two columns, top and bottom respectively) and of molecules (*R*)-**3** and (*R*)-**4** (right columns, top and bottom respectively). Calculated spectra are Boltzmann averages from calculated spectra of each single conformer (see Table 3). Color coding as in Fig. 4. (For molecule **2**, the Gaussian width of bands was assumed to be 0.3 eV, for the other molecules it is 0.2 eV-see Experimental Section). ORD experimental curves are given for both enantiomers.
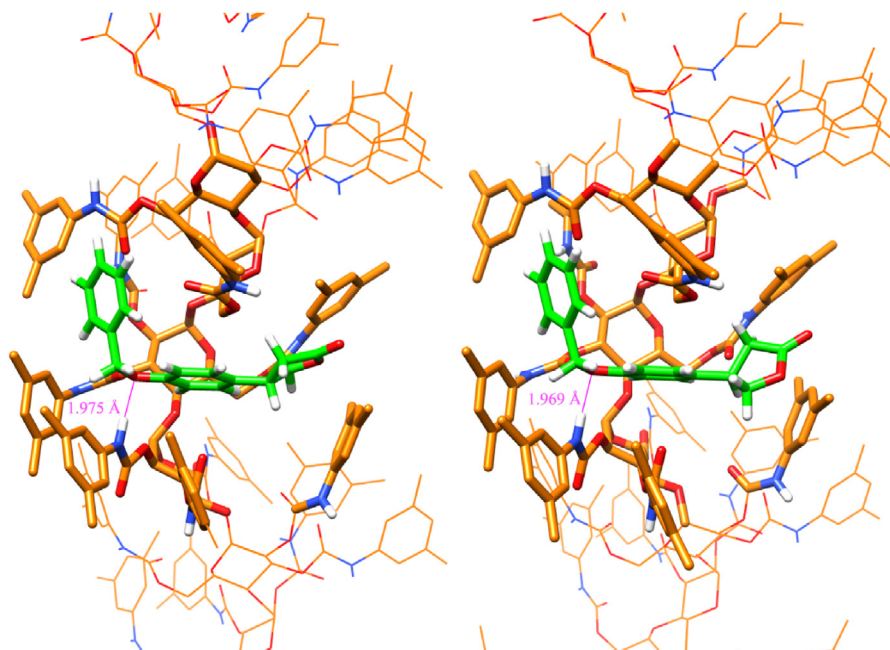

Fig. 6. Molecular docking analysis for compound **3** in the two enantiomeric forms (*S*) (green "tube-mode", left) and (*R*) (green "tube-mode", right) onto polymeric forms of *Amylose tris-(3,5-dimethylphenylcarbamate)* – Chiralpak® AD-H. The structure presented for molecule **3** is the lowest energy conformer among one hundred geometries found during the docking process (see text for details). For the structure of the stationary phase we referred to the PDB file presented in Ref. [53]. The proximal amylose interacting moieties are orange-"tube-mode" displayed.

docking energy, over the most populated cluster, of (*R*) and (*S*) enantiomers of **1**-**4** and are compared therein. The energies are consistent with the chromatography results: longer elution times are indeed systematically associated with stronger calculated binding energy values in each one of the four enantiomeric pairs.

The results are quite explicative about the systematic preference of the (*S*) configuration in being first eluted: indeed (*S*) enantiomers have lower binding energies for all molecules **1**-**4**; this may be

further appreciated by looking at Fig. 6 where the structure of amylose tris-(3,5-dimethylphenylcarbamate) polymer with either one of the two enantiomers of **3** is reported. One may see that the (*R*) enantiomer fits into amylose better than the (*S*) enantiomer; binding is ensured by a shorter hydrogen bonding.

A similar approach and similar conclusions may be found in analogous instances in the literature [55,56], even though in general the approximation in the molecular docking approach does not

allow one to confidently correlate results with the real enantio-selectivity mechanism.

4. Conclusions

In this work we have carried out the HPLC enantiomeric separation in semi-preparative scale of four closely related chiral 3-aryl-substituted-γ-butyrolactones, which are intermediates for reactions to several pharmaceutically relevant molecules, including novel sigma 1 receptor ligands as well as novel PKC ligands. We demonstrated that the first eluted enantiomer has always (S) configuration. The determination of the absolute configuration has been made possible by three chiroptical spectroscopies, ECD, VCD and ORD and by DFT calculations. The three methods have given a unanimous answer to the problem of the absolute configuration assignment, which is rather an exception than a rule [30,32,38]. Finally we have been able to justify the observed constancy in elution order, through Molecular Docking numerical experiments, by evaluating free energy values of interaction of each enantiomeric pair to amylose derived chiral stationary phase of the employed columns.

Appendix A. Supplementary data

Supplementary data associated with this article can be found, in the online version, at http://dx.doi.org/10.1016/j.jpba.2017.01.007.

References

[1] A. Ghantous, H. Gali-Muhtasib, H. Vuorela, N.A. Saliba, N. Darwiche, What made sesquiterpene lactones reach cancer clinical trials? Drug Discov. Today 15 (2010) 668–679.
[2] F. Jun-Tao, W. De-Long, W. Yong-Ling, Y. He, Z. Xing, New antifungal scaffold derived from a natural pharmacophore: synthesis of a-methylene-c-butyrolactone derivatives and their antifungal activity against Colletotrichum lagenarium, Bioorg. Med. Chem. Lett. 23 (2013) 4393–4397.
[3] W. G1adkowski, A. Skrobiszewski, M. Mazur, M. Siepka, A. Pawlak, B. Obminska-Mrukowicz, A. Bia1onska, D. Poradowski, A. Drynda, M. Urbaniak, Synthesis and anticancer activity of novel halolactones with b-aryl substituents from simple aromatic aldehydes, Tetrahedron 69 (2013) 10414–10423.
[4] A. Skrobiszewski, W. Gladkowski, P. Walczak, A. Gliszczyn'Ska, G. Maciejewska, T. Klejdysz, J. Nawrot, C. Wawrzen'Czyk, Synthesis of β-aryl-γ-lactones and relationship: structure – antifeedant and antifungal activity, J. Chem. Sci. 127 (2015) 687–699.
[5] J.J. Bourguignon, A. Schoenfelder, M. Schmitt, C.G. Wermuth, V. Hechler, S.B. Charlier, M. Maitre, Analogues of γ-hydroxybutyric acid. synthesis and binding studies, J. Med. Chem. 31 (1988) 893–897.
[6] S. Englisch-Peters, Synthesis of ω-hydroxy analogues of valine leucine and isoleucine, Tetrahedron 45 (1989) 6127–6134.
[7] D. Rossi, V. Talman, G. Boije Af Gennas, A. Marra, P. Picconi, R. Nasti, M. Serra, J. Ann, M. Amadio, A. Pascale, R.K. Tuominen, J. Yli Kauhaloma, J. Lee, S. Collina, Beyond the affinity for protein kinase C: exploring 2-phenyl-3-hydroxypropyl pivalate analogues as C1 domain-targeting ligands, Med. Chem. Commun. 6 (2015) 547–554.
[8] Università di Pavia Use of Arylalkanolamines as Sigma-1 receptor antagonists. WO2015132733 (2015).
[9] A. Marra, D. Rossi, L. Pignataro, C. Bigogno, A. Canta, N. Oggioni, A. Malacrida, M. Corbo, G. Cavaletti, M. Peviani, D. Curti, G. Dondio, S. Collina, Toward the identification of neuroprotective agents: g-scale synthesis, pharmacokinetic evaluation and CNS distribution of (R)-RC-33, a promising sigma1 receptor agonist, Future Med. Chem. 8 (2016) 287–295.
[10] M. Peviani, E. Salvaneschi, L. Bontempi, A. Petese, A. Manzo, D. Rossi, M. Salmona, S. Collina, P. Bigini, D. Curti, Neuroprotective effects of the Sigma-1

[11] receptor (S1R) agonist PRE-084, in a mouse model of motor neuron disease not linked to SOD1 mutation, Neurobiol. Dis. 62 (2014) 218–232.
[12] S. Collina, R. Gaggeri, A. Marra, A. Bassi, S. Negrinotti, F. Negri, D. Rossi Sigma, receptor modulators: a patent review, Expert Opin. Ther. Pat. 23 (2013) 597–613.
[13] D. Rossi, A. Pedrali, A. Marra, L. Pignataro, D. Schepmann, B. Wünsch, L. Ye, K. Leuner, M. Peviani, D. Curti, O. Azzolina, Studies on the enantiomers of RC-33 as neuroprotective agents: isolation, configurational assignment, and preliminary biological profile, Chirality 25 (2013) 814–822.
[14] D. Rossi, A. Pedrali, R. Gaggeri, A. Marra, L. Pignataro, E. Laurini, V. DalCol, M. Fermeglia, S. Pricl, D. Schepmann, B. Wünsch, M. Peviani, D. Curti, S. Collina, Chemical, pharmacological, and in vitro metabolic stability studies on enantiomerically pure RC-33 compounds: promising neuroprotective agents acting as σ1 receptor agonists, Chem. Med. Chem. 8 (2013) 1514–1527.
[15] D. Rossi, A. Marra, P. Picconi, M. Serra, L. Catenacci, M. Sorrenti, E. Laurini, M. Fermeglia, S. Price, S. Brambilla, N. Almirante, M. Peviani, D. Curti, S. Collina, Identification of RC-33 as a potent and selective sigma.1 receptor agonist potentiating NGF-induced neurite outgrowth in PC12 cells. Part 2: g-scalesynthesis, physicochemical characterization and in vitro metabolic stability, Bioorg. Med. Chem. 21 (2013) 2577–2586.
[16] D. Rossi, A. Pedrali, M. Urbano, R. Gaggeri, M. Serra, L. Fernández, M. Fernández, J. Caballero, S. Ronsisvalle, O. Prezzavento, D. Schepmann, B. Wuensch, M. Peviani, D. Curti, O. Azzolina, S. Collina, Identification of a potent and selective ρ1 receptor agonist potentiating NGF-induced neurite outgrowth in PC12 cells, Bioorg. Med. Chem. 19 (2011) 6210–6224.
[17] D. Rossi, M. Urbano, A. Pedrali, M. Serra, D. Zampieri, M.G. Mamolo, C. Laggner, C. Zanette, C. Florio, D. Schepmann, B. Wuensch, O. Azzolina, S. Collina, Design, synthesis and SAR analysis of novel selective σ1 ligands (Part 2), Bioorg. Med. Chem. 18 (2010) 1204–1212.
[18] D. Zampieri, M.G. Mamolo, E. Laurini, C. Zanette, C. Florio, S. Collina, D. Rossi, O. Azzolina, L. Vio, Substituted benzo[d]oxazol-2(3H)-one derivatives with preference for the σ1 binding site, Eur. J. Med. Chem. 44 (2009) 124–130.
[19] S. Collina, G. Loddo, M. Urbano, L. Linati, A. Callegari, F. Ortuso, S. Alcaro, C. Laggner, T. Langer, O. Prezzavento, G. Ronsisvallef, O. Azzolina, Design synthesis, and SAR analysis of novel selective σ1 ligands, Bioorg. Med. Chem. 15 (2007) 771–783.
[20] I. Agranat, H. Caner, J. Caldwell, Putting chirality to work: the strategy of chiral switches, Nat. Rev. Drug Discov. 1 (2002) 753–768.
[21] T. Andersson, Single-isomer drugs: true therapeutic advances, Clin. Pharmacokinet. 43 (2004) 279–285.
[22] Y. Okamoto, T. Ikai, Chiral HPLC for efficient resolution of enantiomers, Chem. Soc. Rev. 37 (2008) 2593–2608.
[23] S. Collina, G. Loddo, M. Urbano, D. Rossi, M.G. Mamolo, D. Zampieri, S. Alcaro, A.A. Gallelli, O. Azzolina, Enantioselective chromatography and absolute configuration of N,N-dimethyl-3-(naphthalen-2-yl)-butan-1-amines: potential sigma1 ligands, Chirality 18 (2006) 245–253.
[24] R. Gaggeri, D. Rossi, S. Collina, B. Mannucci, M. Baierl, M. Juza, Quick development of an analytical enantioselective high performance liquid chromatography separation and preparative scale-up for the flavonoid Naringenin, J. Chromatogr. A 1218 (2011) 5414–5422.
[25] D. Rossi, A. Marra, M. Rui, S. Brambilla, M. Juza, S. Collina, Fit-for-purpose development of analytical and (semi)preparative enantioselective high performance liquid and supercritical fluid chromatography for the access to a novel σ1 receptor agonist, J. Pharm. Biom. Anal. 118 (2016) 363–369.
[26] Y. Luo, A.J. Carnell, Chemoenzymatic synthesis and application of bicyclo[2.2.2]octadiene ligands: increased efficiency in rhodium-catalyzed asymmetric conjugate additions by electronic tuning, Angew. Chem. Int. Ed. 49 (2010) 2750–2754.
[27] P. Scafato, F. Caprioli, L. Pisani, P. Padula, F. Santoro, G. Mazzeo, S. Abbate, F. Lebon, G. Longhi, Combined use of three forms of chiroptical spectroscopies in the study of the absolute configuration and conformational properties of 3-phenylcyclopentanone, 3-phenylcyclohexanone, and 3-phenylcycloheptanone, Tetrahedron 69 (2013) 10752–10762.
[28] P.L. Polavarapu, Determination of the structures of chiral natural products using vibrational circular dichroism, Chapter 11, in: N. Berova, P.L. Polavarapu, K. Nakanishi, R.W. Woody (Eds.), Comprehensive Chiroptical Spectroscopy (Applications in Stereochemical Analysis of Synthetic Compounds, Natural Products, and Biomolecules), Vol. 2, John Wiley & Sons, NY, 2012, pp. 387–420.
[29] G. Marcin, Configurational and conformational study of (-)-oseltamivir using a multi-chiroptical approach, Org. Biomol. Chem. 13 (2015) 2999–3011.
[30] P.L. Polavarapu, Determination of the absolute configurations of chiral drugs using chiroptical spectroscopy, Molecules 21 (2016) 1056, http://dx.doi.org/10.3390/molecules21081056.
[31] P.L. Polavarapu, Why is it important to simultaneously use more than one chiroptical spectroscopic method for determining the structures of chiral molecules, Chirality 20 (2008) 664–672.
[32] D. Rossi, R. Nasti, A. Marra, S. Meneghini, G. Mazzeo, G. Longhi, M. Memo, B. Cosimelli, G. Greco, E. Novellino, F. Da Settimo, C. Martini, S. Taliani, S. Abbate, S. Collina, Enantiomeric 4-acylamino-6-alkyloxy-2 alkylthiopyrimidines as potential A3 adenosine receptor antagonists: HPLC chiral resolution and absolute configuration assignment by a full set of chiroptical spectroscopy, Chirality 28 (2016) 434–440.
[33] L.A. Nafie, Vibrational Optical Activity-Principles and Applications, Wiley, NY, 2011.

[33] S. Abbate, G. Longhi, F. Lebon, M. Tommasini, Electronic and vibrational circular dichroism spectra of (R)-(-)-apomorphine, Chem. Phys. 405 (2012) 197–206.

[34] S. Abbate, L.F. Burgi, F. Gangemi, R. Gangemi, F. Lebon, G. Longhi, V.M. Pultz, D.A. Lightner, Comparative analysis of IR and vibrational circular dichroism spectra for a series of camphor related molecules, J. Phys. Chem. A 113 (42) (2009) 11390–11405.

[35] S. Abbate, G. Longhi, E. Castiglioni, F. Lebon, P.M. Wood, W.L. Woo Lawrence, Barry V.L. Potter, Determination of the absolute configuration of aromatase and dual aromatase-sulfatase inhibitors by vibrational and electronic circular dichroism spectra analysis, Chirality 21 (2009) 802–809.

[36] P.M. Wood, L.W. Lawrence Woo, J.R. Labrosse, M.N. Trusselle, S. Abbate, G. Longhi, E. Castiglioni, F. Lebon, A. Purohit, M.J. Reed, B.V.L. Potter, Chiral aromatase and dual aromatase-steroid sulfatase inhibitors from the letrozole template: synthesis, absolute configuration, and in vitro activity, J. Med. Chem. 51 (2008) 4226–4238.

[37] S. Abbate, L.F. Burgi, E. Castiglioni, F. Lebon, G. Longhi, E. Toscano, S. Caccamese, Assessment of configurational and conformational properties of naringenin by vibrational circular dichroism, Chirality 21 (2009) 436–441.

[38] Y. He, W. Bo, R.K. Dukor, L.A. Nafie, Determination of absolute configuration of chiral molecules using vibrational optical activity: a review, Appl. Spectrosc. 65 (2011) 699–723.

[39] L.S. Ettore, Nomenclature for chromatography, Pure Appl. Chem. 65 (1993) 819–872.

[40] European Pharmacopoeia, 2.2.29. LIQUID CHROMATOGRAPHY, 8th ed., EDQM,European Pharmacopoeia, Council of Europe, B.P. 907, 67029 Strasbourg,France, July 2013.

[41] Gaussian 09, Revision A.02, M.J. Frisch, G.W. Trucks, H.B. Schlegel, G.E. Scuseria, M.A. Robb, J.R. Cheeseman, G. Scalmani, V. Barone, B. Mennucci, G.A. Petersson, H. Nakatsuji, M. Caricato, X. Li, H.P. Hratchian, A.F. Izmaylov, J. Bloino, G. Zheng, J.L. Sonnenberg, M. Hada, M. Ehara, K. Toyota, R. Fukuda, J. Hasegawa, M. Ishida, T. Nakajima, Y. Honda, O. Kitao, H. Nakai, T. Vreven, J.A. Montgomery Jr., J.E. Peralta, Ogliaro F.M. Bearpark, J.J. Heyd, E. Brothers, K.N. Kudin, V.N. Staroverov, R. Kobayashi, J. Normand, K. Raghavachari, A. Rendell, J.C. Burant, S.S. Iyengar, J. Tomasi, M. Cossi, N. Rega, J.M. Millam, M. Klene, J.E. Knox, J.B. Cross, V. Bakken, C. Adamo, J. Jaramillo, R. Gomperts, R.E. Stratmann, O. Yazyev, A.J. Austin, R. Cammi, C. Pomelli, J.W. Ochterski, R.L. Martin, K. Morokuma, V.G. Zakrzewski, G. Voth, P. Salvador, S. Dannenberg, S. Dapprich, A.D. Daniels, Ö. Farkas, J.B. Foresman, J.V. Ortiz, J. Cioslowski, D.J. Fox Gaussian. Gaussian, Inc.: Wallingford CT (2009).

[42] J. Tomasi, B. Mennucci, R. Cammi, Quantum mechanical continuum solvation models, Chem. Rev. 105 (2005) 2999–3093.

[43] P.L. Polavarapu, Chiroptical Spectroscopy Fundamentals and Applications, CRC Press, Taylor & Francis Group Boca Raton, FL, 2017, page 180.

[44] G. Mazzeo, G. Longhi, S. Abbate, A. Cimmino, M. Masi, L. Maddau, A. Evidente. VCD, ECD and ORD spectra of natural products: phytotoxic pyrones and furanones, produced by Diplodia Corticola, a cork oak pathogen. Chiritaly Conference, Catania, Italy, September 3–5, 2016.

[45] H. Izumi, S. Futamura, L.A. Nafie, R.K. Dukor, Determination of molecular stereochemistry using vibrational circular dichroism spectroscopy: absolute configuration and solution conformation of 5-formyl-cis,cis-1,5-trimethyl-3-hydroxymethylcyclohexane-1-carboxylic acid lactone, Chem. Rec. 3 (2003) 112–119.

[46] F.J. Devlin, P.J. Stephens, B. Figadère, Determination of the absolute configuration of the natural product klaivanolide via density functional calculations of vibrational circular dichroism (VCD), Chirality 21 (2009) E48–E53.

[47] Z. Tomankova, V. Setnicka, M. Urbanova, P. Matejka, V. Kral, K. Volka, P. Bour, Conformational flexibility of corey lactone derivatives indicated by absorption and vibrational circular dichroism spectra, J. Org. Chem. 69 (2004) 26–32.

[48] J.P. Jennings, W. Klyne, P.M. Scopes, Optical rotatory dispersion. Part XXIV, J. Chem. Soc. (1965) 7211–7229.

[49] J.P. Jennings, W. Klyne, P.M. Scopes, Optical rotatory dispersion. Part XXVI. Some bridged ring lactones, J. Chem. Soc. (1965) 7229–7237.

[50] W. Klyne, P.M. Scopes, A. Williams, Optical rotatory dispersion. Part XXVII. The hudson sector rule, J. Chem. Soc. (1965) 7237–7242.

[51] C. Bertucci, L.F. Lopes Guimarães, P. Sueli Bonato, K. Bastos Borges, L. Tiemi Okano, G. Mazzeo, C. Rosini, Assignment of the absolute configuration at the sulfur atom of thioridazine metabolites by the analysis of their chiroptical properties: the case of thioridazine 2-sulfoxide, J. Pharm. Biomed. Anal. 76 (2013) 588–599.

[52] G. Mazzeo, E. Santoro, A. Andolfi, A. Cimmino, P. Troselj, A.G. Petrovic, S. Superchi, A. Evidente, N. Berova, Absolute configurations of fungal and plant metabolites by chiroptical methods. ORD ECD, and VCD studies on phyllostin, scytolide, and oxysporone, J. Nat. Prod. 52 (2010) 796–801.

[53] Y.K. Ye, S. Bai, S. Vyas, M.J. Wirth, NMR and computational studies of chiral discrimination by amylose tris(3,5-dimethylphenylcarbamate), J. Phys. Chem. B (2007) 1189–1198.

[54] G.M. Morris, R. Huey, W. Lindstrom, M.F. Sanner, R.K. Belew, D.S. Goodsell, A.J. Olson, J. Comput. Chem. 16 (2009) 2785–2791.

[55] S. Ravichandran, J.R. Collins, N. Singh, I.W. Wainer, A molecular model of the enantioselective liquid chromatographic separation of (R,S)-ifosfamide and its Ndechloroethylated metabolites on a teicoplanin aglycon chiral stationary phase, J. Chromatogr. A 21 (1269) (2012) 218–225.

[56] Y. Li, D. Liu, P. Wang, Z. Zhou, Computational study of enantioseparation by amylose tris(3,5-dimethylphenylcarbamate)-based chiral stationary phase, J. Sep. Sci. 33 (2010) 3245–3255.